Reversible and photolabile inhibitors for human tissue transglutaminase

Kim Yang-Ping Apperley

A thesis submitted to the
Faculty of Graduate and Postdoctoral Studies
in partial fulfillment of the requirements for the
Doctorate in Philosophy degree in Chemistry

Department of Chemistry and Biomolecular Sciences
Faculty of Science
University of Ottawa

Abstract

Tissue transglutaminase (TG2) is a calcium-dependent enzyme that natively catalyses the formation of isopeptidic bonds between protein- or peptide-bound glutamine and lysine residues. Physiologically, it is ubiquitously expressed in tissues, with roles in cellular differentiation, extracellular matrix stabilisation, and apoptosis, among others. However, its unregulated activity has been associated with various pathologies including fibrosis, cancer and celiac disease.

Since most pathologies are associated with an increased transamidation activity, efforts have been directed towards the development of TG2 inhibitors. In this context, the work described in this thesis is centred on reversible inhibitors, building on recent work done within the Keillor group in two directions, namely localisation and potency.

In a localisation-driven approach, we developed a photolabile derivative of a known reversible inhibitor, in order to form a covalent bond with the enzyme and determine the inhibitor's binding site. In tandem, we optimised a protocol for the expression of TG2 incorporating ArgΔ10 and LysΔ8, amino acids that are ^{13}C- and ^{15}N-labelled to provide a mass shift of 10 and 8 Da, respectively, compared to the corresponding unlabelled amino acids. This "heavy" TG2 was developed as a tool for reference in the analysis of the tryptic digest of labelled protein.

In a potency-driven approach, based on the observation that previous *trans* cinnamoyl inhibitor scaffolds were susceptible to nucleophilic attack by glutathione, we developed a bis(triazole) scaffold with reduced electrophilicity. The preparation of a small library of compounds showed that this scaffold demonstrates a preference for electron-withdrawing substituents, such as nitro groups.

Continuing in a potency-driven approach, and inspired by work done in the identification of glutathione-resistant scaffolds, we studied a new alkynyl scaffold. While still susceptible to glutathione addition, these compounds showed a marked improvement in potency, with the lead compound having an IC_{50} of 930 nM and being established as a competitive inhibitor with a K_i of 420 nM, our most potent reversible inhibitor to date. Furthermore, this scaffold also produced an inhibitor lacking nitro groups (to limit eventual cellular toxicity), but maintaining good potency, with an IC_{50} value of 3.03 μM.

Keywords: enzyme, transglutaminase, enzyme kinetics, photolabelling, reversible inhibition, competitive inhibition

Acknowledgements

First and foremost, I owe thanks to Jeff for welcoming me into his research group five years ago, and for his constant help and support. I may not be able to identify even half the songs on your playlist, but I still learned a lot over my time in your group – how to co-author a review (or three) is definitely a skill I owe to you!

To Olivier, our time in the Keillor group may not have overlapped, but you were the catalyst that started this wonderful adventure. To the Keillor group members whose time overlapped with mine, who are almost too many to mention, thanks for always being ready for a laugh, a drink, or a loud and animated conversation in the office. To the postdocs – Christophe, Chris, Yingche, Nicole and Mark – thanks for always having a minute (or an hour) to teach me something new. To the grad students – Amina, Mirka, Samuel, Abdullah, Dan, Kelvin, Sydney and Karine – thanks for sharing in all the ups and downs of grad school (and for Abdullah, the particular ups and downs of TG2!). To the undergrads, especially those I got to supervise – Catherine, Sara-Pier, Mireille, Vincent and Nicholas – thanks for letting me learn to teach and demonstrate with you.

To my skating family, both in Pierrefonds and at Minto – thanks for helping me maintain balance both in life and on my skates. Special thanks to my coaches for teaching me skills completely different from medicinal chemistry – Donna, thanks for sticking by me for my gold skills and my fourth degree; Mariève, thanks for teaching me the power of positive thinking and for believing in me; Jamie, thanks for pushing me (sometimes very far) outside my comfort zone and teaching me the value of learning to do things correctly the first time.

Anne-Sophie and Alyson, you were there when I had my doubts and I wouldn't have survived this adventure away from Montreal without you. Yingche, you were there no matter

how many kilometers separated us since the day we watched those pigeons kiss outside our window, and you are the genius behind the concept of “truffle days”. Chris, you let me climb with you and from there made my social life in Ottawa a real thing. Samuel, for always answering my “one more question” and for being my Rogers boyfriend; the hashtag #TeamSkim will last beyond grad school. Kelvin, thanks for being my sounding board and for adding just the right level of sarcasm to my life. SP, you were the first to return to the Keillor group after working with me, and sent me Nicholas, who was a second set of hands... and eyes... and a second brain... *bref*, Nicholas, you were a (very much taller) second me.

To my family – mom, dad and Nina – I may have been away in Ottawa but none of this would have been possible without having you by my side, even when the words atom, molecule and enzyme were all synonymous to you. Thanks for loving me unconditionally.

Dedication

This thesis is dedicated to everyone in my support system, even those who are no longer physically here

Table of Contents

List of Tables

List of Figures

List of Schemes

List of Symbols, Abbreviations and Nomenclature

Symbol	Definition
% v/v	percent by volume
°C	degrees Celcius
Å	Angström
Ac	acetyl
ACN	acetonitrile
Acr	acryloyl
ACT	2-aryl-5-carboxytetrazole
AL5	*N*-Cbz-Glu(γ-*p*-nitrophenylester)Gly
anh.	anhydrous
Arg	arginine
ArgΔ10	$^{13}C_6$,$^{15}N_4$-arginine
Asp	aspartic acid
ATP	adenosine 5'-triphosphate
AU	absorbance units
b	y-intercept
B.C.E.	Before the Current Era
BOC	*tert*-butyloxycarbonyl
br	broad
calc.	calculated
Cbz	carboxybenzyl
cDNA	complementary DNA
CE	capillary electrophoresis
CFP	cyan fluorescent protein
CuAAC	copper-catalysed azide-alkyne cycloaddition
Cys	cysteine
d	doublet
Da	dalton
DCM	dichloromethane
dd	doublet of doublets
dec.	decomposition
DIPEA	*N*,*N*-diisopropylethylamine
DMAP	4-(dimethylamino)pyridine
DMF	*N*,*N*-dimethylformamide
DMP	Dess-Martin periodinane
DMSO	dimethysulfoxide
DON	6-diazo-5-oxo-L-norleucine
DPPE	*N*,*N*-diethyl-2-[4-(phenylmethyl)phenoxy]ethanamine HCl
E	enzyme
E. coli	*Escherichia coli*
E.C.	Enzyme Commission number
EDTA	ethylenediaminetetraacetic acid
EI	electron impact
eq.	equation

equiv	molar equivalent
ESI	electrospray ionization
FDA	Food and Drug Administration
FMOC	9'-fluorenylmethyloxycarbonyl
FRET	Förster resonance energy transfer
FRET-FLIM	Förster resonance energy transfer – fluorescence lifetime measurement
fXIII	factor XIII
fXIIIa	activated fXIII
GDP	guanosine 5'-diphosphate
Gln	glutamine
Gly	glycine
GmbH	*Gesellschaft mit beschränkter Haftung* (company with limited liability)
GMP-PCP	β,γ-methyleneguanosine 5′-triphosphate
gplTG	guinea pig liver TGase
GSH	glutathione, reduced form
GSSG	glutathione, oxidised form
GST	glutathione S-transferase
GTP	guanosine 5'-triphosphate
GTPγS	guanosine 5'-*O*-(3-thio)triphosphate
h	hour
His	histidine
HPLC	high-performance liquid chromatography
HRMS	high-resolution mass spectrometry
hTG2	human tissue transglutaminase
Hz	hertz
hν	UV light
I	inhibitor
IC_{50}	concentration of inhibitor required to decrease the enzyme's activity to 50% of what is observed in the absence of inhibitor
Im	imidazole
IPTG	isopropyl-β-D-thiogalactoside
J	coupling constant
J. Med. Chem.	Journal of Medicinal Chemistry
k_{cat}	turnover number
K_{eq}	equilibrium constant
K_I	irreversible inhibitor inhibition constant
K_i	reversible inhibitor inhibition constant
K_i^{app}	apparent K_i
k_{inact}	inactivation rate constant
K_M	Michaelis-Menten constant
K_M^{app}	apparent K_M
LB	Luria-Bertani
LC	liquid chromatography
LC-MS	liquid chromatography-mass spectrometry

LC-MS/MS	liquid chromatography-tandem mass spectrometry
Lys	lysine
LysΔ6	$^{13}C_6$-lysine
LysΔ8	$^{13}C_6$,$^{15}N_2$-lysine
m	slope
m	multiplet
m.p.	melting point
min	minute
MOPS	3-(*N*-morpholino)propanesulfonic acid
MPAB	(5-allyl-1-methyl-5-phenyl)barbituric acid
mRNA	messenger RNA
MS	mass spectrometry
n.d.	not detected
Na-(L)Asc	sodium L-ascorbate
nAChR	nicotinic acetylchlorine receptors
NMP	*N*-methyl-2-pyrrolidone
NMR	nuclear magnetic resonance
NOESY	nuclear Overhauser effect spectroscopy
nPAGE	native polyacrylamide gel electrophoresis
[O]	oxidant
o/n	overnight
obt.	obtained
OD_{600}	optical density at 600 nm
P	product
PAGE	polyacrylamide gel electrophoresis
PCC	pyridinium chlorochromate
PDB	Protein Data Bank
pKa	negative logarithm of the acidity constant K_a
PSP	PreScission™ Protease
py	pyridine
q	quadruplet
R_f	retention factor
RNA	ribonucleic acid
rpm	revolutions per minute
RT	room temperature
S	substrate
s	singlet
SAR	structure-activity relationship
SAXS	small-angle X-ray scattering
S_b	standard error on *b*
SDS-PAGE	sodium dodecylsulfate polyacrylamide gel electrophoresis
SILAC	stable isotopic labelling of amino acids in cell culture
SILACE	SILAC optimized for *E. coli*
S_m	standard error on *m*
t	time
t	triplet

TB	terrific broth
TBAF	tetrabutylammonium fluoride
TBDMS	*t*-butyldimethylsilyl
TCEP	tris(2-carboxyethyl)phosphine
TCICA	trichloroisocyanuric acid
TEMPO	2,2,6,6-tetramethyl-1-piperidinyloxyl
TFD	trifluoromethyldiazirinyl
TG1	transglutaminase 1, keratinocyte transglutaminase
TG2	transglutaminase 2, tissue transglutaminase
TG3	transglutaminase 3, epidermal transglutaminase
TG4	transglutaminase 4, prostate transglutaminase
TG5	transglutaminase 5
TG6	transglutaminase 6
TG7	transglutaminase 7
TGase or TG	transglutaminase
THF	tetrahydrofuran
THP	tetrahydropyran
Thr	threonine
TIP47	tail-interacting protein 47
TLC	thin layer chromatography
TMS	tetramethylsilane or trimethylsilyl
Tris	tris(hydroxymethyl)aminomethane
Trp	tryptophan
Ts	toluenesulfonyl
Tyr	tyrosine
U	enzyme activity unit
UV	ultraviolet
v	rate
v_0	initial rate in the absence of inhibitor
Val	valine
V_{max}	maximum rate
YFP	yellow fluorescent protein
ZYP	autoinduction medium with N-Z-amine (Z), yeast extract (Y) and salts (P)
α	inhibition factor (eq. 3.2; $\alpha=1+[I]/K_i$)
δ	chemical shift

Epigraph

Now this is not the end. It is not even the beginning of the end.

But it is perhaps the end of the beginning.

– Winston Churchill

Chapter One: **Introduction**

1.1 Medicinal chemistry

Medicinal chemistry is a branch of chemistry at the intersection of chemistry and biology, where isolated or synthesized compounds are evaluated for their biological activities as they pertain to disease. However, over the course of history, the standards and expectations for drugs have changed. For example, one of the most well-known drugs, Aspirin (acetylsalicylic acid), despite its current popularity, would not likely be approved by the FDA by modern standards, due to its various side-effects. As far back as the first century B.C.E., Hippocrates had records of pain relief treatments including a powder made from the bark and leaves of the willow tree to help heal headaches, pains and fevers. In time, scientists discovered that the active compound was salicyn, which is metabolised to salicylic acid, a stomach irritant. In 1853, Charles Frederic Gerhardt neutralised the acid by buffering it in sodium and acetyl chloride, creating acetyl salicylic acid. This product worked well as a drug but, with no intent to market it, Gerhardt abandoned it. Felix Hoffman rediscovered this work in 1899; following the observation that the formulation worked well for his father's arthritis, he convinced Bayer to market the drug, and Aspirin was patented on March 6th, 1899.

While the tale of Aspirin is a great story, the modern approach remains similar in certain respects. Generally, research begins with the identification of a first "hit" compound, and then its derivatisation to obtain a molecule with the desired characteristics for the targeted protein. In relation with this approach, Alexander Crum Brown pioneered the idea of a relationship between a compound's structure and its physiological effect, by showing[1] in 1969 that the methylation of alkaloids, known to cause muscle spasms, resulted in the opposite physiological effect, namely

muscle relaxation. This work was the beginning of what are now termed structure-activity relationships (SAR) in medicinal chemistry.

In the early 1900's, chemist Paul Erhlich (1908 Nobel laureate for his work in immunology) and bacteriologist Sahachiro Hata produced[2] the antiprotozoal arsphenamine, a more selective (and therefore safer) derivative of atoxyl, an antiprotozoal. Arsphenamine was obtained by combining chemical synthesis and biological screening, in an approach even closer to the modern one. Ehrlich was also the first scientist to consider the selectivity of drugs, and he defined the chemotherapeutic index, namely the ratio of the minimum curative dose to the maximum tolerated dose of a therapeutic compound.

Based on those early precedents, modern medicinal chemistry uses SAR in a combination of synthesis and biological screening to fine-tune the characteristics of target compounds. Within the Keillor group, we focus on the development of inhibitors for tissue transglutaminase, a small area in the broad field of medicinal chemistry.

1.2 Transglutaminases

Transglutaminases (TGases, EC 2.3.2.13) are a family of calcium (Ca^{2+})-dependent enzymes that natively catalyse the formation of isopeptidic N^{ε}(γ-glutaminyl)lysine bonds between protein- or peptide-bound glutamine and lysine residues. They are evolutionarily related[3] to papain-like cysteine proteases, through their core domain structure and catalytic mechanism. The general reaction is shown below in Scheme 1.1. The catalytic triad, consisting of the residues cysteine, histidine and aspartate, is conserved throughout the transamidation-active members of the family.

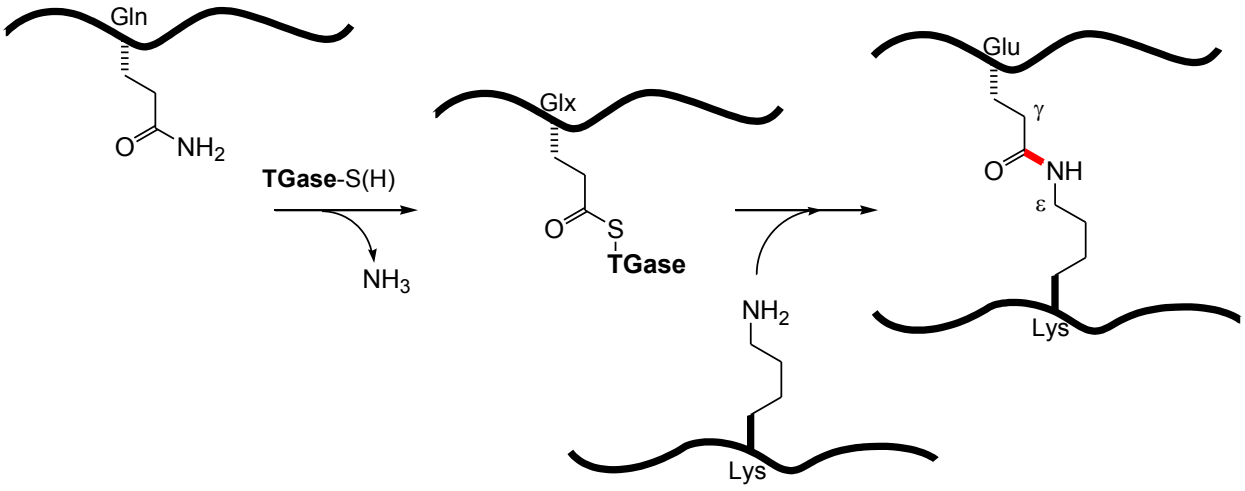

Scheme 1.1. Transamidation reaction catalysed by TGases

Reproduced with permission from Keillor *et al*., Bioorganic Chemistry (2014)[4]

The family of human isoforms is composed of nine members: TGases 1 through 7, factor XIII (fXIII), and the catalytically-inactive erythrocyte membrane protein band 4.2. Of these isozymes, the three-dimensional structures of three have been solved: fXIII, TG2 and TG3; the representative TGase structure (using TG2, PDB code 1KV3), which is consistent between all three crystal structures, is shown below.

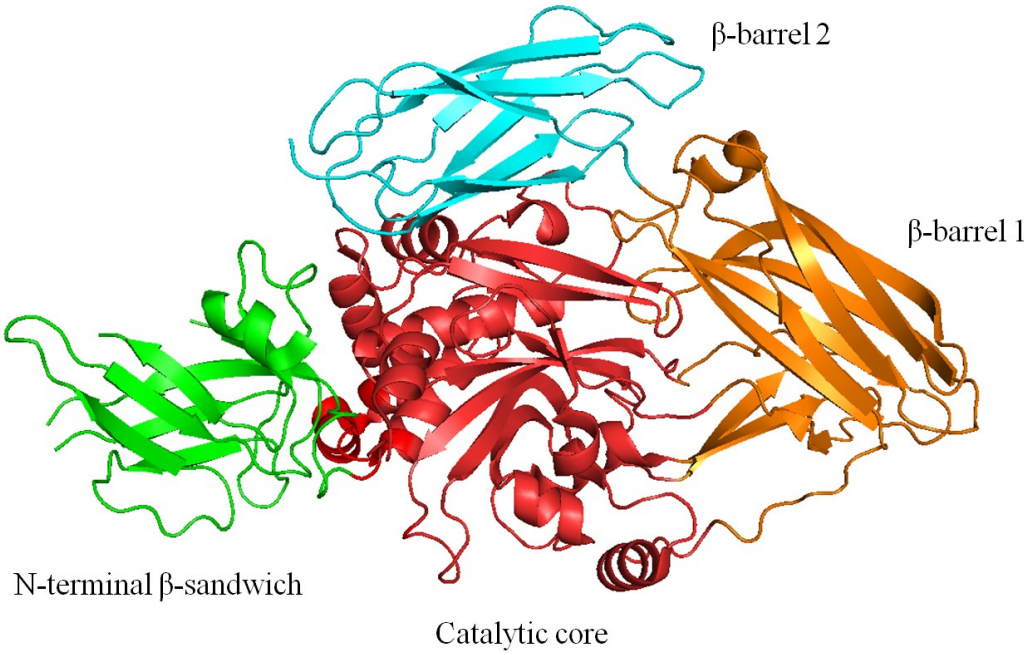

Figure 1.1. Representative TGase structure (TG2, PDB 1KV3)

Each of the human isoforms consists of four domains that are organised in a similar manner[3], as indicated in Figure 1.1: an N-terminal β-sandwich domain, that forms a functional unit within the core domain, a catalytic core domain, that contains the conserved active site triad, and two C-terminal β-barrel domains, that are involved in the regulation of the enzyme's activity. The human isoforms are described individually below.

1.2.1 TG1 (keratinocyte TGase)

TG1, also known as keratinocyte TGase[5], is epidermal-specific. It is mostly found anchored to the keratinocyte plasma membrane via fatty acyl linkages at its N-terminus, a characteristic that makes it unique among TGases. A 90-kDa protein, it is also found in the cytosol, and has a function in the assembly of the cornified envelope, a multi-protein structure of

cross-linked proteins beneath the plasma membrane, in surface epithelia. TG1 is associated with lamellar ichytosis, a disorder of cornification that affects both the epidermis and hair.

1.2.2 TG2 (tissue TGase)

TG2, or tissue TGase[4], is ubiquitously expressed in tissues; as such, this 686-amino acid, 77.3 kDa protein has a variety of physiological roles. It is composed of the typical four TGase domains, with a catalytic triad[6] consisting of Cys277, His335 and Asp358, which are located at the end of a tunnel bordered by residues Trp241, Trp332 and Thr360, each identified[7] by solving the crystal structure of the active form. Like all TGases, TG2 is activated by Ca^{2+}, but it is also deactivated[4] by GTP, an allosteric regulator that results in a more compact conformation[8]. Historically, this GTP-binding role of TG2 led to its double identification as the $G_h\alpha$ G-protein[9]. TG2 is predominantly found in the cytosol, but it is also localised in the nucleus, membrane, cell surface and extracellular matrix. TG2 has been implicated[10] in cellular differentiation, apoptosis, cell adhesion, and matrix assembly. However, its unregulated activity has also been associated[11] with fibrosis, atherosclerosis, and Alzheimer's and Huntington's diseases, as well as celiac disease. As the enzyme studied in the course of the work presented in this thesis, TG2 will be described in greater detail in Section 1.3.

1.2.3 TG3 (epidermal TGase)

TG3, or epidermal TGase, is a 77-kDa protein[5] that is found in the cytosol in the upper epidermal layers, and has a role in cornified envelope assembly in surface epithelia, in a similar manner to TG1. However, unlike TG1, TG3 requires proteolytic cleavage for activation; its zymogen is composed[12] of the four folded domains that comprise the common structure of the

TGase family. The catalytic triad, composed of Cys272, His330 and Asp353, is buried in a narrow cleft, lined[13] by the side chains of Trp236 and Trp327; residue Tyr525 is also within hydrogen-bonding distance of Cys272. TG3 binds Ca^{2+} in both its zymogen (for stability) and active forms, although the latter includes two extra ions. Similarly to TG2, TG3 has been proposed[13] to bind guanine nucleotides; however, a supporting article[14] by the same group in the same year has since been withdrawn. Physiologically, while gluten sensitivity typically presents as celiac disease (associated primarily with TG2), TG3 has been suggested[5] to serve as the auto-antigen responsible for the skin phenotype in dermatitis herpetiformis, a blistering skin disease in response to gluten sensitivity.

1.2.4 TG4 (prostate TGase)

TG4, also known as prostate TGase[15], is confined to the prostate gland, both intra- and extra-cellularly. Its role is not entirely clear, although it has been found to have a role in prostate cancer, since TG4 is involved in the invasion and motility of those cancer cells. More specifically, TG4, through its core domain, is involved in the adhesion of cancer cells to the extracellular matrix; this interaction is abolished by the presence of an antibody for integrin-β1, suggesting a potential biological pathway interaction for TG4 and integrin. While it is not found in all prostate cancer cells, increased levels of TG4 have been linked to increased tumour aggressiveness, thus inferring that levels of TG4 may be used to determine the best course of treatment.

1.2.5 TG5

As one the more recently-discovered[16] members of TGase family, TG5 has not fully been characterised at the functional level, although it is mainly expressed[17] in stratified squamous epithelia, such as the upper layers of the epidermis and in human hair follicles, in a similar manner to TG1 and TG3, and it is structurally similar to TG2. Full-length TG5 (80 kDa) displays very low enzymatic activity but, upon proteolytic cleavage[17], the N-terminal 53-kDa fragment, comprised of the N-terminal and catalytic domains, shows high activity. In a manner similar[18] to TG2 and TG3, TG5 contains a GTP-binding site, and both GTP and ATP inhibit[18] its activity *in vitro*. However, the presence of Ca^{2+} completely restores its transamidation activity, and the role of its GTP-binding activity in regulating cell function is unknown[5]. Overexpressed TG5 can also induce[19] cell death, a characteristic that makes it different from the other epidermal TGases, although its expression is not restricted to epidermal tissue. Physiologically, mutations in the TG5 gene are known to cause[20] acral peeling skin syndrome, an autosomal recessive skin disorder.

1.2.6 TG6

Another recently-discovered member of the TGase family, TG6 was first characterised[3] in 2011. It has a calculated molecular mass of 79.3 kDa, and displays high sequence similarity to TG3 (50% overall, but 59% within the catalytic core domain); as such, its structure was modelled on that of activated TG3. Its catalytic triad is composed of Cys274, His333 and Asp356, residues that are located at the base of a hydrophobic cavity; unlike TG3, TG6 displays a high specific activity without proteolytic processing. However, similarly to TG2, TG6 is sensitive to oxidative inactivation through its Cys residues, and it is inhibited by guanine

nucleotides in a manner that suggests that it may also act as a guanine exchange factor. TG6 has been associated with neuronal differentiation in the central nervous system and it can be detected in the cell cytosol and at the cell surface, suggesting that it may have independent intra- and extra-cellular roles depending on the binding of its allosteric regulators.

1.2.7 TG7

TG7 was initially identified[16] at the transcriptional level by taking advantage of the sequence homology between TGase family members, thus without any knowledge of its physiological significance. As such, the first step in elucidating its physiological significance has been to detect[21] its activity and identify its peptidic substrates, including peptide pepZ3S, which is being studied as a probe for TG7 activity. So far, no reports associate TG7 with any known disease, although its mRNA has been found to be highly expressed[21] in kidneys, testis and thymus.

1.2.8 fXIII (plasma TGase)

Factor XIII, the plasma TGase[22], exists as a heterotetramer in circulation in blood plasma, and as a homodimer (factor XIIIA) in the cytosol; its structure has been elucidated[23] by X-ray crystallography. It circulates in the blood as a proenzyme of the blood clotting factor, which is activated by thrombin in the presence of Ca^{2+} in the final steps of blood coagulation. Factor XIII is composed of two A subunits and two B subunits; in the final step of the enzyme's activation, the B subunit and a 37-amino acid peptide from the N-terminal end of the A subunit (83 kDa) dissociate to yield active fXIIIa, in which the active site is accessible. fXIIIa has several known protein substrates, including proteins of the coagulation and fibrinolytic systems, adhesive

proteins, and cytoskeletal proteins; these classes of substrates correlate with the three major functional roles for fXIIIa, namely its involvement in blood coagulation and fibrinolysis, wound healing, and other less well-defined cellular functions.

1.2.9 Erythrocyte membrane protein band 4.2

The amino acid sequence for erythrocyte membrane protein band 4.2 (band 4.2), which has a role in erythrocyte viability, was derived[24] from the full-length cDNA, in turn obtained from a human reticulocyte cDNA library. This protein, which shows no evidence of Ca^{2+}-stimulated TGase activity, has homology with guinea pig liver TGase (32%) and with the A subunit of human FXIII (27%). The greatest degree of homology is observed in a region containing the respective active sites of both enzymes, where the consensus residues of the TGase active site are Gly-Gln-Cys-Trp-Val. However, band 4.2 has an alanine residue in the place of the catalytic cysteine, a substitution which is likely responsible for the lack of transamidative activity.

1.3 Tissue transglutaminase

Tissue transglutaminase (TG2) is the predominant enzyme studied in the Keillor group. Along with TG3, TG5 and TG6, it is a TGase that also acts as a guanine nucleotide-binding protein. Furthermore, a distinguishing characteristic of TG2 is the large conformational change that it undergoes in going from a more compact catalytically-inactive “closed” form to the active “open” form. TG2 is the only TGase to have been crystallised in a form different from the “closed” one, presented in Figure 1.1.

1.3.1 Mechanism

TG2 catalyses[4] the aforementioned isopeptidic bond formation via a modified ping-pong mechanism[25]; in the first part, the active site cysteine thiolate attacks the amide side chain of a glutamine residue, resulting in the formation of a thiolester acyl-enzyme intermediate and the release of ammonia. In the second part, the amine side chain of a lysine residue acts as a nucleophile, resulting in the formation of the isopeptidic bond and the regeneration of the free enzyme. In the absence of a primary amine substrate, water can assume the role of the nucleophile, resulting in the deamidation of the glutamine residue to glutamate, and the regeneration of the free enzyme. However, hydrolysis has been observed to be much slower than aminolysis, and deacylation appears to be rate-limiting over acylation[26]. A more detailed representation of the mechanism is shown below in Scheme 1.2. Beyond the catalytic triad, the mutation of key tryptophan residues W241 and W332 to alanine results in a protein with no detectable activity[7], thus reaffirming the role of these tunnel-lining residues in catalysis. The third amino acid involved in tunnel formation, Thr360, is also involved in the transamidation activity; the T360A mutant displays[7] a marked preference for hydrolysis over aminolysis.

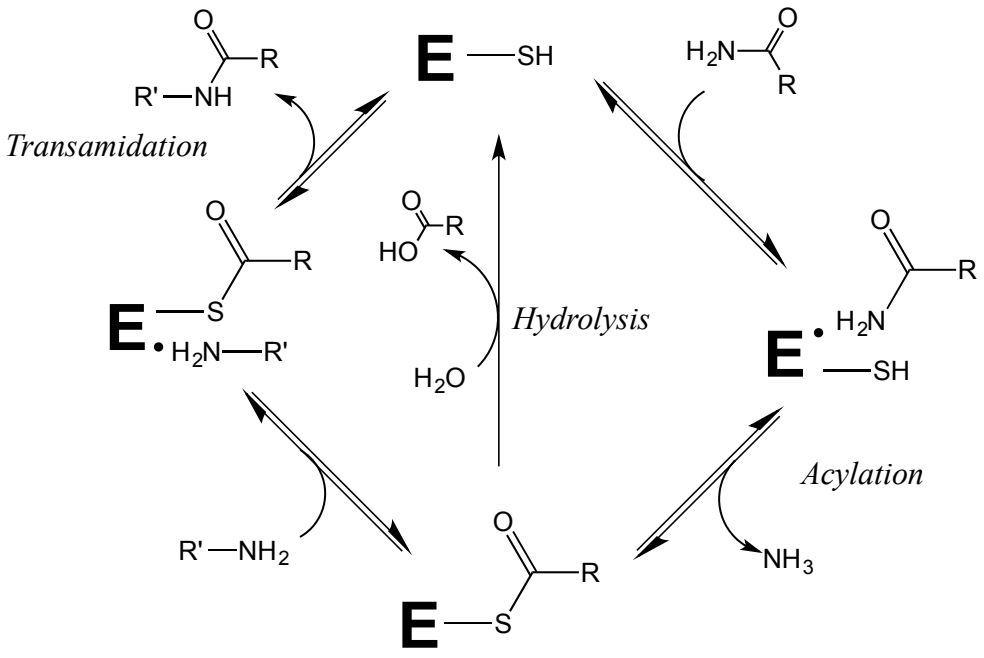

Scheme 1.2. Catalytic cycle for TGases

Reproduced with permission from Keillor *et al.*, Bioorganic Chemistry (2014)[4]

TG2 is relatively selective with respect to the glutamine residues that it will modify, but much less so for lysine or primary amine substrates. An *N*-terminal Cbz protecting group confers affinity[27] for small peptidic (glutamine-donor) substrates; as such, given its simple structure, reasonable affinity and commercial availability, Cbz-Gln-Gly has been the most commonly-used non-protein acyl donor substrate. Overall[4], TG2 has a high affinity for glutamine peptides of the sequence *z*QXP*h*, where *z* is a polar amino acid, X is any amino acid, and *h* is a hydrophobic amino acid.

1.3.2 Allosteric regulation

TG2 is allosterically[28] activated[29] by Ca^{2+}, and deactivated[30] by GTP. In the cytosol, the transamidation activity is likely dormant, due to the low concentration of Ca^{2+} and the high concentration of GTP, and TG2 acts[31] as a classical GTP-binding protein; however, extracellularly, the higher concentration of Ca^{2+} results in an increase in its transamidation activity. TG2 may also be regulated[7, 32] by disulfide bond formation[32] within its tertiary structure, through the residues Cys230, Cys370 and Cys371. The oxidation of Cys230 initiates the cascade of intramolecular disulfide bond formation within the listed residues, resulting in the inactivation of the enzyme. However, this oxidation is also influenced by the presence of Ca^{2+} and substrate, suggesting that there is a fine-tuning of TG2 activation beyond the simplistic view that it is active in the presence of Ca^{2+} and inactive with GTP. In its active form, TG2 binds up to six Ca^{2+} ions; its transamidation activity is decreased or lost when any of the Ca^{2+}-binding sites are mutated[33]. Furthermore, the binding of GTP may be abrogated by point mutations such as arginine mutant R580A, which results[34] in greater sensitivity to the activation by Ca^{2+}. This activation moves the C-terminal β barrels farther apart, into an open form where the active site is accessible. This allosteric regulation is therefore closely associated with the enzyme's conformational change.

1.3.3 Conformational change

Unlike most members of the transglutaminase family, TG2 undergoes a large conformational change, that is regulated[28] by the binding of Ca^{2+} (catalytically active form) and guanosine nucleotides[10] (catalytically inactive). In the closed, catalytically-inactive form, the enzyme assumes a globular, compact conformation, as shown in part A of Figure 1.2 below. This

form shows considerable interaction between the catalytic domain and the two C-terminal β-barrels, thus reducing the accessibility to and the activity of the catalytic site[10]. However, in the open form (part B of Figure 1.2), the active site is solvent-exposed; this conformation was successfully crystallised[7] by using a substrate-mimicking irreversible inhibitor.

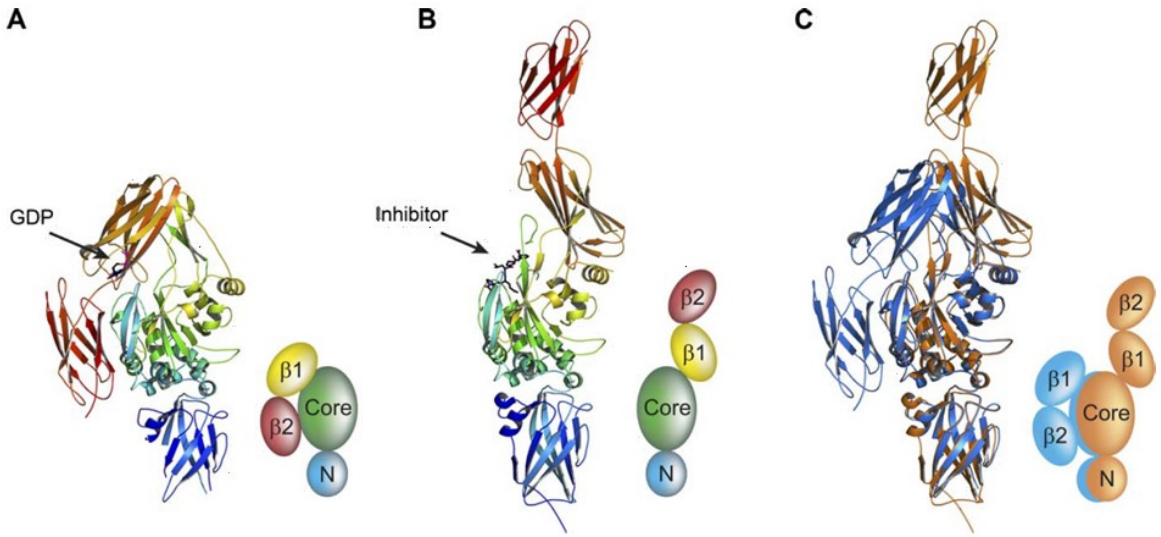

Figure 1.2. Conformations of TG2: A) closed B) open C) overlap of the closed (blue) and open (orange) conformations

Reproduced (open access) from Pinkas *et al*., PloS Biology (2007)[7]

Prior to the availability of crystal structures for TG2, this change in conformation was observed[35] by small-angle X-ray scattering (SAXS) in the form of a considerable increase in the radius of gyration of the activated enzyme in solution. Since then, X-ray crystallography has shown[7-8] that TG2 can adopt at least two dramatically different tertiary structures, as shown in Figure 1.2, that are representative of the large conformational changes related to ligand binding and the regulation of activity. The distance[36] between the termini goes from less than 10 Å in the closed form to approximately 150 Å in the open form; this large conformational change has been

confirmed[7] not to be an artefact of crystallography by measuring the hydrodynamic radii of TG2 in solution. During this conformational change, the C-terminal β-sandwich domains are displaced by approximately 120 Å, while the N-terminal and catalytic domains remain mostly unchanged (part C of Figure 1.2); the conformational regulation of activity is therefore suggested to be due to the occlusion of the substrate binding sites, and not to the perturbation of the catalytic machinery[8]. Furthermore, native polyacrylamide gel electrophoresis (nPAGE) confirms[7, 37] the presence of two conformations in solution, as does kinetic capillary electrophoresis (CE)[38]. The latter experiment showed that the interconversion rates between the open and closed forms are slower than k_{cat}, suggesting that the conformational changes do not occur during the catalytic cycle, but rather as part of the tight functional regulation of TG2. Finally, FRET[36b] (with YFP-hTG2-CFP) and FRET-FLIM[36a] (with CFP-hTG2-YFP) experiments *in cellulo* have confirmed the effect of Ca^{2+} in promoting the open form of the enzyme; FRET was used as a tool since it would only be observed for the closed form of the enzyme, where the termini are in close proximity.

1.3.4 Physiological roles

TG2 has[10] various roles in signalling at the cell surface and in the extracellular matrix; these roles pertain to its varied functions in transamidation, but also as a G-protein, as a non-enzymatic adapter, as a scaffold protein, and as a regulator of signal transduction. TG2 interacts with the extracellular matrix to enhance cell adhesion, by serving as a receptor for fibronectin[39], and also supports integrin-mediated signalling by enhancing the fibronectin-integrin interaction. Its role in matrix assembly[40] relates to the crosslinking and stabilisation of extracellular matrix proteins such as[41] collagen, fibronectin and elastin. In cytoplasmic signalling, TG2 incorporates[10]

amines such as serotonin, histamine, dopamine and norepinephrine in the monoamination of target proteins through its transamidative capacity. However, TG2 has also been observed[42] to promote cell survival through a signalling role associated with its conformation. Beyond signalling, TG2 has been associated with roles ranging from cellular differentiation in neuroblastoma SH-SY5Y cells[43] (where its transamidation capacity is key[10]), astrocytes and fibroblasts[39], to apoptosis, where TG2's function as a G-protein mediates[44] adrenergic signalling, and its crosslinking activity stabilises[44] the integrity of dying cells.

1.3.5 Associated pathologies

1.3.5.1 General

In general[11], the pathogenecity of TG2 seems to be associated with its protein cross-linking and deamidation roles, and less with its behaviour as a G-protein. TG2 has been implicated in various neurodegenerative diseases, such as Alzheimer's disease, where TG2 is associated with the accumulation of fibrillar amyloids in extracellular plaques; these plaques, along with the tau protein, are substrates[45] for the enzyme, whose activity is increased[46] in diseased brains. In Huntington's disease, the cytosolic protein huntingtin is a substrate for TG2[47]; however, huntingtin containing a pathological length of poly-glutamine residues[48] is a superior substrate for TG2 than its shorter, non-diseased counterpart[49]. Recent research has also led to the targeting of the interaction between TG2 and the proteoglycan Sdc-4 as a potential treatment for kidney disease[50]. Furthermore, TG2's role in the stabilisation of the extracellular matrix leads to its role in atherosclerosis[51], possibly through the incorporation of lipoprotein(a) into atherosclerotic plaque[52], as well as in fibrosis. Overall, the greatest potential in disease treatment for TG2 at the moment appears to be centred around fibrosis, cancer and celiac disease, due to

the specific nature of the enzyme's role in their pathologies, but also its concise physiological location.

1.3.5.2 Fibrosis

Recently, TG2 has been postulated as a novel target in pulmonary fibrosis[53], where small electrophilic compounds have been used to inhibit[41] its expression and profibrotic effector functions. In liver fibrosis, where an imbalance in the extracellular matrix processes of production and degradation leads to scarring, TG2 is involved in the increase in production of protein crosslinks; as such, sulfonium inhibitors limited[54] to the extracellular environment have been targeted[55] to the liver by using liposomes to minimise general toxicity and reverse the scarring associated with fibrosis.

1.3.5.3 Cancer

TG2 has also been implicated in cancer, where it is associated with high levels of glycolysis[56], a hallmark of cancer cells, but also with cell migration. In particular, the aberrant expression of this pro-inflammatory protein is associated[57] with the development of drug resistance and metastatic phenotype in multiple cancer types. In accordance with this observation, TG2 expression has been observed to be low in primary tumours, but its activity is increased in drug-resistant and metastatic tumours[10]. TG2 is implicated[58] as a regulator of migration in clonal cell types, where its overexpression may result in the inhibition of or an increase in migration, depending on the cell type, suggesting that it has different roles in a context- and cell-type-specific manner. TG2 has been proposed as a novel therapeutic target in castration-resistant prostate cancer[57], where the level of TG2 expression in prostate cancer cells

has been associated with increased invasion and resistance to chemotherapy. Furthermore, TG2 has been implicated[58] in the migration of astrocytes, where it requires both its transamidation and GTP-binding functions to facilitate astrocyte migration. However, this role may be ablated by a single irreversible inhibitor of its transamidation function.

1.3.5.4 Celiac disease

Celiac disease is an autoimmune disorder caused by an abnormal response to an array of epitopes of wheat gluten and related proteins. Wheat gliadin, in particular, is a preferred substrate[59] for TG2, with up to 36% of its glutamine residues being accessible[60] for TG2-catalysed modification; following deamidation[61] by TG2, the recognition of gliadin by T-cells is enhanced. TG2 is also the autoantigen[62] for antibodies responsible for the immune response: neoepitopes in the TG2-gliadin complex initiate an immune response against both proteins. Today, methods that are based on the detection of TG2 antigen are widely used in the diagnosis of celiac disease[63], and recent results suggest that celiac patient immunoglobulin-A antibodies also modulate the extracellular transamidation function of TG2[64], thus affecting all cell-extracellular matrix interactions.

1.4 Known inhibitors

The range of TG2-associated pathologies demonstrates[65] the need for potent TG2-specific inhibitors. Early work with TG2 used alternative substrates as "inhibitors"; these amine compounds were incorporated into glutamine-containing proteins in lieu of the native amine substrates, thus preventing the formation of the desired crosslinked products *in cellulo*. However,

in this work, we focus on the use of inhibitors in the more traditional sense, namely compounds which prevent the enzyme's native transamidation reaction.

1.4.1 Irreversible inhibitors

We have recently reviewed the field of TG2 inhibitors from both the recent academic literature[11] and the overall patent literature[66]. As such, for the irreversible inhibitors, we will highlight the recent work of two of the more active groups in this field, namely the Khosla and Keillor groups. Using a 3-halo-4,5-dihydroisoxazole group as a reactive electrophilic moiety, the Khosla group developed[67] compound **KCC009** (see Figure 1.3), an irreversible inhibitor (k_{inact}/K_I = 2.00 x 10^3 M^{-1} min^{-1}, k_{inact} = 1.3 min^{-1}, K_I = 0.74 mM) with high specificity for TG2 and effective *in vivo* (mouse model). Further optimisation of this scaffold led[68] to compound **ERW1041E** (k_{inact}/K_I = 16.9 x 10^3 M^{-1} min^{-1}, k_{inact} = 0.110 min^{-1}), which is more efficient and has also been shown to inhibit the activity of TG2 in the small intestine of a mouse[69].

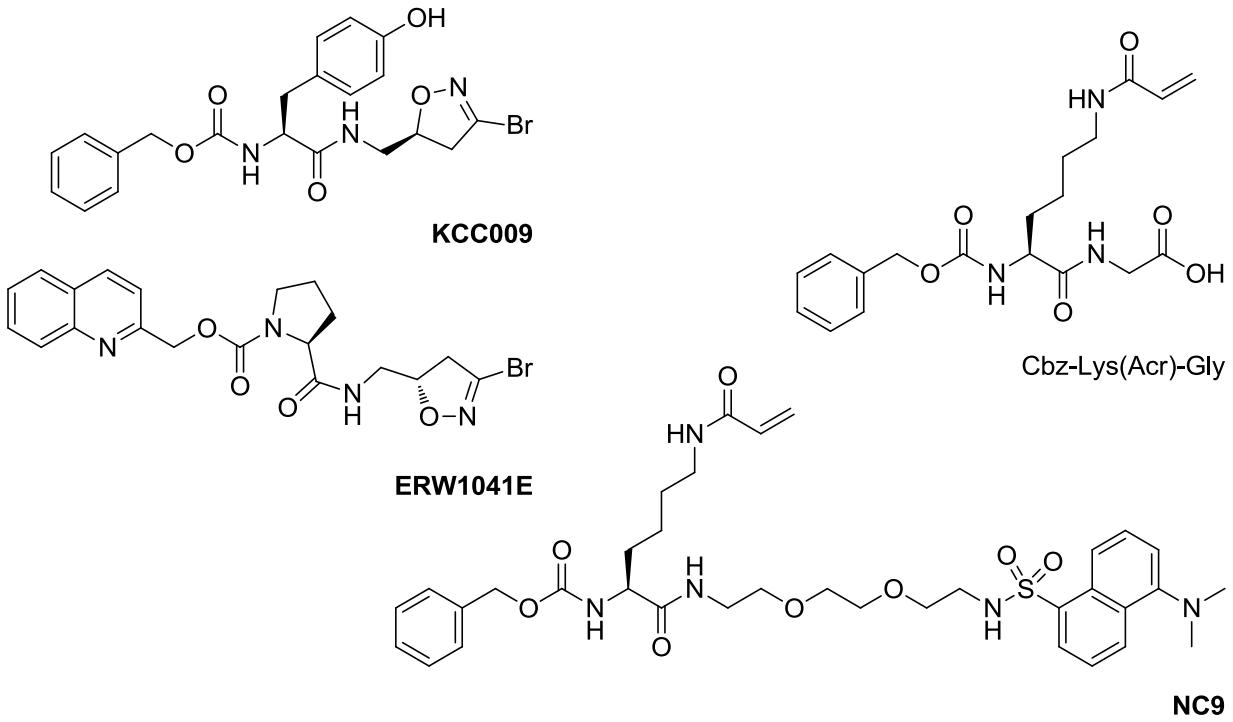

Figure 1.3. Key irreversible TG2 inhibitors from the Khosla and Keillor groups

The Keillor group developed an inhibitor based on the well-known substrate Cbz-Gln-Gly by replacing[70] the glutamine side-chain with an acryloyl group, resulting in Cbz-Lys(Acr)-Gly as their most efficient irreversible inhibitor (k_{inact}/K_I = 3.0 x 10^6 M^{-1} min^{-1}, K_I = 150 nM against guinea pig liver TGase (gplTG), used as a model for TG2). Derivative **NC9** has a lower efficiency[70] (k_{inact}/K_I = 1.4 x 10^4 M^{-1} min^{-1}, K_I = 29 μM against gplTG) but its fluorescent dansyl group allows its use as a probe[71] in cellular studies for TG2 localisation.

Recently, Zedira GmbH have brought an irreversible inhibitor to phase I clinical trials[72] for the dampening of the immune response to gluten in celiac patients. Compound **ZED1227** (Figure 1.4) is the first direct-acting transglutaminase blocker to reach clinical trials.

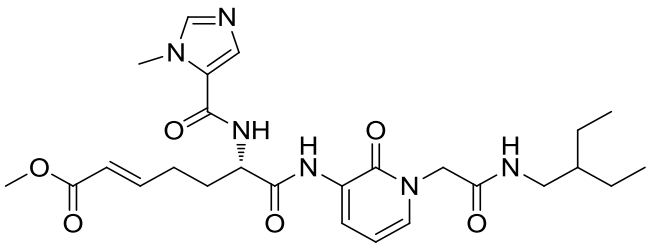

Figure 1.4. Compound **ZED1227**, the first TGase inhibitor to reach clinical trials

1.4.2 Reversible inhibitors

Non-hydrolysable GTP analogues, such as GTPγS (guanosine 5′-*O*-(3-thiotriphosphate)) and GMP-PCP (guanosine 5′-[(β,γ)-methyleno]triphosphate), have also been used[30] as TGase inhibitors, likely as mimics of the negative regulator GTP, which promotes the closed, catalytically-inactive form of the enzyme. While various inhibitors have been reported in recent years, we will focus on those that have been kinetically characterised with respect to the enzyme. The first reported reversible[73] (allosteric) inhibitors were published[74] by Duval *et al*. in 2005, as a series of thieno[2,3-*d*]pyrimidin-4-one acylhydrazides, where compound **1.1** (Figure 1.5) was the most potent, with an IC_{50} value between 0.25 and 0.8 μM depending on the assay used. Continuation of this work by Case and Stein led to inhibitor **LDN-27219**, published[75] in 2007, where one phenyl group has been replaced by a smaller methyl unit. This compound was determined to be an allosteric inhibitor, which was non-competitive with respect to both substrates (acyl donor and acyl acceptor) and mutually exclusive with GTP binding. Follow-up work has shown[76] that these compounds do not compete with a GTP probe, suggesting an allosteric modulation of GTP binding as well. These compounds are also better inhibitors of TG3 than TG2, and no other novel small molecule analogues of **1.1** were observed to inhibit TG2.

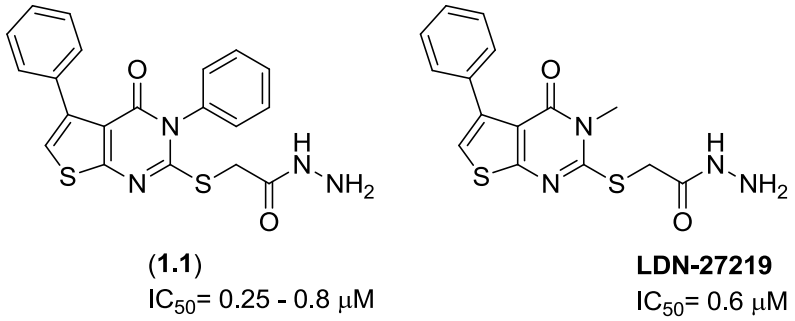

Figure 1.5. First published reversible (allosteric) TG2 inhibitors

These initial inhibitors were followed by work done primarily by the Keillor and Khosla groups in the area of reversible inhibitors. The Khosla group optimised[77] an isatin scaffold (Figure 1.6), starting from a first hit with acylidene oxoindole **10** (IC_{50} = 1.5 μM, K_i = 0.7 μM) and culminating in compound **41**, which is also competitive with respect to the acyl donor substrate and has a K_i value of 0.25 μM.

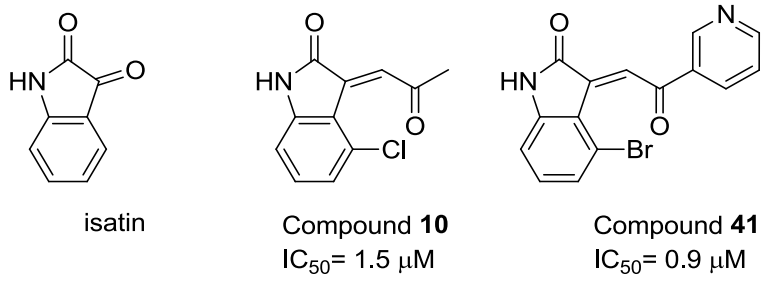

Figure 1.6. Reversible inhibitor isatin scaffold optimised by the Khosla group

The Keillor group focused on a *trans*-cinnamoyl scaffold, where the core represented a mimic[78] of the Cbz protecting group, observed[79] in peptidic substrates to confer improved affinity to the enzyme. Among the scaffolds evaluated (Figure 1.7) were cinnamoyl

benzotriazoles[78] (**CP15n**), azachalcones[78] (**CP30a**), and cinnamoyl triazoles[80] (**CP4d**), with the most potent inhibitor of each family indicated in brackets and reproduced below in Figure 1.7. Inhibitor **CP4d** was the most potent as of 2012, when the research presented in this thesis was begun, with a K_i of 1.0 μM with human TG2[81]. Furthermore, as a competitive, reversible and selective inhibitor, **CP4d** has been observed to favour the closed form of the enzyme, as determined by a FRET experiment[36a] in ST*Hdh*$^{Q7/Q7}$ cells.

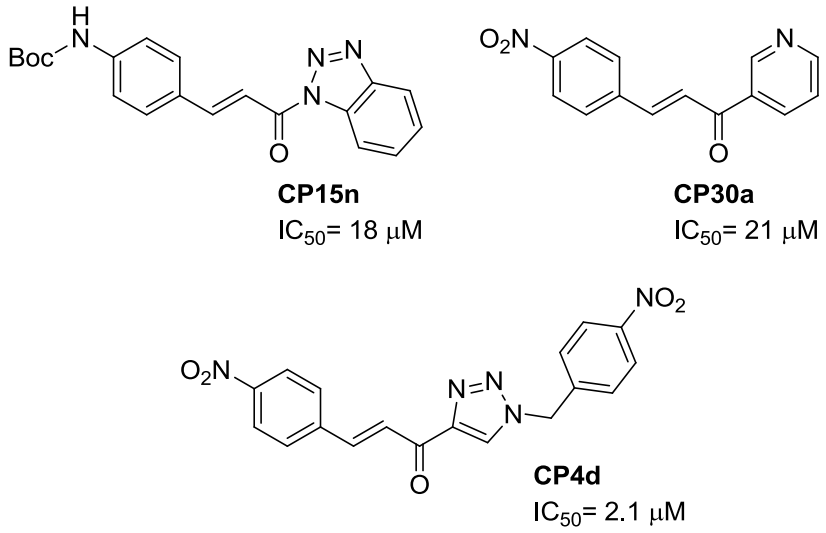

Figure 1.7. Reversible inhibitor cinnamoyl scaffold optimised by the Keillor group

1.4.3 Inhibitor binding locations

Initially, TG2 was crystallised[8] in its closed, inactive form, as were other related TGases, such as fXIII[23], red sea bream TGase[82], and TG3[13]. However, in each of these structures, the active site cysteine was occluded; the Khosla group was the first to solve[7] the crystal structure for TG2 in its open, active form, using Ac-P(DON)LPF-NH_2, a pentapeptide with an electrophilic 6-diazo-5-oxo-L-norleucine (DON) residue (see compound **1.2** in Figure 1.8

below). The stabilisation of the catalytically active form was rendered possible by using this irreversible inhibitor **1.2**, which "locked" the enzyme in its open conformation. From this crystal structure, it was possible to see that the active site cysteine is at the end of a tunnel that is bridged by two tryptophan residues, Trp241 and Trp332, and to visualise the protein-inhibitor complex to help guide subsequent inhibitor optimisation. Studies of **NC9** with TG2 by CE have also shown[38] that this irreversible inhibitor locks the enzyme in its open conformation; in general[4], it appears that any ligand that is irreversibly-bound in the acyl-donor substrate binding site and presents sufficient steric bulk can disfavour the closed conformation.

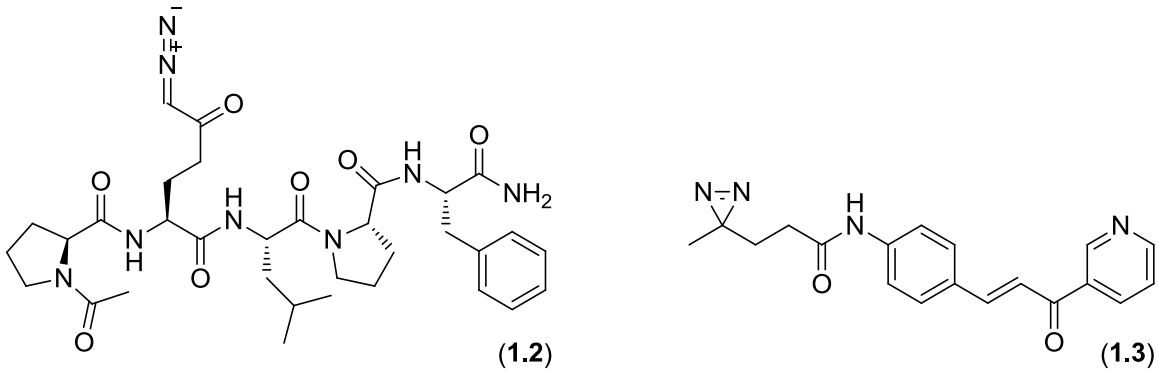

Figure 1.8. Covalent inhibitors used to probe their binding to TG2

In a different approach, the Keillor group prepared a photolabile derivative (compound **1.3**, Figure 1.8) of an azachalcone inhibitor to determine[37] its binding location on gplTG. Guinea pig liver TGase shares significant sequence homology with several TGases from the vertebrate family, including human TG2 (hTG2). As one of the most thoroughly characterised TGases, gplTG was a common choice for inhibition studies, and obtained[26] by isolation from guinea pig livers in good yield and activity. By LC-MS/MS analysis of the photolabelled protein, Cys230, a

residue at the entrance of the tunnel leading to the active site, was identified as the labelling site. Furthermore, nPAGE experiments showed that the photolabile inhibitor interacted with the open form of the enzyme. However, despite the high degree of sequence homology between gplTG and hTG2 (90%), the application of hTG2 models to gplTG gave inconclusive results with respect to the form to which the inhibitor would bind in hTG2.

1.5 Goal of the research presented herein

The primary aim of the research presented herein was to gain more knowledge of the reversible inhibitors of hTG2 (abbreviated simply as TG2 hereafter), by probing their binding location and/or by optimising their stability and potency. Most of the work was done starting from the lead reversible inhibitor **CP4d**, where the cinnamoyl extremity is designated as the West end, while the triazole end is called the East end. Overall, the research presented may be grouped into three categories, as described in greater detail below.

1.5.1 Photolabelling

Following the photolabelling work described above concerning inhibitor binding modes, we aimed to determine the binding location of our lead reversible inhibitor, **CP4d**. To do so, we prepared a photolabile derivative of the inhibitor that could covalently bind to TG2 (Chapter 3). In order to facilitate the subsequent analysis by LC-MS/MS, we also expressed and purified a "heavy" isotopically-labelled form of TG2, which incorporated $^{13}C_6$,$^{15}N_4$-arginine and $^{13}C_6$,$^{15}N_2$-lysine (Chapter 2).

1.5.2 Glutathione resistance

In the optimisation of the reversible inhibitors, we continued previous work[81] begun on the development of compounds with reduced electrophilicity in order to prevent the formation of adducts with intracellular nucleophiles such as glutathione. In particular, most of the key inhibitors (Figure 1.6) feature an α,β-unsaturated carbonyl moiety, commonly referred to as a Michael acceptor, which may result in the formation of adducts *in vivo*. Over the course of this work, we developed a simple ^{1}H NMR assay to estimate the susceptibility of key compounds to glutathione addition, and evaluated a novel family of bis(triazole) compounds as TG2 inhibitors (Chapter 4).

1.5.3 Exploration of the alkynyl scaffold for reversible inhibitors

Following on the work done in the development of glutathione-resistant inhibitors, a sub-category of alkynyl derivatives was developed further. While the initial alkynyl compounds prepared displayed equal susceptibility to glutathione addition, they also exhibited significantly enhanced inhibitory potency against TG2. In this respect, and continuing in the vein of trying to replace the nitro group in our compounds while maintaining their inhibitory potency, we prepared a small library of compounds in order to probe the characteristics of the substituents at the West end of the alkynyl derivative of the cinnamoyl scaffold (Chapter 5).

Chapter Two: **Isotopically-labelled TG2**

2.1 Isotopically-labelled proteins

Isotopically-labelled proteins have applications in the study of either a protein itself, or its interaction with a ligand. Within the Keillor group, our interest lies in the second case, namely the covalent modification of TG2 with various small molecules, either irreversible inhibitors or photolabile derivatives of reversible ones. The two main tools used to analyse isotopically-labelled proteins are NMR and mass spectrometry, depending on the type of labelling chosen.

In protein NMR, various nuclei may be replaced by their NMR-relevant isotopes, either ^{2}H, for smaller proteins, or, more commonly, ^{13}C and ^{15}N. The use of the latter two (NMR-visible) isotopes results in a greater peak separation on the spectrum, when compared to ^{1}H NMR, since the range of chemical shifts spans approximately 200 ppm instead of ~12 ppm. Conversely, the use of deuterium, which is NMR-invisible, increases the sharpness of ^{13}C and ^{15}N peaks by reducing their relaxation times and increasing the amount of magnetisation transferred[83]. In these experiments, all nuclei of the atom chosen for spectroscopic analysis are replaced by their chosen isotope, whether they are a part of the protein backbone or its side chains. To do so, proteins are expressed (or synthesized) in a minimal medium containing any combination of D_2O, $^{13}C_6$-glucose and $^{15}NH_4Cl$ as the sole sources of deuterium, carbon and nitrogen, respectively, to incorporate these labels exclusively into the protein.

In mass spectrometry (MS) experiments, the most commonly used in proteomics, so-called "heavy" proteins (incorporating ^{13}C- and ^{15}N-labelled, "heavy" amino acids) are used as an internal standard for the quantification of peptides. The "light" proteins (constituted with the standard amino acids) and "heavy" proteins are treated in a similar manner, including protease digestion, to ensure that a direct comparison may be made. Peptidic digests of both "light" and

"heavy" protein samples behave in the same manner by liquid chromatography (LC), thus resulting in their co-elution. The intensity of the MS peak corresponding to the "heavy" peptide can be used as an internal standard to which the intensity of the variable "light" peptide may be compared, since both peptides have the same ionisation characteristics. This approach is most often applied to the study of the variation in protein quantities in proteomics, following treatment of the "light" protein, but it may also be used in the analysis of tryptic digests of covalently-labelled proteins. In all cases, the perturbed system corresponds to the "light" experiment, while the "heavy" protein is used as a reference.

2.2 Overview of general SILAC experiments

Stable Isotopic Labelling of Amino acids in Cell culture (SILAC) is generally applied in metabolic proteomics studies, where two cell populations are grown in identical media, except that one incorporates the "heavy" version of the selected amino acids. In this manner, both the studied (perturbed) "light" cells and the reference "heavy" ones undergo the same treatment except for the perturbation, the effect of which is the aspect being studied. This concept is illustrated in a graphical manner in Figure 2.1 below, where the graph on the left is indicative of proteins unaffected by the perturbation, as evidenced by the equal ratio between the MS peaks from proteins in the perturbed population and those in the unperturbed, reference population. Conversely, in the graph on the right, the lower peak of the "light" protein suggests that the perturbation resulted in a lower amount of that protein than what was observed in the reference population.

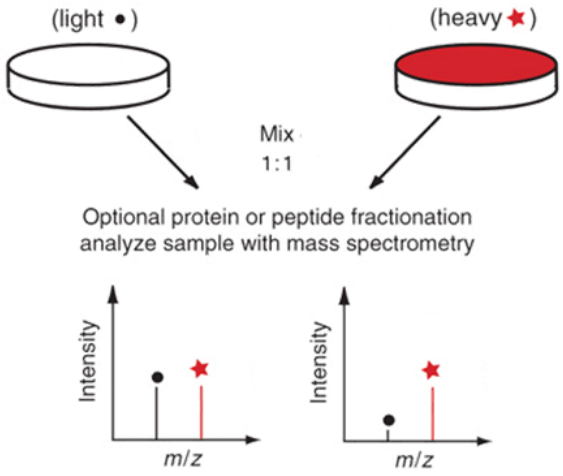

Figure 2.1. Schematic representation of a SILAC experiment, adapted from "A practical recipe for stable isotope labeling by amino acids in cell culture (SILAC)"[84]

This standard SILAC approach has been used successfully to identify contaminants in a study[85] of the role of various organelles in the formation of phagosomes. In order to determine whether isolated proteins were from true phagosome formation or simply carried over as contaminants through the method used to recover the studied phagosomes, a SILAC study was undertaken. Cells were grown in either a regular "light" medium, or a medium containing "heavy" $^{13}C_6$,$^{15}N_4$-arginine and $^{13}C_6$,$^{15}N_2$-lysine, abbreviated as ArgΔ10 and LysΔ8, respectively, to indicate their mass shift in daltons from the light isotopes. The cells in the "heavy" medium were allowed to grow normally, while those in the "light" medium were supplemented with a reagent to induce phagosome formation. After combining the "light" and "heavy" cells in a 1:1 ratio (by cell count), the phagosomes were isolated in the usual manner prior to analysis of their proteome following digestion with trypsin, a protease that cleaves the peptide backbone on the C-terminal end of arginine and lysine residues (hence their selection as "heavy" amino acids for

incorporation). In the case of contaminants, a 1:1 ratio of "light" to "heavy" peptide fragments would be expected, since they would be obtained regardless of the induction of phagosome formation. However, since phagosome formation was only induced for the cells grown in "light" medium, a much higher ratio would be expected for proteins truly part of the phagosomes, because they would be obtained in a larger quantity from the experiment from cells grown in "light" medium. This experiment successfully identified the organelles involved in phagosome formation.

2.3 Application to TG2

Given the size of TG2, as well as previous experience within the Keillor group in using[37, 81] MS experiments to detect labelling events on the protein, we opted for an analysis of ligand binding through an approach similar to SILAC, but working only with isolated, purified protein, instead of whole cells. We therefore designed an experiment to label "light" TG2, and use "heavy" TG2 as a reference for later LC-MS analysis. The choice of the "heavy" amino acids to incorporate was based on the selectivity of the protease used for protein digestion, prior to analysis. The most commonly-used protease is trypsin, as demonstrated in the example above; we therefore opted to label our protein with ArgΔ10 and LysΔ8 as well. In this manner, each peptidic digest would end in either arginine or lysine; in a sample containing both regular and "heavy" protein, in a 1:1 molar ratio, each LC-MS spectrum would show one peak on the LC chromatograph, but two equal peaks in its mass spectrum, separated by the difference in mass for the "heavy" amino acid. This result would be expected for all peptides except those having been covalently labelled; in those cases, we would expect to see a lower intensity peak for the "light" peptide when compared to the "heavy" one, such as is illustrated in the right-hand-side graph in

Figure 2.1. This difference in peak intensities would be an indicator that the particular peptide had been labelled, and would also indicate that a different LC fraction would require analysis, one with only one MS peak, corresponding to the sum of the masses of the peptide and of the label.

2.4 Preparation of the isotopically-labelled enzyme

2.4.1 Methods to obtain isotopically-labelled proteins

There exist two main methods to prepare isotopically-labelled proteins; one is to use whole cells grown in culture, and the second is to express in a cell-free manner, by providing all of the enzymatic machinery required for protein expression, often obtained from a cell lysate. Generally, whole cells in culture are better for preparing large-scale recombinant proteins, while cell-free expression is done on a smaller scale, for various reasons including the expression of proteins that may be toxic to the host, the use of unnatural amino acids[86], post-translational modifications, or to study the components required for protein folding and stability.

In practice, cell-free protein expression is most often used in the literature to prepare protein for NMR, by ubiquitously incorporating NMR-active nuclei. However, in a few cases, it has also been used to prepare isotopically-labelled proteins, such as in the incorporation of selenomethionine, ArgΔ10, and LysΔ6 ($^{13}C_6$-lysine) for absolute protein quantification[87]; this method is still used much more rarely than whole cells grown in culture in the context of the incorporation of isotopically-labelled amino acids. Given the prevalence of the use of whole cells for purposes similar to ours, and that our standard manner of expressing TG2 is in whole *E. coli* cells in culture, we chose to continue in this approach. In particular, a SILAC medium optimised

for expressions in *E. coli* cells (SILACE) has been published[88]; this approach was applied in that same study to express GST-4DSK2 labelled with LysΔ6.

2.4.2 Optimisation of a protocol for the expression and purification of ArgΔ10-LysΔ8 TG2

Starting from this SILACE medium, we optimised the expression conditions for our target protein, knowing that the yields of hTG2 in TB, a rich medium, are already low, at 3 mg per litre of culture[89]; for comparison, gplTG was obtained in much higher amounts, at 22 mg per litre of culture[90]. The SILACE complex medium contains most of the amino acids, including arginine and lysine, thus enabling an easy replacement of those particular two amino acids by their "heavy" counterparts, without affecting any of the other residues in the protein.

The Keillor group has published[89] a protocol for the expression of GST-PSP-hTG2, a glutathione S-transferase (GST) fusion protein with a PreScission™ Protease (PSP) cleavage site, which is used for the expression and purification of hTG2 from *E. coli*. This protocol has been optimised for cell culture in TB; in comparison, SILACE is a complex medium with 29 components, including 12 of the standard 20 amino acids.

The expression of TG2 was therefore optimised with this medium. In particular, while most proteins expressed under control of the lac operon use isopropyl-β-D-thiogalactoside (IPTG) as a stable inducer, including the GST-4DSK2 example[88] above, the expression of TG2 in TB normally relies on the "leaky" nature of the promoter, thus expressing constant low levels of the protein. The T7 RNA polymerase is so active that a basal level of expression can lead to a substantial expression of the target protein in the absence of inducer[91]; while this characteristic represents a problem in some cases, we take advantage of this quality in the expression of TG2. In particular, this slower expression of TG2 has been associated with a higher concentration of

correctly-folded protein[89]. Our optimisation of the expression conditions was therefore centred on the concentration of IPTG used for induction.

2.4.2.1 Induction of expression

The SILACE medium normally uses glucose (10 g) as a general carbon food source, and IPTG (1 mM) for the induction of the protein expression. As a first attempt, we tried to express TG2 without IPTG, thus replicating the standard conditions in TB medium. However, SILACE is a not as rich a medium as TB and, perhaps unsurprisingly, we obtained no protein under these conditions. We therefore increased the concentration of IPTG until we obtained TG2 in the soluble fraction. The results, listed by increasing concentration of IPTG, are grouped in Table 2.1, where the columns "lysate", "insoluble fraction" and "TG2 (gel)" refer to the appearance of the TG2 band after SDS-PAGE staining with Coomassie blue, and the final "TG2 yield" column refers to the mass of enzyme obtained (as determined by a Bradford assay) and its activity (as determined by our standard **AL5** assay[26]), presented as an average of two experiments. For comparison, the first entry represents a standard expression in TB medium.

Table 2.1. Optimisation of the concentration of IPTG used for induction in SILACE medium

[IPTG] (μM)	**Lysate**	**Insoluble fraction**	**TG2 (gel)**	**TG2 yield**
0 – TB standard	Overexpressed	Faint	Strong	2.4 mg (0.78 mg/mL) 0.33 U/mg
0	Too dilute	Not run	Nothing	Nothing
1	Too dilute	Faint	Nothing	Nothing
2	Faint	Faint	Faint, multiple bands	0.45 mg (0.16 mg/mL) 0.01 U/mg
20	Faint	Faint	Faint, multiple bands	0.26 mg (0.10 mg/mL) 0.04 U/mg
1 000	Faint	Overexpressed	Nothing	Nothing

Overall, while concentrations of both 2 μM and 20 μM IPTG resulted in the expression of soluble TG2, the protein obtained at 20 μM was consistently purer than that obtained with 2 μM, as observed by fewer bands being present by SDS-PAGE, but also by its relative activity. While the mass quantity of protein obtained at 2 μM IPTG was 70% higher than at 20 μM, the latter concentration of IPTG resulted in a more active protein, suggesting a greater amount of TG2 and

fewer impurities in the overall protein fraction, when taken in conjunction with the SDS-PAGE results.

Since we found no concentration of IPTG that resulted in pure TG2, we tried the glucose and lactose combination from the rich auto-induction ZYP-5052 medium[91], at both half (1.25 g total) and double (5 g total) the standard amounts of sugar, which brought the total mass of sugar to still only half of the 10 g prescribed for SILACE. However, higher concentrations of lactose are known[91] to reduce cell viability and result in the loss of the expression plasmid when used in the ZYP medium. Since neither amount of sugars yielded any TG2 in the soluble fraction, and only resulted in a faint band in the lysate by SDS-PAGE, we re-focused our efforts on induction with the constant inducer, IPTG.

2.4.2.2 Buffer modifications

Working from the knowledge that a concentration of 20 μM IPTG in SILACE resulted in the cleanest TG2 with hydrolytic activity, we modified the phosphate buffer used in the medium. While SILACE requires 47.8 mM Na_2HPO_4 and 22.0 mM KH_2PO_4, resulting in a pH of 7.5, TB uses potassium as the counterion for both phosphate salts, in concentrations of 72.0 mM K_2HPO_4 and 17.0 mM KH_2PO_4, for a slightly higher pH of 7.8. Since no concentrations were tested between 20 and 1000 μM IPTG, we also tried 100 μM IPTG, to determine whether an intermediate concentration of inducer would result in higher yields of soluble protein.

Table 2.2. Optimisation of the concentration of IPTG in SILACE medium with the TB buffer

Concentration of IPTG (μM)	**Lysate**	**Insoluble fraction**	**TG2 (gel)**	**TG2 (quantity)**
20	Faint	Too concentrated	Faint, impurity from PSP	0.08 mg (0.08 mg/mL) 0.24 U/mg
100	Faint	Too concentrated	Nothing	Nothing

Since the higher concentration of IPTG resulted in the absence of protein, we repeated the experiment with 20 μM IPTG on a full 1-litre scale, using the same stocks of buffers, resin, and PSP as would be used in the "heavy" experiment, to maximise reproducibility between this control experiment and the one to be done with the isotopically-labelled amino acids. TG2 was obtained at a concentration of 0.30 mg/mL and a specific activity of 0.13 U/mg in a total of 0.45 mg; while this activity is lower than what had been observed on the attempt recorded in Table 2.2, the protein was obtained in significantly higher yield. This increase in yield, compared to the smaller scale experiments used to generate the data in the tables (500-mL cultures), may be due to a lesser loss in transfer on the larger scale. The quantity is also in agreement with the amount of protein obtained at the same concentration of IPTG (20 μM) in the unmodified SILACE medium. The goal of this experiment was to have TG2 for MS analysis, and as such, activity was deemed to be of lesser importance than the amount of protein, since 50 μg would be required per series of MS experiments.

2.4.3 Final medium recipe and expression and purification of ArgΔ10-LysΔ8 TG2

Overall, only two modifications were made to the SILACE expression protocol; the medium buffer was prepared using a pair of potassium phosphate salts, in a total concentration of phosphate of 89 mM at pH 7.8, and expression was induced with 20 μM IPTG instead of the standard 1 mM. These conditions resulted in a workable yield of TG2 for future experiments, in a reproducible manner. Isotopically-labelled ArgΔ10 and LysΔ8 were purchased from Silantes and used in place of the corresponding "light" amino acids in the SILACE medium. Following the optimised protocol, ArgΔ10-LysΔ8 TG2 was obtained in a final amount of 0.15 mg (Bradford assay) and an activity of 0.13 U/mg (**AL5** assay), consistent with the numbers obtained previously. Purity was established by Coomassie-stained SDS-PAGE, shown below in Figure 2.2; the minor impurity was established to be PSP, and was determined not to be an issue for later MS experiments.

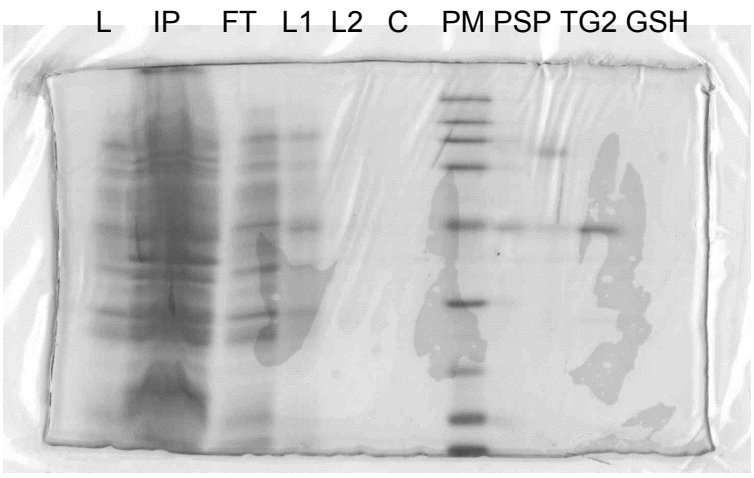

Figure 2.2. SDS-PAGE of the various fractions from the expression and purification of ArgΔ10-LysΔ8 TG2

Legend: L (total lysate), IP (insoluble protein fraction), FT (flow-through from the column), L1 (wash with lysis buffer and 0.5% Triton X-100), L2 (wash with lysis buffer), C (wash with cleavage buffer), PM (Bio-Rad Broad range protein marker), PSP (elution from the initial addition of PSP), TG2 (purified protein), GSH (elution from the resin wash with cleavage buffer with 10 mM GSH).

2.5 Perspectives

Overall, while the **AL5** activity assay and the SDS-PAGE results suggest that we successfully obtained TG2, it would be ideal to verify the total mass of the protein in order to confirm the incorporation of the isotopically-labelled amino acids ArgΔ10 and LysΔ8, an experiment which was not carried out by our collaborator at the Université de Montréal. In a practical sense, given the low quantities of protein required for analysis, the current protocol is

sufficient for our requirements. In the future, should this type of experiment become more common, it may be necessary to further optimise the expression protocol, perhaps by modifying the temperature of expression in order to increase the yield of protein.

Chapter Three: **Synthesis and evaluation of a photolabile inhibitor**

3.1 Methods to identify binding modes for ligands

Two types of methods exist to identify the binding modes for ligands and proteins. Some are theoretical, or computational; molecular docking allows for the prediction of possible binding modes, but the results depend heavily on the chosen parameters for the *in silico* experiment. Conversely, experimental methods rely, as the name suggests, on experiments, sometimes requiring modifications to the ligands or proteins in order to provide results. These types of methods include crystallography, NMR, and photolabelling.

3.1.1 Computational methods

As mentioned above, the main computational method to study protein-ligand interactions is molecular docking. While this method takes into account several factors, such as charged states and steric clashes, the obtained results are theoretical, and remain hypothetical until proven experimentally. As such, computational methods are used in the Keillor group as tools to help design inhibitors and understand the effect of various substitutions on the compounds. They are also used to generate binding models that can be compared against the kinetic results obtained.

3.1.2 Experimental methods

Various experimental methods are used to study the interactions of proteins with their ligands. One of the more commonly-used techniques is X-ray crystallography, where the ligand is either co-crystallised with the protein, or soaked into a protein crystal. The former method was used successfully by the Khosla group at Stanford University to obtain[7] the first crystal structure of the open form of TG2, using a irreversible inhibitor that stabilised the open form over the

previously elucidated structure of the closed form (Sections 1.3.3 and 1.4.3). However, this method only offers a static view of the protein-ligand complex, namely the most stable crystalline form, and the conformational flexibility of TG2 makes it difficult to crystallise in native conditions. There is also the risk of cracking a crystal during the post-crystallisation addition of the ligand.

Another method used to study ligand-protein interactions is protein NMR, which allows for the study of the protein in solution. For proteins smaller than 15 kDa, ^{1}H NMR spectra can be sufficient; however, for larger ones, it may be necessary to use correlation data with additional nuclei, such as ^{13}C and ^{15}N, in order to have a greater separation of peaks, since most of the protons will have overlapping signals in the same region of the spectrum. As described in Chapter 2, the incorporation of these NMR-visible nuclei requires the expression of the protein in minimal medium with $^{13}C_6$-glucose and $^{15}NH_4Cl$ as the sole sources of carbon and nitrogen, respectively, to ensure that the protein contains the desired labels. With those techniques, the generally accepted protein size limit is 35 kDa, which is half the size of TG2 (77 kDa). While more advanced molecular biology techniques, such as protein splicing and modular expression, combined with advances in spectroscopy[92] have led to the analysis of proteins up to 1.1 MDa in size[93], this kind of experiment in the context of ligand binding would first require the analysis of TG2 in that experiment, and then the analysis of the protein-inhibitor complex.

Photolabelling is a technique that allows for the formation of a covalent bond between a ligand and a protein, following irradiation at a given wavelength (dependent on the selected photolabile group). However, the ligand must be modified in order to incorporate a photolabile moiety, without affecting its binding to the target and while still being proximal to the binding site in order to yield results of interest. Previous work done within the Keillor group using a

diazirine-derivatised version of inhibitor **CP30a** led to the identification[37] of the binding site of the inhibitor, but with gplTG (Section 1.4.3). Continuing in the same vein, after developing a protocol for the expression and purification of isotopically-labelled hTG2 (Chapter 2), we focused on the identification of the binding site of reversible inhibitors with hTG2, using photolabelling as the method of choice.

3.2 Identification of binding modes for reversible inhibitors

Based on molecular docking results obtained by Dr. Christopher M. Clouthier, it appears that **CP4d** could bind to both the open and closed forms of the enzyme. These results correlate well with the determination that **CP4d** is a competitive inhibitor of TG2 (in its active, open form), but also that it demonstrates slow binding behaviour to the closed form of the enzyme (C.M.C., *unpublished results*). This dual type of inhibition is demonstrated in Scheme 3.1 below. By binding to the closed form of the enzyme, **CP4d** effectively removes a portion of the closed enzyme from the available pool of enzyme with no ligand bound, thus shifting the equilibrium towards the closed form, according to Le Châtelier's principle. It may also result in the closing of the enzyme, as shown by the K_{eq2} relationship.

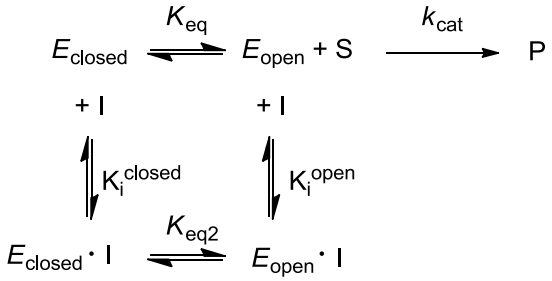

Scheme 3.1. Kinetic scheme demonstrating the possible mode of inhibition by **CP4d**

Indeed, experiments in capillary electrophoresis (Dr. Christopher M. Clouthier, *unpublished data*) have demonstrated that **CP4d** shifts the conformational equilibrium towards the closed (catalytically inactive) form. These two putative binding positions are shown below in Figure 3.1.

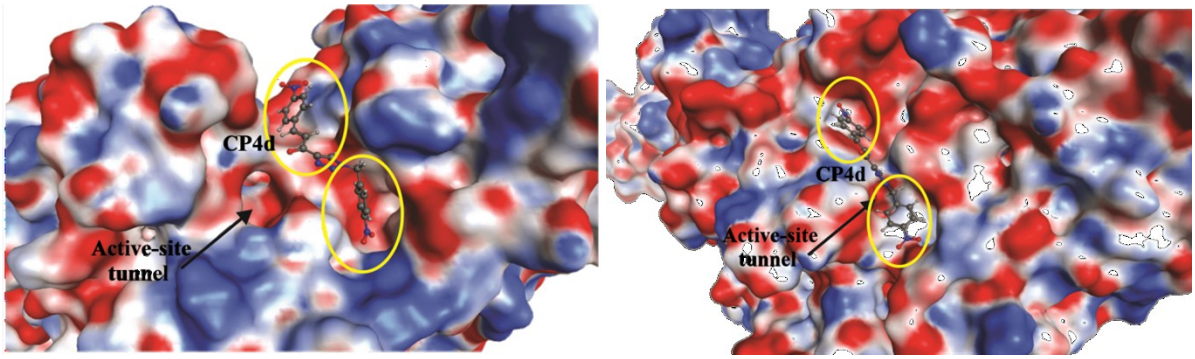

Figure 3.1. Docking results of **CP4d** in both the (left) open and (right) closed forms of TG2

In order to study the binding interactions between **CP4d** and TG2, we sought to design and prepare a photolabile derivative of the inhibitor, which we could then use to photolabel the enzyme to experimentally determine the binding sites.

3.3 Development of a photolabile inhibitor

3.3.1 Potential photolabile moieties

The most commonly used photolabile groups are[94] benzophenone, phenyl azide, and aryldiazirine. These are shown in Scheme 3.2 with their respective major photolysis products, namely a triplet diradical, a nitrene, and a singlet carbene. Each of these groups has different

characteristics that were considered prior to selecting one for the photoaffinity labelling study of inhibitor **CP4d**.

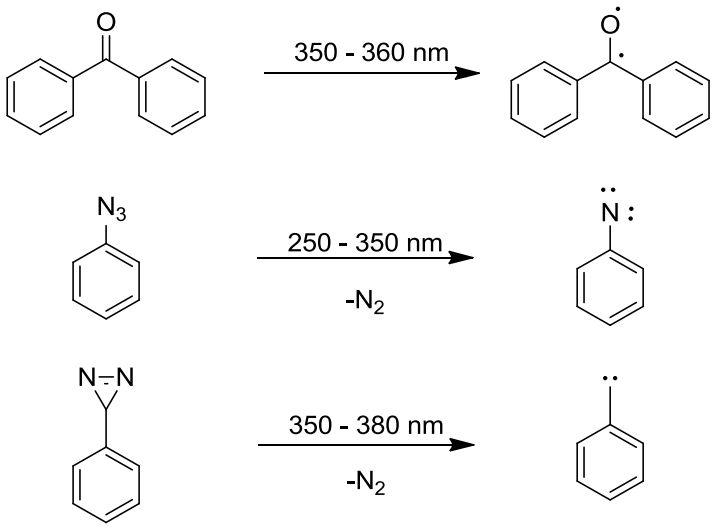

Scheme 3.2. Most commonly-used photolabile groups and their photolysis products

3.3.1.1 Benzophenone

Benzophenone is a useful photolabelling group due to its inertness to solvent and to its easy preparation. Its diradical is generated at longer UV wavelengths, which reduces the potential damage to biomolecules. Excess absorption of UV light by proteins leads to electronically-excited molecules that can then undergo degradative chemical transformations; in this respect, a longer wavelength is therefore desirable. However, benzophenone also requires longer irradiation times than other photolabile groups, thus increasing the amount of non-specific labelling. Due to its larger size, benzophenone also has the potential to affect binding through sterics and through its highly hydrophobic character.

For example, benzophenone has successfully been used[95] to identify the target proteins of the antitumour drug tamoxifen. This photolabile moiety was incorporated into a ligand similar to *N*,*N*-diethyl-2-[4-(phenylmethyl)phenoxy]ethanamine HCl (DPPE), a compound that competes with tamoxifen for the antiestrogen binding site. The resulting photolabel is shown in Figure 3.2, next to the parent DPPE ligand. The tritium labels were added as reporters in order to identify the labelled proteins, namely subunits of the antiestrogen binding sites, by radioactivity.

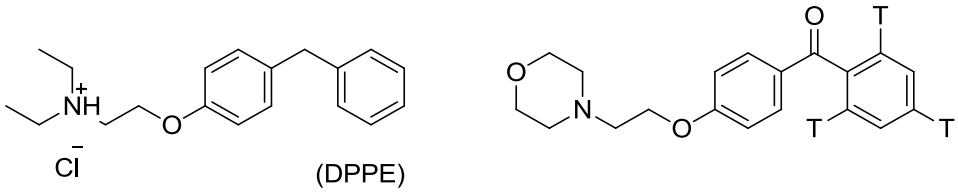

Figure 3.2. Parent DPPE (left) and the corresponding benzophenone photolabel (right) used to label antiestrogen binding site subunits

3.3.1.2 Phenylazide

Similarly to benzophenone, phenylazides are easy to work with due to their commercial availability and ease of synthesis. However, they may also be reduced to amines by nucleophilic thiols at physiological pH[96], although this reaction is more prevalent in alkaline solutions[94]. They require irradiation at shorter wavelength UV light than other photolabile groups, which may result in greater damage to biomolecules, and the resulting nitrene is less reactive than carbenes. This product nitrene is also known to undergo rearrangements to form more stable benzazirines and ketenimines, thus limiting the amount of labelling observed[94].

Phenylazide has successfully been used[97] on 3,5-diaryl-oxadiazoles that had been observed to induce apoptosis in tumour cells. A chloro-pyridinyl group was replaced by the phenylazide derivative, including tritium labels as reporters for downstream SDS-PAGE analysis by radioactivity, in order to covalently modify proteins interacting with these active compounds (Figure 3.3). Tail-interacting protein 47 (TIP47), an insulin-like growth factor-II receptor binding protein, was identified as the ligand-binding protein in this manner, and validated using knockout experiments.

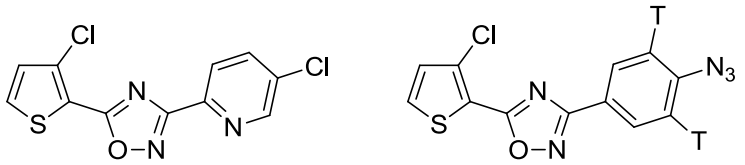

(**MX-126374**) (**MX-126911**)

Figure 3.3. Parent (**MX-126374**) and photolabile derivative (**MX-126911**) inhibitors of apoptosis, found to target TIP47

3.3.1.3 Diazirine

While diazirines have been used in both aliphatic and aromatic scaffolds, the most common one is the trifluoromethylphenyldiazirine (shown in Scheme 3.3 further below), due to its greater chemical stability than other diazirines. Similarly to benzophenones, aryldiazirines are photolysed at longer UV wavelengths, resulting in less potential damage to the biomolecules of interest. The generated carbene is very reactive, with a short half-life; while this characteristic can lead to quenching by water, and therefore a reduced amount of protein labelling, it also limits

the amount of non-specific labelling. The singlet-state carbene can insert into O-H and N-H bonds, as well as C-H bonds, thus minimising bias from selective reactivity.

The trifluoromethylphenyl diazirine has been applied to the study of barbiturate general anaesthetics, which act as allosteric inhibitors of muscle-type nicotinic acetylchlorine receptors (nAChRs). In particular, the barbiturate (5-allyl-1-methyl-5-phenyl)barbituric acid (MPAB) was derivatised[98] to incorporate a trifluoromethyldiazirinyl (TFD) component, thus allowing the identification of barbiturate binding sites in the *Torpedo* nAChR. As was the case in the previous photolabelling examples, tritium labels were incorporated into the photolabile inhibitor in order to detect bound proteins after SDS-PAGE; these compounds are shown in Figure 3.4.

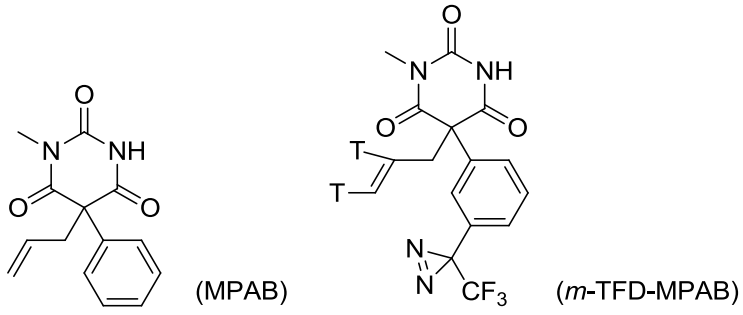

Figure 3.4. Parent barbiturate general anaesthetic MPAB and its photolabile derivative *m*-TFD-MPAB

3.3.2 Choice of the photolabile moiety for the study of CP4d

Having considered the advantages and disadvantages of each of the photolabile groups with respect to our inhibitor structure and experimental setup, we chose to work with the trifluoromethylaryldiazirine moiety. The significant hydrophobic character of benzophenone would likely have reduced the already-limited solubility of parent compound **CP4d** (~33 μM in

our assay buffer), and its larger size may have had a detrimental effect on binding to the enzyme. TCEP (tris(2-carboxyethyl)phosphine) is used as a reducing agent in our buffers with TG2 in order to ensure that the enzyme remains in its reduced, active form, but this could lead to the potential reduction of a phenylazide group to the corresponding aniline. Furthermore, we use an azide-alkyne cycloaddition as the final step in the synthesis of **CP4d**, which may result in side reactions with an incorporated phenyl azide group instead of the benzyl azide used in the synthesis. Finally, diazirines, while synthetically more involved, are easily photolysed to a reactive carbene, and can be used in either aliphatic or aromatic form. Aromatic diazirines have been noted to produce higher yields of carbene than their aliphatic counterparts[99]; this aromatic group could replace either phenyl group of **CP4d**, thus minimising the effect on inhibitor binding. We therefore elected to work with the aromatic trifluoromethylphenyldiazirine, which is activated by the electron-withdrawing trifluoromethyl group and stabilised by the phenyl group. The product carbene is generally[96] formed in approximately 65% yield, and the acid-stable diazo derivative in the remaining 35% yield, as shown in Scheme 3.3. The advantages of the trifluoromethylphenyldiazirine are that it can be heated to 75°C for 30 minutes, or kept in 1 M solutions of acid (HCl) or base (NaOH) for two hours at room temperature without decomposition, as long as it is shielded from light. The half-life for the photolysis of the diazirine is approximately 25 seconds, while that of the diazoisomer is much longer, at 22 minutes; previous experiments have determined[81] that TG2 is stable for at least 10 minutes under irradiation at 350 nm, a time that represents over 20 half-lives for the generation of the carbene, and only half the half-life of the diazoisomer side-product.

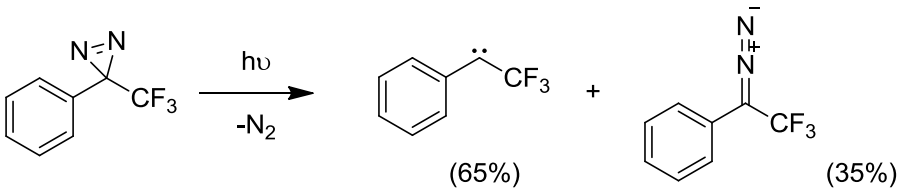

Scheme 3.3. Products of UV irradiation of 3-trifluoromethyl-3-phenyldiazirine

3.3.3 Synthetic approach for the photolabile inhibitor

Given that the last step in the synthesis[80] of **CP4d** is a copper(I)-catalysed azide-alkyne cycloaddition (CuAAC) to form the triazole, we chose to prepare a 4-(trifluoromethyldiazirine)benzyl azide that we could then use in a convergent synthetic strategy. This projected approach is shown schematically in Figure 3.5, where **CP3** is the common ynone intermediate. While the examples shown above featured tritium on the photolabel in order to allow radioactive detection of labelled proteins following SDS-PAGE, we already know the identity of our target protein and chose to integrate the isotopic labels into the protein (Chapter 2) as an aid in sample analysis.

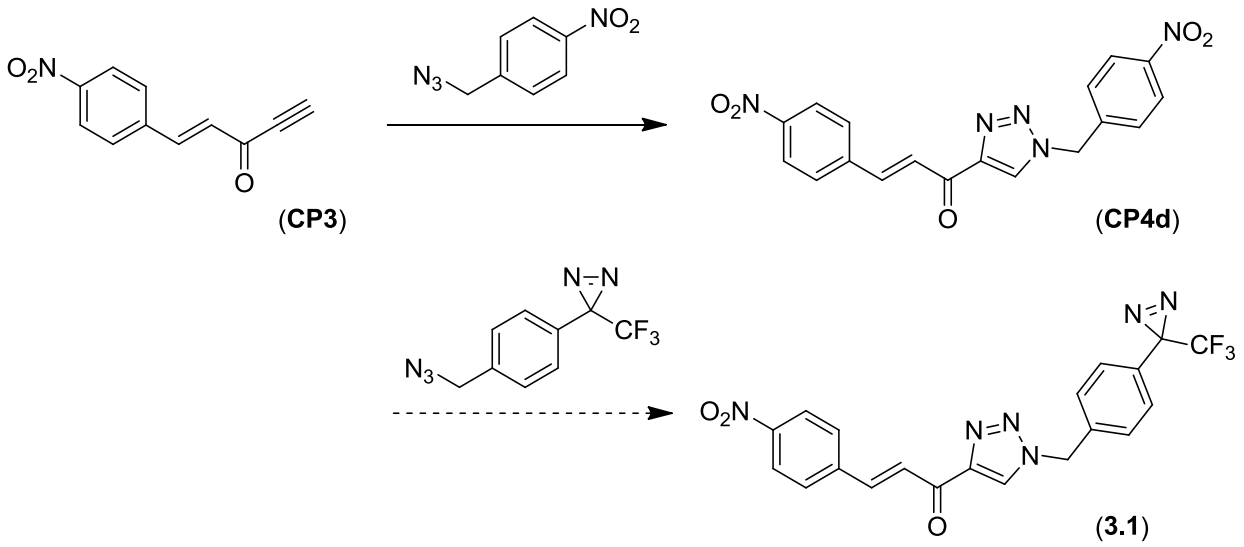

Figure 3.5. Proposed approach for the preparation of the photolabile derivative **3.1** of **CP4d**

3.3.4 Synthesis of the photolabile inhibitor

Trifluoromethylphenyldiazirines are generally prepared from the corresponding ketones, so a logical starting point was 4-iodobenzyl alcohol, from which we could prepare the trifluoromethylketone in one step using a lithiation followed by coupling to ethyl trifluoroacetate, provided that the hydroxyl group had been adequately protected. This projected approach is shown in Scheme 3.4 below, with the key reagents indicated above each transformation arrow. More specifically, the protecting group (indicated as R in Scheme 3.4) was required to be stable to *n*-butyllithium lithiation and subsequent acylation, tosylation, the diaziridine formation with ammonia, and possibly to the oxidation with iodine. However, the oxidation was the last step prior to deprotection, therefore it was not crucial that the protecting group be stable to those reaction conditions, only that it either remain or be removed, but not form a side-product.

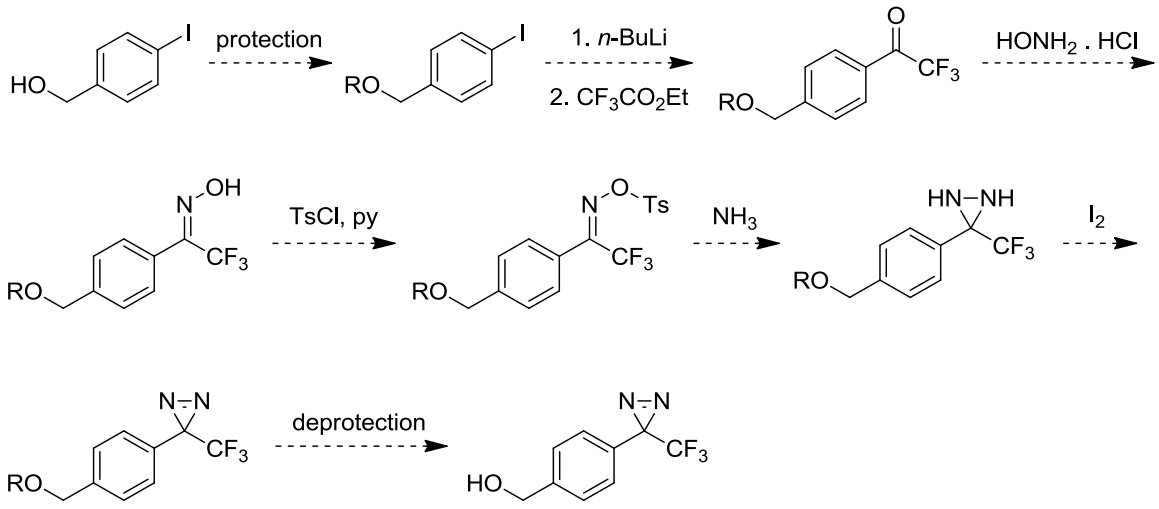

Scheme 3.4. Approach for the synthesis of the diazirine

We began with the use of tetrahydropyran (THP) as a protecting group, thus forming the corresponding acetal. While the preparation of the final diazirine was successful on one occasion using the THP protecting group, it was also unsuccessful on several occasions, and the THP group was observed to decompose as early as during the transformation to the oxime. A methyl group has been used[100] to protect a phenol (instead of our benzyl alcohol) as an ether in the preparation of a trifluoromethylphenyldiazirine, but decomposition was observed during the single-pot preparation of our diazirine, which was the initial synthetic route[101] used prior to optimization. The deprotection conditions on a phenol instead of a benzyl alcohol also involved a different chemistry, due to the increased relative stability of the phenolate by resonance, such that we were not able to directly apply the literature deprotection conditions to our scaffold. Finally, we chose a silyl group, namely *t*-butyldimethylsilyl (TBDMS), to protect the alcohol, since it is reasonably acid-stable and specifically requires the fluoride anion in order to be

cleaved. The TBDMS group was observed to be stable to all of the reaction conditions used in the formation of the diazirine, thus allowing efforts to be focused on yield optimisation.

The transformation of the benzyl alcohol into a benzyl azide was also investigated prior to working with the diazirinyl derivative. Initially, a conversion *via* the tosylate was considered, thus enabling a simple nucleophilic substitution to the corresponding azide, as shown in Scheme 3.5 below. Standard solvents for the proposed reactions are dichloromethane (DCM) for the tosylation, and DMSO for the substitution, as shown further below in Scheme 3.6. However, given that tosylates can be oxidised[102] to aldehydes in DMSO, in a Swern-like oxidation, we chose to use DMF as a similar polar aprotic solvent, but without an oxidant quality.

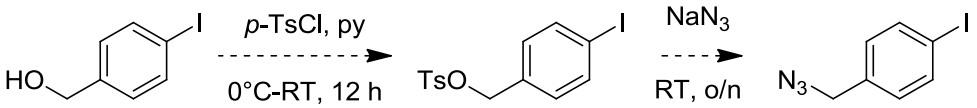

Scheme 3.5. Proposed transformations to prepare the desired benzyl azide from a benzyl alcohol

The first attempt was to prepare the azide in a one-pot synthesis, using DCM as the solvent for both steps. However, sodium azide was observed to be insoluble in DCM. This result was consistent with the fact that a 0.5 M solution of sodium azide in DMSO (a more polar solvent) requires 24 hours of stirring at room temperature for full dissolution; while this approach is possible with DMSO given its high boiling point (189°C), it is inconvenient with the highly-volatile DCM. Instead, the sodium azide was dissolved in DMF, and this solution was added to the solution of the tosylate in DCM, without any workup performed. Three distinct products were obtained by TLC analysis, but they were lost in flash column chromatography. In

a final attempt, both reactions were run in DMF, in a single-pot reaction, but the starting alcohol was recovered in 75% yield after workup. The sodium azide was also observed to only partially dissolve in DMF, unlike in DMSO, and therefore this approach was discontinued.

At the same time as this work was being carried out, a former Keillor group member, Dr. Christophe Pardin, was working in the Boddy group, preparing the same diazirinyl benzyl azide. His synthetic scheme involved the use of an Appel reaction to prepare the benzyl bromide from the benzyl alcohol and CBr_4/PPh_3, and then a nucleophilic substitution with sodium azide in DMSO, as was done in the original cinnamoyl triazole study[80]. These reactions were incorporated into the optimised synthetic scheme, presented below as Scheme 3.6. As part of the optimisation, starting from a preparation[96] of the diazirine from the ketone with minimal workup and no purification, as had been used in the synthesis of a 3-trifluoromethyl-3-(3-iodophenyl)diazirine, the tosylation and oxidation to the diazirine steps were modified in order to optimise the yield. In particular, it was difficult to determine the source of problems when no product was obtained after a combined four steps without analysis; in Scheme 3.6, products indicated in square brackets were subjected to reaction workup and the crude product was analysed by ^{1}H and ^{19}F NMR prior to moving on to the next step.

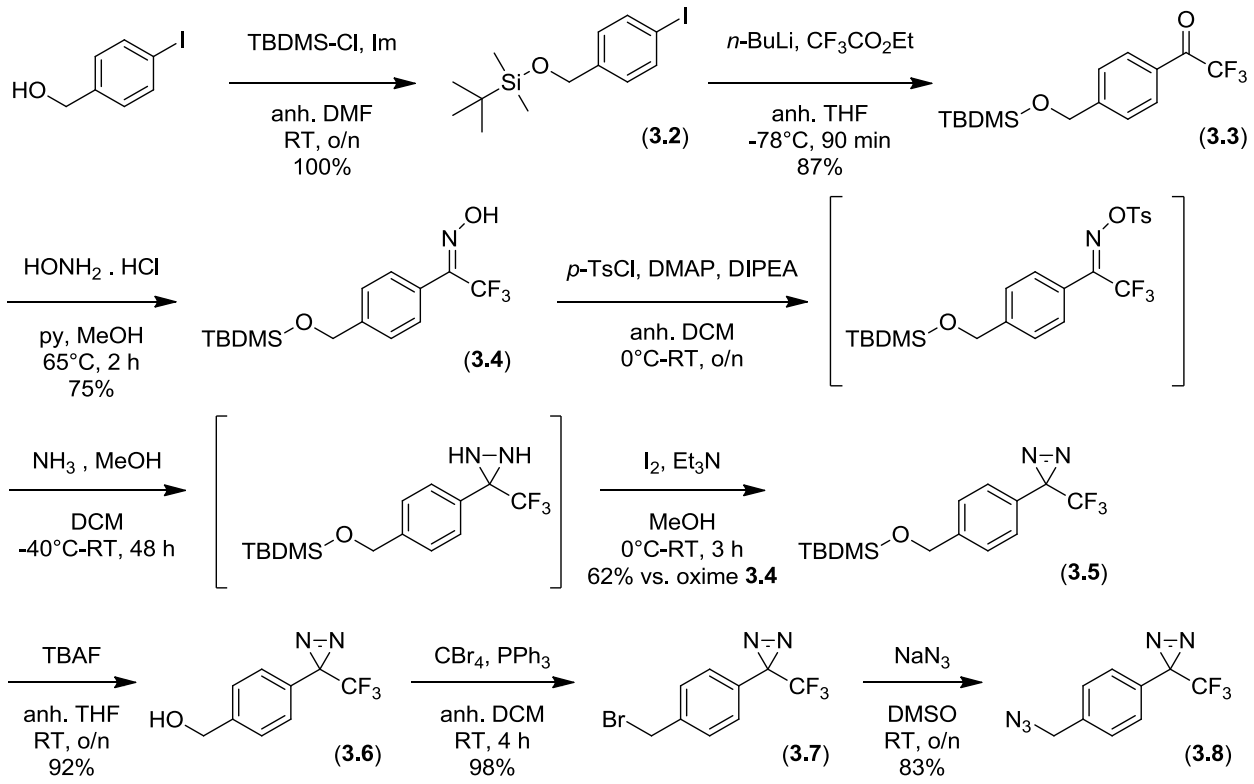

Scheme 3.6. Synthesis of the diazirinyl benzyl azide **3.8**

Starting from 4-iodobenzyl alcohol, we first protected[103] the alcohol as a *tert*-butyldimethylsilyl ether, thereby removing an acidic proton in order to allow a lithiation and coupling reaction[101] on **3.2** to substitute a trifluoromethylacyl group for the iodide in **3.3**. From there, we prepared the diazirine in the standard manner, namely preparing the oxime[101] **3.4**, then tosylating[104] it prior to using ammonia to form the diaziridine[101, 104], which was oxidised[100] to the more stable diazirine **3.5**. Once the photoreactive moiety had been prepared, the TBDMS protecting group was removed[105] with tetrabutylammonium fluoride, prior to the Appel reaction on **3.6**, as suggested by Dr. Pardin, to form **3.7**. Finally, nucleophilic substitution[80] of bromide with sodium azide afforded the key compound **3.8**.

The cinnamoyl ynone scaffold (**CP3**) was synthesised from *trans* 4-nitrocinnamic acid as published previously[80]; however, the original synthesis of **CP4d** called for an overnight CuAAC at 75°C, conditions that risked decomposing the diazirinyl group due to prolonged high temperatures. Instead, we used one equivalent of copper(I) iodide, and the cycloaddition was performed at room temperature[106](Scheme 3.7). The isolated yields were comparable between both reaction conditions, as determined by first trying the new reaction conditions in the synthesis of **CP4d** (36% yield).

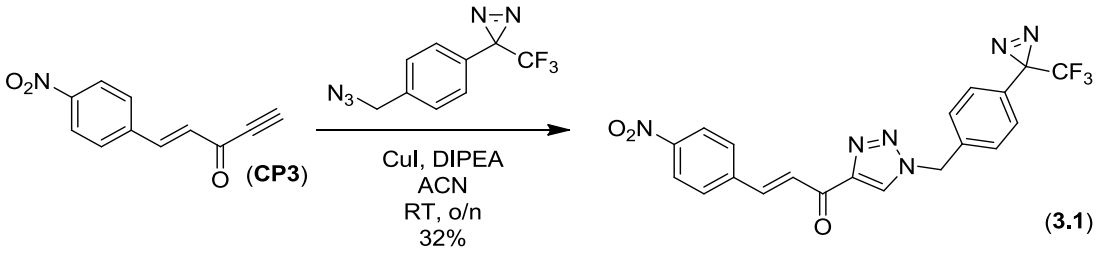

Scheme 3.7. Synthesis of the photolabile inhibitor **3.1**

While the percent isolated yields were comparable to those obtained with the original CuAAC, they remained low. This result is likely due to the strong electron withdrawing quality of the nitro group, thus rendering the alkyne less nucleophilic.

3.4 Evaluation of the photolabile inhibitor

3.4.1 Enzyme inhibition kinetics – IC_{50}

In order to determine the potency of this photolabile derivative of **CP4d**, we began by determining its IC_{50} value. By definition, the IC_{50} is the concentration of inhibitor required to decrease the enzyme's activity to 50% of what is observed in the absence of inhibitor; the value

obtained is therefore relative to the concentrations of substrate and enzyme used. However, if all assays are carried out in the same manner, the values are comparable relative to each other, and offer a quick method for the initial evaluation of compounds. All IC_{50} experiments presented within this thesis were measured under the same conditions, described in more detail in Chapter 7; for compound **3.1**, we determined an IC_{50} value of 44.8 ± 4.4 μM, at a concentration of 54.4 μM substrate **AL5**.

3.4.2 Enzyme inhibition kinetics – modes of inhibition

However, the IC_{50} only gives an idea of the potency, offering no information on the mode of inhibition. More extensive evaluation, wherein we determined the apparent K_M and V_{max} values with our substrate[26], **AL5** (*N*-Cbz-Glu(γ-*p*-nitrophenylester)Gly), in the presence of varying concentrations of our inhibitor, allowed us to determine the type of reversible inhibition, namely competitive, uncompetitive, or (mixed) non-competitive. These apparent values are obtained by non-linear regression on the experimental data, by fitting plots of the initial rate vs. the concentration of substrate **AL5** to the hyperbolic Michaelis-Menten equation shown below (eq. 3.1).

$$v = \frac{V_{max}[S]}{K_M + [S]} \qquad \text{(eq. 3.1)}$$

In competitive inhibition, as the name implies, the inhibitor competes with the substrate to bind to the free form of the enzyme. While the simplest form involves the inhibitor and the substrate competing for the active site, it is also possible that the inhibitor binds to a distinct site on the enzyme, resulting in the occlusion of the active site to which the substrate would bind,

either in a situation of steric hindrance or a rapid shift in the enzyme's conformation upon inhibitor binding. In this mode, K_M appears to increase by a factor of α (eq. 3.2), since more substrate is required to reach a rate of 50% V_{max} due to competition by the inhibitor. However, V_{max} is unchanged, since it can still be reached at a higher concentration of substrate (thus out-competing the inhibitor).

$$\alpha = 1 + \frac{[inhibitor]}{K_i} \qquad \text{(eq. 3.2)}$$

In uncompetitive inhibition, the inhibitor binds to the enzyme-substrate complex, without affecting the free enzyme. By removing some of the reactive Michaelis complex from the product-forming pathway, V_{max} decreases (by a factor of α), since not all of the enzyme is available for turnover no matter how much substrate is added. Therefore, K_M appears to decrease by a factor of α as well, since V_{max} is mathematically lower, so proportionately less substrate is required for apparent saturation.

In mixed non-competitive inhibition, the inhibitor may bind to either free enzyme (competitive) or to the Michaelis complex (uncompetitive). Since competitive inhibition has no effect on V_{max}, and uncompetitive inhibition decreases that value, mixed non-competitive inhibition will result in a decrease of V_{max}. However, the effect on K_M depends on which mode of inhibition is stronger; since K_M increases by a factor of α_{comp} through competitive inhibition, but decreases by a factor of α_{uncomp} through uncompetitive inhibition, the more potent mode (larger value of α) will dictate the overall effect on the apparent K_M value.

The table below summarises the associated changes in the apparent K_M and V_{max} values for all three modes of inhibition. These changes are used to determine whether a given inhibitor is competitive, uncompetitive, or non-competitive with respect to the substrate.

Table 3.1. Effect on kinetic parameters of different modes of inhibition

Mode of inhibition	**Effect on K_M**	**Effect on V_{max}**
Competitive	increases	none
Uncompetitive	decreases	decreases
Mixed non-competitive	may increase or decrease	decreases

3.4.3 Evaluation of inhibitor 3.1

Given that the parent inhibitor **CP4d** is competitive with respect to the acyl donor substrate (**AL5**), we first estimated K_i (as K_i^{app}) for inhibitor **3.1** using the Cheng-Prusoff equation[107]. This equation allows us to estimate the K_i value from the IC_{50}, assuming that the mode of inhibition is known. The equation for a competitive inhibitor is shown below (eq. 3.3); for **3.1**, using a K_M value[81] of 14.0 μM, we calculated a K_i^{app} value of 9.2 μM.

$$IC_{50} = \frac{K_i^{app}}{K_M}[S] + K_i^{app} \qquad \text{(eq. 3.3)}$$

In order to confirm the mode of inhibition and determine an experimental value for K_i, we designed the standard experiment using 0.5, 1, 2, and 5 times the value of K_M (for the

substrate concentrations) and 0, 0.5, 1, 2, and 5 times the value of K_i^{app} (for the inhibitor concentrations) to generate Michaelis-Menten curves at fixed inhibitor concentrations, using the curve with no inhibitor as a positive control.

However, within this experiment with compound **3.1**, we noted significant issues with the compound's solubility, namely its solubility limit of 14 μM in **AL5** buffer (a MOPS-based buffer at pH 7.2). We were therefore only able to test inhibitor concentrations corresponding to factors of 0, 0.25, 0.5, 0.75, and 1 for K_i^{app}. While not ideal, this lower concentration range ensured that we saw no artifacts relating to incomplete dissolution of the inhibitor in solution, which were observed in experiments nearing the compound's solubility limit. Following the generation of Michaelis-Menten curves at various concentrations of **3.1** (Figure 3.6), we performed non-linear regression using GraphPad Prism 6 according to equation 3.1 in order to obtain values for K_M^{app} and V_{max} at each concentration of inhibitor. However, the generated Michaelis-Menten curves overlap (within error) despite the increasing concentrations of inhibitor; the extrapolated values for the kinetic parameters are therefore limited by the data.

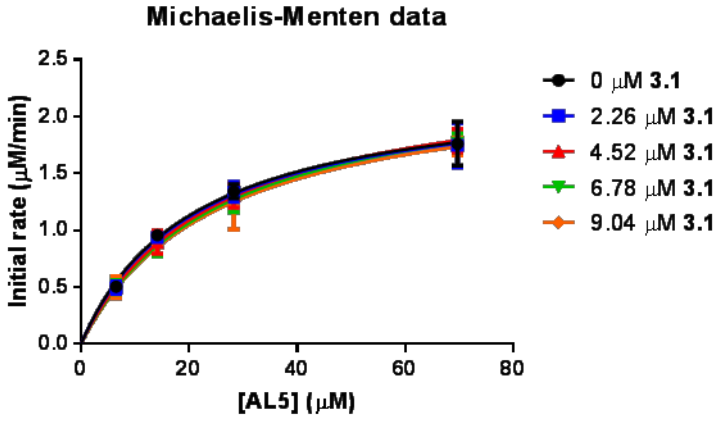

Figure 3.6. Michaelis-Menten curves at increasing concentrations of **3.1**

We then plotted the extrapolated constants against the concentration of **3.1**, as shown in Figure 3.7, to determine that the inhibitor is competitive with respect to **AL5**, the acyl donor substrate, given that K_M^{app} increases proportionately to the concentration of substrate while V_{max} remains constant (slope of 0.0097 ± 0.0072 min^{-1} for the linear regression of V_{max} vs. [**3.1**]). We determined a K_M value of 20.9 ± 0.8 µM for **AL5** in this experiment, a value that correlates well with the literature value[81] of 14.0 µM. The K_i value for inhibitor **3.1** was extrapolated as the negative x-intercept of the plot of K_M^{app} vs. the concentration of inhibitor, since the apparent K_M value is the product of the true K_M value and α (eq. 3.2), yielding a K_i of 37.8 ± 9.9 µM. The larger error in K_i arises in part from the fact that the highest concentration that we tested was roughly one quarter of K_i, due to solubility limitations.

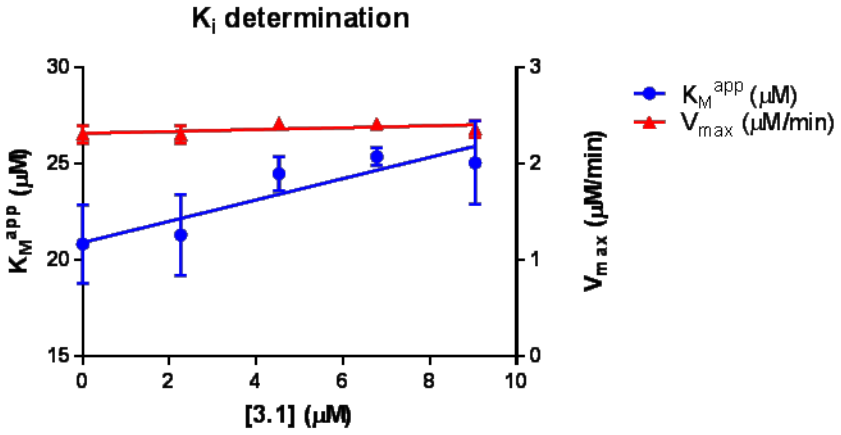

Figure 3.7. K_i determination for inhibitor **3.1**

3.4.4 Attempts at photolabelling

The photolabelling experiment was carried out using a maximal concentration of photolabel, namely 14 µM. The enzyme was incubated with the photolabel in **AL5** buffer for

10 minutes in a Luzchem photoreactor LZC4 with an LZC-UVA lamp (315-400 nm), corresponding to a range of wavelengths known to photolyse the diazirine and over a time period corresponding to 20 times the diazirine's half-life of photolysis. The sample was then subjected to dialysis into simple Tris buffer (pH 7.2) for digestion and analysis, prior to analysis by collaborator Peter Kubiniok, a Ph.D. candidate in Prof. Pierre Thibault's group at Université de Montréal.

Complete coverage of the protein sequence was obtained through its tryptic digest, although no labelled peptides were detected, suggesting an absence of protein labelling events. We hypothesise that the lack of labelling events is likely due to the low concentration of photolabel in solution, relative to its apparent affinity for the enzyme, which is an issue that we were not able to predict at the beginning of this experiment. It is likely that the carbene was quenched by water, instead of inserting itself into the protein, due to its high reactivity.

3.5 Further work done

Given that the lack of results was due in significant part to the low solubility of the photolabile inhibitor, several efforts were made in an attempt to circumvent this problem. We studied the effect of both the nature and concentration of organic solvent, and the replacement of a phenyl group by a pyridine, with the goal of increasing the concentration of photolabel in solution.

3.5.1 Increasing the volume of organic co-solvent

The premise of this photolabelling experiment was to identify the binding site of the inhibitor on the enzyme; as such, maximal catalytic activity was not a requirement. The standard

solvent, DMF, is normally used in a volume percentage of 2.5%, coming from the stock solution of substrate **AL5**. At a concentration of 20% v/v of DMF, the relative activity was approximately 60% of its maximum (Figure 3.8); however, the solubility of the photolabel did not increase. We repeated the assay with DMSO (Figure 3.8), in which 30% relative activity was retained at 40% v/v, but again saw no notable effect on solubility at this increased volume of co-solvent. The third solvent tested, *N*-methyl-2-pyrrolidone (NMP), is used in peptide synthesis as a more hydrophobic replacement for DMF, and it is also water-miscible. However, at only 2.5% v/v NMP, the enzyme's activity was decreased to approximately 15% of what was observed at a same volume of DMF.

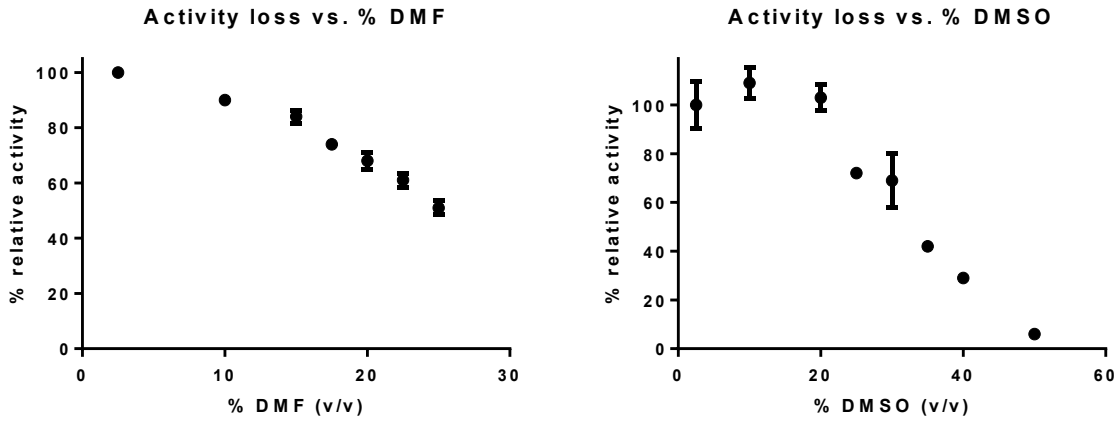

Figure 3.8. Hydrolytic activity of TG2 at various amounts of DMF and DMSO

3.5.2 Scaffold modification

A recent publication[99] in Chemical Communications suggested that the replacement of a phenyldiazirine with a pyridinyl or pyrimidinyl diazirine may increase solubility of trifluoromethylaryldiazirines by 30- to 250-fold or 100- to 7500-fold, respectively. Pyridinyl

groups increase the polarity of aromatic compounds, by rendering the aromatic group more polarised by the electronegative nitrogen, although the heterocyclic nitrogen is not protonated under physiological conditions. Specifically, its pK_a value is generally below 6 for substitutions at the 2-position, while physiological pH is 7.4. Furthermore, the original study[80] of cinnamoyl triazole derivatives compared lead compound **CP4d**, with a 4-nitrophenyl group, to a simple phenyl (**CP4a**) or a pyridinyl group (**CP4e**), as shown in Figure 3.9 below. With gplTG, the IC_{50} for **CP4e** was four times higher than **CP4a**, but still good at 18 ± 2 μM; however, with hTG2, the IC_{50} for **CP4e** was observed to be greater than 100 μM. This loss of potency was not accompanied by an increase in aqueous solubility, as both compounds showed a maximal solubility of approximately 35 μM in **AL5** buffer.

Figure 3.9. Proposed minimal structural modification to increase solubility

3.6 Conclusion and future directions

Overall, we were able to successfully synthesize a diazirinyl derivative of **CP4d**, and determine that the new compound **3.1** is also a competitive inhibitor with respect to the acyl donor substrate, with a K_i value of 38 μM. However, in order for the labelling aspect of this project to be successful, we would require a photolabile inhibitor with either greater solubility, or, ideally, greater affinity for the protein. Greater solubility would allow us to increase the concentration of photolabel in solution, thereby increasing the probability of labelling the

enzyme instead of having the carbene quenched by water; however, an increased concentration may result in additional non-specific binding to the protein, given the relatively lower affinity compared to the parent compounds. In contrast, having an increased affinity for the protein would ensure that a similar (or lower) concentration of photolabel would be required in solution, thus reducing the risk of unspecific labelling events while maintaining a sufficient concentration to optimise binding.

While the limitations of other photolabile moieties were outlined at the beginning of this chapter, it may be worthwhile to investigate the effect of 2-aryl-5-carboxytetrazoles (ACT)[108] as a different photolabile moiety. This functional group has recently been applied to well-studied drugs Dasatinib and JQ-1, respective kinase and bromodomain protein inhibitors, in a comparison between benzophenone, diazirine and this ACT photolabile group. The ACT moiety forms a less-reactive carboxynitrile imine as its photolysis product and, as such, it requires a nucleophilic side chain in its vicinity on the protein in order to form a covalent linkage. However, this group also resulted in the highest photolabelling efficiency on the two proteins studied. The ACT may be applied to our TG2 inhibitors by being incorporated directly into **CP4d** in lieu of the acyl triazole (Figure 3.10); however, work would be necessary to ensure that the removal of the methylene group linked to the triazole does not negatively affect the inhibitory activity of the compound. In particular, cinnamoyl benzotriazole derivatives, which lack that methylene-associated rotatable bond, were observed to have higher IC_{50} values with gplTG, thus resulting in the potential requirement of a significantly higher concentration for labelling. However, in a similar approach to the replacement of the phenyl group with a pyridinyl one (Section 3.5.2), a decrease in affinity may be compensated by greater solubility, as would be expected from the tetrazole ring.

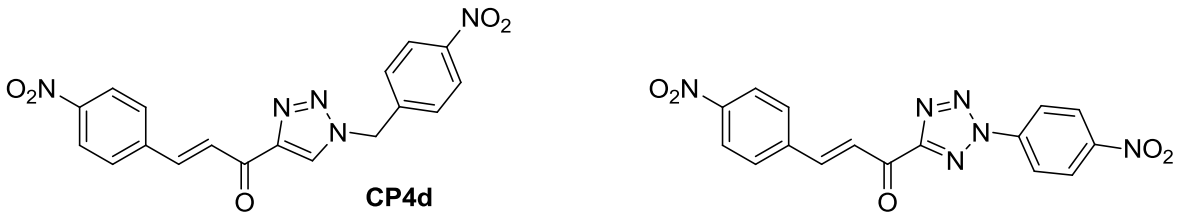

Figure 3.10. Proposed structure for a future photolabile tetrazole inhibitor

Chapter Four: **Synthesis of glutathione-resistant reversible inhibitors**

4.1 Glutathione

Glutathione (GSH, shown below in Figure 4.1) is the naturally-occurring tripeptide γ-glutaminylcysteinylglycine. It plays a major role as a cellular antioxidant through the intracellular equilibrium established with its disulfide form (GSSG), thus offering protection[109] against reactive oxygen and nitrogen species. Inside cells, the concentration of GSH may reach[110] 10 mM; however, its concentration is one to three orders of magnitude lower outside cells, reaching values as low as 5 μM in plasma[111]. GSH also plays other roles in metabolic processes, such as[111] acting as a cysteine reserve, storing and transporting nitric oxide, helping in the operation of certain transcription factors and mediating the detoxification of various endogenous and foreign compounds. The latter category likely encompasses the inactivation of certain compounds that may include our TG2 inhibitors, hence our interest in verifying the extent of this reactivity.

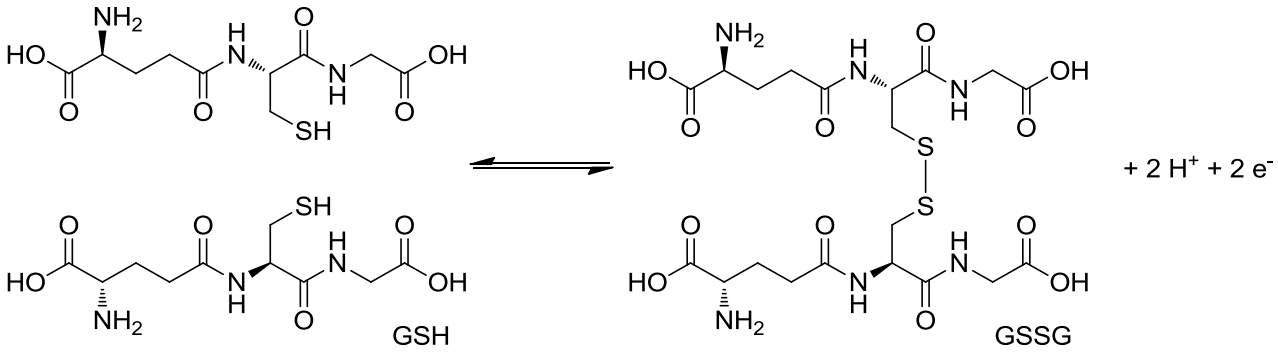

Figure 4.1. Structures of glutathione, both reduced (GSH) and oxidised (GSSG)

4.1.1 Potential reactivity of key inhibitors with GSH

Some of our key inhibitors, previously developed against gplTG, are reproduced in Figure 4.2 below; one common feature that can be observed is the α,β-unsaturated carbonyl motif, also called a Michael acceptor, highlighted in blue in each of the structures. These moieties are relatively strong electrophiles; as such, we were concerned that GSH would react with our compounds and form adducts that may have significantly decreased potency against intracellular TG2.

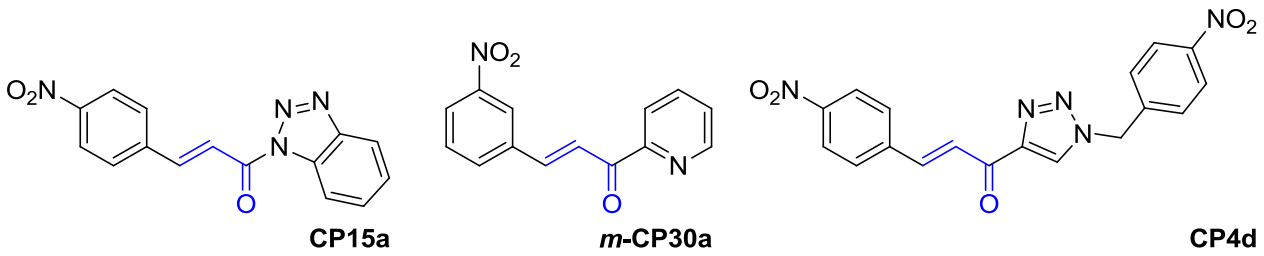

Figure 4.2. Common electrophilic motif in our most potent inhibitors

4.2 Previous work done within the group

A previous student in the Keillor group, Isabelle Roy, prepared[81] various analogues of known inhibitors **CP15a** and ***m*-CP30a** in an effort to maintain potency against TG2 while reducing the electrophilicity associated with the parent α,β-unsaturated alkene. Some of the key compounds she prepared are shown below in Figure 4.3, with the parent compounds shown at the end of each row. The asterisk indicates IC_{50} values that were obtained with gplTG, prior to the development and optimisation of an expression and purification protocol for hTG2, while the entry "n.d." denotes that no inhibition was detected at the compound's solubility limit. However,

kinetic parameters determined with both forms of the enzyme have been shown[89] to be close to one another, suggesting that the parent compounds **CP15a** and ***m*-CP30a** remain as good starting points for new scaffolds for inhibitors against hTG2.

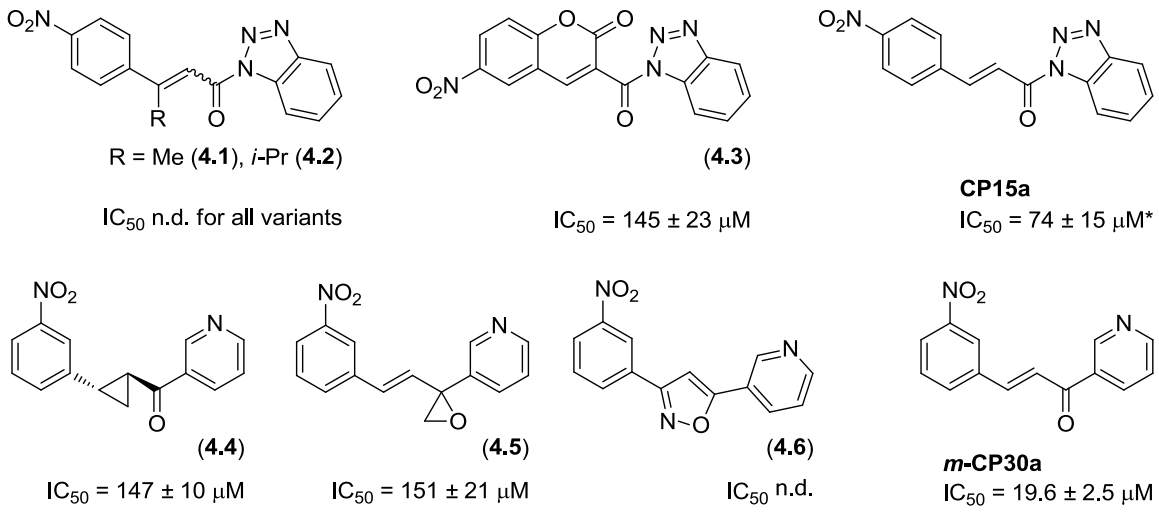

Figure 4.3. Previous scaffolds developed in an attempt to decrease the electrophilicity of cinnamoyl inhibitors

As can be seen in Figure 4.3, several different approaches were taken in an attempt to reduce electrophilicity. In the first, the β position was alkylated with either a methyl (**4.1**) or an isopropyl (**4.2**) group, to increase resistance to nucleophilic attack through both steric hindrance and a minor electron donating effect from the added alkyl group. Unfortunately, both modifications resulted in a complete loss of inhibitory potency. In a second approach, the electrophilic alkene was incorporated into a coumarin, under the reasoning that aromaticity would reduce reactivity due to the stability conferred by the extended π system. The resulting compound **4.3** was a weak inhibitor; as such, it was not evaluated for GSH resistance. Starting

from inhibitor ***m*-CP30a**, each of the double bonds of the alkene and carbonyl were replaced by a three-member ring, namely a *trans* cyclopropyl (**4.4**) for the *trans* alkene, and an epoxide (**4.5**) for the carbonyl. Both modified compounds showed reduced potency against hTG2, with IC_{50} values of approximately 150 μM. In another approach, both reactive double bonds were incorporated into an aromatic isoxazole (**4.6**), in an effort to reduce reactivity by again taking advantage of the stability conferred by aromaticity. However, the resulting compound retained no inhibitory potency, suggesting that the restricted geometry may have played a role in the compound's binding to the enzyme.

Returning to lead compound **CP15a**, in an electronically-motivated approach, the alkene was replaced with an alkyne (Figure 4.4). It was hypothesized that the additional π bond would reduce electrophilicity by increasing the electron density at that position in the molecule. This modification was the first to display an increase in potency, with compound **4.7** having an IC_{50} of 2.6 ± 0.2 μM.

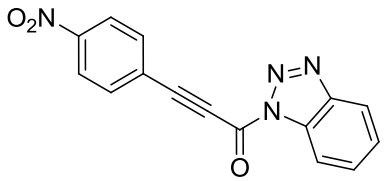

(**4.7**)

Figure 4.4. Alkynyl derivative of **CP15a**

4.3 Development of a method to determine susceptibility to glutathione addition

4.3.1 ^{1}H NMR assay development

In order to study the reactivity of our compounds with glutathione, we were inspired by work published in the Journal of Medicinal Chemistry, in which the authors evaluated[112] the stability of a substituted maleimide core that also functions as a Michael acceptor. They chose to use GSH as the nucleophile in the addition-elimination reaction with their compounds; the three representative derivatives that were evaluated are shown in Figure 4.5 below.

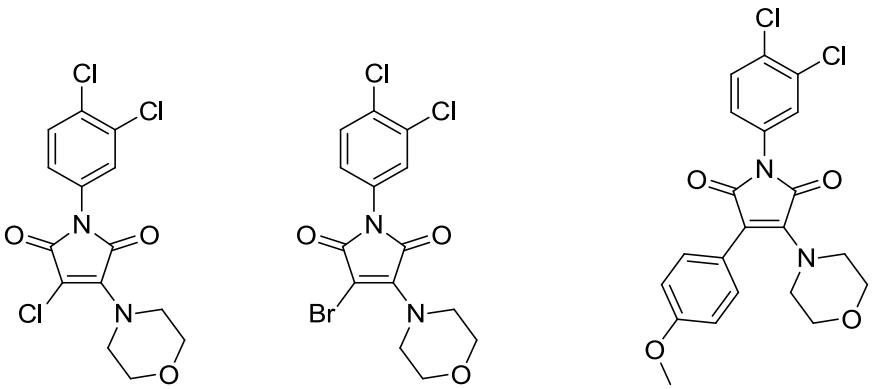

Figure 4.5. Michael acceptor maleimide derivatives studied for GSH stability

These compounds were incubated at 37°C in DMSO with a 5-fold molar excess of GSH, and aliquots were taken every hour (starting at time zero) and analysed by HPLC to determine how much substrate remained. Compound **B1**, as the starting point, had a half life of approximately 2 h. Compound **B9b**, with a bromine instead of the chlorine, was expected to react more quickly due to its superior leaving group, while compound **B7a** would likely react much more slowly by virtue of its methoxyphenyl substituent. These hypotheses were confirmed by the

result that **B9b** had fully reacted with GSH prior to the one-hour time point, while **B7a** showed no reactivity with GSH after 24 hours.

Previous studies[81] undertaken while the Keillor group was at Université de Montréal were performed by incubating our inhibitors under conditions mimicking a cellular environment, namely 50 mM HEPES buffer at pH 7.4, with 0.2 mM GSH and 3% acetonitrile by volume to solubilise the inhibitor, used at a concentration of 0.03 mM. For each inhibitor, the mixture was incubated at room temperature and aliquots taken over a total time of 40 minutes to 5 hours were analysed by LC-MS. However, several compounds, including lead inhibitor **CP4d** and alkynyl derivative **4.7**, were observed not to ionise well, thus limiting the potential for analysis by MS. As a starting point in the University of Ottawa Chemistry and Biomolecular Sciences department, we worked with representative compound **CP4d** and tried to establish HPLC standards for the inhibitor alone and its GSH adduct, under the same conditions as used previously. However, we were unable to resolve peaks corresponding to the inhibitor and to the formed adduct; furthermore, attempts to analyse the reaction by ^{1}H NMR in D_2O, to mimic the HPLC assay conditions, were unsuccessful due to the low aqueous solubility of **CP4d**. The addition of organic co-solvents (DMSO-d_6, methanol-d_4) up to 50% by volume was also insufficient to solubilise enough of the inhibitor in order to record its NMR spectrum. Given these issues, we opted to continue with 6.7 equivalents of GSH at room temperature, as had been done at the Université de Montréal, but to run the experiment in DMSO as had been done in the *J. Med. Chem.* work described above. At first, we chose to follow the reaction by ^{1}H NMR, using deuterated DMSO, in order to determine a rough time scale for our experiment, prior to reserving time on an LC-MS system. We also analysed the obtained adducts by mass spectrometry, after

recording the NMR spectra, in order to confirm the molecular weight of the products and determine whether we had single or double additions of the thiol.

4.3.2 Preliminary results with lead inhibitors

Using compound ***m*-CP30a** as a test compound, we determined that the reaction with glutathione proceeded to a significant extent within the first ten minutes (the time required to prepare the sample and record its ^{1}H NMR spectrum), and that it was complete within the first hour, with no further reaction after four hours. A similar reactivity was observed with **CP4d**, where the shifting of a characteristic methylene peak (calibrated to TMS) showed that the reaction had proceeded to more than 50% completion after 10 minutes; this observation was also supported by a significant change in the peaks in the aromatic region of the spectrum. Again, the reaction was complete after one hour and the compound did not react further after a total of four hours. In both cases, given the rapidity of the reaction and the difficulties previously observed in separating the inhibitor and its GSH adduct by HPLC, we chose not to analyse the products by HPLC but to continue with ^{1}H NMR for our analyses; however, for both compounds, mono-additions of glutathione were confirmed experimentally by mass spectrometry. The ^{1}H NMR spectra for both experiments are shown below (Figure 4.6).

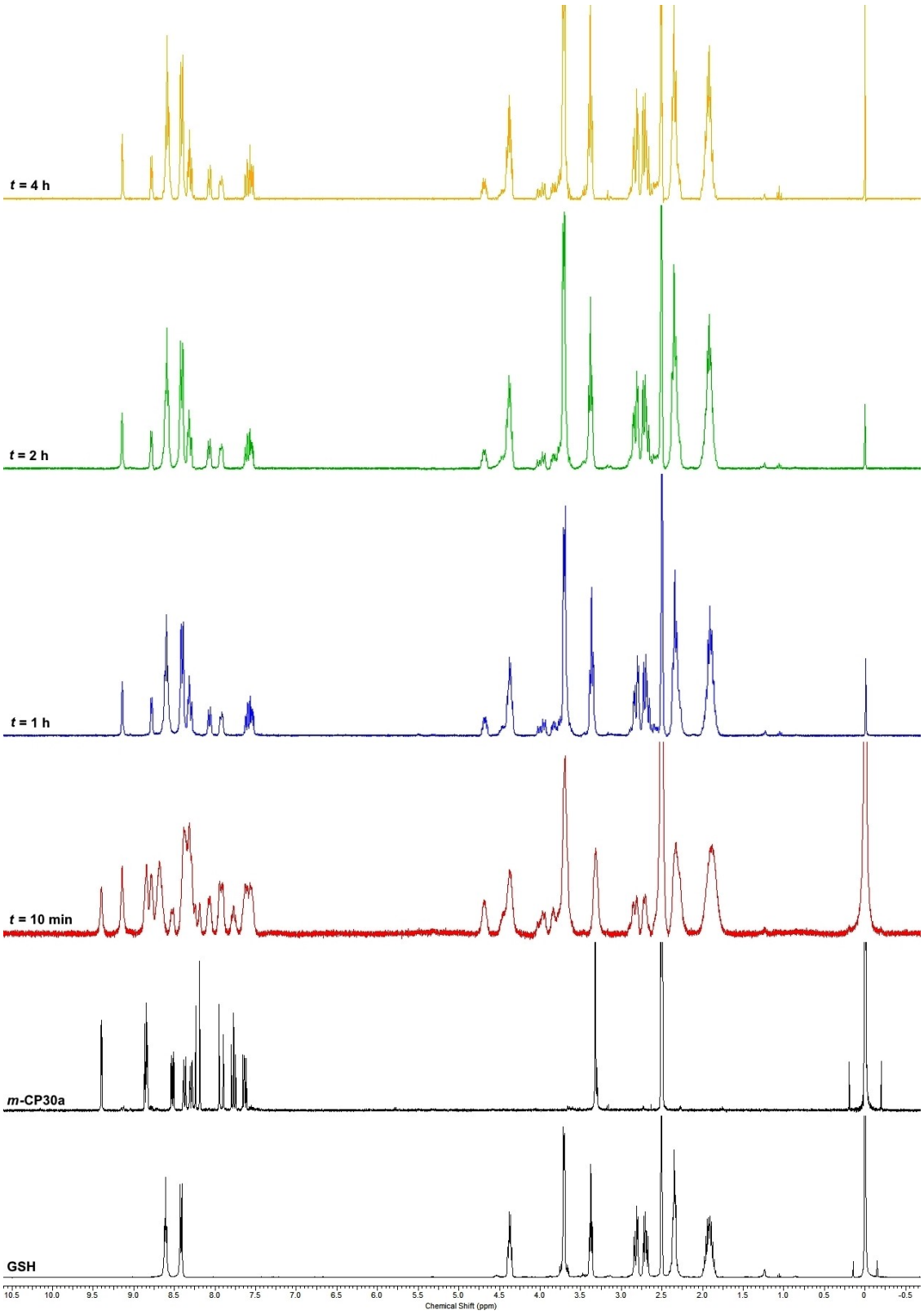
t = 4 h
t = 2 h
t = 1 h
t = 10 min
m-CP30a
GSH
10.5 10.0 9.5 9.0 8.5 8.0 7.5 7.0 6.5 6.0 5.5 5.0 4.5 4.0 3.5 3.0 2.5 2.0 1.5 1.0 0.5 0 -0.5
Chemical Shift (ppm)

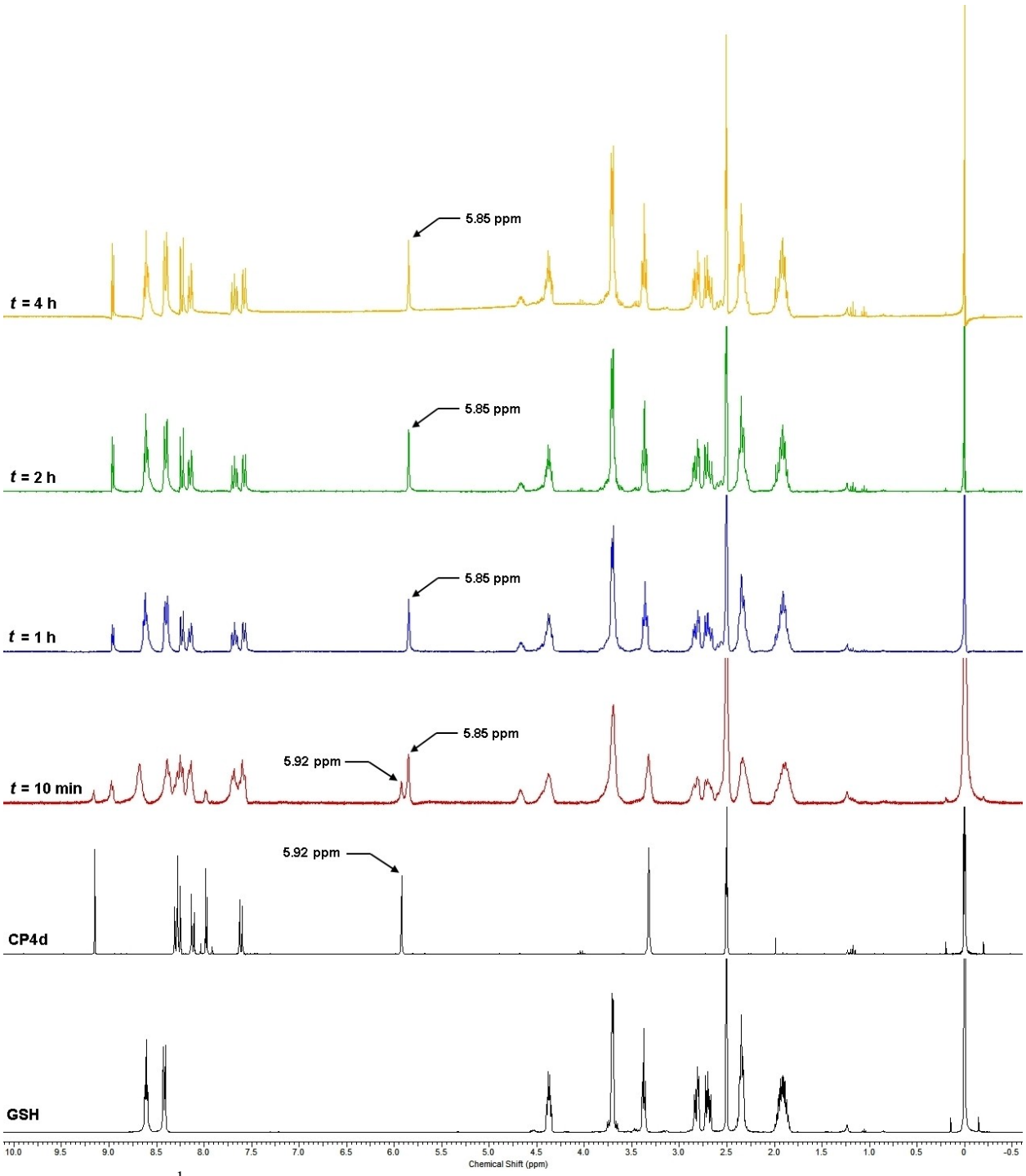

Figure 4.6. ^{1}H NMR assay for GSH resistance with ***m*-CP30a** (top) and **CP4d** (bottom)

4.4 Evaluating an alkynyl scaffold

Building on the work done by Isabelle Roy with the alkynyl derivative (**4.7**) of **CP15a**, we prepared alkynyl derivatives of **CP4a** and **CP4d**, hoping to see a similar increase in potency. These inhibitors (**4.8** and **4.9**, respectively) are shown below in Figure 4.7 with their parent cinnamoyl compounds. Gratifyingly, we observed IC_{50} values of 0.61 ± 0.05 μM for compound **4.8** (published[113] as **22a**) and 0.79 ± 0.05 μM for compound **4.9** (published[113] as **22b**), at a concentration of 54.4 μM substrate **AL5**.

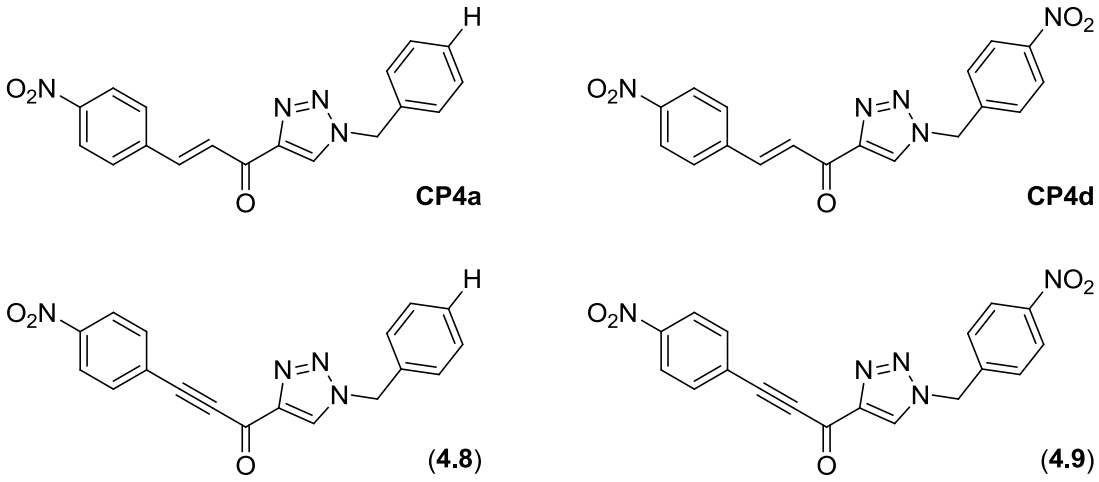

Figure 4.7. CP4a and **CP4d** alkynyl derivatives **4.8** and **4.9**

Initial efforts to determine the reactivity of inhibitor **4.7** had been unsuccessful due to the compound's weak ionisation by MS. We therefore applied our ^{1}H NMR assay to inhibitor **4.9** (Figure 4.8), which showed that this alkynyl derivative of **CP4d** was just as susceptible to GSH addition as the parent **CP4d**, and perhaps even more so, with both compounds showing significant reaction after only 10 minutes, the minimum time for collecting the NMR spectrum following the mixing of our inhibitor with GSH. Since there were no vinylic peaks to monitor,

we looked for changes in the overall spectra that were different from a simple overlap of both initial spectra, and also monitored the chemical shift (relative to TMS) of the methylene peak, in a similar approach to the analysis with **CP4d**.

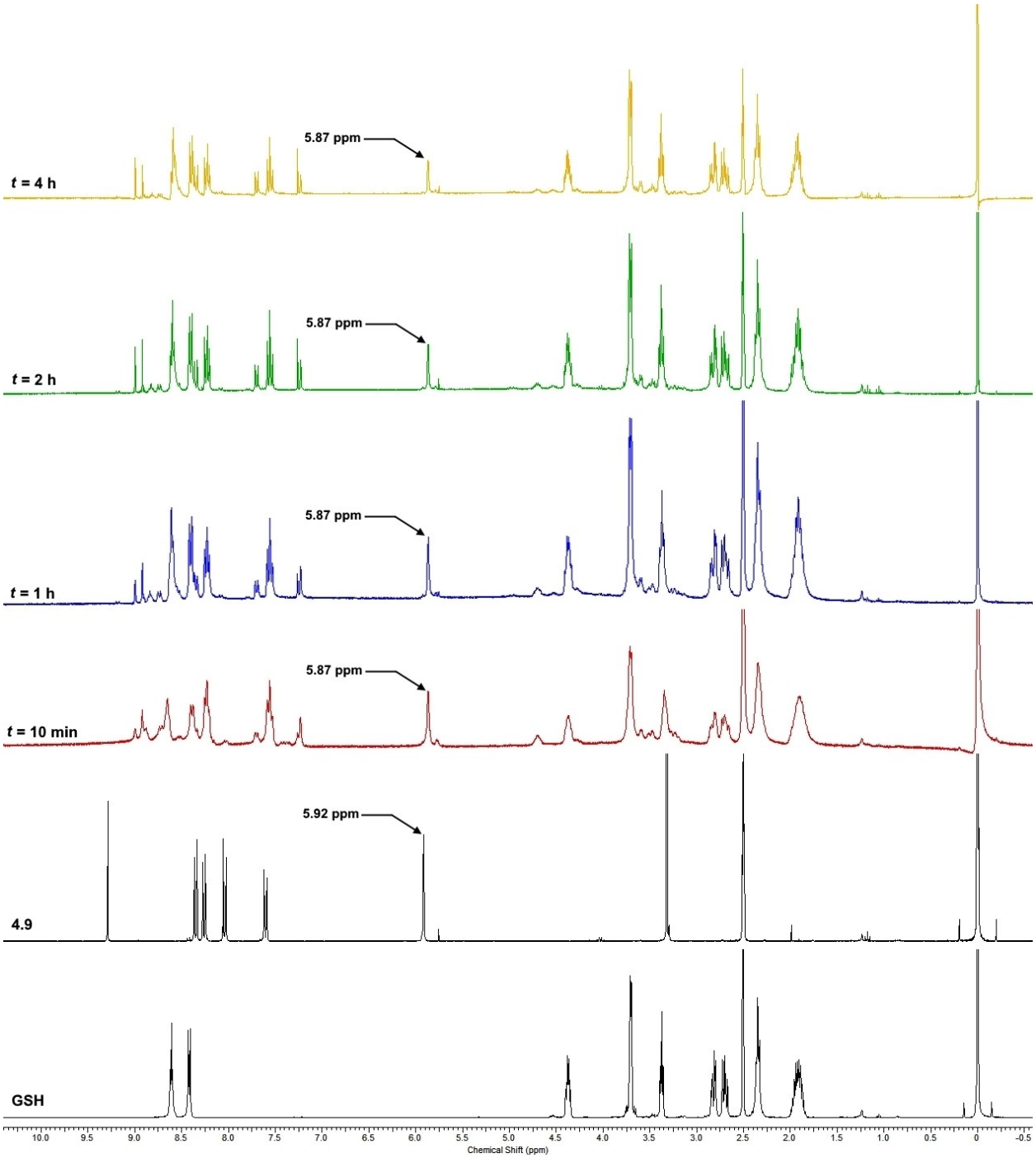

Figure 4.8. GSH susceptibility of inhibitor **4.9**

Given the significant reactivity observed between GSH and inhibitor **4.9**, we did not pursue this scaffold further for GSH resistance. However, we prepared a small library of compounds in order to study the effect of the West substituents on the inhibitory potency against TG2; this work is the topic of Chapter 5.

4.5 Development of a bis(triazole) scaffold

Looking back at the lead compound, we observed that **CP4d** has several symmetrical components centred around the carbonyl group, namely a 4-nitrophenyl group at its two extremities, and two carbon-carbon double bonds between these groups and the central carbonyl. However, one double bond is present as a simple alkene, and the other is incorporated into an aromatic triazole. We hypothesized that the incorporation of the alkene into a second triazole (Figure 4.9) may decrease its electrophilicity, given the stability conferred by aromaticity.

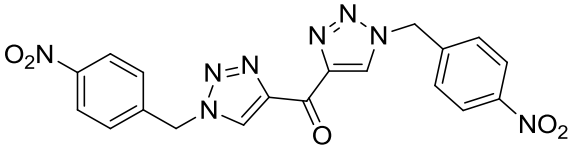

(**4.10**)

Figure 4.9. Suggested bis(triazole) inhibitor **4.10**, based on **CP4d**

Furthermore, docking studies performed by Dr. Christopher M. Clouthier (Figure 4.10) suggested that a bis(triazole) derivative of **CP4d** would bind in a similar location near the

enzyme's active site, and may have an additional interaction with Trp241 that, along with Trp332, bridges[7] the entrance to the active site tunnel.

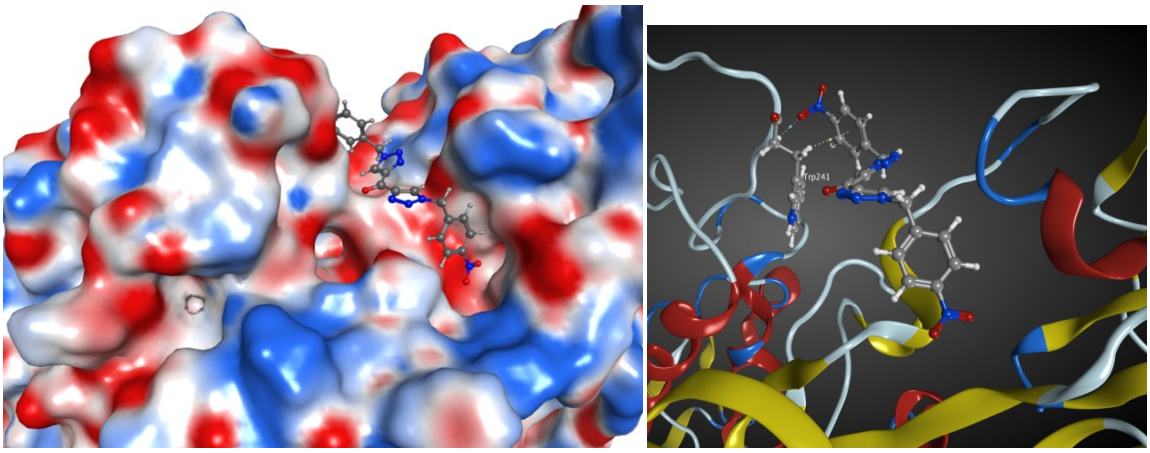

Figure 4.10. Docking experiments with compound **4.10**, shown (left) in the standard orientation of previous figures and (right) in ribbon form to show the projected interaction with Trp241

4.6 General synthetic approach to the bis(triazole) derivatives

4.6.1 First synthetic route

Since the target compound was symmetrical, we started from a central core with the goal of preparing penta-1,4-diyn-3-one (**4.13**, a known compound[114]), then using a double CuAAC to prepare both triazole groups in one step. We were also inspired by the synthesis of alkynyl compounds (Chapter 5), which was ongoing around the same time, and therefore proposed the synthetic scheme shown below (Scheme 4.1). Unfortunately, we observed that aldehyde **4.11** appeared to be lost during the evaporation of solvent under reduced pressure, a fact which correlates well with its literature[115] boiling point of 54-57°C.

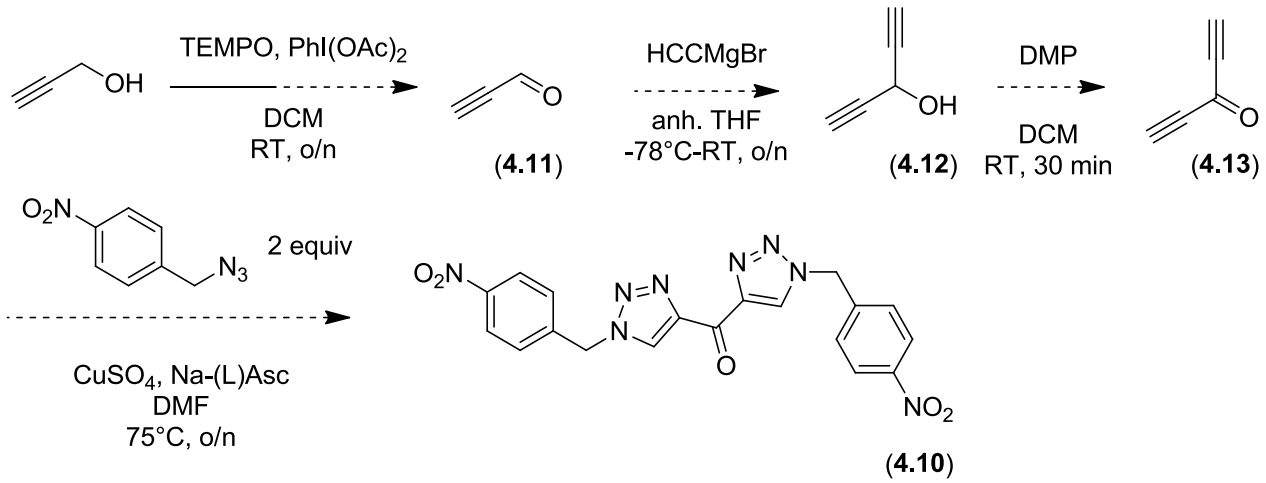

Scheme 4.1. First proposed synthesis of compound **4.10**

4.6.2 Second synthetic route

In a second approach, we tried to prepare intermediate **4.13** in a similar manner to the synthesis[80] of **CP4d**, which proceeds from 4-nitrocinnamic acid through the corresponding acyl chloride prior to an electrophilic desilylation with ethynyltrimethylsilane to prepare intermediate **CP3** (Fig. 3.5). In the approach for intermediate **4.13**, we began from propynoic acid and followed similar steps as the synthesis of **CP3**, with our synthetic route shown below (Scheme 4.2).

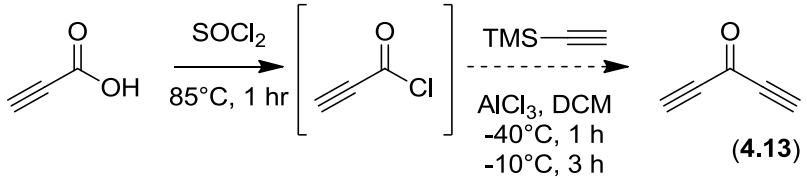

Scheme 4.2. Second proposed synthesis for intermediate **4.13**

However, the isolated yield of product was negligible in this second approach, and thus we were unable to confirm that any of the many products obtained was intermediate **4.13**. Another issue with the reliance on this intermediate is the possible isomerisation of the ketone to the dienol **4.14**, shown below in Figure 4.11. While the isomers are shown in equilibrium, we did not collect data to confirm whether this enolisation was taking place; in particular, it has been shown in the liteature[116] that the compound decomposes rapidly at room temperature. Given this knowledge and the fact that a symmetrical approach would limit our options in building a small library of these compounds, we chose to pursue a different synthetic route.

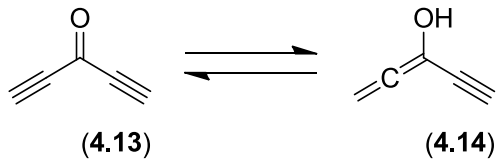

Figure 4.11. Possible enolisation of intermediate **4.13**

4.6.3 Third synthetic route

In our third approach, we chose to build the target compound from one extremity to the other, thus beginning and ending with a CuAAC. The advantage of this scheme over the previous two was the possibility of making modifications at one extremity of the molecule following the preparation of a common intermediate (compound **4.18** in Scheme 4.3 below), in order to generate a small library of compounds all maintaining the presence of one nitro group. We chose to follow this approach to mimic the original study[80] that yielded **CP4d**.

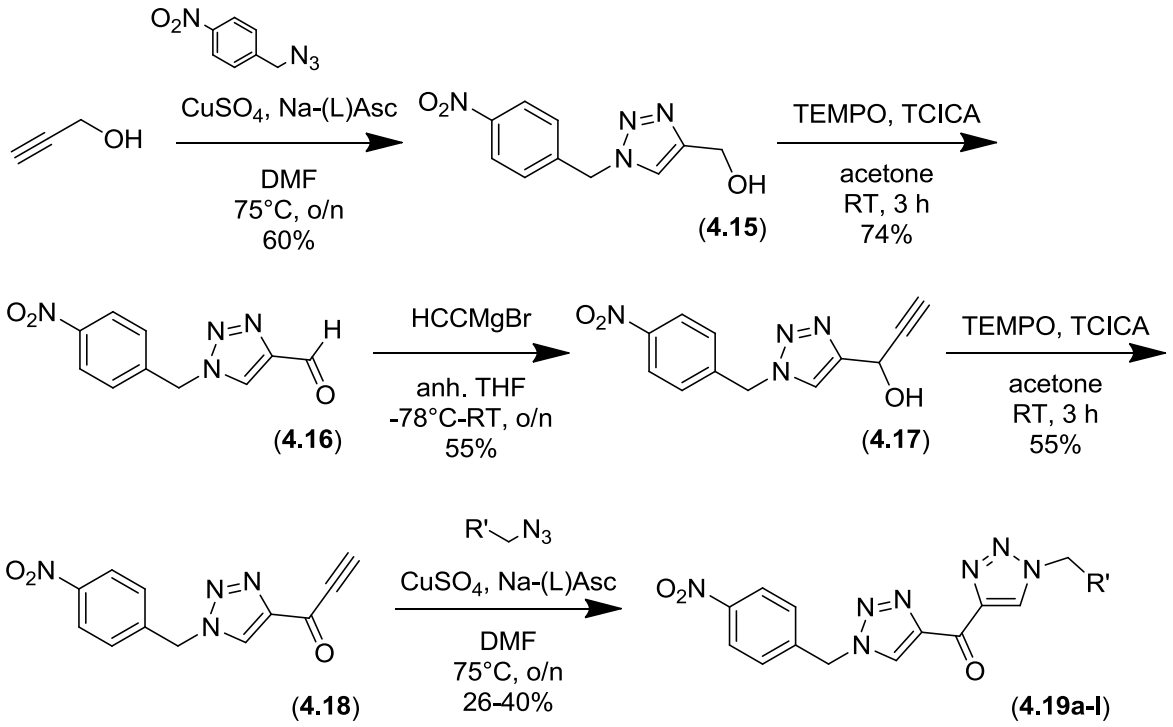

Scheme 4.3. Synthetic approach for the library of bis(triazole) compounds

In the oxidation steps, the low solubility of our intermediate alcohols (**4.15** and **4.17**) in DCM led us to use acetone as the solvent for the reaction. Following the completion of the transformation, the solvent was removed by evaporation under reduced pressure and the crude carbonyl product was dissolved in DCM prior to the washing steps, given that acetone is water-miscible. In the first CuAAC, the low 60% yield of **4.15** is attributed to a loss of product in the aqueous phases due to the presence of DMF as a co-solvent in the extraction with ethyl acetate. In particular, working on a larger scale, the volumes of aqueous washes were reduced for practical purposes, thus likely leading to a greater solubilisation of the product in the aqueous phases due to the presence of a significant volume of DMF. The low yields of the second CuAAC (**4.19**) are attributed to the electron deficient nature of the alkyne, due to its conjugation

with the carbonyl; the yields of the CuAAC varied between 26% and 40%, but without a trend with respect to the electronic effects of the substituent on the azide, suggesting that the low yield is associated with the electron deficient ynone. These yields are also in agreement with those previously observed on the **CP4** series[80].

Given the good potency observed with the trifluoromethyl derivative **4.19e** (Table 4.1 below), we also prepared a symmetrical bis(trifluoromethyl)derivative (**4.24a** in Scheme 4.4), following the same synthetic approach as outlined in Scheme 4.3, but starting with 4-(trifluoromethyl)benzyl azide. As a curiosity, we also prepared a simple bis(triazole) compound with unsubstituted phenyl groups at both extremities of the compound (**4.24b**).

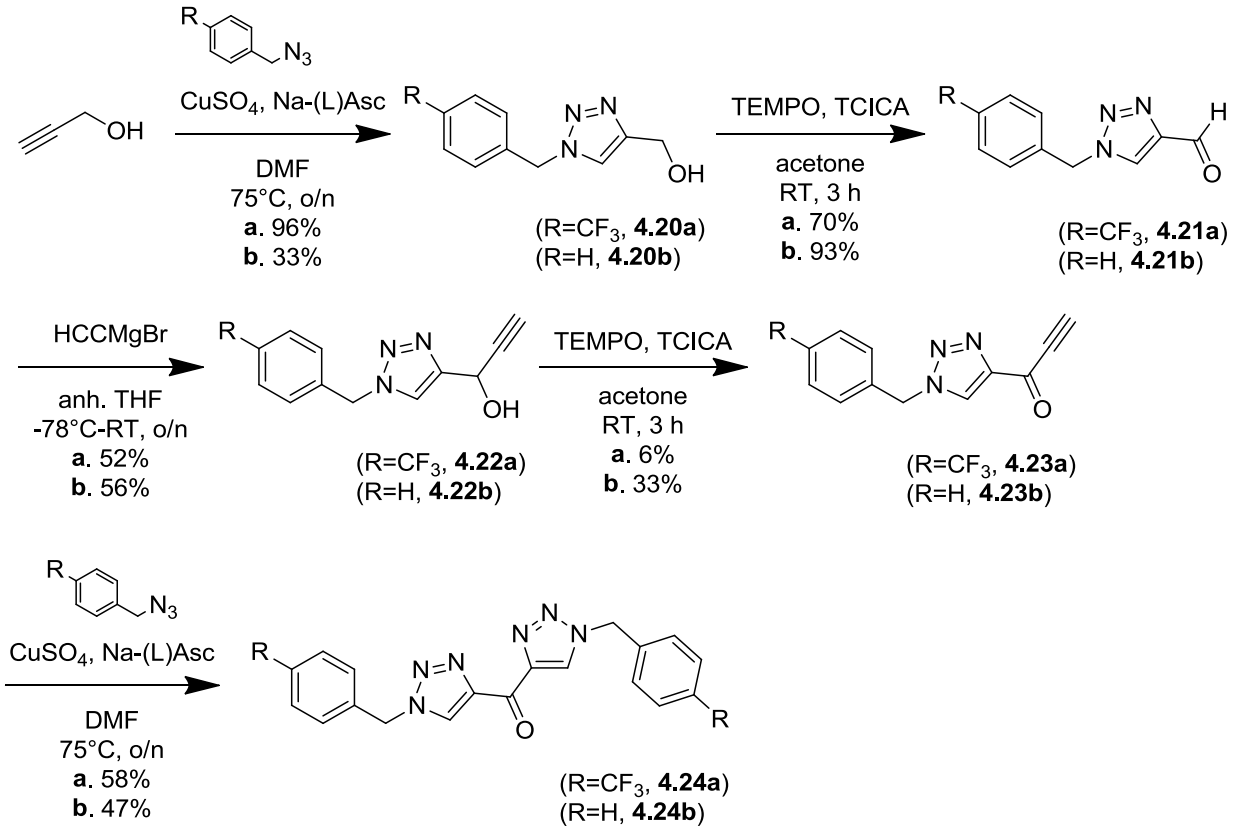

Scheme 4.4. Synthesis of symmetrical 4-(trifluoromethyl)phenyl and phenyl compounds

While some yields were lower than normally expected (particularly **4.20b** at 33% and **4.23a** at 6%), we chose to proceed forward without further optimization, since we had enough material for full characterization and for the final inhibition assays. Had these compounds been the start of another family of compounds as potential inhibitors, we would have optimised those steps in order to have a greater amount of the intermediate ynones (**4.23a** and **4.23b**) for a divergent synthesis of final products.

4.7 Inhibitory potential of the bis(triazole) derivatives

4.7.1 Results of the bis(triazole) library of compounds

The full list of prepared compounds is shown in Table 4.1, along with their inhibitory potency, evaluated using our standard IC_{50} assay (see Section 3.4.1). In this table, as was done previously, the entry "n.d." denotes that inhibition was not detected at the compound's indicated solubility limit. The entry ">100" denotes that inhibition was observed, but that we were unable to quantify the IC_{50} value due to the large error inherent to the Dixon plot. In particular, we chose 100 μM as the cutoff value due to the fact that all those IC_{50} values were evidently above 100 μM, as estimated by the extrapolation to the (negative) x-intercept of the Dixon plot, and that the highest concentration of inhibitor in solution generally ranged between 5 and 30 μM.

Table 4.1. Bis(triazole) compounds and their inhibitory potency

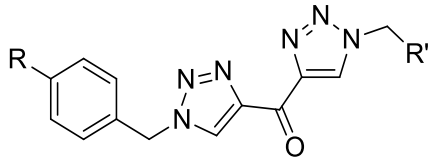

Compound	R group	R' group	IC_{50} (μM)
CP4d	N/A	N/A	2.1 ± 0.3
4.19a	$-NO_2$	-Ph	n.d. @ 32 μM
4.19b	$-NO_2$	-(2-NO_2)Ph	64.1 ± 4.6
4.19c	$-NO_2$	-(3-NO_2)Ph	> 100
4.10	$-NO_2$	-(4-NO_2)Ph	14.1 ± 1.7
4.19e	$-NO_2$	-(4-CF_3)Ph	25.9 ± 1.8
4.19f	$-NO_2$	-(4-OCF_3)Ph	> 100
4.19g	$-NO_2$	-(4-CN)Ph	> 100
4.19h	$-NO_2$	-(4-CH_3)Ph	n.d. @ 12 μM
4.19i	$-NO_2$	-(4-OCH_3)Ph	n.d. @ 15 μM
4.19j	$-NO_2$	-(4-F)Ph	n.d. @ 15 μM
4.19k	$-NO_2$	-(4-Br)Ph	n.d. @ 5 μM
4.19l	$-NO_2$	-cyclohexyl	n.d. @ 32 μM
4.24a	$-CF_3$	-(4-CF_3)Ph	n.d. @ 31 μM
4.24b	-H	-Ph	n.d. @ 32 μM

Assay run with a concentration of 54.5 μM **AL5**

4.7.2 Discussion of the bis(triazole) compound results

Given the strong inhibition observed with compound **4.10**, the first compound that we prepared, we began with a typical medicinal chemistry approach, first removing one nitro group (**4.19a**) and then walking it around the aromatic ring, in order to determine the optimal position for substitution, among *ortho* (**4.19b**), *meta* (**4.19c**), and *para* (**4.10**) positions, prior to modifying that substituent. Unlike inhibitor **CP4a**, which maintains good inhibitory potency despite the removal of the East nitro group compared to **CP4d**, the removal of one nitro group on this scaffold (**4.19a**) resulted in a complete loss of potency at the compound's solubility limit. However, among the three positions evaluated for the nitro group, we observed that, once again, the *para* position (**4.10**) is favoured, leading to the lowest IC_{50}.

In a second approach, we were inspired by the Hammett parameters, which relate the electron withdrawing effect of substituents to the dissociation of benzoic acid. In a more general sense, they may be used to qualitatively compare the electron withdrawing or donating effect of a variety of substituents on an aromatic ring. Following the Hammett parameter scale, we compared *para* substituents nitro, cyano and trifluromethyl, which have respective decreasing sigma parameter (σ_{para}) values[117] of 0.78, 0.66 and 0.54 in the *para* position. However, our results did not correlate with this trend; while both **4.19g** and **4.19e** had lower IC_{50} values than nitro derivative **4.10**, the less electron-withdrawing trifluoromethyl **4.19e** resulted in a stronger inhibitor (IC_{50} = 26 μM) than the cyano derivative **4.19g** (IC_{50} > 100 μM).

We also looked at the steric and electron donating effect of substituents, by comparing trifluoromethyl derivative **4.19e** with methyl (**4.19h**), methoxy (**4.19i**) and trifluoromethoxy (**4.19f**) derivatives. The trifluoromethoxy group is unusual in that it is electron donating by resonance with the oxygen, but electron withdrawing with its trifluoromethyl group; overall, the

trifluoromethoxy group[118] is not conjugated to the aromatic ring to which it is bound, due to the p-orbital electrons of the oxygen being delocalised in the σ* orbitals of the C-F bonds. This group also increases lipophilicity more than trifluoromethyl and methoxy substituents alone. On our inhibitor scaffold, the trifluoromethoxy group resulted in a weak inhibitor, but more potent than either methyl derivative. This result suggests that there is a greater affinity for electron withdrawing substituents than electron donating ones at that position on the scaffold.

Compounds **4.19j** and **4.19k** featured a simple halogen at the 4-position of the aromatic ring, thus placing an electron-withdrawing substituent on the phenyl group, albeit less electron withdrawing than the nitro, cyano and trifluoromethyl groups. However, these compounds showed no inhibitory potency at their solubility limits, suggesting that the scaffold may require stronger electron withdrawing groups on both phenyl rings, as evidenced by the fact that few compounds showed inhibitory effects on TG2. In the case of bromide derivative **4.19k**, the size of the atom may also have played a role in the sterics of binding to the enzyme.

Cyclohexyl derivative **4.19l** was prepared with the goal of probing the importance of the aromatic ring, which has the potential for π-related interactions. The lack of any inhibition at the compound's solubility limit may suggest that the aromatic group is necessary, although we saw no inhibition with the unsubstituted phenyl in **4.19a**, thus rendering this result inconclusive.

As alluded to above, we also prepared a symmetrical bis(trifluoromethyl) derivative **4.24a**, based on the good inhibition seen with the mono(trifluoromethyl) inhibitor **4.19e**. However, this symmetrical compound showed no inhibition at its solubility limit, a result which again suggests that the bis(triazole) scaffold has little tolerance for substitutions, and reaffirms the importance of a nitro group for potency. The nitro group has been a staple of many reversible

inhibitors (shown below in Figure 4.12), notably ***m*-CP30a**, **CP4d**, and now compounds **4.8** and **4.9**, as well as **4.10** and **4.19e**. We also observed no inhibition with the symmetrical unsubstituted compound **4.24b**.

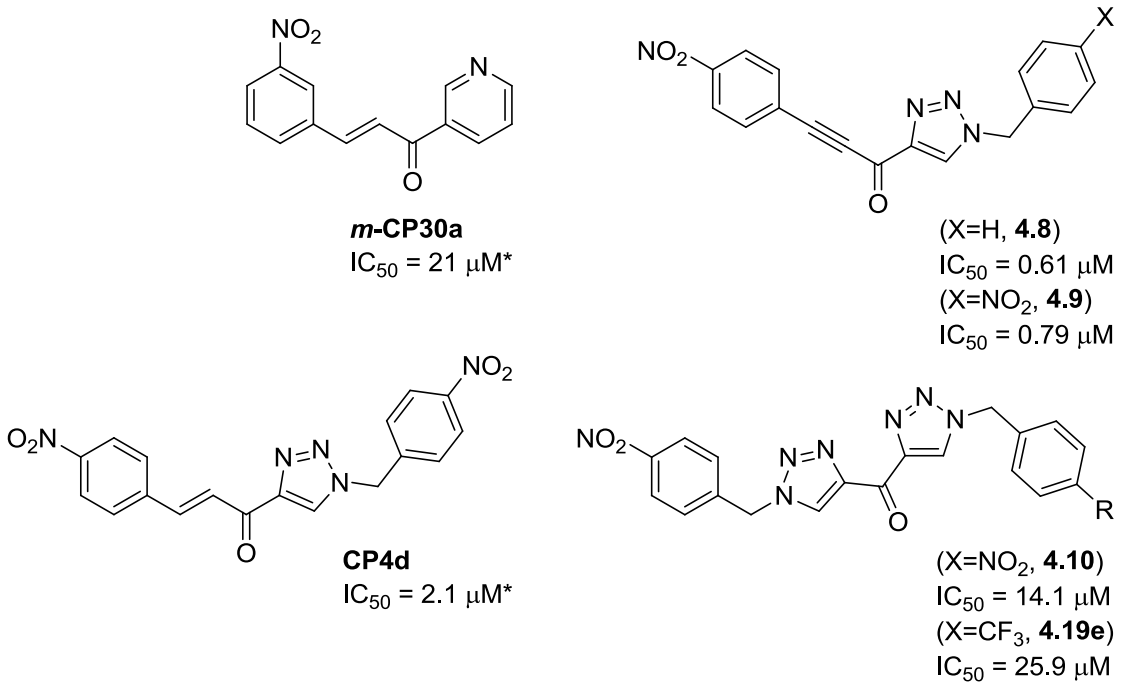

Figure 4.12. Potent nitro-containing reversible inhibitors and their respective IC_{50} values (those obtained with gplTG are indicated with an asterisk)

Among the family of compounds shown in Table 4.1, we also attempted to prepare a trifluoromethylketone variant (**4.30**), shown below in Scheme 4.5. This substituent would have been interesting to study due to its strong electron-withdrawing quality, as well as the presence of an sp²-hybridised oxygen. In previous work, performed[78] in the discovery of the original cinnamoyl inhibitors, the presence of a nitro group, a BOC or an FMOC protecting group, or a methyl ester on the West end of the cinnamoyl benzotriazole compounds resulted in an increase

in inhibitory potency against gplTG, thus suggesting a preference for substituents with an sp^2-hybridised oxygen. While the preparation of the azide **4.29** was more involved than the previous ones used in the various CuAAC described to date, it was inspired by the synthesis of diazirinyl azide **3.8**, and we obtained the new azide **4.29** in reasonable yield (11% overall). However, the electrophilic carbonyl appeared to interfere in the CuAAC with scaffold intermediate ynone **4.18**, such that we only recovered decomposition products. The potential interference of the electrophilic carbonyl was also observed in the preparation of bromide **4.28**; the Appel reaction on the diazirine scaffold to prepare the corresponding bromide **3.7** had a much higher yield (98%) than the 22% observed with **4.28**.

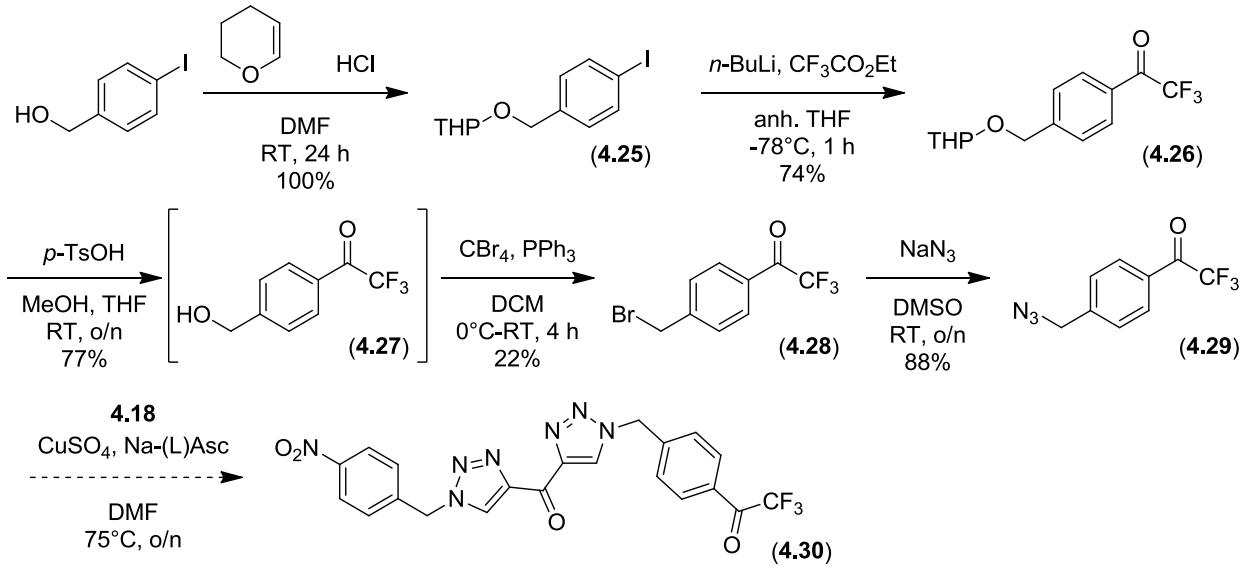

Scheme 4.5. Preparation of azide **4.29** towards bis(triazole) **4.30**

4.7.3 K_i determination

Similarly to the approach taken with the photolabile inhibitor **3.1**, we determined the mode of inhibition of our most potent bis(triazole) inhibitor, compound **4.10**. As outlined in Sections 3.4.2 and 3.4.3, we determined apparent K_M and V_{max} values for substrate[26] **AL5** at increasing concentrations of inhibitor, as shown below in Figure 4.13.

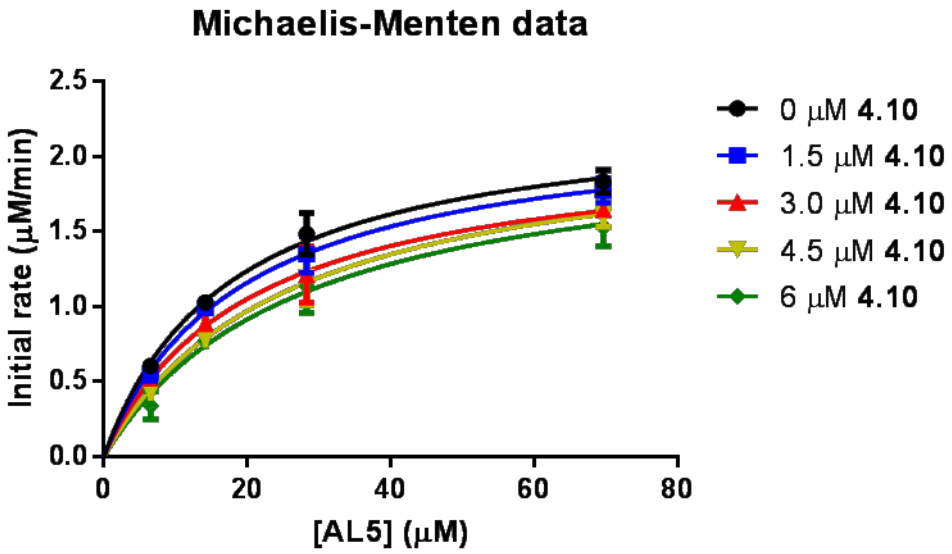

Figure 4.13. Michaelis-Menten curves at increasing concentrations of **4.10**

By non-linear regression fitting of the curves in Figure 4.13 to the hyperbolic Michaelis-Menten equation (eq. 3.1), we established the apparent K_M and V_{max} values at each concentration of inhibitor, and these extrapolated constants were plotted in Figure 4.14 below.

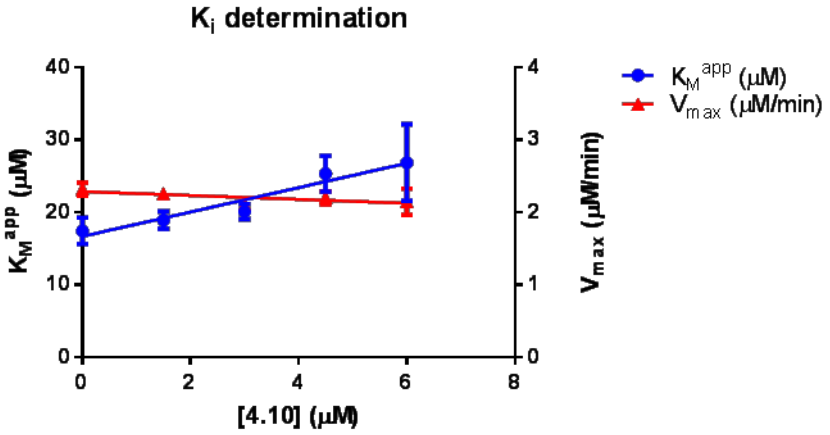

Figure 4.14. K_i determination for inhibitor **4.10**

Given that the value of V_{max} remains relatively constant, with a slope of -0.027 ± 0.013 min^{-1}, and that K_M^{app} clearly increases proportionately to the concentration of inhibitor, we established that inhibitor **4.10** is also competitive with respect to the acyl-donor substrate, with a K_i value of 9.9 ± 1.6 μM.

4.8 Glutathione resistance

Following the kinetic evaluation of the most potent compound of the series, inhibitor **4.10**, we subjected it to our ^{1}H NMR assay for GSH resistance. Unlike previous inhibitors, the spectra of this inhibitor and GSH in solution together resulted in a simple additive spectrum, even at the last time-point evaluated (72 hours, Figure 4.15). The only peaks in the aromatic region that appear to be affected over time are those that correspond to GSH, suggesting a redox reaction between GSH and the solvent, DMSO, a known oxidant[102]. These results were highly encouraging and led us to believe that we had prepared an inhibitor with significantly increased resistance to glutathione addition, a quality that more than offset the slightly weaker potency (K_i of 10 μM, compared to 1 μM for **CP4d**).

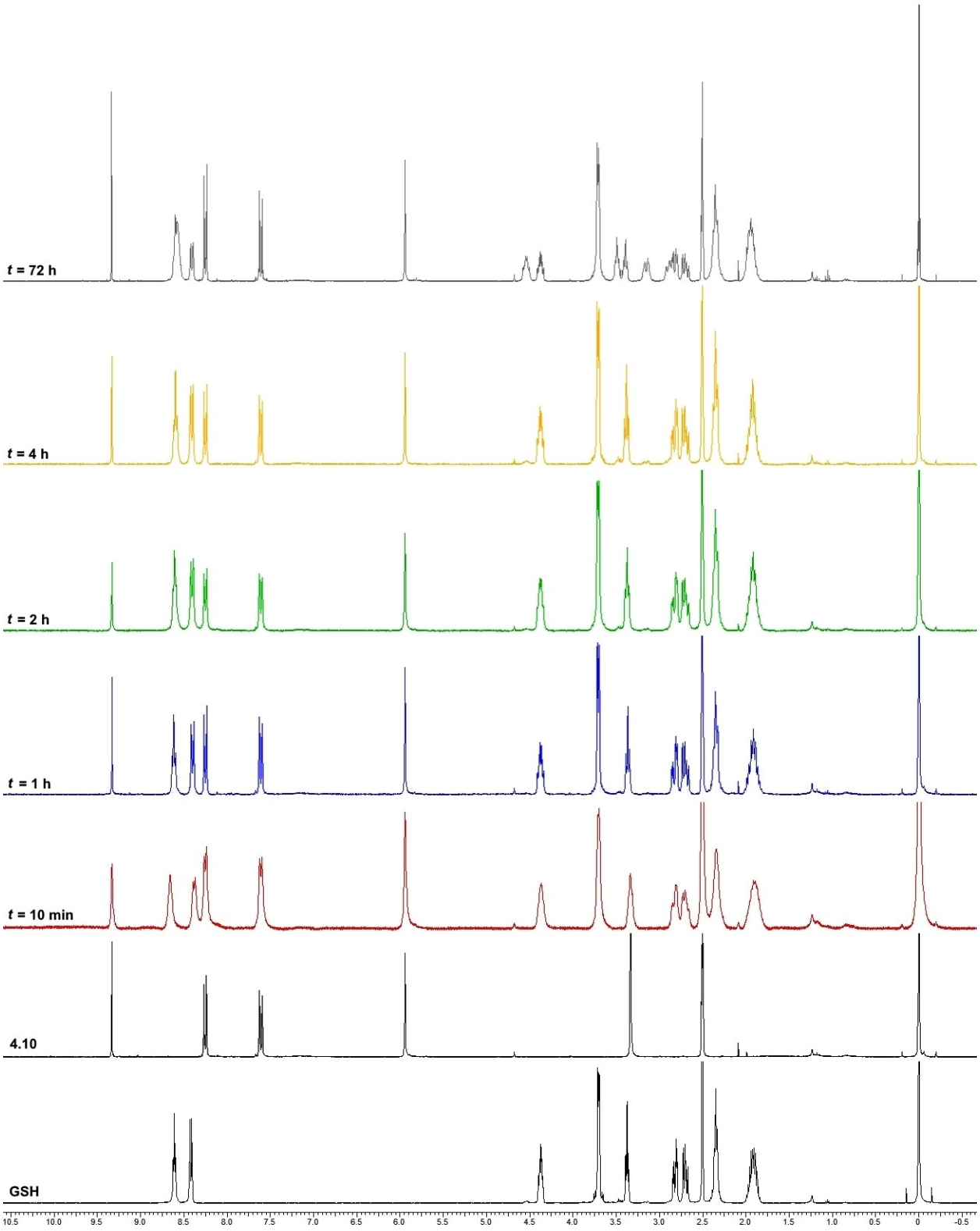

Figure 4.15. GSH susceptibility of inhibitor **4.10**

4.9 Evaluation *in vitro*

Following the positive results obtained with our ^{1}H NMR assay, we evaluated the potency of inhibitor **4.10** under our standard assay conditions (Section 3.4.1), in a buffer supplemented with 1 mM GSH, to mimic intracellular conditions. We ran both a blank (substrate, no enzyme) and a positive control (substrate, enzyme, no inhibitor) with each experiment in order to confirm that GSH did not result in an increased release of *para*-nitrophenolate and that the tripeptide did not affect the enzyme's activity.

The inhibitor was added to the GSH-doped buffer and incubated at room temperature for one hour prior to the addition of substrate **AL5** and enzyme and the subsequent monitoring of the enzyme-catalysed hydrolysis. However, we observed no detectable inhibition following incubation between the inhibitor and GSH (Figure 4.16 below). By reducing the incubation time as much as possible, we observed some residual inhibition, but less than was observed in the absence of GSH. This experiment suggested that the inhibitor reacted on a minute time-scale with GSH, and that it remained susceptible to GSH addition despite evidence of the contrary in our ^{1}H NMR experiment.

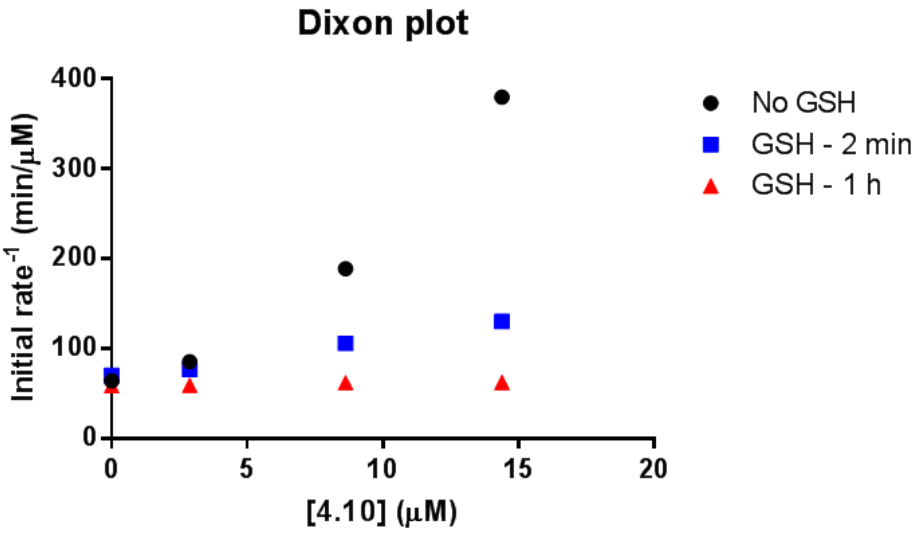

Figure 4.16. Comparison of the reciprocal initial rates for inhibitor **4.10** under different conditions

4.10 Future directions

Overall, while our initial ^{1}H NMR results with these compounds suggested good resistance to nucleophilic attack by glutathione, the *in vitro* experiments showed a different result. This difference may be related to the significantly different assay conditions between GSH resistance and inhibitory potency; ideally, the reactivity of our compounds with GSH would be investigated in a similar buffer to that used in the inhibition assays, instead of DMSO-d_6. With a more accurate assay for GSH resistance, our inhibitors and their derivatives would be better evaluated and the results could be used to guide the next series of inhibitors. We propose that the nucleophilic thiolate of GSH (present in greater concentration in water than in DMSO) attacks our compound **4.10** at its carbonyl carbon, resulting in the hemithioketal shown below (Figure 4.17).

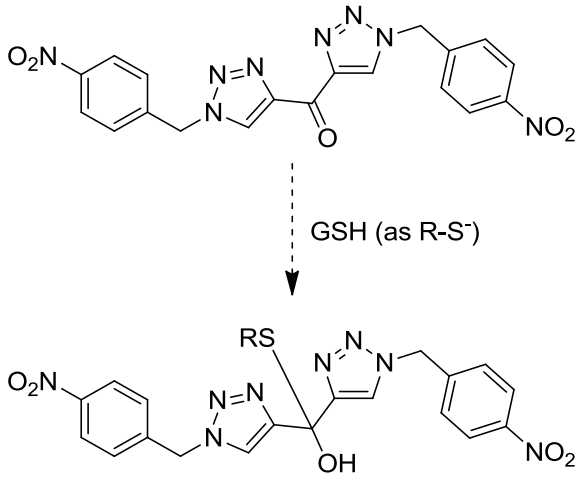

Figure 4.17. Proposed adduct formed between GSH and inhibitor **4.10**

Chapter Five: **Probing of the alkynyl scaffold as reversible inhibitors**

5.1 Synthesis and evaluation of the alkynyl derivatives prepared previously

Following the development of a scaffold with greater resistance to glutathione addition in DMSO (Chapter 4), we chose to study the alkynyl scaffold (of compounds **4.8** and **4.9**) in greater detail. While the compounds, shown below in Figure 5.1, remained susceptible to GSH addition, they were also the most potent reversible inhibitors prepared by the Keillor group to date.

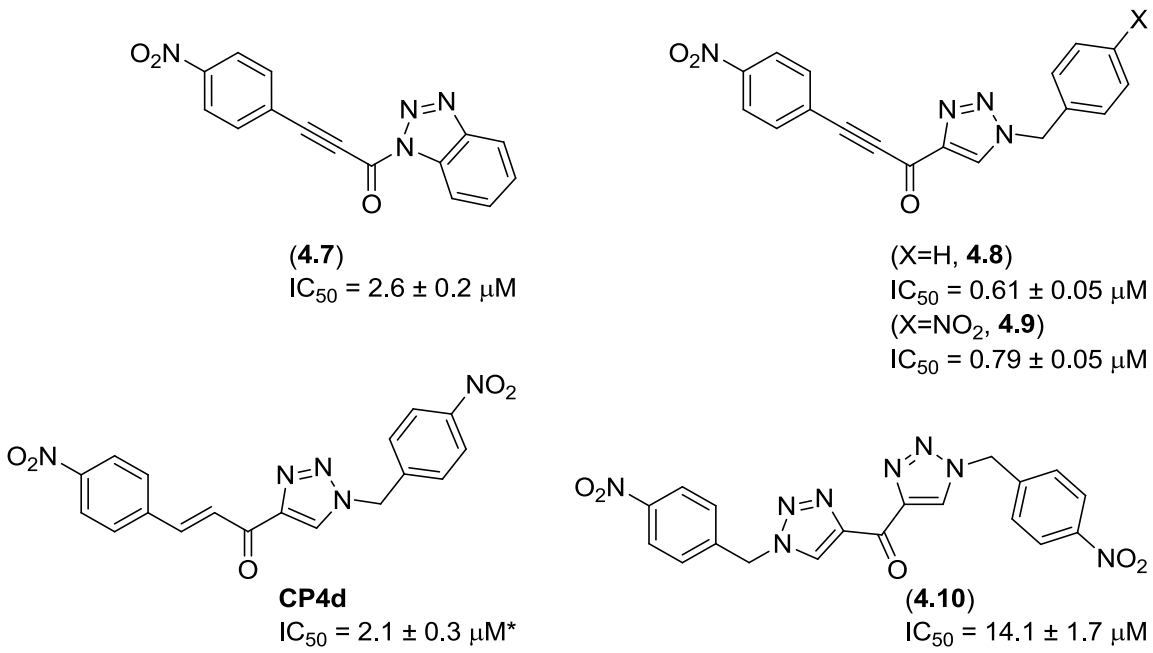

Figure 5.1. Initial alkynyl compounds and the previous key inhibitors **CP4d** and **4.10**

Prior to studying this inhibitor scaffold in further detail, we determined the mode of inhibition for compound **4.9**, in order to compare it to **CP4d** and **4.10**, both of which present a nitro group at each extremity of the molecule (Figure 5.1), and both of which are competitive

inhibitors with respect to the acyl donor substrate. In the same process as described in Sections 3.4.2 and 3.4.3, we first determined apparent K_M and V_{max} values at increasing concentrations of **4.9**, as shown in Figure 5.2 below.

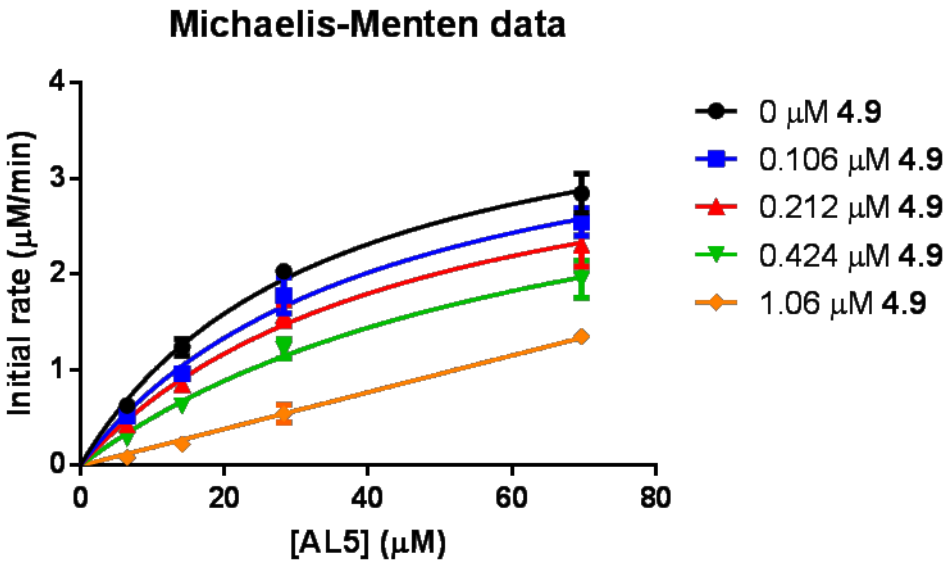

Figure 5.2. Michaelis-Menten curves at increasing concentrations of **4.9**

From those curves, fitted to the hyperbolic Michaelis-Menten equation (eq. 3.1) by non-linear regression using GraphPad Prism 6, we extrapolated the apparent K_M and V_{max} values. We disregarded the data obtained at a concentration of 1.06 µM **4.9** (orange trace in Figure 5.2) due to the fact that the curve did not show hyperbolic behaviour over the range of concentrations of substrate **AL5** that were used in this experiment. The K_M^{app} and V_{max} values thus obtained were then plotted against the concentration of **4.9**, as shown below in Figure 5.3.

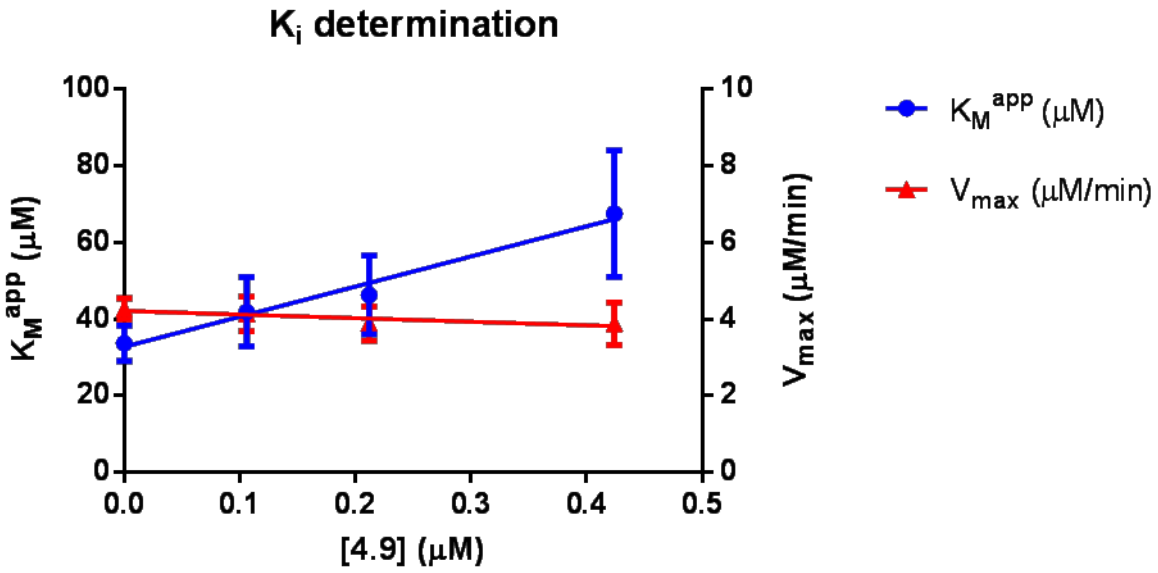

Figure 5.3. K_i determination for inhibitor **4.9**

In a fashion similar to that observed for inhibitors **3.1** and **4.10**, the apparent K_M values increased proportionately to the concentration of inhibitor, while V_{max} remained relatively constant, with a slope of -0.94 ± 0.36 min^{-1}. These combined results show that, like **CP4d** and **4.10**, inhibitor **4.9** is also competitive with respect to the acyl donor substrate. By plotting the K_M^{app} values against the concentration of **4.9**, we calculated a K_i of 0.42 ± 0.05 μM. This K_i value is the lowest that has been established in the Keillor group for reversible hTG2 inhibitors; **CP4d** had a K_i value[80] of 174 nM with gplTG, but that value[89] increased to 1.0 μM with hTG2. In light of the strong inhibitory potency displayed by compounds **4.8** and **4.9**, we therefore chose to probe the relevance of the West substituent by preparing a small family of derivatives of this alkynyl scaffold.

5.1.1 Development of a synthetic route for the synthesis of inhibitor 4.9

In the initial synthesis of the alkynyl compounds, of which compound **4.9** was representative, we chose to follow a linear synthesis ending with a CuAAC with two different benzyl azides; this approach would allow us to vary the substituents on the East end of the molecule, similar to what had been done in the original study[80]. As shown below in Scheme 5.1, a Sonogashira coupling between propargyl alcohol and 4-iodonitrobenzene led to primary alcohol **5.1**, which was oxidised (where [O] denotes any oxidant) to the corresponding aldehyde **5.2** using either Dess-Martin periodinane (DMP) or 2,2,6,6-tetramethyl-1-piperidinyloxyl (TEMPO), as described below in Section 5.1.2. The Grignard addition of ethynylmagnesium bromide allowed us to install the second alkyne functionality in **5.3**, in a compound that was then reoxidised to a ketone (**5.4**) under the same conditions as those used for aldehyde **5.2**, prior to the final CuAAC to obtain inhibitors **4.8** and **4.9**. While the conditions for the Sonogashira coupling and the Grignard addition were well-established, we optimised the oxidation and CuAAC steps in order to maximise the overall yield of the ynone intermediate **5.4** and of the final compounds **4.8** and **4.9**.

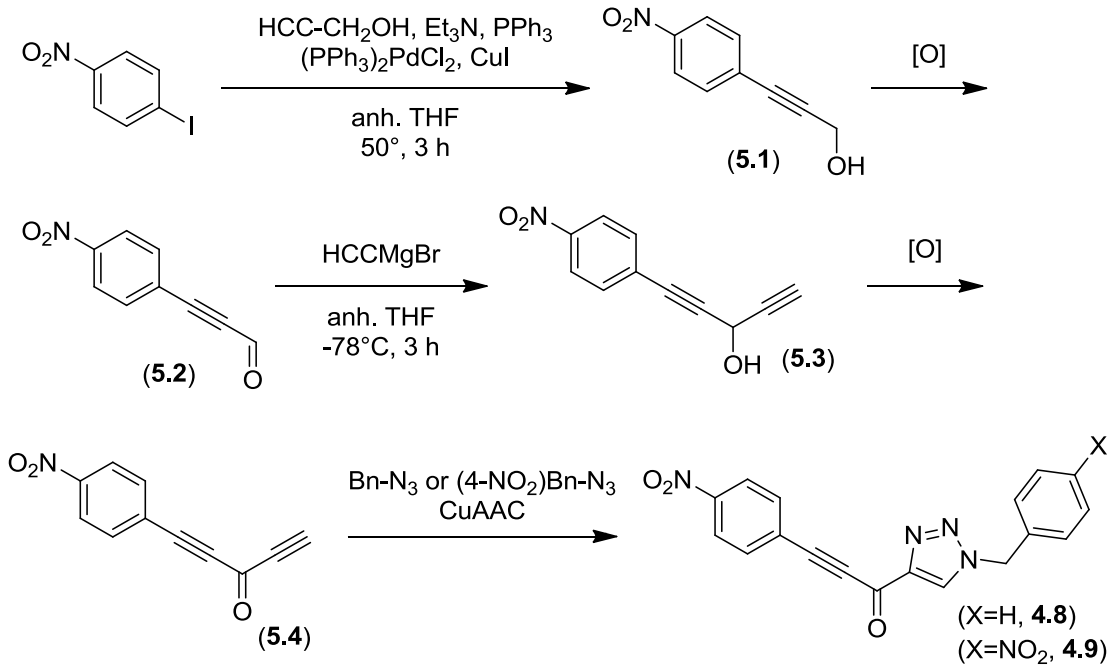

Scheme 5.1. Basic approach for the synthesis of the alkynyl compounds

5.1.1.1 Choice of the oxidant

The initial synthetic scheme for the alkynyl derivatives of **CP4d** was developed by Dr. Christophe Pardin, along with Élise de Francesco, an undergraduate student in the group, for the synthesis of inhibitor **4.8**. Élise tested both Dess-Martin periodinane (DMP) and pyridinium chlorochromate (PCC) in the preparation of aldehyde **5.2**; given that the respective yields were 65% and 32%, we opted to use DMP for the oxidation steps. However, because of the high cost of DMP and the large quantities necessary (1.2 molar equivalents), we optimized the use of a different oxidant, namely TEMPO, in the study of this scaffold. TEMPO is used in a catalytic amount, and a second reagent, such as sodium hypochlorite or a hypervalent iodine as in periodic acid or iodosobenzene, is used to regenerate the radical. Initial work, done on the bis(triazole) scaffolds described in Chapter 4, involved the use of trichloroisocyanuric acid (TCICA) as a

radical-regenerating agent, and produced the corresponding aldehyde **4.16** in good yield (74%) and the ketone **4.18** in moderate yield (55%). Unfortunately, the use of TCICA in the oxidation on the alkynyl scaffold resulted in two products from the reaction with alcohol **5.1**, both containing a *para*-substituted benzene ring and an aldehyde functionality, with no other protons seen by ^{1}H NMR. We obtained moderate results with (diacetoxyiodo)benzene, with an average yield of 53% for the aldehyde **5.2** and 48% for the ketone **5.4**. Other ongoing research projects within the Keillor group required DMP; once a less expensive supplier was found, we returned to the use of DMP, given its shorter reaction time (less than 3 hours, compared to 16 hours for TEMPO) and higher yields. In this return to DMP, we obtained yields of 94% and 88% for the aldehyde **5.2** and ketone **5.4**, respectively; these higher yields than those obtained earlier are attributed to having gained more experience from working in the synthesis lab over time.

5.1.1.2 Optimisation of the azide-alkyne cycloaddition

At that point in time, the previously reported CuAAC conditions[80] (75°C overnight) were still being used; while inhibitor **4.8** was first obtained in low yield (8%), a second attempt[119] resulted in isolating **4.8** in 36% yield but **4.9** in even lower yield, at 2%, although the isolated regioisomer was not identified. The issue of regioselectivity arose in trying to prepare more of compound **4.9** in order to repeat the kinetic assays. Two regioisomers were isolated, namely the 1,4-substituted triazole (desired) and the 1,5-substituted triazole. Efforts to separate the two compounds by flash column chromatography (7:3 hexanes:ethyl acetate) were unsuccessful, as was trituration with acetonitrile. In light of the difficulties that were being observed with this synthesis, other avenues were pursued, outlined below in Section 5.1.4. However, ultimately, the use of the cycloaddition conditions outlined for photolabile inhibitor

3.1, namely the use of one equivalent of copper(I) iodide instead of a catalytic amount, along with a DCM/ethyl acetate eluent system for column chromatography, allowed us to obtain pure **4.9**. This result was confirmed by NOESY, as judged by the interaction between the methylene and triazole protons (Spectrum for **4.9** in the Appendix). It is expected that, by performing the reaction at room temperature, instead of 80°C, the 1,4-substituted triazole was favoured over the more sterically-hindered 1,5-substituted triazole; as for the purification, the use of DCM as the less polar phase, instead of hexanes, resulted in better solubility of the crude product, and thus a tighter band of product migrating through the column, leading to improved separation. The optimized synthesis is shown below in Scheme 5.2.

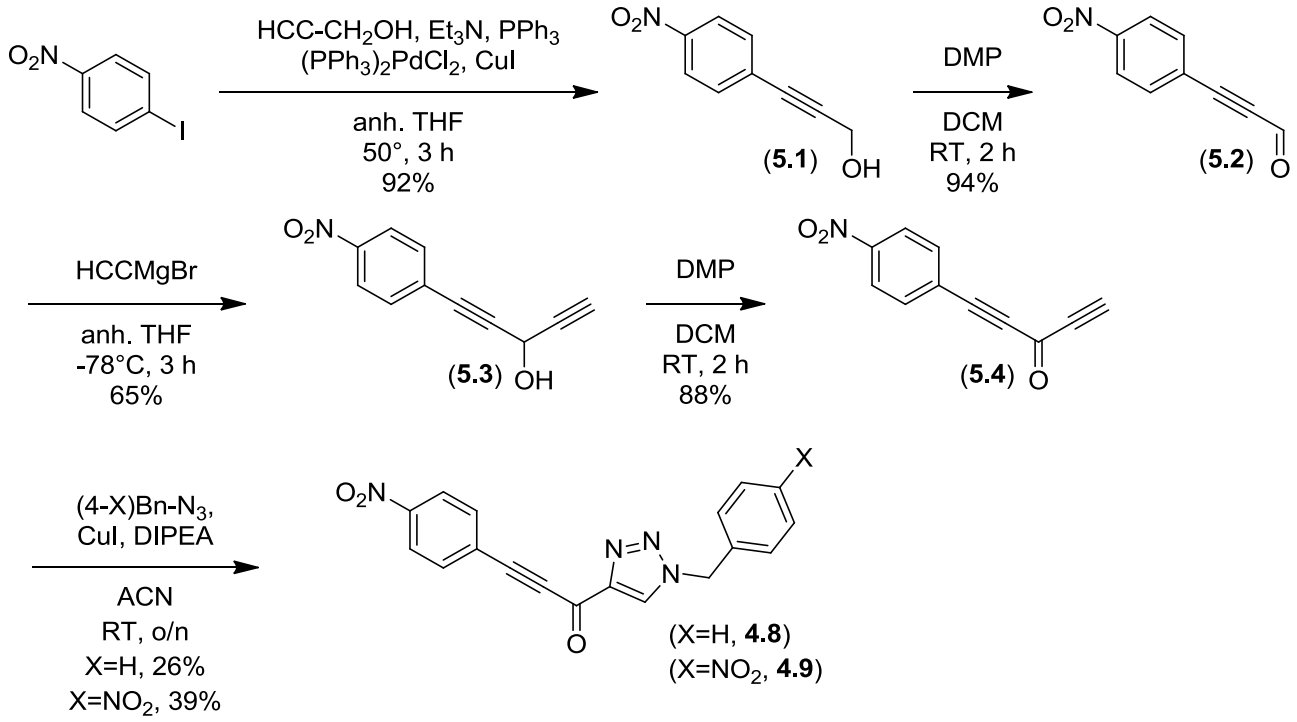

Scheme 5.2. Optimised synthesis of the alkynyl derivatives

5.1.2 Other attempted synthetic routes in the synthesis of inhibitor 4.9

As we alluded to in the previous section, we also attempted different synthetic routes to obtain inhibitor **4.9**. While the first scheme (Scheme 5.2 above) was eventually successful, the negative results also had an impact on the approach to the study of the alkynyl scaffold, as discussed further below in Section 5.2. In particular, we were forced to build each compound from the West end to the East end, despite having only two substituents at the East end, but seven at the West. In that respect, it would have been easier to build the molecule in the other direction, in a reverse approach, as outlined below.

5.1.2.1 Reverse approach to the synthesis

Because of the mixed regioselectivity observed in using the CuAAC as the final step, we tried to build the target compound **4.9** in the reverse direction, beginning with the CuAAC and ending with the Sonogashira coupling. In particular, we knew that we could prepare ynone **4.18** according to Scheme 4.3 in the synthesis of the bis(triazole) compounds, and so we aimed to use that common intermediate in the synthesis of the alkynyl derivatives, ending with a Sonogashira coupling to the substituted iodobenzene of our choice, as shown below (Scheme 5.3). We also tried the Sonogashira coupling with the intermediate alcohol **4.17**, such that the produced **5.5** may then be oxidized to the desired inhibitor **4.9**.

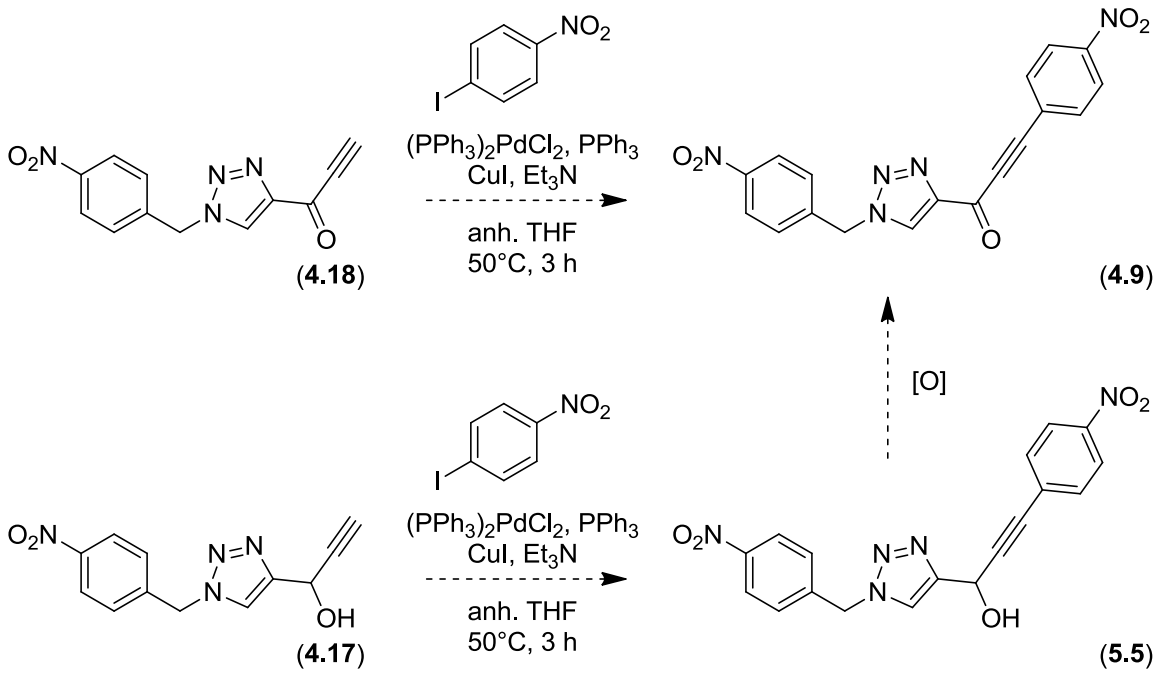

Scheme 5.3. Sonogashira coupling of **4.18** or **4.17** and 4-iodonitrobenzene to prepare inhibitor **4.9**, either directly or through intermediate alcohol **5.5**

However, both Sonogashira couplings were unsuccessful despite multiple attempts, likely due to the interference of the various functionalities in the intermediate alkynes **4.17** and **4.18**. In particular, we recovered none of the target product, as verified by ^{1}H NMR, but also no starting material. We therefore disregarded this synthetic route, despite its potential elegant simplicity in promoting a divergent synthesis for two key classes of inhibitors, namely the bis(triazole) and alkynyl derivatives.

5.1.2.2 Alternative convergent approach to the synthesis

In a different approach, we chose to build up both sides of the scaffold and to join them through the bond between the alkyne and the carbonyl functionalities. We first proposed a nucleophilic addition of a carbanion to an aldehyde, using the intermediate aldehyde **4.16** from the bis(triazole) synthesis (Scheme 4.3). We prepared the alkyne **5.7** in a manner similar to the synthesis of **5.1**, but using ethynyltrimethylsilane for the Sonogashira coupling to form intermediate **5.6**, that was then deprotected to generate the terminal alkyne of **5.7**. To generate the carbanion, we used *n*-butyllithium to deprotonate the terminal alkyne formed according to Scheme 5.4 below, and the acetylide was then used in a nucleophilic addition to aldehyde **4.16**. In a similar approach to that described in Scheme 5.3, the resulting alcohol **5.5** would have been oxidized to prepare final inhibitor **4.9**.

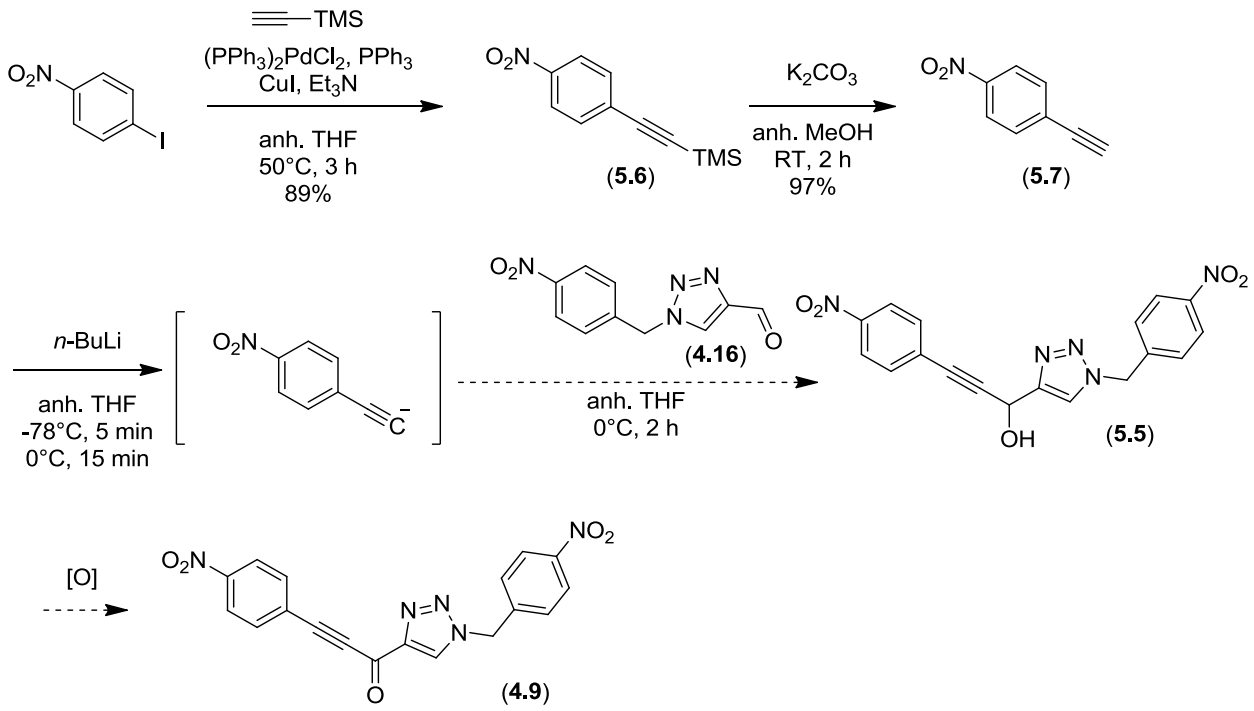

Scheme 5.4. Coupling of an acetylide with an aldehyde to prepare inhibitor **4.9** through intermediate alcohol **5.5**

At the conclusion of the coupling step between alkyne **5.7** and aldehyde **4.16**, we recovered none of the targeted alcohol **5.5**, but rather varying amounts of the aldehyde **4.16** and a significant quantity of alkyne **5.7**. In order to verify that we were generating the acetylide, we quenched the reaction with D_2O, such that the acetylide would become deuterated upon workup, and the signal for the terminal proton would not be observed by ^1H NMR. In this manner, we were able to conclude that the issue stemmed from the nucleophilic attack of the carbanion on the aldehyde, and not the generation of the acetylide. The varying quantities of recovered aldehyde **4.16** may be attributed to either its decomposition from the slight excess of base that was used, or to its low solubility in the 90% hexanes eluent system used in column

chromatography. A better approach would have been to use a different eluent system for the column, such as replacing hexanes by DCM, which solubilised the crude product to a greater extent. However, the low polarity of the alkyne **5.7** required a system that was less polar than possible with a combination of DCM and ethyl acetate. We also added[120] zinc(II) chloride in an attempt to enhance the electrophilicity of the aldehyde by virtue of the ability of the Lewis acid to coordinate to the carbonyl oxygen, and thus increase the partial positive charge of the carbonyl carbon and render it more electrophilic. However, we again recovered starting aldehyde **4.16** and deuterated **5.7**.

In an effort to increase the electrophilicity of the carbonyl compound in a different manner, we prepared the acid chloride derivative of aldehyde **4.16**, by going through a carboxylic acid (**5.8**), as shown in Scheme 5.5 below. This acid chloride would then be used in the coupling reaction with terminal alkyne **5.7** to obtain inhibitor **4.9** directly.

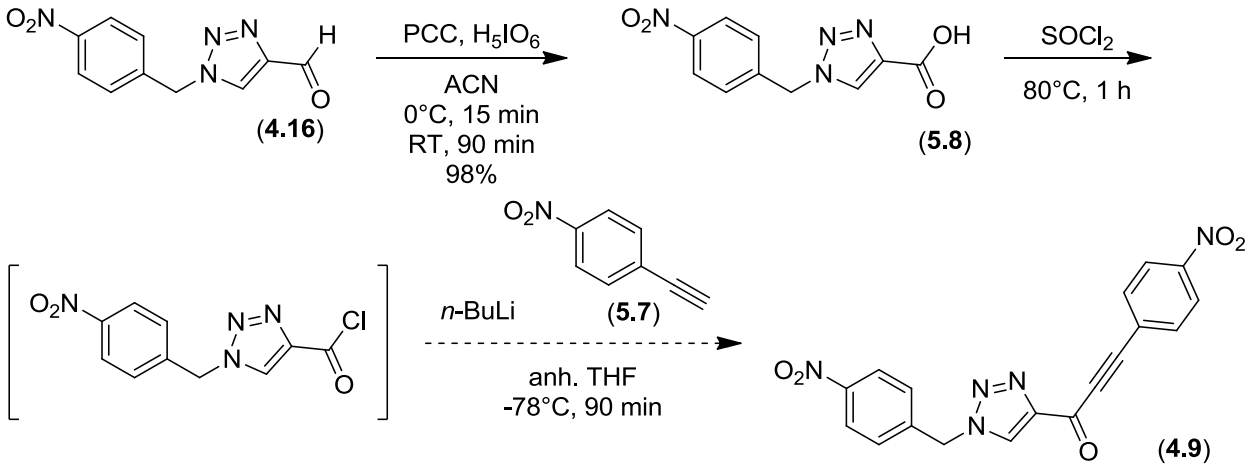

Scheme 5.5. Coupling of an acetylide with an acid chloride to prepare inhibitor **4.9**

While the oxidation to the carboxylic acid **5.8** was highly successful, in essentially quantitative yield, we recovered various products of decomposition, and the alkyne **5.7** from the attempted coupling reaction. However, after quenching the reaction with D_2O, the recovered alkyne **5.7** was approximately 90% deuterated (as determined by ^1H NMR), suggesting again that the issue remained with the low nucleophilicity of the acetylide. Furthermore, we were able to confirm that the acid chloride had indeed been formed; otherwise, the acetylide would have been quenched by the carboxylic acid proton, and we would not have deuterated it upon workup.

After all these experiments, upon reattempting the synthesis outlined in Scheme 5.2, inhibitor **4.9** was obtained in moderate yield, although the lessons learned during the pursuit of a different synthetic route were not lost. Specifically, the work provided us with the knowledge that the reverse and alternative convergent synthetic routes would not be applicable in the preparation of the alkynyl library of compounds, which would therefore have to be built from the West to the East end.

5.2 Synthesis and evaluation of a library of substituted alkynyl derivatives

In order to optimise the screening of multiple scaffold modifications, we varied the substituent at the West end, and then prepared two compounds for each West substituent. We opted for the simple benzyl and 4-nitrobenzyl derivatives on the East end, mimicking the distinction between **CP4a** and **CP4d**, and thus also allowing us to probe the importance of the East nitro group, as shown in Figure 5.4.

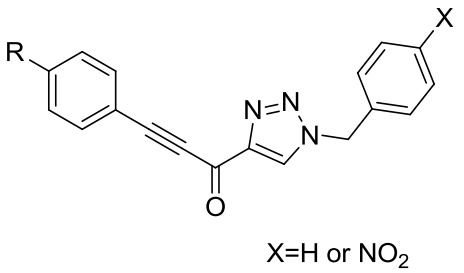

Figure 5.4. Basic alkynyl scaffold, where R was varied and X was maintained as H or NO_2

Synthetically, our experiences with other synthetic pathways as outlined in section 5.1.4 led us to prepare each compound in a linear fashion, following Scheme 5.6, in the same approach as presented in Scheme 5.2. Each class of West substituents is designated by letters **a** through **f**.

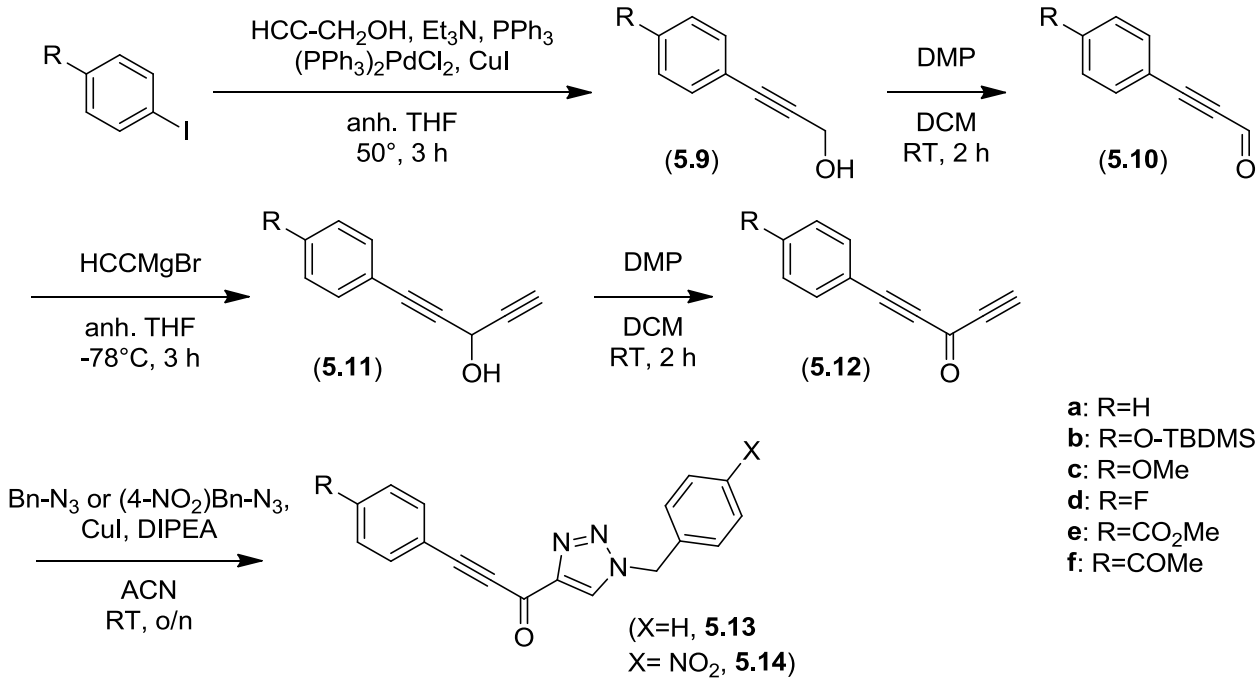

Scheme 5.6. Preparation of the library of alkynyl derivatives, similarly to Scheme 5.2, where letters **a** through **f** are used to identify the R substituent for each compound

5.2.1 Efforts to replace the nitro group

Nitroaromatic compounds have been known to be toxic to biological systems for several decades. In particular, nitrobenzene has been the subject of an extensive review[121] on its mode of action in causing tumours of the liver, kidney and thyroid. While the evidence for the mode of action in the latter two cases appears to be rodent-specific, there remains cause for concern given the high incidence of tumours resulting from the chronic exposure to nitrobenzene even though no human toxicological studies have been done. However, the relationship between nitrobenzene and hepatocellular tumours has been well-established. Nitrobenzene results in an increased production of oxidative and reductive metabolites, which overwhelms the capacity of the liver to quench free radicals and repair damage to macromolecules. Furthermore, the reductive pathways of nitrobenzene result in the formation of nitrosobenzene and phenylhydroxylamine, which oxidise[122] hemoglobin-Fe^{2+} to methemoglobin-Fe^{3+}; the latter cannot complex O_2, thus reducing the oxygen-carrying capacity of blood and leading to the hemolysis of red blood cells.

In a more general sense, nitroaromatics[122] are myelosuppressive agents, leading to bone marrow depression, but they are also activated towards nucleophilic displacement, resulting in phenylated proteins that act as immunogens, capable of inducing an immune response. Nitroaromatics are also known carcinogens; once reduced to anilines, they may be *N*-hydroxylated and react with specific proteins that are important growth-limiting factors, an interaction that leads to the uncontrolled growth of tumours.

In light of the toxicity issues relative to nitroaromatic compounds, we would prefer to substitute a different group onto our inhibitors, while maintaining a strong inhibitory potency against TG2. Our most potent compounds (reproduced below in Figure 5.5) to date all contained

at least one nitro group (***m*-CP30a**, **4.8**) and several contained two (**CP4d**, **4.9**, **4.10**); in this work, we aimed to explore the substitution possibilities at the West end of the alkynyl scaffold to replace this toxic group.

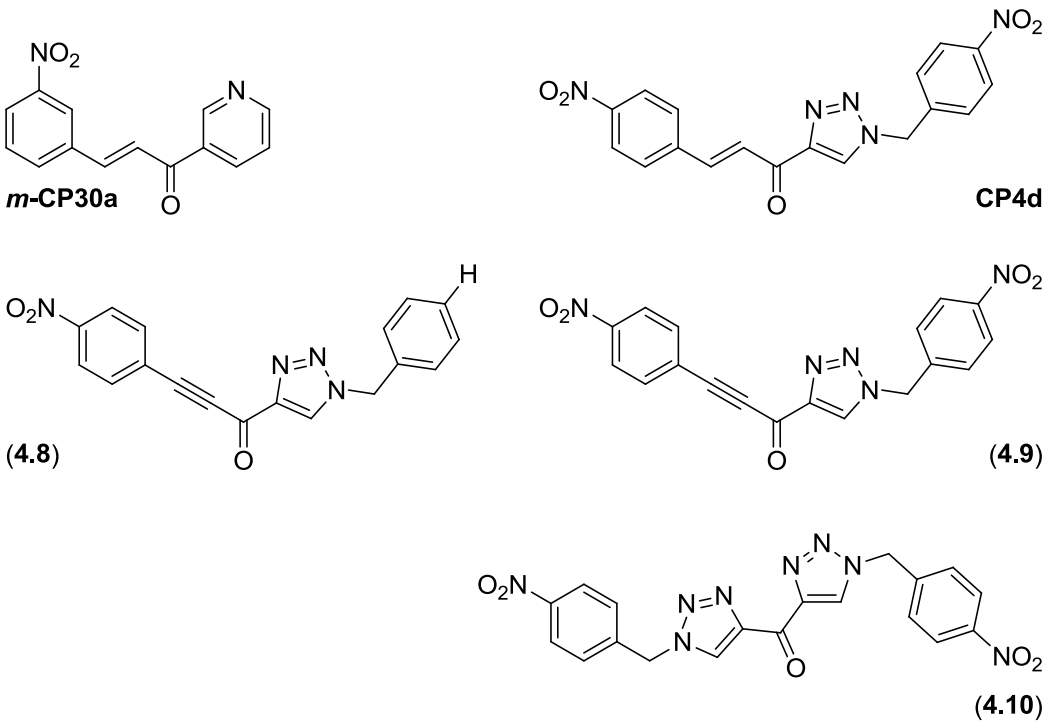

Figure 5.5. Potent reversible inhibitors featuring a nitro group

5.2.2 Choice of substituents

The successfully synthesized compounds are shown below in Figure 5.6. As noted in Scheme 5.6, letters were used to designate the substitents for each intermediate and final compound. In the case of silyl ethers **b**, the TBDMS protecting group was used to mask the phenol moiety for the synthesis. The final compounds evaluated as inhibitors (**5.16** and **5.17**) are featured in Scheme 5.7 further below.

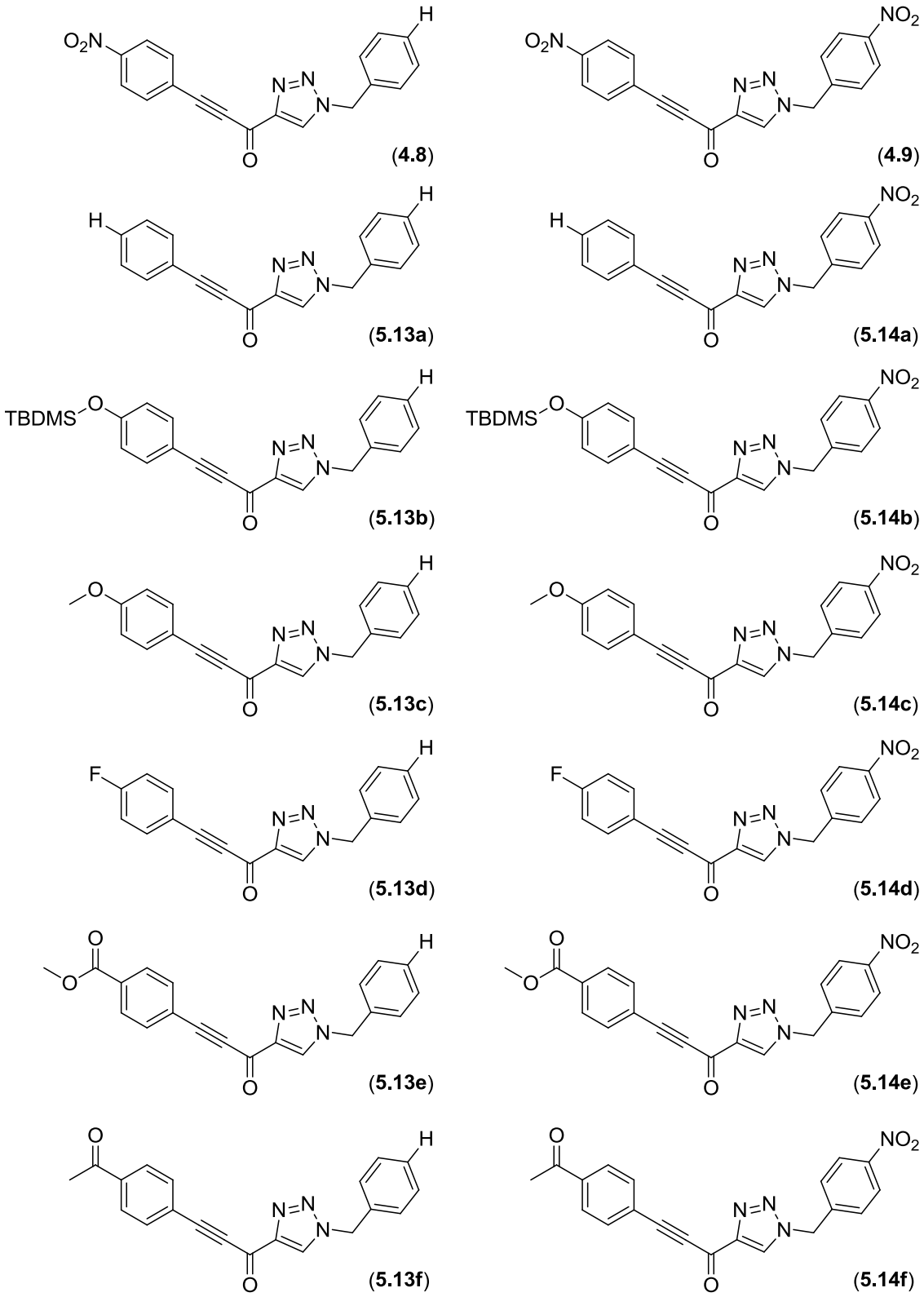

Figure 5.6. Library of alkynyl derivatives synthesised according to Scheme 5.6

The first substitution was to remove the West nitro group (derivatives **a**) to determine whether the bare alkynyl scaffold (**5.15a**) retained potency. This substitution was also of interest given the slight increase in potency observed for the parent compound **4.8** when compared to **4.9**. Molecular docking studies performed in the group by Dr. Christopher M. Clouthier had previously suggested[119] that the alkynyl scaffolds were bound in the same pockets of the enzyme as **CP4d**, but in opposite orientations. The East nitro derivative of the West benzyl scaffold (**5.14a**) would therefore allow us to compare opposite substitutions and determine whether this hypothesis of directional binding was applicable. We also worked with two electron donating groups, namely *t*-butyldimethylsilyl ether (derivatives **b**, protected phenols) and methoxy[123] (derivatives **c**) groups on the West end. While the eventual phenol derivatives **5.16** and **5.17**, obtained from the deprotection of the silyl ethers **5.13b** and **5.14b**, had the ability to act as a hydrogen bond donor and acceptor, the anisole derivatives held only the latter characteristic. These electron-donating groups may also reduce the reactivity at the triple bond, by rendering it less electrophilic than with electron-withdrawing substituents at the West end. Since the 4-position on benzyl rings is easily oxidised *in vivo* by cytochromes, a common practice[124] to increase metabolic stability of such compounds is to place a fluorine (derivatives **d**) at that position, to prevent potential oxidation. Finally, we also tried a methyl ester (derivatives **e**) and a methyl ketone (derivatives **f**), both electron withdrawing groups for the aromatic cycle, but with the ester having the additional oxygen available as a hydrogen bond acceptor.

Of all the substituents shown in Figure 5.6, only the phenol derivative required additional protection and deprotection steps, as mentioned above. We chose to prepare a silyl ether, as had been used previously in the synthesis of the photolabile inhibitor **3.1**, given the ease of preparation and good yield for both the protection and deprotection steps with this group. The

extra transformations are shown in Scheme 5.7, where the initial silyl ether **5.15** was used in the Sonogashira coupling to form primary alcohol **5.11b**, and where the cycloaddition products **5.13b** and **5.14b** were deprotected with TBAF to obtain final compounds **5.16** and **5.17**, respectively.

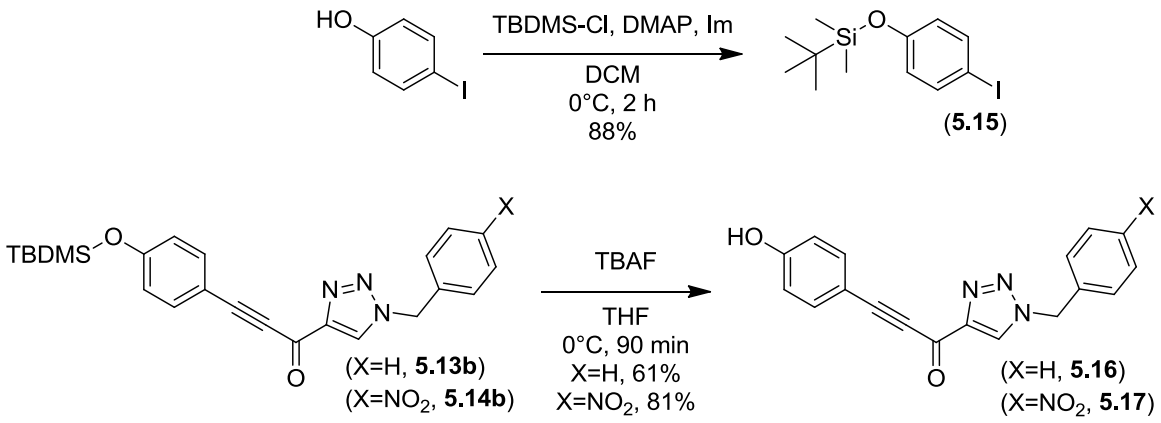

Scheme 5.7. Protection and deprotection in the preparation of the phenol derivatives **5.16** and **5.17**

Other scaffolds that we wanted to evaluate at the West end were aniline, sulfonamide, acetamide, carboxamide and carboxylic acid derivatives, starting from their corresponding 4-iodobenzenes. However, these scaffolds were incompatible with the Sonogashira coupling, likely due to the poisoning of the palladium catalyst by the protons on heteroatoms. As described above, we were able to protect the single hydroxyl proton of phenol with TBDMS, but this approach was unsuccessful with the carboxylic acid, on which the silyl ester was much more labile. In a different approach, the saponification of the corresponding methyl esters (**e**) with lithium hydroxide led to the formation of three different aryl-containing products, likely due to

partial hydrolysis of the triple bond. With the aniline, sulfonamide and carboxamide iodobenzenes, we were unsuccessful in replacing both acidic protons; neither TBDMS nor BOC protecting groups offered complete protection. Finally, the acetamide would have been prepared by acetylating the aniline derivative, but we were unable to prepare the latter. In a different approach, we tried to reduce the nitro derivatives (**4.8** and **4.9**) to the corresponding anilines using the standard approach[125] of tin(II) chloride, but we recovered decomposition products, suggesting that the densely functionalised compounds were undergoing side reactions with the catalyst.

5.2.3 Evaluation of the various scaffold modifications

5.2.3.1 Enzyme kinetics - assay modifications

Between the work presented in Chapter 4 and the work presented in this chapter (excluding the K_i determination for inhibitor **4.9**, which had been done previously), we observed a change in the K_M value for our substrate **AL5**, which increased from the experimentally determined value of 23 μM (from the average of values obtained in K_i determination experiments for **3.1**, **4.10** and **4.8**) to 200 μM (work done in conjunction with Dr. Nicole M. R. McNeil). In tandem with this increase in K_M, we also observed that the activity of enzyme freshly eluted from an affinity column after expression and purification increased significantly, going from an average of 0.3 U/mg to 4.5 U/mg. These novel results were verified on three separate instruments in order to confirm consistency (work done in conjunction with Dr. Nicole M. R. McNeil and Abdullah Akbar). We believe that the enzyme being expressed and purified has a higher value of k_{cat}, due to the higher specific activity being measured. As k_{cat} increases, so does K_M, since the latter is defined as a collection of rate constants that includes k_{cat} in the numerator.

In light of this change, we re-optimised the IC_{50} assay to ensure that we could accurately determine initial rates. The results presented in this chapter were obtained by running the inhibition assay on a microplate reader, in order to reduce the mass of substrate **AL5** that was used for each assay, given that we used higher concentrations in light of the new K_M value.

Table 5.1. Modifications made to the IC_{50} assay setup

	Old data	**New data**
K_M for **AL5**	23 μM	200 μM
Final [**AL5**] in solution	54.5 μM (2.3 x K_M)	500 μM (2.5 x K_M)
Final [hTG2] in solution	2.5 mU/mL	5.0 mU/mL

However, while the data in Table 5.1 above suggests that the new inhibition assays were run with twice the concentration of enzyme as had been used previously, the new range of specific activity values for the recombinant expression of hTG2 is so much higher than what had been used previously that we were actually adding a significantly lower molar concentration of enzyme. However, since these enzyme kinetic assays are run under saturating conditions, this change in concentration, whether molar or with respect to activity, had no effect on the kinetic values being measured. We used the IC_{50} values of inhibitors **4.8** and **4.9** to compare both assays; gratifyingly, the values remained close. The IC_{50} for inhibitor **4.8** went from 0.61 ± 0.05 μM to 1.47 ± 0.08 μM, and that of **4.9** increased from 0.79 ± 0.05 μM to 0.93 ± 0.05 μM. The non-coincidental proximity of these values is attributed to the fact that we remained at a similar

concentration of substrate **AL5** relative to its K_M value; mathematically, according to the Cheng-Prussoff equation[107] (eq. 3.3, reproduced below),

$$IC_{50} = \frac{K_i^{app}}{K_M}[S] + K_i^{app} \qquad \text{(eq. 3.3).}$$

we note that the ratio of $[S]/K_M$ was essentially unchanged, and therefore the experimental IC_{50} values ought to remain the same since K_i is a constant for the inhibitor.

5.2.3.2 Results and discussion

The IC_{50} values for the synthesised alkynyl compounds are grouped in Table 5.2 below. Each indicated value represents the average of two triplicate experiments, and the error is propagated from the errors in the linear regression slope (m) and y-intercept (b) coefficients, as calculated using Microsoft Excel's LINEST function, as described in Section 7.3.1. As was done previously, the expression "n.d." denotes that no inhibition was detected at the compound's indicated solubility limit.

Table 5.2. Inhibitory potency of the synthesised alkynyl compounds

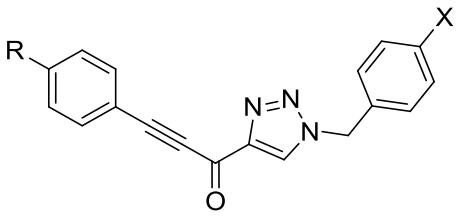

Compound	R group	X group	IC_{50} (μM)
4.8	NO_2	H	1.47 ± 0.08
4.9	NO_2	NO_2	0.93 ± 0.05
5.13a	H	H	59.6 ± 4.7
5.14a	H	NO_2	n.d. @ 38 μM
5.16	OH	H	59.1 ± 3.4
5.17	OH	NO_2	n.d. @ 18 μM
5.13c	OMe	H	90 ± 13
5.14c	OMe	NO_2	n.d. @ 34 μM
5.13d	F	H	24.6 ± 2.1
5.14d	F	NO_2	n.d. @ 9 μM
5.13e	CO_2Me	H	n.d. @ 36 μM
5.14e	CO_2Me	NO_2	n.d. @ 32 μM
5.13f	COMe	H	3.03 ± 0.40
5.14f	COMe	NO_2	8.19 ± 0.91

Assay run with a concentration of 500 μM **AL5**

In an interesting result, the compounds with an East benzyl group were generally more potent than those with an East *p*-nitrobenzyl group, except for the West nitro scaffold, where both compounds **4.8** and **4.9** were similarly potent. The only other East nitro compound that inhibited TG2 below its solubility limit was **5.14f**, with the acetyl group; in that pair, the compound with the simple benzyl (**5.13f**) was still more potent, and almost in line with the parent nitro compounds. This result is important to note with respect to the goal of removing nitro groups from our inhibitors, as **5.13f** contains none but has similar potency to mononitro derivative **4.8**.

Despite the moderate symmetry within this scaffold, we also observed that while compound **4.8** is a potent inhibitor, the reverse substitution pattern (West hydrogen, East nitro, **5.14a**) showed no detectable inhibition at its solubility limit. However, the bare alkynyl scaffold, with no substitutions on either extremity (**5.13a**), was moderately potent, suggesting that the affinity is not solely reliant on the substituents, and that a nitro group may even be detrimental to binding at the East end of the compound in some cases.

Furthermore, we observed no inhibitory difference between the West hydrogen (**5.13a**) and the West phenol (**5.16**), and a moderate loss in inhibition with the West anisole (**5.13c**). When taken in conjunction with the good potency observed with the fluoro (**5.13d**), nitro (**4.8**) and acetyl (**5.13f**) derivatives, we observed a similar trend to that established with previous scaffolds, namely the increase in potency observed with electron-withdrawing substituents. However, in most of those cases, the corresponding East nitro derivative showed no inhibition, suggesting again that the electron withdrawing substituent at that position has a more detrimental effect on potency.

Finally, while we observed good potency with both acetyl compounds **5.13f** and **5.14f**, we saw none for the corresponding methyl ester derivatives **5.13e** and **5.14e**, suggesting an important role for the ester oxygen in decreasing the binding affinity for the enzyme. Overall, it appears that this alkynyl scaffold is much more tolerant to substitutions than the bis(triazole) one, and the IC_{50} values obtained in this work are lower than those obtained previously, suggesting a better scaffold affinity for the enzyme. In particular, we also observed good affinity with compound **5.13f**, our first potent reversible inhibitor that does not include a nitro group in its structure, thus minimising its potential cellular toxicity.

5.3 Future directions

While only seven derivatives were prepared for each of the West substituents, the alkynyl scaffold seems promising due to the overall stronger potency observed for compounds with a simple East benzyl group, without the nitro group that had been key in many previous inhibitors (**CP4d**, **CP30a**, **4.10**). However, the trend associating potency with electron withdrawing groups at the West end of the molecule was maintained, with the most potent compounds bearing a nitro (**4.8**), fluorine (**5.13d**) or ketone (**5.13f**) on the West end, but a simple benzyl on the East end.

In light of the increased potency displayed by inhibitor **4.9** (K_i = 420 nM) compared to **CP4d** (K_i = 1.0 μM), we propose to integrate the diazirinyl azide **3.8** into the alkynyl scaffold, in hopes of improving the affinity of the inhibitor for the enzyme and obtaining better results in a subsequent photolabelling project (à la Chapter 3). Since the synthesis was established so that the azide-alkyne cycloaddition was the last step in the synthesis of the photolabel, we could replace

the cinnamoyl ynone **CP3** with intermediate **5.4** or **5.12f** (Scheme 5.8 below) to prepare a different photolabile inhibitor.

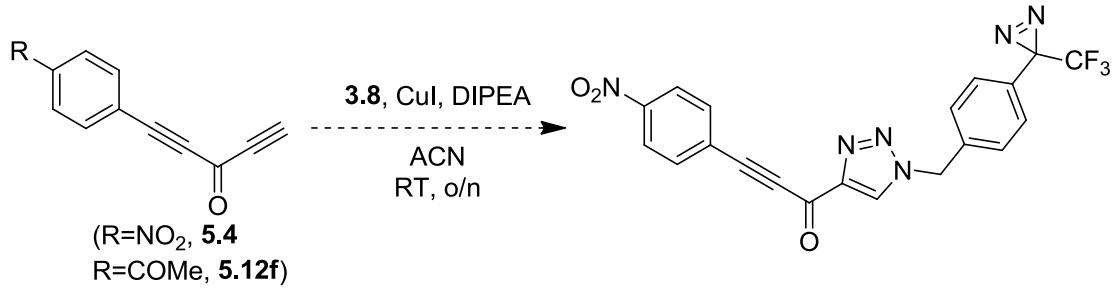

Scheme 5.8. Proposed alkynyl photolabile compound

Chapter Six: **Conclusions and perspectives**

6.1 Photolabelling project

6.1.1 Goal of the project

This project was developed as a method to study the binding of various reversible inhibitors, starting from lead inhibitor **CP4d**. In a two-part approach, we aimed to express and purify TG2 labelled with ArgΔ10 and LyΔ8 as a reference for LC-MS/MS analysis, and to prepare a photolabile derivative of **CP4d**, compound **3.1** (reproduced below in Figure 6.1), that would covalently bind to the enzyme upon photoirradiation. The resulting covalent linkage would then be used in the analysis of the tryptic digest to determine the binding sites of our inhibitor.

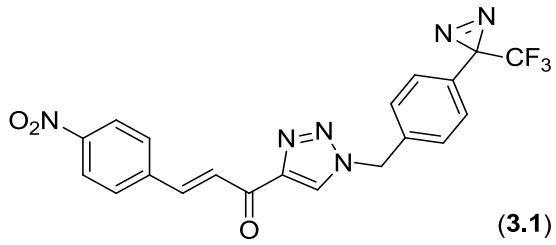

Figure 6.1. Photolabile inhibitor **3.1**

6.1.2 Results

We successfully optimised the protocol for the expression and purification of TG2 from a complex medium (SILAC optimised for *E.coli*) and obtained 150 μg of ArgΔ10-LysΔ8 TG2. Although objectively low, this amount would be sufficient for 3 series of experiments performed in quintuplicate, since the "heavy" protein was only to be used as a reference for LC-MS/MS analysis.

We successfully synthesised compound **3.1** and evaluated it as an inhibitor against TG2, obtaining an IC_{50} of 44.8 ± 4.4 μM. Further kinetic experiments determined that inhibitor **3.1** is competitive with respect to the acyl donor substrate, like its parent **CP4d**, with a K_i of 37.8 ± 9.9 μM. However, our photolabel had a solubility limit between 9 and 14 μM in aqueous buffer, which was far below its K_i value. In this respect, the low solubility of our compound (combined with a relatively low affinity for the enzyme) limited its potential application as a photolabel, since the small amount of carbene that was generated was likely quenched by water instead of inserting itself into the enzyme.

6.1.3 Perspectives

We tried two methods to improve the aqueous solubility of our photolabel – an increase in the percentage volume of organic co-solvent (DMF, DMSO, NMP), and the replacement of a phenyl group by a pyridinyl one, in order to increase the polarity of our compound. However, neither method resulted in an increase in the concentration of photolabel in solution.

We propose two potential approaches for the future of this project. A novel photoactivatable group, a 2-aryl-5-carboxytetrazole (ACT), may be used to replace the acyltriazole, if the removal of the methylene group does not affect the affinity for the enzyme, as shown in Figure 6.2 below.

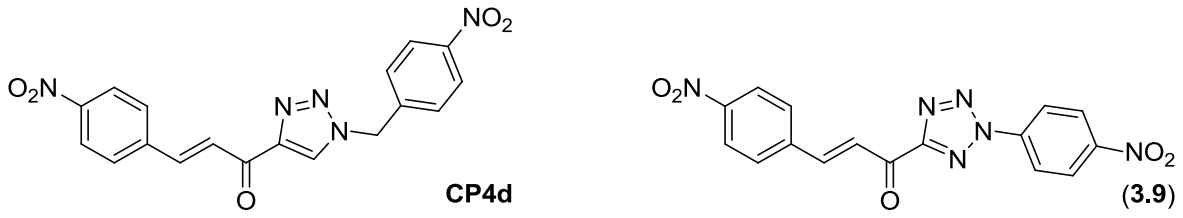

Figure 6.2. Potential application of the ACT photoactivatable group

A second approach would be to combine the alkynyl scaffold developed in Chapter 5 with the diazirinyl azide **3.8**, as shown below (Scheme 6.1). This approach would take advantage of the increased affinity observed with the alkynyl scaffold (either West nitro or West acetyl), although it may have a similar solubility limit as the original compound **3.1**. Ideally, a similar solubility would be offset by a great affinity for the enzyme with the novel scaffold, thus allowing maximum binding to the enzyme and increased potential for photolabelling.

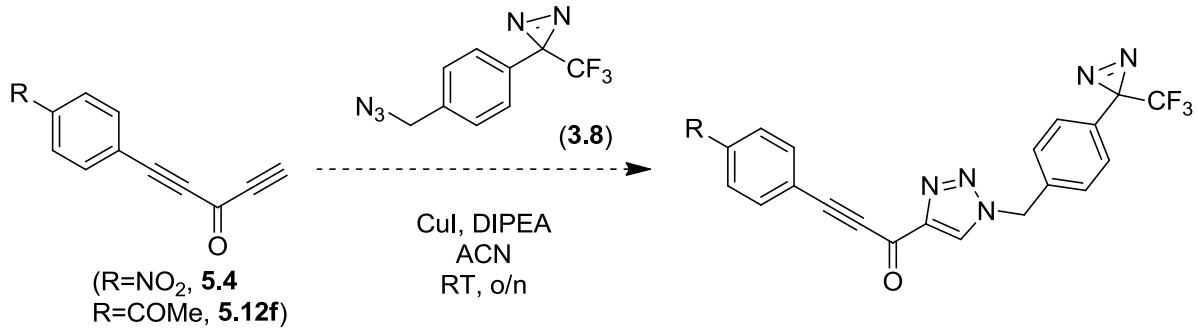

Scheme 6.1. Addition of trifluoromethylphenyldiazirine **3.8** to the alkynyl scaffold

6.2 Glutathione-resistant inhibitors

6.2.1 Goal of the project

The aim of this project was to evaluate the susceptibility to glutathione of earlier key reversible inhibitors (**CP4d**, ***m*-CP30a**), and then to develop a series of compounds with greater resistance to electrophilic addition, while maintaining a similar inhibitory potency.

6.2.2 Results

We developed a ^{1}H NMR assay to test for the reactivity of our compounds with glutathione, and confirmed the significant susceptibility of **CP4d** and ***m*-CP30a** to nucleophilic addition. After making several modifications to the original cinnamoyl inhibitor scaffold, we evaluated a series of bis(triazole) derivatives, led by compound **4.10** (reproduced below in Figure 6.3), with an IC_{50} value of 14.1 ± 1.7 μM. This inhibitor showed no reaction with glutathione after 72 hours in DMSO at room temperature. Like previous inhibitors in the cinnamoyl family, inhibitor **4.10** was found to be competitive with respect to the acyl donor substrate, with a K_i of 9.9 ± 1.6 μM.

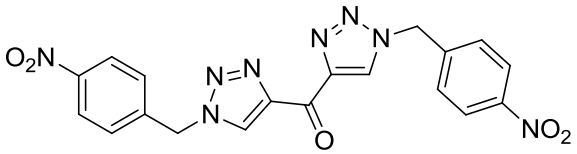

(**4.10**)

Figure 6.3. Bis(triazole) inhibitor **4.10**

However, in aqueous buffer supplemented with 1 mM glutathione, we observed a significant loss in potency for **4.10** after a 2-minute incubation period at room temperature, and a complete loss of inhibition after one hour.

6.2.3 Perspectives

A significant drawback of our chosen method to study the electrophilicity of our inhibitors was the difference in the conditions under which the reaction with glutathione was studied, compared to the inhibition assay. We chose to analyse the reactivity in DMSO-d_6, a solvent that solubilised both our inhibitors and glutathione to a sufficient extent for the analysis by ^{1}H NMR. However, the kinetic assays were performed in an aqueous buffer. In order to optimise the identification of scaffolds with enhanced resistance to nucleophilic addition, the next step would be to develop a glutathione assay that mimics the inhibition assay as closely as possible. Ideally, the separation of the inhibitor and its glutathione adduct by HPLC would be possible, such that the assay may be run in aqueous conditions instead of DMSO.

Given the low aqueous solubility limit observed with this inhibitory scaffold, as well as the previous cinnamoyl one, in our assay buffer (see Table 6.1 below), it would be interesting to pursue a completely different scaffold, also lacking in an electrophilic Michael acceptor, but with greater hydrophilic character. In particular, of the compounds developed in the work presented herein, both the photolabel **3.1** and bis(triazole) **4.10** have a solubility limit near their K_i value. The third key compound, alkyne **4.9**, has the lowest absolute solubility limit, but this low concentration in solution is partially offset by its high potency.

Table 6.1. Comparison of K_i values and solubility limits of notable reversible inhibitors

Inhibitor	**K_i (μM)**	**Solubility limit (μM)**	**Ratio Solubility/K_i**
CP4d	1.0 ± 0.1	33	33
***m*-CP30a**	4.0 ± 0.6	49	12
3.1	38 ± 9.9	11	0.30
4.9	0.42 ± 0.05	8	19
4.10	9.9 ± 1.6	14	1.4

In this respect, preliminary work has been done by undergraduate Honours student Nicholas Brunet-Filion on the synthesis of unreactive mimics of the protected dipeptide Cbz-Gln-Gly, a known TG2 substrate. While the replacement of glutamine with 5-hydroxynorvaline (see Figure 6.4 below) did not demonstrate inhibition of the transamidation reaction, we reached a concentration of 385 μM in solution in our assay buffer, which is an order of magnitude higher than the most soluble small molecule inhibitors. The hydroxyl group is likely a poor mimic of the terminal amide; its replacement with a different group, such as a nitrile, may increase affinity for the enzyme such that the inhibitor may compete with our substrate **AL5**, which is based on the same dipeptide.

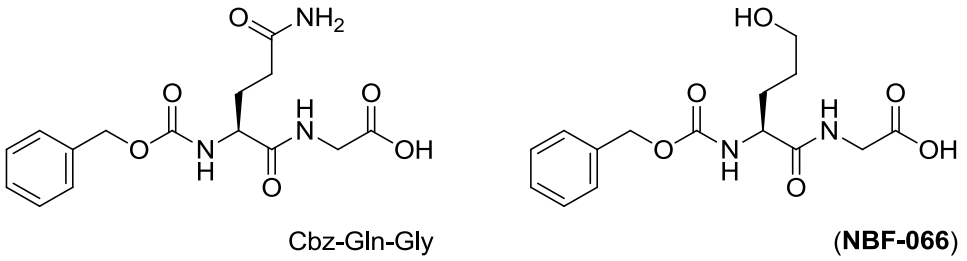

Figure 6.4. Reversible inhibitor scaffold based on the substrate Cbz-Gln-Gly

6.3 Probing the alkynyl triazole scaffold

6.3.1 Goal of the project

In the pursuit of glutathione-resistant inhibitor scaffolds, we prepared an alkynyl derivative of **CP4d**, compound **4.9** (reproduced below in Figure 6.5), which displayed equal susceptibility to glutathione addition, but an increased potency against TG2, with a K_i value of 420 nM. In this project, we probed the effect of the West substituents on the potency of the compounds, while maintaining the East substituent as either a simple benzyl or a 4-nitrobenzyl. Knowing that nitro groups tend to be cytotoxic, and that the electron-withdrawing groups on the West end increase the electrophilicity of the π bonds, we aimed to determine whether both could be replaced while maintaining the same degree of inhibitory potency.

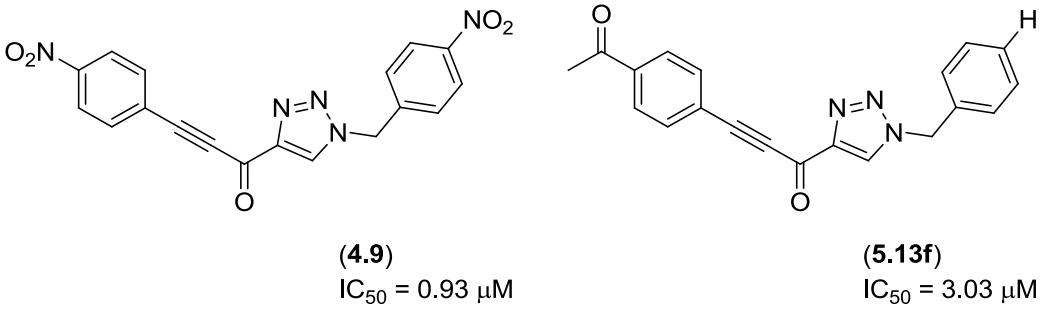

Figure 6.5. Alkynyl inhibitors **4.9** and **5.13f**

6.3.2 Results

Within the library of compounds that were prepared, we observed that electron-withdrawing substituents at the West end generally resulted in greater potency, mimicking a trend seen with the earlier cinnamoyl inhibitors. However, we observed better overall inhibition by the compounds bearing a simple benzyl group at the East end, instead of the previously favoured 4-nitrobenzyl group. Furthermore, we observed a similar potency for derivative **5.13f** (reproduced in Figure 6.5), with an acetyl group at the West end and a simple benzyl at the East end (IC_{50} = 3.03 ± 0.40 μM), when compared to the parent **4.9** (IC_{50} = 0.93 ± 0.05 μM). This compound is the first reversible inhibitor in the Keillor group to maintain strong potency against TG2 without possessing a nitro group in its structure, thus minimising its potential cellular toxicity.

6.3.3 Perspectives

Within the 14 derivatives of the alkynyl scaffold that were prepared, we were encouraged by the observation that better potency is observed with a simple benzyl at the East end, thus removing one nitro group. The next step for this project would be to try a greater variation of substituents at the West end and determine their effect on the inhibitory potency. It was previously observed that substituents containing an sp^2-hybridised oxygen resulted in stronger inhibition; as such, the carboxamide and acetamide derivatives would be interesting to evaluate, especially in light of the observation that the acetyl derivatives are potent inhibitors, but the corresponding methyl esters have no effect on TG2.

Furthermore, while evaluating these compounds as inhibitors for TG2, we observed that parent **4.9** displays slow-binding behaviour. After incubation of the inhibitor with the enzyme for

3 minutes at room temperature, we observed lower initial rates after initiating the reaction with the addition of substrate **AL5** than the rates recorded directly after initiating the reaction with the addition of the enzyme. After incubation of the inhibitor with the enzyme for 10 minutes at room temperature, we observed no activity directly after initiating the reaction with the addition of substrate **AL5**, but saw a gradual increase in product formation as the inhibitor was out-competed by the substrate, which was used in a greater concentration. This slow-binding behaviour would be interesting to study for this scaffold, but also in the context of other inhibitors (***m*-CP30a**, **CP4d**) that had previously been observed to display similar behaviour.

6.4 Conclusion

Overall, the research presented in this thesis increased the knowledge associated with reversible TG2 inhibitors, both in the progress towards the determination of their binding sites on the enzyme and in the improvement of their potency. Starting from lead inhibitor **CP4d**, we developed compounds **3.1** (photolabel), **4.10** (bis(triazole)) and **4.9** (parent alkyne), each a key inhibitor in furthering our knowledge of the SAR of these classes of inhibitors. We also developed a potent reversible inhibitor lacking nitro groups (**5.13f**). Furthermore, the alkynyl inhibitors may represent the future in reversible TG2 inhibitors, as compounds to target the extracellular protein, where the concentration of glutathione is much lower than inside cells. However, while there remain limitations for these compounds as eventual drugs, these inhibitors may also be used as probes for conformation-dependent biological roles. In particular, the slow-binding behaviour displayed by inhibitor **4.9** may relate to a conformational change in the enzyme, which may be an interesting manner to study TG2.

Chapter Seven: **Experimental section**

7.1 General comments

Chemicals and solvents were obtained from Sigma-Aldrich or Fisher Scientific and used without further purification, as were deuterated solvents obtained from Cambridge Isotope Laboratories. NMR spectra were recorded on Bruker AVANCE 300 and 400 instruments, while mass spectrometry results were obtained by the John Holmes Mass Spectrometry facility of the University of Ottawa. Melting points were recorded for powder compounds on a Stanford Research Systems EZ-Melt instrument. Previously published compounds (***m*-CP30a**, **CP3**, **CP4d**, **CP4e**) were obtained according to the published[78, 80] procedures.

7.2 Experimental section for Chapter 2

7.2.1 Preparation of buffers and media

Media and buffers were prepared with milliQ water; reagents were obtained from BioShop and Sigma-Aldrich, and used without further purification. TB medium and milliQ water used in the preparation of the SILACE medium were sterilised by autoclave, while the prepared stock solutions for the SILACE medium used autoclaved milliQ water and were re-sterilised following dissolution of the components by filtration through a 0.22 μM filter.

7.2.2 Expression and purification of ArgΔ10-LysΔ8 hTG2

BL21(DE3) *E. coli* cells containing the expression plasmid pGST-PSP-hTG2 were grown overnight at 37°C with shaking (240 rpm) in LB medium (75 mL) containing 100 μg/mL ampicillin prior to being spun down (2700 rpm, 15 min, 4°C) and resuspended in SILACE[88] medium (75 mL) containing 100 μg/mL ampicillin. This bacterial suspension was then used to

inoculate 925 mL of SILACE medium containing 100 μg/mL ampicillin and the culture was incubated at 37°C with shaking (240 rpm) until the optical density at 600 nm (OD_{600}) reached a value between 0.5 and 0.7, at which point IPTG was added and the culture was incubated for an additional 20 hours at 28°C with shaking (240 rpm). Cells were then harvested by centrifugation (4500 rpm, 20 minutes) and the protein was purified according to a published protocol[89].

7.2.3 Activity assay

The activity of the enzyme was assessed by taking a 50-μL aliquot and adding it to 950 μL **AL5** buffer (111 mM MOPS (pH 7.0), 3.33 mM $CaCl_2$, and 0.05 mM EDTA) and 25 μL of a solution of substrate[26] *N*-Cbz-Glu(γ-*p*-nitrophenylester)Gly (**AL5**) at a concentration of 8.0 mg/mL (17.4 mM) in DMF. The initial rate was converted from AU/min to μmol hydrolysed/min using an extinction coefficient of 8040 cm^{-1} M^{-1}, according to the Beer-Lambert Law. One unit (U) of enzyme activity is defined[89] as the amount of TGase that catalyses the formation of 1 μmol of *p*-nitrophenolate per minute. The specific activity of our enzyme is reported in the units of U/mg; the mass of enzyme was determined using a Bradford assay (external calibration curve).

7.3 Experimental section for Chapter 3

7.3.1 Inhibition kinetics – IC_{50} mathematics

Experimentally, the IC_{50} is determined by taking the negative x-intercept of a Dixon plot, which correlates the reciprocal initial rates with the concentration of inhibitor. Mathematically, this value is obtained by manipulating the linear Dixon plot equation, using m as the value for the slope and $1/v_0$ as the y-intercept, which is the reciprocal of the initial rate in the absence of inhibitor.

$$\frac{1}{v} = m\,[inhibitor] + \frac{1}{v_0} \qquad \text{eq. 7.1}$$

Knowing that, by definition, the IC_{50} is the concentration of inhibitor required for the initial rate v to be half of what it was in the absence of inhibitor (v_0), we obtain the equation below.

$$\frac{2}{v_0} = m \times IC_{50} + \frac{1}{v_0} \qquad \text{eq. 7.2}$$

Rearranging that equation, we obtain the IC_{50} as a function of the slope and y-intercept, and basic algebra indicates that, for a linear equation of the form y = mx+b, the x-intercept is -b/m, and so the IC_{50} value is the negative of the x-intercept value.

$$\frac{2}{v_0} - \frac{1}{v_0} = m \times IC_{50} \qquad \text{eq. 7.3}$$

$$\frac{1}{v_0} \times \frac{1}{m} = IC_{50} = \frac{b}{m} = -x_{int} \qquad \text{eq. 7.4}$$

The error on each individual IC_{50} value, determined by a triplicate experiment, is taken by propagating the errors from the linear regression, namely S_b and S_m as obtained from the Microsoft Excel LINEST function.

$$\delta IC_{50} = IC_{50} \times \sqrt{\left(\frac{S_b}{b}\right)^2 + \left(\frac{S_m}{m}\right)^2} \qquad \text{eq. 7.5}$$

Since the final IC_{50} value presented in the results sections represents an average of two or three experiments, the overall IC_{50} error is taken as the propagation of the errors of each IC_{50} value on the mean, as shown below in equation 7.6, where *n* represents the number of individual values used in the average.

$$\Delta IC_{50} = \frac{\sqrt{\sum_n [(\delta IC_{50})_n]^2}}{n} \qquad \text{eq. 7.6}$$

7.3.2 Inhibition kinetics – IC_{50} experiment

The maximal solubility of the inhibitor in our assay setup was determined by preparing sequential dilutions of a stock solution of 1 mg/mL of the photolabel in DMF and adding 25 µL of the solution to 900 µL of **AL5** buffer, mixing, and verifying after 10 minutes at room temperature that no precipitate was observable to the naked eye. The concentrations tested, and their associated results, are combined below in Table 7.1 for compound **3.1**; a similar approach was taken for each inhibitor tested.

Table 7.1. Determination of the solubility limit of photolabel **3.1**

Stock concentration	**Overall concentration of 3.1**	**Observed result**
1.0 mg/mL	61 µM	Cloudy
0.50 mg/mL	31 µM	Cloudy
0.25 mg/mL	15 µM	Cloudy
0.13 mg/mL	7.6 µM	Clear after 10 minutes at RT
0.20 mg/mL	12 µM	Clear after 10 minutes at RT

The stock solution for the assay was therefore established to be 0.20 mg/mL. While working in molar units of concentration (μM) is more logical for the reporting of final values, using mass units of concentration was easier when working with a series of inhibitors, and these concentration values were generally converted to molar at the end of the experiment.

Kinetic runs were recorded on a Varian Cary 100 Bio UV-visible spectrophotometer, by monitoring the absorbance at 405 nm; the reaction was initiated by the addition of enzyme, which was expressed and purified according to a published protocol[89]. Initial slopes were obtained from the instrument's software by performing a zeroth order linear fit over the first five minutes. This range was verified to be linear after doing the fitting, to ensure that initial rates were being measured accurately. A range of 5 concentrations of inhibitor, along with one positive control (no inhibitor) and one blank (no enzyme) were recorded in triplicate in order to generate a Dixon plot (reciprocal of the initial rate vs. inhibitor concentration) and extrapolate an IC_{50} value. In each cuvette, the volume of DMF was adjusted so that it stayed constant at 5% v/v. The full cuvette contents are indicated in Table 7.2 below; the only value that changes between inhibitors is the concentration of the inhibitor stock, which depends on the solubility limit as determined in the method outlined above.

Table 7.2. Cuvette contents (in μL) for the determination of an IC_{50} value

AL5 buffer	**Inhibitor (3.1, 0.20 mg/mL)**	**AL5 (1 mg/mL)**	**DMF**	**TG2 (0.050 U/mL)**
950	0	25	25	0
900	0	25	25	50
900	5	25	20	50
900	10	25	15	50
900	15	25	10	50
900	20	25	5	50
900	25	25	0	50

The recorded initial rates were then converted from AU/min to μM/min, using an extinction coefficient[26] of 8040 cm^{-1} M^{-1} in the Beer-Lambert law, and plotted in a Dixon plot. The negative x-intercept then gives the IC_{50} value, as established in section above in equation 7.4. A typical Dixon plot, shown here for inhibitor **3.1**, is presented in Figure 7.1. For each inhibitor, the IC_{50} experiment was repeated on at least two separate days, to ensure consistency in the obtained values.

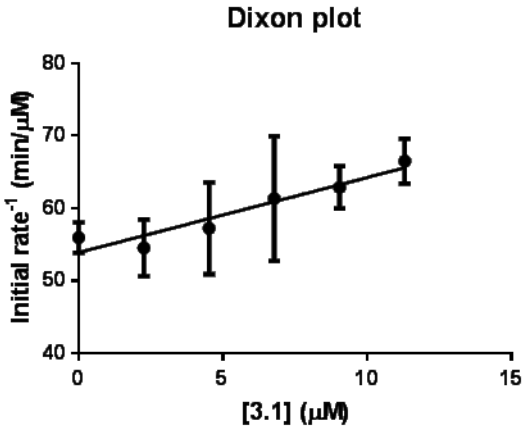

Figure 7.1. Typical Dixon plot for an IC_{50} determination experiment, shown here for compound **3.1**

7.3.3 Inhibition kinetics – K_i determination

Kinetic runs were recorded on a Varian Cary 100 Bio UV-visible spectrophotometer, by monitoring the absorbance at 405 nm; the reaction was initiated by the addition of enzyme, expressed and purified according to a published protocol[89]. Initial slopes were obtained from the instrument's software by performing a zeroth order linear fit over the first five minutes. This range was verified to be linear after doing the fitting, to ensure that initial rates were being measured accurately. These initial rates were then used to general Michaelis-Menten curves, from which values of K_M and V_{max} were extracted by non-linear regression using GraphPad Prism 6, by fitting to the hyperbolic equation 3.1.

For each Michaelis-Menten curve generated, 4 concentrations of substrate **AL5** were used, corresponding to 0.5, 1, 2, and 5 times its K_M value (14.0 μM[81]), as well as a blank run at each concentration of **AL5** (no enzyme), to account for the background hydrolysis reaction. Each set of reaction conditions was run in triplicate for each of the 4 concentrations of inhibitor used,

as well as the positive control (no inhibitor). In total, 5 Michaelis-Menten curves were generated, corresponding to 0, 0.25, 0.5, 0.75, and 1 times K_i^{app}; while higher concentrations of inhibitor would have been desirable, we were limited by the compound's low aqueous solubility.

The full cuvette contents are indicated in Table 7.3 below; the volume added of the stock of **AL5** (2.2 mM DMF) varied for each established substrate concentration, so the volume of added DMF was adjusted so that the overall percentage volume of organic co-solvent remained constant at 5%. For 0.5 x K_M, 3 µL of the **AL5** solution were added; for 1 x K_M, 6.5 µL were added; for 2 x K_M, 13 µL were added and for 5 x K_M, 32 µL of the stock solution of **AL5** were added.

Table 7.3. Cuvette contents (in µL) for the determination of a K_i value

AL5 buffer	**Inhibitor (3.1, 0.25 mg/mL)**	**AL5 (1 mg/mL)**	**DMF**	**TG2 (0.050 U/mL)**
950	0	50 µL total		0
900	0	50 µL total		50
900	4	46 µL total		50
900	8	42 µL total		50
900	12	38 µL total		50
900	16	34 µL total		50

The recorded initial rates were then converted from AU/min to μM/min, using an extinction coefficient of 8040 cm^{-1} M^{-1}, and the generated curves were fitted as described above to extrapolate the values shown in Table 7.4 below.

Table 7.4. Calculated values for K_M^{app} and V_{max} at various concentrations of inhibitor **3.1**, reported with the standard error given by GraphPad

Concentration of 3.1 (μM)	0.00	2.26	4.52	6.78	9.04
K_M^{app} (μM)	20.8 ± 2.0	21.3 ± 2.1	24.49 ± 0.87	25.37 ± 0.46	25.1 ± 2.2
V_{max} (μM/min)	2.305 ± 0.090	2.304 ± 0.091	2.420 ± 0.036	2.414 ± 0.019	2.360 ± 0.087

In each case, while the K_i experiment was performed only once, the positive control (no inhibitor) curve was used to determine that the data obtained was valid, namely by comparing the experimentally-obtained K_M for **AL5** to its established[81] value of 14.0 μM.

The error on the calculated value of K_i was propagated from the errors in each of the K_M^{app} values, as obtained by non-linear regression by GraphPad. The K_i is calculated as the negative x-intercept of the plot of K_M^{app} vs. [inhibitor] (Figure 3.6), in a similar manner to an IC_{50}, and so the propagated error is calculated according to eq. 7.5.

7.3.4 Labelling experimental setup

hTG2 was expressed and purified according to a published protocol[89], and obtained in a concentration of 0.577 mg/mL, as determined by a Bradford quantification assay. This protein

had been stored frozen at -80°C in the standard hTG2 cleavage buffer (25 mM Tris (pH 7.2), 150 mM NaCl, 1 mM EDTA, 1 mM TCEP, 15% glycerol) in an aliquot of 400 µL, and was used following thawing to 0°C without further dilution or concentration.

The photolabelling solution was prepared in a quartz cuvette, using 400 µL of the hTG2 solution as described above, 30 µL of a solution of the photolabel (0.2 mg/mL in DMF), and 570 µL of **AL5** buffer to complete the volume to 1 mL. This solution (3 µM hTG2, 14 µM photolabel) was irradiated for 10 minutes using a Luzchem photoreactor LZC4 with an LZC-UVA lamp (315-400 nm, peak centred at 351 nm), with a simple solution of buffer as a negative control in a second quartz cuvette. The photolabelling solution showed the presence of bubbles at the end of the labelling experiment, as expected from the release of nitrogen following the photolysis of the diazirine, while the negative control did not.

The photolysed sample and a sample of ArgΔ10-LysΔ8 TG2 were dialysed separately into 25 mM Tris buffer (pH 7.2) overnight prior to shipping to Université de Montréal for further analysis by Peter Kubiniok, a graduate student in Prof. Pierre Thibault's group.

7.3.5 Photolabile inhibitor synthesis

7.3.5.1 *tert*-butyl((4-iodobenzyl)oxy)dimethylsilane (**3.2**)

To a solution of 4-iodobenzyl alcohol (3.519 g, 15.04 mmol, 1.000 equiv) in anhydrous DMF (15 mL) were added[103] imidazole (2.082 g, 30.57 mmol, 2.033 equiv) and *tert*-butyldimethylsilyl chloride (3.419 g, 22.69 mmol, 1.509 equiv); the resulting solution was stirred at room temperature under nitrogen overnight prior to being quenched with a heterogeneous mixture (1:1:2 saturated aqueous $NaHCO_3$: water : diethyl ether, 60 mL). The resulting mixture was stirred until CO_2 evolution had ceased, and the product was extracted with diethyl ether (2 x 70 mL). The combined organic extracts were washed with water (2 x 100 mL) and brine (75 mL) prior to being dried over anhydrous magnesium sulfate, filtered, and evaporated to dryness to obtain the product **3.2** as white crystals (5.255 g, 15.09 mmol) in quantitative yield.

^{1}H NMR (400 MHz, $CDCl_3$) δ 7.66 (d, *J*=*J*=8.3 Hz, 2 H), 7.08 (d, *J*=8.3 Hz, 2 H), 4.68 (s, 2 H), 0.94 (s, 9 H), 0.10 (s, 6 H).

^{13}C NMR (100 MHz, $CDCl_3$) δ 151.2, 137.2, 128.0, 92.0, 64.4, 25.9, 18.4, -5.3.

MS (EI) 348 (2, M), 291 (100, M – *t*-Bu), 261 (16, M – *t*-BuMe_2), 217 (58, M – O-TBDMS).

m.p. < 50°C.

7.3.5.2 1-(4-(((*tert*-butyldimethylsilyl)oxy)methyl)phenyl)-2,2,2-trifluoroethanone (**3.3**)

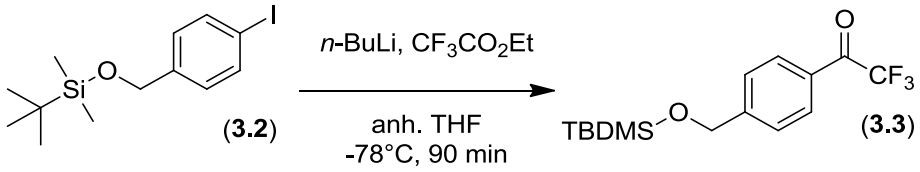

A three-necked flask was charged with anhydrous THF (140 mL) and cooled to -78°C prior to the addition[101] of *n*-butyllithium (~1.2 M in hexanes, 22 mL, 26 mmol, 1.7 equiv), followed by the addition of a solution of aryl iodide **3.2** (5.255 g, 15.09 mmol, 1.000 equiv) in anhydrous THF (15 mL). The resulting solution was stirred at -78°C for 90 minutes prior to the addition of ethyl trifluoroacetate (5.80 mL, 48.5 mmol, 3.21 equiv). The solution was divided between hexanes (125 mL) and water (125 mL), and the organic phase was additionally washed with brine (125 mL) prior to being dried over anhydrous magnesium sulfate, filtered, and evaporated under reduced pressure. The product **3.3** was purified by flash column chromatography (9:1 to 7:3 hexanes:dichloromethane) to obtain a yellow oil (4.174 g, 13.11 mmol) in 87% yield.

^{1}H NMR (400 MHz, $CDCl_3$) δ 8.06 (d, *J*=8.0 Hz, 2 H), 7.51 (d, *J*=8.2 Hz, 2 H), 4.84 (s, 2 H), 0.97 (s, 9 H), 0.13 (s, 6 H).

^{19}F NMR (400 MHz, $CDCl_3$) -71.3.

^{13}C NMR (100 MHz, $CDCl_3$) δ 180.2 (d, *J*=34.6 Hz), 150.1, 130.2 (q, *J*=2.2 Hz), 128.6, 126.2, 116.7 (q, *J*=290 Hz), 64.3, 25.9, 18.4, -5.4.

MS (EI) 318 (0.5, M), 261 (100, M – *t*-Bu), 231 (37), 211 (41), 187 (19, M – O-TBDMS), 165 (53), 135 (24), 91 (34), 59 (10).

7.3.5.3 1-(4-(((*tert*-butyldimethylsilyl)oxy)methyl)phenyl)-2,2,2-trifluoroethanone oxime (**3.4**)

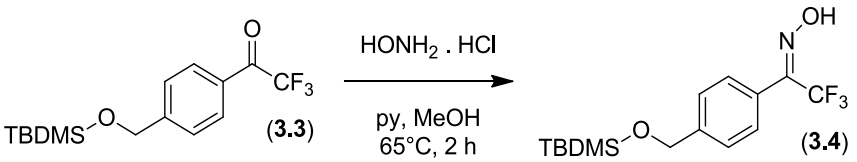

A solution of ketone **3.3** (2.160 g, 6.784 mmol, 1.000 equiv), hydroxylamine hydrochloride (1.426 g, 20.52 mmol, 3.025 equiv) and pyridine (1.1 mL, 16 mmol, 2.4 equiv) in methanol (3 mL) was stirred[101] at reflux for 2 hours prior to being allowed to cool to room temperature. The product was divided between diethyl ether (40 mL) and water (20 mL), and then additionally extracted from the aqueous phase with diethyl ether (40 mL). The combined organic extracts were washed with 1 N HCl (3 x 40 mL), saturated aqueous $NaHCO_3$ (2 x 40 mL) and brine (40 mL) prior to being dried over anhydrous magnesium sulfate, filtered, and evaporated under reduced pressure. The product **3.4** was purified by flash column chromatography (185:15 hexanes:ethyl acetate) to obtain a dense clear oil (1.697 g, 5.090 mmol) in 75% yield.

^{1}H NMR (400 MHz, $CDCl_3$) δ 8.65 (br s, 1 H), 7.48 (d, *J*=8.2 Hz, 2 H), 7.42 (d, *J*= 8.3 Hz, 2 H), 4.77 (s, 2 H), 0.94 (s, 9 H), 0.10 (s, 6 H)

^{13}C NMR (100 MHz, $CDCl_3$) δ 147.8 (d, *J*=32.1 Hz), 144.2, 128.6, 125.9, 124.4, 120.6 (q, *J*=273 Hz), 64.4, 25.9, 18.4, -5.3

^{19}F NMR (40 Hz, $CDCl_3$) δ -66.6

HRMS (EI) calc. for [$C_{15}H_{21}NO_2F_3Si^-$] 332.1294 Da, obt. 332.1290 Da

R_f (9:1 hexanes:ethyl acetate) ~0.28

7.3.5.4 3-(4-(((*tert*-butyldimethylsilyl)oxy)methyl)phenyl)-3-(trifluoromethyl)-3*H*-diazirine (**3.5**)

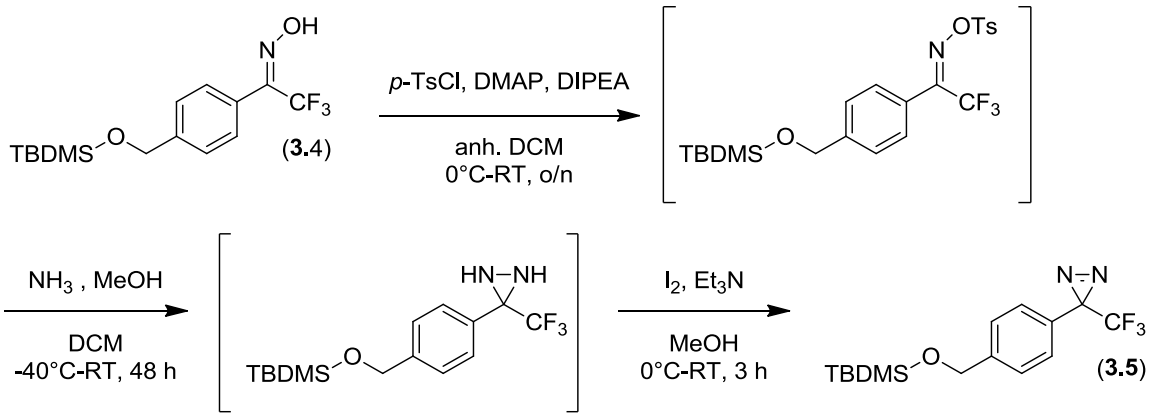

A solution of oxime **3.4** (3.106 g, 9.315 mmol, 1.000 equiv), DMAP (18.7 mg, 153 µmol, 16.4 mequiv) and DIPEA (3.8 mL, 22 mmol, 2.4 equiv) in DCM (25 mL) was cooled to 0°C prior to the addition[104] of a solution of *p*-toluenesulfonylchloride (2.788 g, 14.62 mmol, 1.570 equiv) in DCM (25 mL). The resulting reaction mixture was stirred in the dark for one hour at 0°C prior to being quenched with aqueous citric acid (2 M, 30 mL). The organic phase was washed with water (2 x 45 mL) and brine (45 mL) prior to being dried over anhydrous magnesium sulfate, filtered, and evaporated to dryness. The crude product (5.54 g) was redissolved[101, 104] in DCM (6 mL) and cooled to -50°C prior to the addition of a solution of ammonia in methanol (7 N, 21.4 mL, 150 mmol, 16.1 equiv). The resulting reaction mixture was stirred under a sealed septum in the dark for 48 hours, gradually warming to room temperature, prior to being evaporated under reduced pressure to a white paste. The crude residue was divided between diethyl ether (100 mL) and water (60 mL), and the organic phase was additionally washed with water (2 x 60 mL) before being dried over anhydrous magnesium sulfate, filtered, and evaporated under reduced pressure. The crude diaziridine was dissolved[100] in methanol (20 mL) and triethylamine (3.9 mL, 28 mmol, 3.0 equiv) and cooled to 0°C prior to the addition

of iodine chips (2.688 g, 10.59 mmol, 1.137 equiv). The reaction mixture was allowed to gradually warm to room temperature as it was stirred in the dark for 4 hours prior to being quenched with aqueous solutions of citric acid (10%, 45 mL) and sodium thiosulfate (10%, 45 mL). The product was extracted with diethyl ether (3 x 90 mL) and the combined organic extracts were washed with brine (135 mL) before being dried over anhydrous magnesium sulfate, filtered, and evaporated under reduced pressure. The product **3.5** was purified by flash column chromatography (19:1 hexanes:ethyl acetate) to obtain a dark orange oil (1.910 g, 5.781 mmol) in 62% yield compared to the oxime **3.4**.

^{1}H NMR (400 MHz, $CDCl_3$) δ 7.33 (d, *J*=8.6 Hz, 2 H), 7.14 (d, *J*=8.1 Hz, 2 H), 4.72 (s, 2H), 0.92 (s, 9H), 0.07 (s, 6H)

^{13}C NMR (100 MHz, $CDCl_3$) δ 143.3, 127.6, 126.41, 126.40, 126.3, 122.2 (q, *J*=273 Hz), 64.4, 25.9, 18.4, -5.3

^{19}F NMR (400 MHz, $CDCl_3$) δ -65.3

HRMS (EI) calc. for [$C_{15}H_{21}N_2OF_3Si$] 330.1375 Da, obt. 330.1342 Da.

R_f (9:1 hexanes:ethyl acetate) ~0.86

7.3.5.5 (4-(3-(trifluoromethyl)-3*H*-diazirin-3-yl)phenyl)methanol (**3.6**)

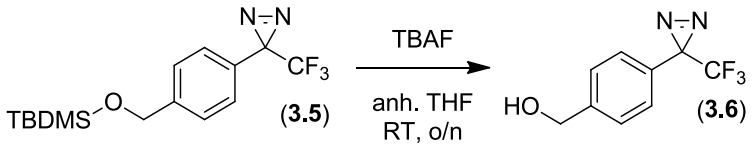

The silyl ether **3.5** (1.910 g, 5.781 mmol, 1.000 equiv) was dissolved[105] in anhydrous THF (7.5 mL) and cooled to 0°C prior to the addition of TBAF (1.0 M in THF, 19 mL, 19 mmol, 3.3 equiv). The resulting reaction mixture was allowed to gradually warm to room temperature was it was stirred under nitrogen in the dark overnight. The reaction was quenched with saturated aqueous NH_4Cl (30 mL), and the product was extracted with diethyl ether (2 x 45 mL). The combined organic extracts were washed with brine (125 mL) prior to being dried over anhydrous magnesium sulfate, filtered, and evaporated under reduced pressure. The product **3.6** was purified by flash column chromatography (7:3 hexanes:ethyl acetate) to obtain a yellow paste (1.155 g, 5.344 mmol) in 92% yield.

^{1}H NMR (400 MHz, $CDCl_3$) δ 7.38 (d, *J*=8.1 Hz, 2 H), 7.18 (d, *J*=8.1 Hz, 2 H), 4.71 (s, 2 H)

^{13}C NMR (100 MHz, $CDCl_3$) δ 142.6, 128.4, 127.1, 126.72, 126.71, 122.1 (q, *J*=273 Hz), 64.5

^{19}F NMR (40 MHz, $CDCl_3$) -65.3

HRMS (EI) calc. for [$C_9H_7OF_3^{2\cdot}$] (loss of N_2) 188.0449 Da, obt. 188.0449 Da

R_f (7:3 hexanes:ethyl acetate) ~0.31

m.p. near room temperature

7.3.5.6 3-(4-(bromomethyl)phenyl)-3-(trifluoromethyl)-3*H*-diazirine (**3.7**)

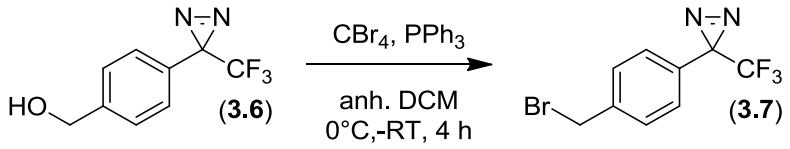

The alcohol **3.6** (1.128 g, 5.218 mmol, 1.000 equiv) and tetrabromomethane (2.008 g, 6.054 mmol, 1.160 equiv) were dissolved in anhydrous DCM (5 mL) and cooled to 0°C prior to the slow addition of triphenylphosphine (1.586 g, 6.045 mmol, 1.158 equiv). The resulting reation mixture was allowed to gradually warm to room temperature as it was stirred under nitrogen in the dark for 3 hours prior to being diluted with hexanes (30 mL). The reaction mixture was filtered over Celite prior to being evaporated under reduced pressure. The product **3.7** was purified by flash column chromatography (19:1 hexanes:ethyl acetate) to obtain a pale yellow oil (1.424 g, 5.105 mmol) in 98% yield.

^{1}H NMR (400 MHz, $CDCl_3$) δ 7.40 (d, *J*=8.6 Hz, 2 H), 7.15 (d, *J*=8.1 Hz, 2 H), 4.45 (s, 2 H)

^{13}C NMR (100 MHz, $CDCl_3$) δ 139.4, 129.4, 129.3, 126.93, 126.92, 122.0 (q, *J*=273 Hz), 32.0

^{19}F NMR (400 MHz, $CDCl_3$) δ -65.2

HRMS (EI) calc. for [$C_9H_6F_3Br^{2\cdot}$] (loss of N_2) 249.9605 Da, obt. 249.9594 Da

R_f (95:5 hexanes:ethyl acetate) ~0.62

7.3.5.7 3-(4-(azidomethyl)phenyl)-3-(trifluoromethyl)-3*H*-diazirine (**3.8**)

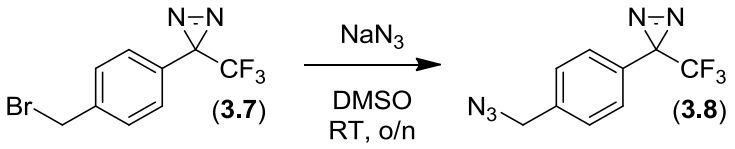

The benzyl bromide (1.424 g, 5.105 mmol, 1.000 equiv) was dissolved[80] in a previously prepared stock solution of sodium azide in DMSO (0.50 M, 13 mL, 6.5 mmol, 1.3 equiv), and the resulting reaction solution was stirred in the dark overnight at room temperature prior to being quenched with water (20 mL). The product was extracted with diethyl ether (3 x 20 mL) and the combined organic extracts were washed with water (2 x 25 mL) and brine (35 mL) prior to being dried over anhydrous magnesium sulfate, filtered, and evaporated to dryness to obtain a pale yellow oil (1.022 g, 4.239 mmol) in 83% yield. Note: this product is extremely volatile and can be lost if evaporated under reduced pressure at a temperature above 22°C.

^{1}H NMR (400 MHz, $CDCl_3$) δ 7.37 (d, *J*=8.6 Hz, 2 H), 7.22 (d, *J*=8.1 Hz, 2 H), 4.38 (s, 2 H)

^{13}C NMR (100 MHz, $CDCl_3$) δ 137.2, 129.2, 128.5, 126.98, 126.97, 122.0 (q, *J*=273 Hz), 54.1

^{19}F NMR (400 MHz, $CDCl_3$) δ -65.2

HRMS (EI) calc. for [$C_9H_6N_3F_3^{2-}$] (loss of N_2) 213.0514 Da, obt. 213.0554 Da

R_f (95:5 hexanes:ethyl acetate) ~0.45

7.3.5.8 (*E*)-3-(4-nitrophenyl)-1-(1-(4-(3-(trifluoromethyl)-3*H*-diazirin-3-yl)benzyl)-1*H*-1,2,3-triazol-4-yl)prop-2-en-1-one (**3.1**)

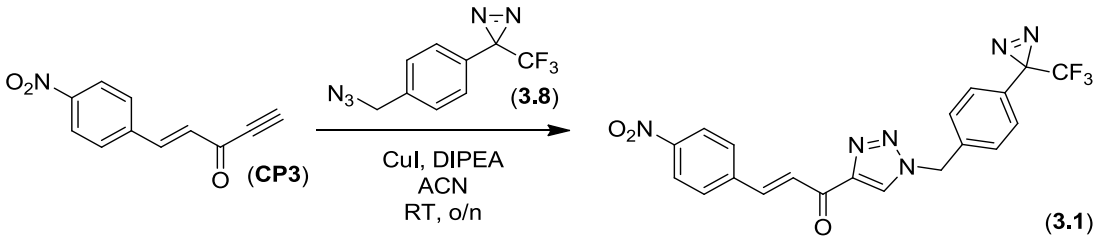

To a solution of the ynone **CP3** (prepared as previously published[80]) (0.203 g, 1.01 mmol, 1.01 equiv) in acetonitrile (10 mL) were added[106] DIPEA (0.17 mL, 1.0 mmol, 1.0 equiv) and copper(I) iodide (0.191 g, 1.00 mmol, 1.00 equiv), resulting in the unexpected solidification of the reaction mixture. Addition of acetonitrile (15 mL) and sonication yielded a heterogeneous mixture, to which was added the diazirinyl azide **3.8** (0.240 g, 0.997 mmol, 1.00 equiv) prior to stirring in the dark at room temperature overnight. The reaction mixture was diluted with DCM (30 mL) and washed with 1 N HCl (2 x 30 mL), water (2 x 30 mL) and brine (2 x 30 mL) prior to being dried over anhydrous magnesium sulfate, filtered, and evaporated under reduced pressure. The product **3.1** was purified by flash column chromatography (7:3 hexanes:ethyl acetate) to obtain a wheat-coloured powder (0.141 g, 0.320 mmol) in 32% yield.

^{1}H NMR (400 MHz, DMSO-d_6) δ 9.10 (s, 1 H), 8.29 (d, *J*=8.8 Hz, 2 H), 8.11 (d, *J*=8.8 Hz, 2 H), 7.99 (d, *J*=16.0 Hz, 1 H), 7.93 (d, *J*=16.2 Hz, 1 H), 7.50 (d, *J*=8.4 Hz, 2 H), 7.34 (d, *J*=8.0 Hz, 2 H), 5.80 (s, 2 H)

^{13}C NMR (100 MHz, DMSO-d_6) δ 181.4, 148.2, 147.2, 140.8, 140.7, 137.7, 129.8, 129.1, 129.0, 127.6, 127.0, 126.3, 124.0, 52.5.

^{19}F NMR (400 MHz, DMSO-d_6) δ -64.6

HRMS (EI) calc. for [$C_{20}H_{13}N_6O_3F_3$] 442.1001 Da, obt. 442.0988 Da

m.p. 103-105°C (dec.)

7.4 Experimental section for Chapter 4

7.4.1 Glutathione resistance assay

^{1}H NMR spectra of a solution of 12 mM inhibitor and 80 mM reduced glutathione in DMSO-d_6 (1 mL) were recorded at the indicated time points. Spectra were collected for each substrate individually, as well as after combining the inhibitor and glutathione, at 10 minutes, one hour, two hours and four hours to monitor for any changes different from an additive spectrum. The product was then analysed by mass spectrometry to confirm the presence of the proposed glutathione adduct.

HRMS (ESI$^+$) for the adduct [***m*-CP30a+GSH**]: calc. for $[C_{24}H_{27}N_5O_9S+Na]^+$ 584.1422 Da, obt. 584.1500 Da

HRMS (ESI$^-$) for the adduct [**CP4d+GSH]**: calc. for $[C_{28}H_{29}N_8O_{11}S]^-$ 685.1682 Da, obt. 685.1677 Da

HRMS (ESI$^+$) for the adduct [**4.9+GSH**]: calc. for $[C_{28}H_{28}N_8O_{11}S+Na]^+$ 707.1490 Da, obt. 707.1525 Da

7.4.2 General procedures

7.4.2.1 Preparation of azides

A solution of sodium azide in DMSO (0.5 M) was prepared by stirring for 24 hours at room temperature to ensure full dissolution of the salt. The substituted benzyl bromide (1.0 equiv) was dissolved[80] in the solution of sodium azide (1.1 equiv) and the resulting reaction solution was stirred at room temperature overnight prior to being quenched with water. The product was extracted with diethyl ether and the combined organic extracts were washed with water and brine prior to being dried over anhydrous magnesium sulfate, filtered, and evaporated to dryness.

Substituted benzyl azides obtained in this manner were verified by ^{1}H NMR and used without further purification.

7.4.2.2 Copper-catalysed azide-alkyne cycloaddition ($CuSO_4$)

To a solution of the alkyne (1.0 equiv) in DMF (0.1 M) were added[80] the substituted benzyl azide (1.0 equiv, prepared according to general procedure 7.4.2.1) and an aqueous solution (5% v/v) of copper(II) sulfate (0.01 equiv) and sodium L-ascorbate (0.1 equiv). The resulting reaction mixture was stirred at 75°C overnight, prior to being quenched with water. The product was extracted with ethyl acetate, and the combined organic extracts were washed with 0.25 N HCl and brine prior to being dried over anhydrous magnesium sulfate, filtered, and evaporated under reduced pressure.

7.4.2.3 TEMPO oxidation (TCICA)

To a solution of the alcohol (1.0 equiv) dissolved in acetone (0.2 M) and cooled to 0°C were added[126] trichloroisocyanuric acid (1.05 equiv) and TEMPO (0.01 equiv). The reaction mixture was allowed to gradually warm to room temperature while it was stirred, until TLC analysis showed complete reactant consumption (generally within three hours). The reaction mixture was then filtered over Celite and evaporated under reduced pressure prior to dissolution of the crude product in DCM. The organic phase was washed with saturated aqueous sodium bicarbonate and 1 N HCl prior to being dried over anhydrous magnesium sulfate, filtered, and evaporated under reduced pressure.

7.4.2.4 Grignard addition (overnight)

To a solution of the aldehyde (1.0 equiv) in anhydrous THF (0.05 M) cooled to -78°C was added ethynylmagnesium bromide (0.5 M in THF, 1.25 to 2.0 equiv), and the resulting reaction solution was allowed to gradually warm to room temperature as it was stirred overnight under nitrogen. The reaction was then quenched with weakly acidic water and the product was extracted with ethyl acetate. The combined organic extracts were washed with brine prior to being dried over anhydrous magnesium sulfate, filtered, and evaporated under reduced pressure.

7.4.3 Inhibitor synthesis

7.4.3.1 (1-(4-nitrobenzyl)-1*H*-1,2,3-triazol-4-yl)methanol (**4.15**)

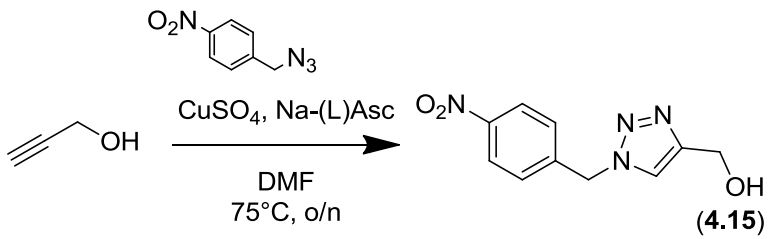

4-Nitrobenzyl azide was prepared from 4-nitrobenzyl bromide according to General Procedure 7.4.2.1. Compound **4.15** was prepared from propargyl alcohol (25.00 mmol) and 4-nitrobenzyl azide according to General Procedure 7.4.2.2, and obtained as an orange power (3.498 g, 14.94 mmol) in 60% yield.

^{1}H NMR (400 MHz, $(CD_3)_2CO$) δ 8.26 (d, *J*=8.8 Hz, 2 H), 7.97 (s, 1 H), 7.59 (d, *J*=8.8 Hz, 2 H), 5.82 (s, 2 H), 4.67 (s, 2 H)

^{13}C NMR (100 MHz, $(CD_3)_2CO$) δ 150.0, 148.8, 144.6, 129.9, 124.8, 123.6, 56.8, 53.2

HRMS (EI) calc. for $[C_{10}H_{10}N_4O_3]$ 234.0753 Da, obt. 234.0740 Da

m.p. 120-123°C

R_f (ethyl acetate) ~0.15

7.4.3.2 1-(4-nitrobenzyl)-1*H*-1,2,3-triazole-4-carbaldehyde (**4.16**)

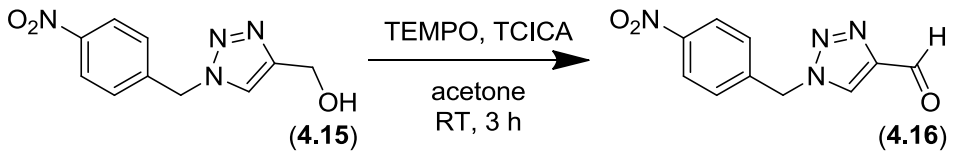

Compound **4.16** was prepared from compound **4.15** (14.93 mmol) according to General Procedure 7.4.2.3, and obtained as a pale yellow powder (2.588 g, 11.15 mmol) in 74% yield.

^{1}H NMR (400 MHz, $(CD_3)_2CO$) δ 10.08 (s, 1 H), 8.78 (s, 1 H), 8.28 (d, *J*=8.8 Hz, 2 H), 7.68 (d, *J*=8.8 Hz, 2 H), 5.97 (s, 2 H)

^{13}C NMR (100 MHz, $(CD_3)_2CO$) δ 185.3, 149.0, 148.9, 143.5, 130.3, 128.2, 124.9, 53.8

HRMS (EI) calc. for $[C_{10}H_8N_4O_3]$ 232.0596 Da, obt. 232.0577 Da

m.p. 109-111°C (dec.)

R_f (ethyl acetate) ~0.68

7.4.3.3 1-(1-(4-nitrobenzyl)-1*H*-1,2,3-triazol-4-yl)prop-2-yn-1-ol (**4.17**)

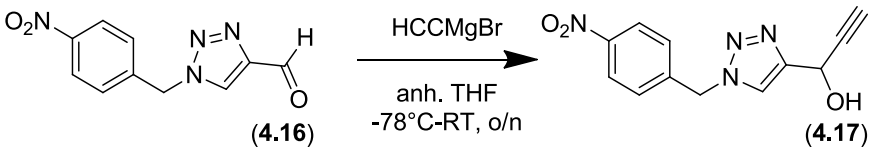

Compound **4.17** was prepared from aldehyde **4.16** (11.15 mmol) according to General Procedure 7.4.2.4 and purified by flash column chromatography (1:2 DCM:ethyl acetate) to obtain a yellow oil (1.584 g, 6.134 mmol) in 55% yield.

^{1}H NMR (400 MHz, $(CD_3)_2CO$) δ 8.27 (d, *J*=8.9 Hz, 2 H), 8.10 (s, 1 H), 7.62 (d, *J*=8.9 Hz, 2 H), 5.84 (s, 2 H), 5.60 (s, 1 H), 3.03 (s, 1 H)

^{13}C NMR (100 MHz, $(CD_3)_2CO$) δ 150.1, 148.8, 144.4, 130.0, 124.8, 123.5, 84.5, 74.4, 57.5, 53.4

HRMS (EI) calc. for $[C_{12}H_9N_4O_3]^-$ 257.0680 Da, obt. 257.0700 Da

R_f (1:2 DCM:ethyl acetate) ~0.41

7.4.3.4 1-(1-(4-nitrobenzyl)-1*H*-1,2,3-triazol-4-yl)prop-2-yn-1-one (**4.18**)

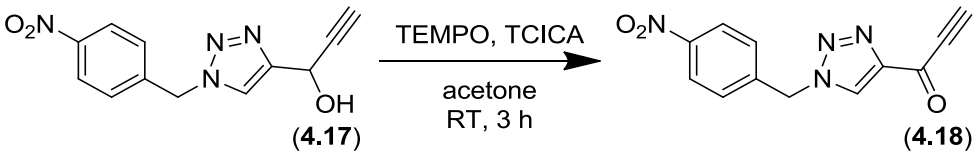

Compound **4.18** was prepared from alcohol **4.17** (6.13 mmol) according to General Procedure 7.4.2.3 and purified by flash column chromatography (1:1 hexanes:ethyl acetate) to obtain of a white powder (864 mg, 3.37 mmol) in 55% yield.

^{1}H NMR (400 MHz, $(CD_3)_2CO$) δ 8.87 (s, 1 H), 8.28 (d, *J*=8.9 Hz, 2 H), 7.69 (d, *J*=8.9 Hz, 2 H), 5.98 (s, 2 H), 4.35 (s, 1 H)

^{13}C NMR (100 MHz, $(CD_3)_2CO$) δ 169.7, 148.9, 148.5, 143.3, 130.3, 130.2, 124.9, 82.9, 81.4, 53.8

HRMS (ESI$^+$) calc. for $[C_{12}H_8N_4O_3]^+$ 279.0494 Da, obt. 279.0508 Da

m.p. 124-126°C (dec.)

R_f (1:1 hexanes:ethyl acetate) ~0.30

7.4.3.5 (1-benzyl-1*H*-1,2,3-triazol-4-yl)(1-(4-nitrobenzyl)-1*H*-1,2,3-triazol-4-yl)methanone (**4.19a**)

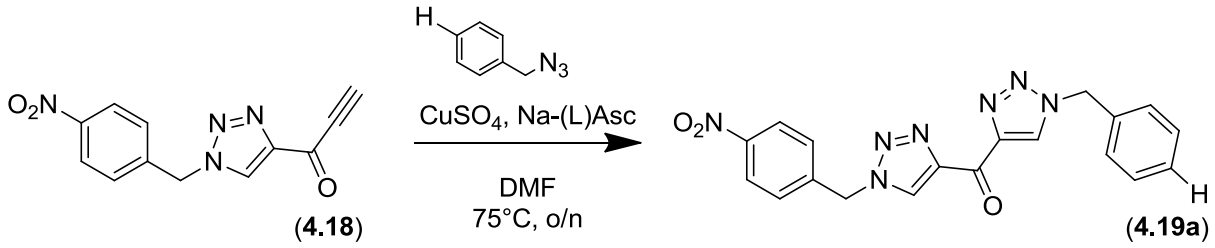

Benzyl azide was prepared from benzyl bromide according to General Procedure 7.4.2.1. Compound **4.19a** was prepared from ynone **4.18** (1.00 mmol) and benzyl azide, according to General Procedure 7.4.2.2 and purified by flash column chromatography (1:1 DCM:ethyl acetate) to obtain a pale yellow powder (105 mg , 0.270 mmol) in 27% yield.

^{1}H NMR (400 MHz, DMSO-d_6) δ 9.32 (s, 1 H), 9.23 (s, 1 H), 8.25 (d, *J*=8.9 Hz, 2 H), 7.60 (d, *J*=8.9 Hz, 2 H), 7.40-7.33 (m, 5 H), 5.93 (s, 2 H), 5.75 (s, 2 H)

^{13}C NMR (100 MHz, DMSO-d_6) δ 175.2. 147.3, 145.13, 145.06, 142.7, 135.4, 130.7, 130.1, 129.1, 128.8, 128.3, 128.0, 123.9, 53.0, 52.1.

HRMS (ESI$^+$) calc. for $[C_{19}H_{15}N_7O_3+Na]^+$ 412.1129 Da, obt. 412.1155 Da

m.p. 168-170°C (dec.)

R_f (1:1 DCM:ethyl acetate) ~0.42

7.4.3.6 (1-(2-nitrobenzyl)-1*H*-1,2,3-triazol-4-yl)(1-(4-nitrobenzyl)-1*H*-1,2,3-triazol-4-yl)methanone (**4.19b**)

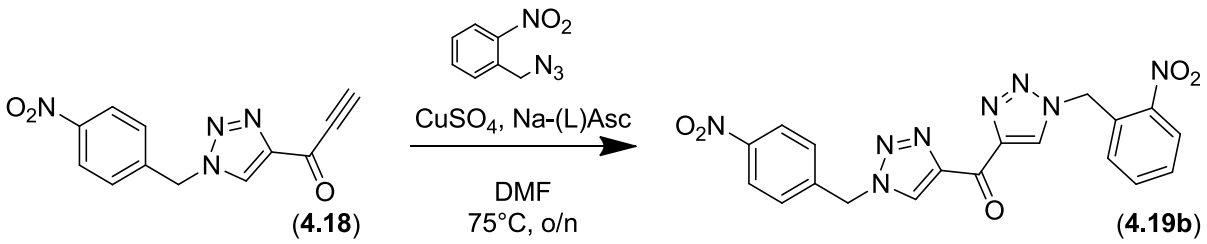

(**4.18**) (**4.19b**)

2-Nitrobenzyl azide was prepared from 2-nitrobenzyl bromide according to General Procedure 7.4.2.1. Compound **4.19b** was prepared from ynone **4.18** (1.00 mmol) and 2-nitrobenzyl azide according to General Procedure 7.4.2.2 and purified by flash column chromatography (7:3 DCM:ethyl acetate) to obtain a yellow powder (130 mg, 0.299 mmol) in 30% yield.

^{1}H NMR (400 MHz, DMSO-d_6) δ 9.34 (s, 1 H), 9.23 (s, 1 H), 8.25 (d, *J*=8.9 Hz, 2 H), 8.17 (dd, *J*=7.7 Hz, *J*=1.3 Hz, 1 H), 7.76 (ddd, *J*=7.7 Hz, *J*=7.7 Hz, *J*=1.3 Hz, 1 H), 7.66 (ddd, *J*=7.7 Hz, *J*=7.7 Hz, *J*=1.3 Hz, 1 H), 7.61 (d, *J*=8.9 Hz, 2 H), 7.17 (dd, *J*=7.7 Hz, *J*=1.3 Hz, 1 H), 6.12 (s, 2 H), 5.94 (s, 2 H)

^{13}C NMR (100 MHz, DMSO-d_6) δ 175.2, 147.6, 147.3, 145.2, 145.0, 142.8, 134.5, 131.1, 130.8, 130.3, 129.8, 129.2, 125.2, 124.0, 52.2, 50.3

HRMS (ESI$^+$) calc. for $[C_{19}H_{14}N_8O_5+Na]^+$ 457.0979 Da, obt. 457.0985 Da

m.p. 145-147°C (dec.)

R_f (7:3 DCM:ethyl acetate) ~0.28

7.4.3.7 (1-(3-nitrobenzyl)-1*H*-1,2,3-triazol-4-yl)(1-(4-nitrobenzyl)-1*H*-1,2,3-triazol-4-yl)methanone (**4.19c**)

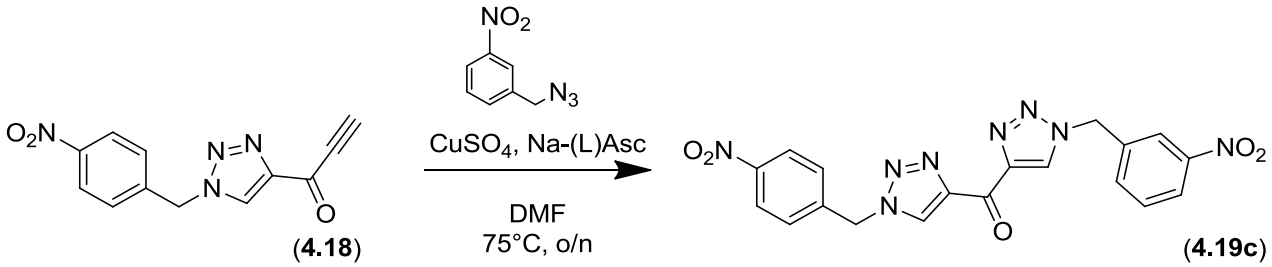

3-Nitrobenzyl azide was prepared from 3-nitrobenzyl bromide according to General Procedure 7.4.2.1. Compound **4.19c** was prepared from ynone **4.18** (1.00 mmol) and 3-nitrobenzylazide according to General Procedure 7.4.2.2 and purified by flash column chromatography (7:3 DCM:ethyl acetate) to obtain a pale yellow powder (117 mg, 0.269 mmol) in 27% yield.

^{1}H NMR (400 MHz, DMSO-d_6) δ 9.34 (s, 1 H), 9.33 (s, 1 H), 8.33 (dd, *J*=1.8 Hz, *J*=1.8 Hz, 1 H), 8.26-8.21 (m, 3 H), 7.84 (ddd, *J*=7.7 Hz, *J*=1.3 Hz, *J*=1.3 Hz, 1 H), 7.70 (dd, *J*=7.9 Hz, *J*=7.9 Hz, 1 H), 7.60 (d, *J*=8.9 Hz, 2 H), 5.93 (s, 2 H), 5.92 (s, 2 H)

^{13}C NMR (100 MHz, DMSO-d_6) δ 175.2, 147.9, 147.3, 145.14, 145.11, 142.7, 137.4, 134.9, 130.8, 130.6, 130.4, 129.1, 123.9, 123.3, 123.1, 52.1, 52.0

HRMS (ESI^{+}) calc. for $[C_{19}H_{14}N_8O_5+Na]^{+}$ 457.0979 Da, obt. 457.0975 Da

m.p. 173-175°C (dec.)

R_f (7:3 DCM:ethyl acetate) ~0.20

7.4.3.8 bis(1-(4-nitrobenzyl)-1*H*-1,2,3-triazol-4-yl)methanone (**4.10**)

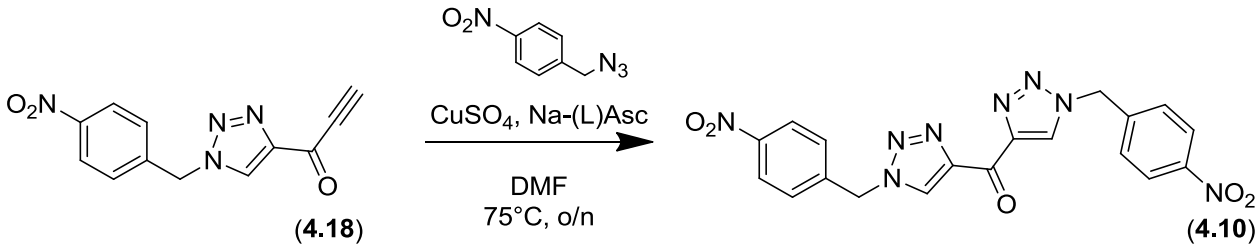

4-Nitrobenzyl azide was prepared from 4-nitrobenzyl bromide according to General Procedure D. Compound **4.10** was prepared from ynone **4.18** (1.00 mmol) and 4-nitrobenzyl azide according to General Procedure E and purified by flash column chromatography (1:1 DCM:ethyl acetate) a yellow powder (174 mg, 0.401 mmol) in 40% yield.

^{1}H NMR (400 MHz, DMSO-d_6) δ 9.33 (s, 2 H), 8.25 (d, *J*=8.9 Hz, 4 H), 7.61 (d, *J*=8.9 Hz, 4 H), 5.94 (s, 4 H)

^{13}C NMR (100 MHz, DMSO-d_6) δ 175.2, 147.4, 145.2, 142.8, 130.8, 129.2, 124.0, 52.2

HRMS (ESI^{+}) calc. for $[C_{19}H_{14}N_8O_5+Na]^{+}$ 457.0985 Da, obt. 457.0978 Da

m.p. 189-191°C (dec.)

R_f (1:1 DCM:ethyl acetate) ~0.36

7.4.3.9 (1-(4-nitrobenzyl)-1*H*-1,2,3-triazol-4-yl)(1-(4-(trifluoromethyl)benzyl)-1*H*-1,2,3-triazol-4-yl)methanone (**4.19e**)

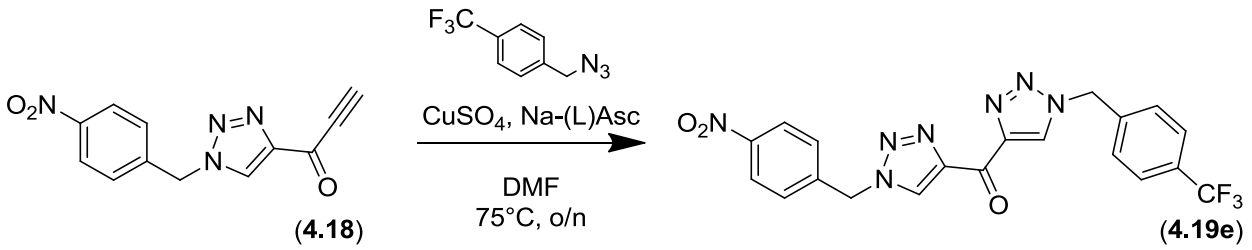

(**4.18**) (**4.19e**)

4-(Trifluoromethyl)benzyl azide was prepared from 4-(trifluoromethyl)benzyl bromide according to General Procedure 7.4.2.1. Compound **4.19e** was prepared from ynone **4.18** (1.00 mmol) and 4-(trifluoromethyl)benzyl azide according to General Procedure 7.4.2.2 and purified by flash column chromatography (7:3 DCM:ethyl acetate) to obtain a yellow powder (183 mg, 0.400 mmol) in 40% yield.

^{1}H NMR (400 MHz, DMSO-d_6) δ 9.32 (s, 1 H), 9.31 (s, 1 H), 8.25 (d, *J*=8.9 Hz, 2 H), 7.77 (d, *J*=8.1 Hz, 2 H), 7.60 (d, *J*=8.9 Hz, 2 H), 7.57 (d, *J*=8.1 Hz, 2 H), 5.94 (s, 2 H), 5.80 (s, 2 H)

^{13}C NMR (100 MHz, DMSO-d_6) δ 175.2, 147.3, 145.14, 145.11, 142.8, 140.1, 130.7, 130.6, 129.1, 128.8 (q, *J*=31.7 Hz), 128.7, 125.7 (q, *J*=3.6 Hz), 124.0 (q, *J*=270 Hz), 123.9, 52.4, 52.1

^{19}F NMR (400 MHz, $(CD_3)_2CO$) δ -63.2

HRMS (ESI$^+$) calc. for $[C_{20}H_{14}N_7O_3F_3+Na]^+$ 480.1002 Da, obt. 480.1025 Da

m.p. 176-178°C (dec.)

R_f (7:3 DCM:ethyl acetate) ~0.3

7.4.3.10 (1-(4-nitrobenzyl)-1*H*-1,2,3-triazol-4-yl)(1-(4-(trifluoromethoxy)benzyl)-1*H*-1,2,3-triazol-4-yl)methanone (**4.19f**)

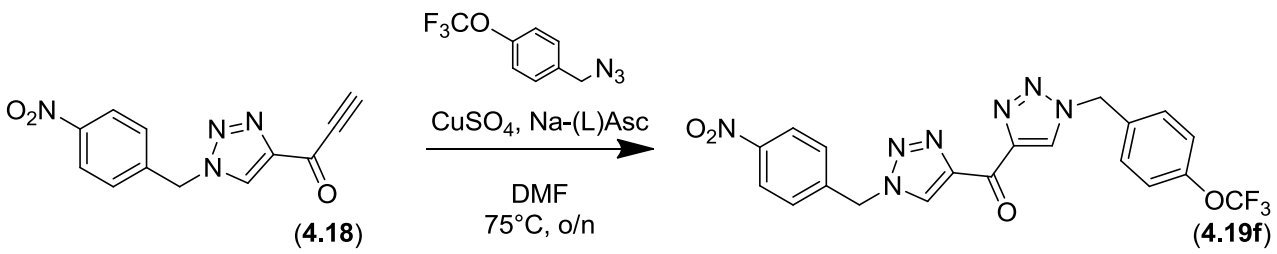

(**4.18**) (**4.19f**)

4-(Trifluoromethoxy)benzyl azide was prepared from 4-(trifluoromethoxy)benzyl bromide according to General Procedure 7.4.2.1. Compound **4.19f** was prepared[127] from ynone **4.18** (1.00 mmol) and 4-(trifluoromethoxy)benzyl azide according to General Procedure 7.4.2.2 and purified by flash column chromatography (2:1 DCM:ethyl acetate) to obtain a white powder (177 mg, 0.374 mmol) in 37% yield.

^{1}H NMR (400 MHz, DMSO-d_6) δ 9.33 (s, 1 H), 9.28 (s, 1 H), 8.25 (d, *J*=8.8 Hz, 2 H), 7.61 (d, *J*=8.8 Hz, 2 H), 7.53 (d, *J*=8.4 Hz, 2 H), 7.40 (d, *J*=8.4 Hz, 2 H), 5.94 (s, 2 H), 5.80 (s, 2 H)

^{13}C NMR (100 MHz, DMSO-d_6) δ 175.4, 148.30, 148.28, 147.4, 145.3, 145.2, 142.9, 135.0, 130.9, 130.5, 130.3, 129.3, 124.0, 121.5, 120.1 (q, *J*=255 Hz), 52.3

^{19}F NMR (400 MHz, DMSO-d_6) δ -56.8

HRMS (ESI$^+$) calc. for $[C_{20}H_{14}N_7O_4F_3+Na]^+$ 472.0957 Da, obt. 472.0951 Da

m.p. 167-169°C (dec.)

R_f (2:1 DCM:ethyl acetate) ~0.50

7.4.3.11 4-((4-(1-(4-nitrobenzyl)-1*H*-1,2,3-triazole-4-carbonyl)-1*H*-1,2,3-triazol-1-yl)methyl)benzonitrile (**4.19g**)

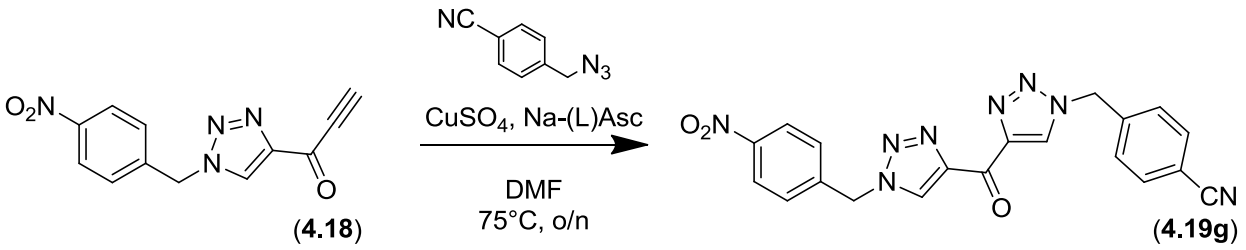

(**4.18**) (**4.19g**)

4-(Azidomethyl)benzonitrile was prepared from 4-(bromomethyl)benzonitrile according to General Procedure 7.4.2.1. Compound **4.19g** was prepared from ynone **4.18** (1.00 mmol) and 4-(azidomethyl)benzonitrile according to General Procedure 7.4.2.2 and purified by flash column chromatography (6:4 DCM:ethyl acetate) to obtain a pale yellow powder (108 mg, 0.261 mmol) in 26% yield.

^{1}H NMR (400 MHz, DMSO-d_6) δ 9.33 (s, 1 H), 9.30 (s, 1 H), 8.25 (d, *J*=8.9 Hz, 2 H), 7.87 (d, *J*=8.4 Hz, 2 H), 7.61 (d, *J*=8.9 Hz, 2 H), 7.53 (d, *J*=8.4 Hz, 2 H), 5.94 (s, 2 H), 5.87 (s, 2 H)

^{13}C NMR (100 MHz, DMSO-d_6) δ 175.2, 147.3, 145.11, 145.09, 142.7, 140.8, 132.7, 130.7, 130.6, 129.1, 128.8, 123.9, 118.4, 111.0, 52.4, 52.1

HRMS (ESI$^+$) calc. for $[C_{20}H_{14}N_8O_3+Na]^+$ 437.1081 Da, obt. 437.1093 Da

m.p. 196-198°C (dec.)

R_f (6:4 DCM:ethyl acetate) ~0.29

7.4.3.12 (1-(4-methylbenzyl)-1*H*-1,2,3-triazol-4-yl)(1-(4-nitrobenzyl)-1*H*-1,2,3-triazol-4-yl)methanone (**4.19h**)

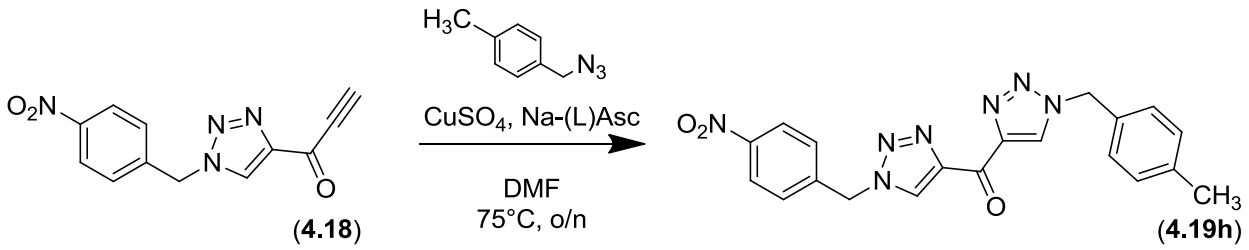

(**4.18**) (**4.19h**)

4-Methylbenzyl azide was prepared from 4-methylbenzyl bromide according to General Procedure 7.4.2.1. Compound **4.19h** was prepared from ynone **4.18** (1.00 mmol) and 4-methylbenzyl azide according to General Procedure 7.4.2.2 and purified by flash column chromatography (7:3 DCM:ethyl acetate) to obtain a yellow powder (157 mg , 0.389 mmol) in 39% yield.

^{1}H NMR (400 MHz, DMSO-d_6) δ 9.32 (s, 1 H), 9.19 (s, 1 H), 8.25 (d, *J*=8.8 Hz, 2 H), 7.60 (d, *J*=8.8 Hz, 2 H), 7.29 (d, *J*=7.9 Hz, 2 H), 7.19 (d, *J*=7.9 Hz, 2 H), 5.93 (s, 2 H), 5.69 (s, 2 H), 2.28 (s, 3 H)

^{13}C NMR (100 MHz, DMSO-d_6) δ 175.3, 147.3, 145.2, 145.1, 142.8, 137.7, 132.5, 130.8, 130.0, 129.4, 129.2, 128.1, 124.0, 52.9, 52.2, 20.7

HRMS (ESI$^+$) calc. for $[C_{20}H_{17}N_7O_3+Na]^+$ 426.1285 Da, obt. 426.1296 Da

m.p. 185-187°C (dec.)

R_f (7:3 DCM:ethyl acetate) ~0.34

7.4.3.13 (1-(4-methoxybenzyl)-1*H*-1,2,3-triazol-4-yl)(1-(4-nitrobenzyl)-1*H*-1,2,3-triazol-4-yl)methanone (**4.19i**)

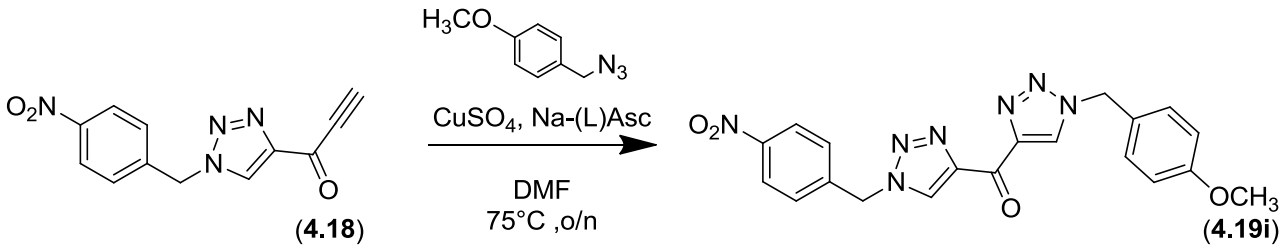

(**4.18**) (**4.19i**)

4-Methoxybenzyl azide was prepared from 4-methoxybenzyl bromide according to General Procedure 7.4.2.1. Compound **4.19i** was prepared from ynone **4.18** (1.00 mmol) and 4-methoxybenzyl azide according to General Procedure 7.4.2.2 and purified by flash column chromatography (6:4 DCM:ethyl acetate) to obtain a pale yellow powder (151 mg, 0.360 mmol) in 36% yield.

^{1}H NMR (400 MHz, DMSO-d_6) δ 9.32 (s, 1 H), 9.17 (s, 1 H), 8.25 (d, *J*=8.9 Hz, 2 H), 7.60 (d, *J*=8.9 Hz, 2 H), 7.37 (d, *J*=8.8 Hz, 2 H), 6.94 (d, *J*=8.8 Hz, 2 H), 5.93 (s, 2 H), 5.66 (s, 2 H), 3.74 (s, 3 H)

^{13}C NMR (100 MHz, DMSO-d_6) δ 175.2, 159.2, 147.2, 145.1, 145.0, 142.7, 130.7, 129.8, 129.7, 129.1, 127.3, 123.9, 114.1, 55.0, 52.6, 52.1

HRMS (ESI$^+$) calc. for $[C_{20}H_{17}N_7O_4+Na]^+$ 442.1234 Da, obt. 442.1237 Da

m.p. 177-179°C (dec.)

R_f (1:1 DCM:ethyl acetate) ~0.47

7.4.3.14 (1-(4-fluorobenzyl)-1*H*-1,2,3-triazol-4-yl)(1-(4-nitrobenzyl)-1*H*-1,2,3-triazol-4-yl)methanone (**4.19j**)

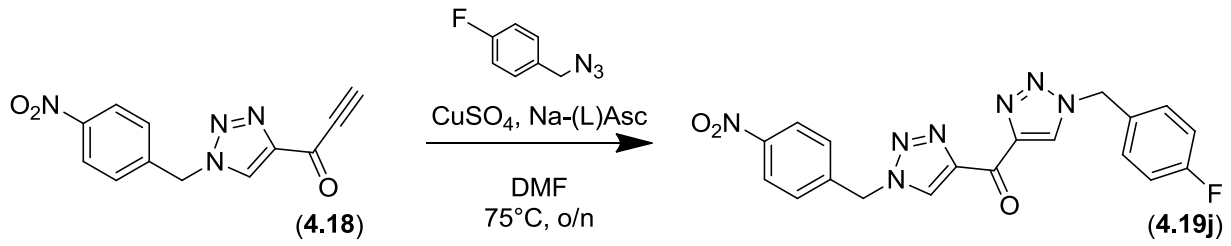

4-Fluorobenzyl azide was prepared from 4-fluorobenzyl bromide according to General Procedure 7.4.2.1. Compound **4.19j** was prepared from ynone **4.18** (1.00 mmol) and 4-fluorobenzyl azide according to General Procedure 7.4.2.2 and purified by flash column chromatography (7:3 DCM:ethyl acetate) to obtain a yellow powder (110 mg, 0.270 mmol) in 27% yield.

^{1}H NMR (400 MHz, DMSO-d_6) δ 9.32 (s, 1 H), 9.24 (s, 1 H), 8.25 (d, *J*=8.8 Hz, 2 H), 7.60 (d, *J*=8.8 Hz, 2 H), 7.47 (dd, *J*=8.9 Hz, *J*=8.9 Hz, 2 H), 7.23 (dd, *J*=8.9 Hz, *J*=8.9 Hz, 2 H), 5.93 (s, 2 H), 5.74 (s, 2 H)

^{13}C NMR (100 MHz, DMSO-d_6) δ 175.3, 147.3, 145.2, 145.1, 142.8, 131.7, 130.8, 130.5, 130.4, 130.2, 129.2, 124.0, 115.7 (d, *J*=21.5 Hz), 52.3, 51.2

^{19}F NMR (400 MHz, $(CD_3)_2CO$) δ -115.0

HRMS (ESI$^+$) calc. for $[C_{19}H_{14}N_7O_3F+Na]^+$ 430.1034 Da, obt. 430.1046 Da

m.p. 178-180°C (dec.)

R_f (7:3 DCM:ethyl acetate) ~0.29

7.4.3.15 (1-(4-bromobenzyl)-1*H*-1,2,3-triazol-4-yl)(1-(4-nitrobenzyl)-1*H*-1,2,3-triazol-4-yl)methanone (**4.19k**)

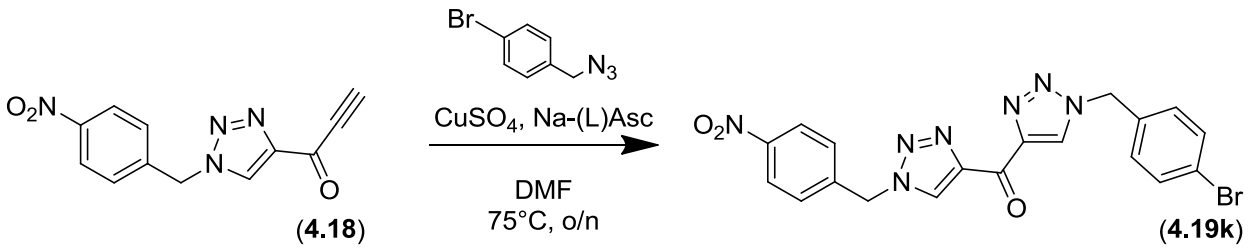

(**4.18**) (**4.19k**)

4-Bromobenzyl azide was prepared from 4-bromobenzyl bromide according to General Procedure 7.4.2.1. Compound **4.19k** was prepared from ynone **4.18** (1.00 mmol) and 4-bromobenzyl azide according to General Procedure 7.4.2.2 and purified by flash column chromatography (7:3 DCM:ethyl acetate) to obtain a yellow powder (140 mg, 0.299 mmol) in 30% yield.

^{1}H NMR (400 MHz, DMSO-d_6) δ 9.32 (s, 1 H), 9.25 (s, 1 H), 8.25 (d, *J*=8.9 Hz, 2 H), 7.603 (d, *J*=8.9 Hz, 2 H), 7.596 (d, *J*=8.5 Hz, 2 H), 7.35 (d, *J*=8.5 Hz, 2 H), 5.93 (s, 2 H), 5.74 (s, 2 H)

^{13}C NMR (100 MHz, DMSO-d_6) δ 175.8, 147.8, 145.6, 143.3, 135.4, 132.2, 131.3, 130.8, 129.7, 124.4, 122.1, 52.8, 52.7

HRMS (ESI^{+}) calc. for $[C_{19}H_{14}N_7O_3Br+Na]^{+}$ 490.0239 Da (^{79}Br), obt. 490.0215 Da

m.p. 202-204°C (dec.)

R_f (7:3 DCM:ethyl acetate) ~0.24

7.4.3.16 (1-(cyclohexylmethyl)-1*H*-1,2,3-triazol-4-yl)(1-(4-nitrobenzyl)-1*H*-1,2,3-triazol-4-yl)methanone (**4.19l**)

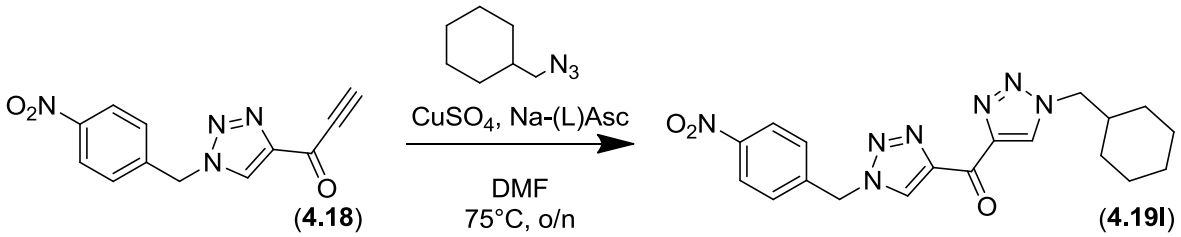

Azidomethylcyclohexane was prepared from bromomethylcyclohexane according to General Procedure 7.4.2.1, and used without further purification. Compound **4.18l** was prepared from ynone **4.18** (1.00 mmol) and azidomethylcyclohexane according to General Procedure E and purified by flash column chromatography (8:2 DCM:ethyl acetate) to obtain a pale yellow powder (119 mg, 0.301 mmol) in 30% yield.

^{1}H NMR (400 MHz, DMSO-d_6) δ 9.35 (s, 1 H), 9.09 (s, 1 H), 8.25 (d, *J*=8.8 Hz, 2 H), 7.61 (d, *J*=8.8 Hz, 2 H), 5.94 (s, 2 H), 4.36 (d, *J*=7.2 Hz, 2 H), 1.94-1.84 (m, 1 H), 1.69-165 (m, 2 H), 1.62-1.58 (m, 1 H), 1.54-1.51 (m, 2 H), 1.23-1.09 (m, 3 H), 1.03-0.93 (m, 2 H)

^{13}C NMR (100 MHz, DMSO-d_6) δ 175.3, 147.3, 144.98, 144.95, 142.8, 130.8, 130.2, 129.1, 123.9, 55.3, 52.1, 37.9, 29.5, 25.6, 24.9

HRMS (ESI^{+}) calc. for $[C_{19}H_{21}N_7O_3+Na]^{+}$ 418.1598 Da, obt. 418.1605 Da

m.p. 169-171°C (dec.)

R_f (8:2 DCM:ethyl acetate) ~0.25

7.4.3.17 (1-(4-(trifluoromethyl)benzyl)-1*H*-1,2,3-triazol-4-yl)methanol (**4.20a**)

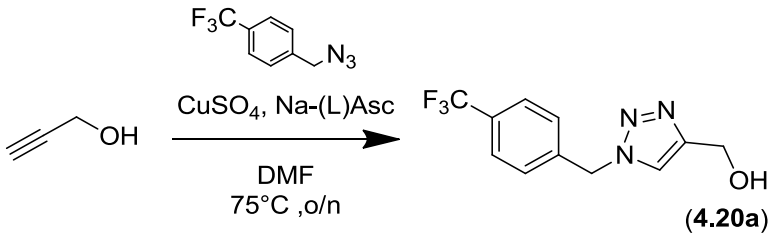

4-(Trifluoromethyl)benzyl azide was prepared from 4-(trifluoromethyl)benzyl bromide according to General Procedure 7.4.2.1. Compound **4.20a** was prepared[127] from propargyl alcohol and 4-(trifluoromethyl)benzyl azide (19.5 mmol) according to General Procedure 7.4.2.2, and obtained as a white powder (4.801 g, 18.67 mmol) in 96% yield.

^{1}H NMR (400 MHz, $(CD_3)_2CO$) δ 7.93 (s, 1 H), 7.73 (d, *J*=8.2 Hz, 2 H), 7.54 (d, *J*=8.2 Hz, 2 H), 5.74 (s, 2 H), 4.66 (s, 2 H)

^{13}C NMR (100 MHz, $(CD_3)_2CO$) δ 149.0, 141.0, 129.7 (q, *J*=32.0), 128.6, 125.7 (q, *J*=3.8), 123.0, 122.4, 55.9, 52.5

^{19}F NMR (400 MHz, $(CD_3)_2CO$) δ -63.1

HRMS (ESI$^+$) calc. for $[C_{10}H_{11}N_3OF_3+H]^+$ 258.0854 Da, obt. 258.0852 Da

m.p. 99-102°C

R_f (1:1 DCM:ethyl acetate) ~0.18

7.4.3.18 (1-benzyl-1*H*-1,2,3-triazol-4-yl)methanol (**4.20b**)

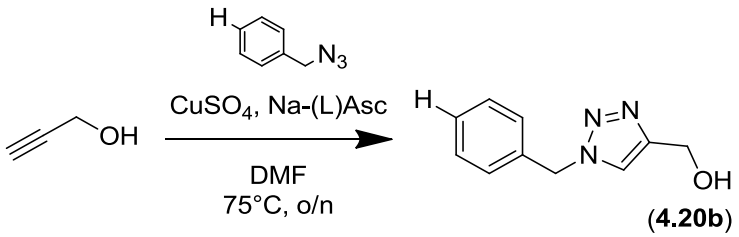

Benzyl azide was prepared from benzyl bromide according to General Procedure 7.4.2.1. Compound **4.20b** was prepared from propargyl alcohol (5.5 mmol) and benzyl azide according to General Procedure 7.4.2.2, and purified by flash column chromatography (ethyl acetate) to obtain a white powder (343 mg, 1.81 mmol) in 33% yield.

^{1}H NMR (400 MHz, $(CD_3)_2CO$) δ 7.82 (s, 1 H), 7.39-7.30 (m, 5 H), 5.59 (s, 2 H), 4.63 (s, 2 H)

^{13}C NMR (100 MHz, $(CD_3)_2CO$) δ 148.8, 136.4, 128.8, 128.2, 128.0, 122.0, 55.9, 53.2

MS (EI) 189 (3, M), 130 (8), 91 (100, tropyllium)

m.p. 77-80°C

R_f (ethyl acetate) ~0.22

7.4.3.19 1-(4-(trifluoromethyl)benzyl)-1*H*-1,2,3-triazole-4-carbaldehyde (**4.21a**)

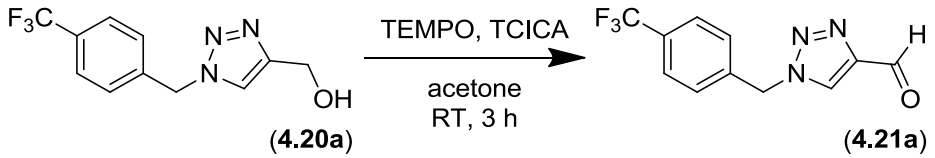

(**4.20a**) (**4.21a**)

Compound **4.21a** was prepared[127] from alcohol **4.20a** (18.67 mmol) according to General Procedure 7.4.2.3, and obtained as a white powder (3.313 g, 12.99 mmol) in 70% yield.

^{1}H NMR (400 MHz, $(CD_3)_2CO$) δ 10.06 (s, 1 H), 8.74 (s, 1 H), 7.75 (d, *J*=8.1 Hz, 2 H), 7.62 (d, *J*=8.1 Hz, 2 H), 5.90 (s, 2 H)

^{13}C NMR (100 MHz, $(CD_3)_2CO$) δ 184.4, 147.9, 139.8, 130.0 (q, *J*=32.1 Hz), 128.9, 127.0, 125.8 (q, *J*=3.8 Hz), 121.6 (q, *J*=270 Hz), 53.1

^{19}F NMR (400 MHz, $(CD_3)_2CO$) δ 63.2

HRMS (ESI$^+$) calc. for $[C_{11}H_8N_3OF_3+Na]^+$ 278.0517 Da, obt. 278.0486 Da

m.p. 86-88°C (dec.)

R_f (1:1 DCM:ethyl acetate) ~0.82

7.4.3.20 1-benzyl-1*H*-1,2,3-triazole-4-carbaldehyde (**4.21b**)

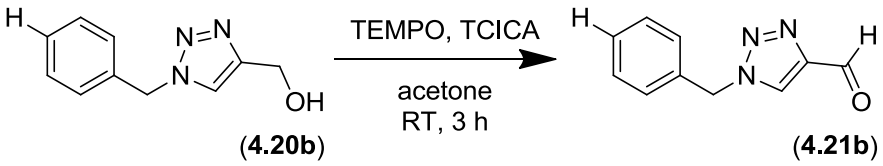

(**4.20b**) (**4.21b**)

Compound **4.21b** was prepared from alcohol **4.20b** (5.13 mmol) according to General Procedure 7.4.2.3 to obtain a orange oil (0.892 g, 4.76 mmol) in 93% yield.

^{1}H NMR (400 MHz, $(CD_3)_2CO$) δ 10.05 (s, 1 H), 8.64 (s, 1 H), 7.43-7.35 (m, 5 H), 5.75 (s, 2 H)

^{13}C NMR (100 MHz, $(CD_3)_2CO$) δ 184.4, 147.9, 135.4, 129.0, 125.6, 124.2, 126.6, 53.7

HRMS (EI) calc. for $[C_{10}H_9N_3O]$ 187.0746 Da, obt. 187.0735 Da

7.4.3.21 1-(1-(4-(trifluoromethyl)benzyl)-1*H*-1,2,3-triazol-4-yl)prop-2-yn-1-ol (**4.22a**)

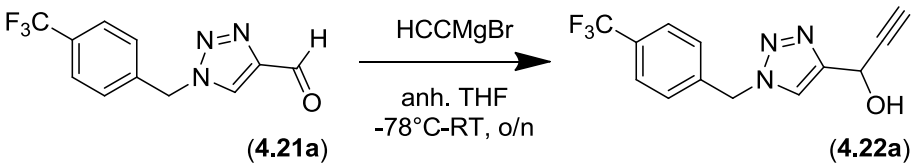

(**4.21a**) (**4.22a**)

Compound **4.22a** was prepared[127] from aldehyde **4.21a** (12.99 mmol) according to General Procedure 7.4.2.4 and purified by flash column chromatography (3:1 DCM:ethyl acetate) to obtain a white powder (1.895 g, 6.743 mmol) in 52% yield.

^{1}H NMR (400 MHz, $(CD_3)_2CO$) δ 8.08 (s, 1 H), 7.74 (d, *J*=8.1 Hz, 2 H), 7.58 (d, *J*=8.1 Hz, 2 H), 5.78 (s, 2 H), 5.63 (d, *J*=2.2 Hz, 1 H), 5.20 (br s, 1 H), 3.02 (d, *J*=2.2 Hz, 1 H)

^{13}C NMR (100 MHz, $(CD_3)_2CO$) δ 150.0, 141.6 (d, *J*=1.1 Hz), 130.7 (q, *J*=32.1 Hz), 129.6, 126.6 (q, *J*=4.0 Hz), 125.2 (q, *J*=270 Hz), 123.3, 84.5, 74.4, 57.5, 53.6

^{19}F NMR (400 MHz, $(CD_3)_2CO$) δ -63.1

HRMS (ESI$^+$) calc. for $[C_{13}H_{10}N_3OF_3+Na]^+$ 304.0674 Da, obt. 304.0674 Da

m.p. 127-135°C

R_f (3:1 DCM:ethyl acetate) ~0.22

7.4.3.22 1-(1-benzyl-1*H*-1,2,3-triazol-4-yl)prop-2-yn-1-ol (**4.22b**)

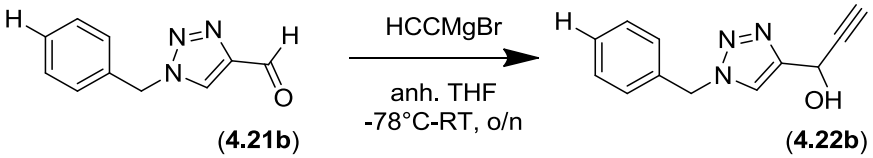

Compound **4.22b** was prepared from aldehyde **4.21b** (4.76 mmol) according to General Procedure 7.4.2.4 and purified by flash column chromatography (65:35 hexanes:ethyl acetate) to obtain a pale yellow powder (567 mg, 2.66 mmol) in 56% yield.

^{1}H NMR (400 MHz, $(CD_3)_2CO$) δ 7.95 (s, 1 H), 7.39-7.32 (m, 5 H), 5.62 (s, 2 H), 5.56 (d, *J*=2.1 Hz, 1 H), 2.99 (d, *J*=2.3 Hz, 1 H)

^{13}C NMR (100 MHz, $(CD_3)_2CO$) δ 148.9, 136.2, 128.8, 128.3, 128.1, 121.9, 83.7, 73.3, 56.6, 53.4

HRMS (EI) calc. for $[C_{12}H_{11}N_3O]$ 213.0902 Da, obt. 213.0893 Da

m.p. 83-85°C (dec.)

R_f (65:35 hexanes:ethyl acetate) ~0.083

7.4.3.23 1-(1-(4-(trifluoromethyl)benzyl)-1*H*-1,2,3-triazol-4-yl)prop-2-yn-1-one (**4.23a**)

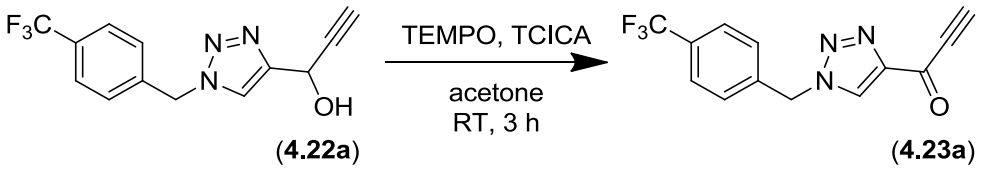

(**4.22a**) (**4.23a**)

Compound **4.23a** was prepared[127] from alcohol **4.22a** (6.74 mmol) according to General Procedure 7.4.2.3 and purified by flash column chromatography (DCM) to obtain a white powder (104 mg, 0.371 mmol) in 6% yield.

^{1}H NMR (400 MHz, $(CD_3)_2CO$) δ 8.82 (s, 1 H), 7.72 (d, *J*=8.2 Hz, 2 H), 7.61 (d, *J*=8.2 Hz, 2 H), 5.88 (s, 2 H), 4.30 (s, 1 H)

^{13}C NMR (100 MHz, $(CD_3)_2CO$) δ 169.7, 148.5, 140.7 (d, *J*=1.5 Hz), 131.0 (q, *J*=32.1 Hz), 130.1, 129.8, 126.8 (q, *J*=3.6 Hz), 125.2 (q, *J*=270 Hz), 82.8, 81.5, 54.1

^{19}F NMR (400 MHz, $(CD_3)_2CO$) δ -63.2

HRMS (ESI$^+$) calc. for $[C_{13}H_8N_3OF_3+Na]^+$ 302.0517 Da, obt. 302.0503 Da

m.p. 115-125°C

R_f (DCM) ~0.20

7.4.3.24 1-(1-benzyl-1*H*-1,2,3-triazol-4-yl)prop-2-yn-1-one (**4.23b**)

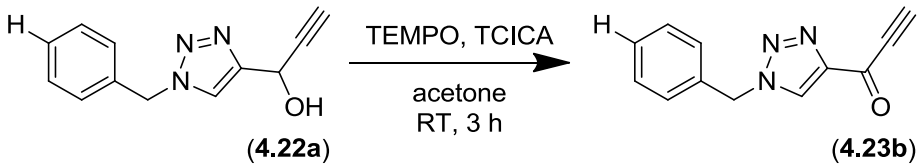

(**4.22a**) (**4.23b**)

Compound **4.23b** was prepared from alcohol **4.22b** (2.66 mmol) according to General Procedure 7.4.2.3 and purified by flash column chromatography (8:2 hexanes:ethyl acetate) to obtain a pale yellow-orange powder (185 mg, 0.875 mmol) in 33% yield.

^{1}H NMR (400 MHz, $(CD_3)_2CO$) δ 8.74 (s, 1 H), 7.44-7.35 (m, 5 H), 5.75 (s, 2 H), 4.30 (s, 1 H)

^{13}C NMR (100 MHz, $(CD_3)_2CO$) δ 168.9, 147.6, 135.3, 129.0, 128.7, 128.6, 128.2, 81.6, 80.6, 53.8

HRMS (EI) calc. for $[C_{12}H_9N_3O]$ 211.0746 Da, obt. 211.0742 Da

m.p. 76-78°C (dec.)

R_f (8:2 hexanes:ethyl acetate) ~0.11

7.4.3.25 bis(1-(4-(trifluoromethyl)benzyl)-1*H*-1,2,3-triazol-4-yl)methanone (**4.24a**)

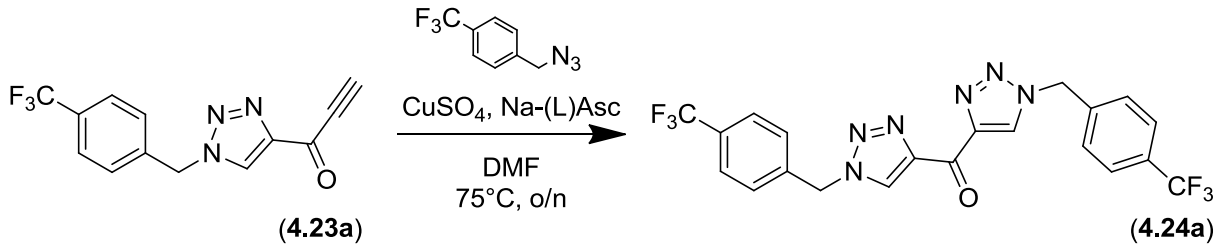

(**4.23a**) (**4.24a**)

4-(Trifluoromethyl)benzyl azide was prepared from 4-(trifluoromethyl)benzyl bromide according to General Procedure 7.4.2.1. Compound **4.24a** was prepared[127] from ynone **4.23a** (0.371 mmol) and 4-(trifluoromethyl)benzylazide according to General Procedure 7.4.2.2 and purified by flash column chromatography (8:2 DCM:ethyl acetate) to obtain a white powder (104 mg, 0.215 mmol) in 58% yield.

^{1}H NMR (400 MHz, DMSO-d_6) δ 9.31 (s, 2 H), 7.76 (d, *J*=8.1 Hz, 4 H), 7.58 (d, *J*=8.1 Hz, 4 H), 5.89 (s, 4 H)

^{13}C NMR (100 MHz, DMSO-d_6) δ175.3, 145.2, 140.1, 130.6, 128.85 (q, *J*=31.7 Hz), 128.80, 125.7 (q, *J*=4.0 Hz), 124.0 (q, *J*=270 Hz), 52.4

^{19}F NMR (400 MHz, DMSO-d_6) δ -61.2

HRMS (ESI^{+}) calc. for $[C_{21}H_{14}N_6OF_6+Na]^{+}$ 503.1031 Da, obt. 503.1049 Da

m.p. 203-205°C

R_f (8:2 DCM:ethyl acetate) ~0.40

7.4.3.26 bis(1-benzyl-1*H*-1,2,3-triazol-4-yl)methanone (**4.24b**)

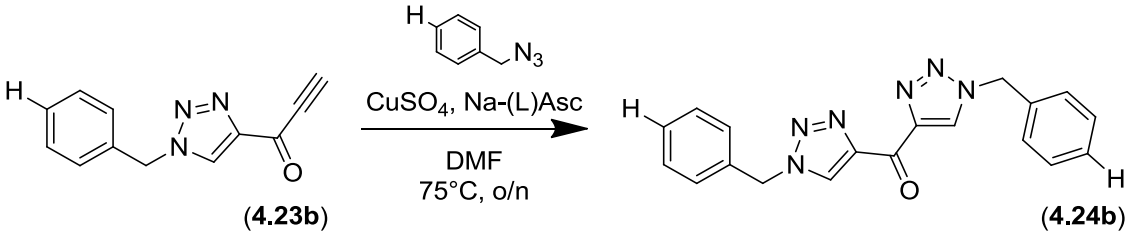

Benzyl azide was prepared from benzyl bromide according to General Procedure 7.4.2.1. Compound **4.24b** was prepared from ynone **4.23b** (0.875 mmol) and benzyl azide according to General Procedure 7.4.2.2 and purified by flash column chromatography (9:1 DCM:ethyl acetate) to obtain a white powder (142 mg, 0.412 mmol) in 47% yield.

^{1}H NMR (400 MHz, DMSO-d_6) δ 9.23 (s, 2 H), 7.40-7.33 (m, 10 H), 5.74 (s, 4 H)

^{13}C NMR (100 MHz, DMSO-d_6) δ 175.9, 145.6, 135.9, 130.7, 129.3, 128.8, 128.6, 53.6

HRMS (ESI^{+}) calc. for $[C_{19}H_{16}N_6O+Na]^{+}$ 367.1283 Da, obt. 367.1270 Da

m.p. 197-199°C

R_f (9:1 DCM:ethyl acetate) ~0.19

7.4.3.27 2-((4-iodobenzyl)oxy)tetrahydro-2*H*-pyran (**4.25**)

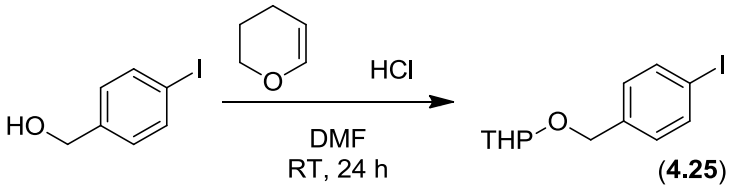

To a solution of 4-iodobenzyl alcohol (3.526 g, 15.06 mmol, 1.000 equiv) in DCM (12 mL) were added[128] 3,4-dihydro-2*H*-pyran (2.0 mL, 22 mmol, 1.5 equiv) and concentrated HCl (7 drops). The resulting heterogeneous mixture was vigorously stirred at room temperature for 24 hours prior to being divided between DCM (70 mL) and water (35 mL). The organic phase was additionally washed with brine (70 mL) prior to being dried over anhydrous magnesium sulfate, filtered, and evaporated to dryness to obtain **4.25** as a yellow oil (5.008 g, 15.74 mmol) in quantitative yield.

^{1}H NMR (400 MHz, $CDCl_3$) δ 7.65 (d, *J*=8.3 Hz, 2 H), 7.09 (d, *J*=8.4 Hz, 2 H), 4.70 (d, *J*=12.3 Hz, 1 H), 4.66 (t, *J*=3.5 Hz, 1 H), 4.42 (d, *J*=12.3 Hz, 1 H), 3.90-3.84 (m, 1 H), 3.55-3.49 (m, 1 H), 1.88-1.49 (m, 6 H)

^{13}C NMR (100 MHz, $CDCl_3$) δ 138.0, 137.4, 129.7, 97.8, 92.9, 68.13, 62.2, 30.5, 25.4, 19.3

MS (EI) 318 (4, M), 272 (9), 234 (9), 218 (2), 217 (100, M – O-THP)

R_f (4:1 hexanes:ethyl acetate) ~0.53

7.4.3.28 2,2,2-trifluoro-1-(4-(((tetrahydro-2*H*-pyran-2-yl)oxy)methyl)phenyl)ethanone (**4.26**)

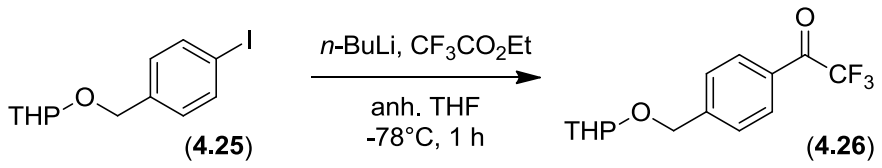

A 3-necked flask was charged[101] with anhydrous THF (140 mL) and cooled to -78°C prior to the addition of *n*-butyllithium (1.6 M in hexanes, 22 mL, 35 mmol, 2.2 equiv), followed by a solution of iodoaryl **4.25** (5.008 g, 15.74 mmol, 1.000 equiv) in anhydrous THF (15 mL). The resulting reaction solution was stirred at -78°C for one hour prior to the addition of ethyl trifluoroacetate (5.8 mL, 49 mmol, 3.1 equiv). The solution was divided between hexanes and water (125 mL each) and the organic phase was washed with brine (125 mL) prior to being dried over anhydrous magnesium sulfate, filtered, and evaporated under reduced pressure. The product **4.26** was purified by flash column chromatography (8:2 hexanes:DCM) to obtain a yellow oil (3.354 g, 11.64 mmol) in 74% yield.

^{1}H NMR (400 MHz, $CDCl_3$) δ 8.04 (d, *J*=7.7 Hz, 2 H), 7.53 (d, *J*=8.1 Hz, 2 H), 4.86 (d, *J*=13.6 Hz, 1 H), 4.72 (t, *J*=3.5 Hz, 1 H), 4.59 (d, *J*=13.6 Hz, 1 H), 3.91-3.84 (m, 1 H), 3.57-3.52 (m, 1 H), 1.92-1.51 (m, 6 H)

^{13}C NMR (100 MHz, $CDCl_3$) δ 180.0, 147.0, 130.3 (q, *J*=8.0 Hz), 129.0, 127.6, 116.7 (q, *J*=289 Hz), 98.2, 67.9, 62.2, 30.5, 25.4, 19.2

^{19}F NMR (400 MHz, $CDCl_3$) δ -71.4

MS (EI) 288 (1.6, M), 219 (15, M – CF_3), 188 (24), 187 (100, M – O-THP), 118 (39, M – O-THP – CF_3), 85 (90, THP)

7.4.3.29 1-(4-(bromomethyl)phenyl)-2,2,2-trifluoroethanone (**4.28**)

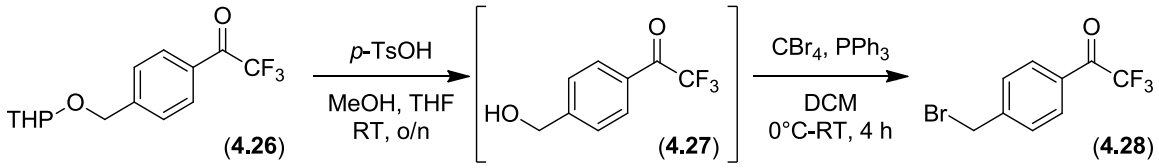

To a solution of the acetal **4.26** (3.100 g, 10.75 mmol, 1.000 equiv) in methanol (90 mL) and THF (55 mL) was added[128] *p*-toluenesulfonic acid monohydrate (0.210 g, 1.11 mmol, 0.103 equiv) prior to stirring the resulting solution at room temperature overnight. The reaction was quenched with sodium bicarbonate (3.6 g, 43 mmol) and the heterogeneous mixture was stirred for 5 minutes prior to being filtered and evaporated to dryness. The crude product **4.27** (1.684 g, ~8.249 mmol) was dissolved directly in DCM (18 mL) and cooled to 0°C prior to the addition of carbon tetrabromide (3.263 g, 9.840 mmol, 1.193 equiv) and triphenylphosphine (2.715 g, 10.35 mmol, 1.255 equiv). The resulting reaction mixture was allowed to warm to room temperature as it was stirred for four hours prior to being evaporated under reduced pressure. The product **4.28** was purified by flash column chromatography (9:1 hexanes:DCM) to obtain a white powder (0.491 g, 1.84 mmol) in 17% yield relative to the starting acetal **4.26.**

^{1}H NMR (400 MHz, $CDCl_3$) δ 8.04 (d, *J*=7.8 Hz, 2 H), 7.55 (d, *J*=8.6 Hz, 2 H), 4.49 (s, 2 H)

^{13}C NMR (100 MHz, $CDCl_3$) δ 179.9 (d, *J*=35.2 Hz), 145.5, 130.6 (q, *J*=2.1 Hz), 129.7, 129.6, 116.6 (q, *J*=289 Hz), 31.4

^{19}F NMR (400 MHz, CCl_3) δ -71.5

MS (EI) calc. for [$C_9H_6OF_3Br$] 265.9554 Da, obt. 265.9553 Da

m.p. 41-42°C

7.4.3.30 1-(4-(azidomethyl)phenyl)-2,2,2-trifluoroethanone (**4.29**)

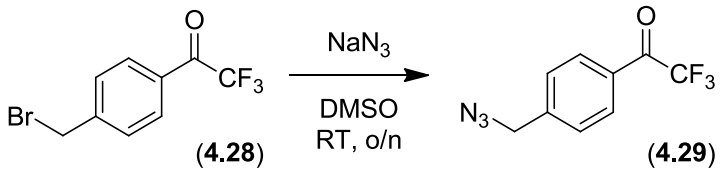

Compound **4.29** was prepared from intermediate **4.28** (1.84 mmol) according to General Procedure 7.4.2.1 to obtain a clear oil (0.369 g, 1.61 mmol) in 88% yield.

^{1}H NMR (400 MHz, $CDCl_3$) δ 8.08 (d, *J*=7.8 Hz, 2 H), 7.49 (d, *J*=8.6 Hz, 2 H), 4.47 (s, 2 H)

^{13}C NMR (100 MHz, $CDCl_3$) δ 180.0 (d, *J*=35.0 Hz), 143.5, 130.7, 129.6, 128.4, 116.6 (q, *J*=289 Hz), 54.1

^{19}F NMR (400 MHz, $CDCl_3$) δ -71.5

MS (EI) calc. for $[C_9H_9OF_3]^{\cdot}$ 187.0371 Da, obt. 187.0360 Da

7.5 Experimental section for Chapter 5

7.5.1 General procedures

7.5.1.1 Modified IC_{50} determination

IC_{50} values were determined in a similar manner to that outlined in section 7.3.2, with the exceptions that the organic co-solvent was changed from DMF to DMSO, the absorbance at 405 nm was measured on a BioTek Synergy H4 hybrid reader microplate reader, and the initial rates were taken over 90 seconds. The adjusted well volumes (in μL) are presented in Table 7.5 below.

Table 7.5. Well contents (in μL) for the determination of an IC_{50} value

AL5 buffer	Inhibitor (DMSO stock)	AL5 (20 mM)	DMSO	TG2 (0.020 U/mL)
190	0	5	5	0
140	0	5	5	50
140	1	5	4	50
140	2	5	3	50
140	3	5	2	50
140	4	5	1	50
140	5	5	0	50

7.5.1.2 Sonogashira coupling

To a solution of the substituted iodobenzene (1.0 equiv) in anhydrous THF (0.33 M) were added triphenylphosphine (20 mequiv), bis(triphenylphosphine)palladium(II) dichloride (6.0 mequiv),

copper(I) iodide (20 mequiv) and propargyl alcohol (1.2 equiv) prior to stirring at 50°C under reflux setup and nitrogen for 3 hours. The reaction was quenched with water, and the product was extracted with ethyl acetate. The combined organic extracts were washed with ammonium hydroxide, water, and brine prior to being dried over anhydrous magnesium sulfate, filtered, and evaporated under reduced pressure.

7.5.1.3 TEMPO oxidation ($PhI(OAc)_2$)

To a solution of the alcohol (**18** or **20**, 1.0 equiv) in DCM (0.2 M) were added[129] (diacetoxyiodo)benzene (1.8 equiv) and TEMPO (0.2 equiv), prior to stirring overnight at room temperature. The reaction solution was washed with saturated aqueous sodium bicarbonate and brine, prior to being dried over anhydrous magnesium sulfate, filtered and evaporated under reduced pressure.

7.5.1.4 DMP oxidation

To a solution of the alcohol (1.0 equiv) in DCM (0.1 M) was added the DMP (1.2 equiv) prior to stirring at room temperature for 75 minutes to 3 hours. Once the reactant consumption was complete, as observed by TLC, the reaction mixture was evaporated under reduced pressure. The crude residue was redissolved in ethyl acetate, resulting in the crashing out of a white precipitate that dissolved upon washing with a saturated aqueous solution of sodium thiosulfate. The organic phase was washed again with the saturated $Na_2S_2O_3$ solution, then with water and brine prior to being dried over anhydrous magnesium sulfate, filtered, and evaporated under reduced pressure.

7.5.1.5 Grignard addition (3 hours)

To a solution of the aldehyde (1.0 equiv) in anhydrous THF (0.05 M) cooled to -78°C was added ethynylmagnesium bromide (0.5 M in THF, 1.25 to 2.0 equiv), and the resulting reaction solution was stirred for three hours under nitrogen. The reaction was quenched with weakly acidic water and the product was extracted with ethyl acetate. The combined organic extracts were washed with brine prior to being dried over anhydrous magnesium sulfate, filtered, and evaporated under reduced pressure

7.5.1.6 Azide-alkyne cycloaddition (CuI)

To a solution of the ynone (1.0 equiv) in acetonitrile (0.1 M) were added[106] copper(I) iodide (1.0 equiv), the azide (1.0 equiv) and *N*,*N*-diisopropylethylamine (1.0 equiv, added dropwise) prior to stirring at room temperature overnight. The reaction mixture was then diluted with DCM prior to being washed with 1 N HCl, water, ammonium hydroxide, water, and brine before being dried over anhydrous magnesium sulfate, filtered, and evaporated under reduced pressure.

7.5.2 Inhibitor synthesis

7.5.2.1 3-(4-nitrophenyl)prop-2-yn-1-ol (**5.1**)

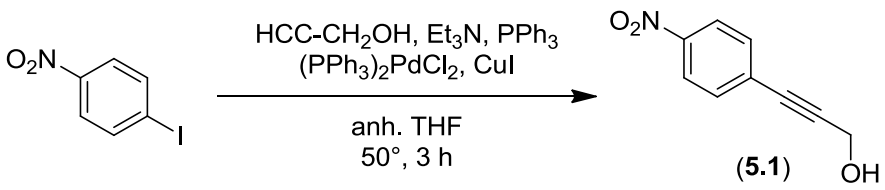

(**5.1**)

Compound **5.1** was prepared according to General Procedure 7.5.1.2 from 4-iodonitrobenzene (4.98 g, 20.0 mmol) and purified by flash column chromatography (1:1 hexanes:ethyl acetate) to obtain a dark orange powder (3.260 g, 18.40 mmol) in 92% yield.

^{1}H NMR (400 MHz, $CDCl_3$) δ 8.20 (d, *J*=8.7 Hz, 2 H), 7.59 (d, *J*=8.7 Hz, 2 H), 4.55 (s, 2 H), 1.70 (br s, 1 H)

^{13}C NMR (100 MHz, $CDCl_3$) δ 147.25, 132.41, 129.41, 123.59, 92.44, 83.84, 51.53

HRMS (EI) calc. for [$C_9H_7NO_3$ 177.0426 Da, obt. 177.0398 Da

m.p. 95-97°C (dec.)

R_f (1:1 hexanes:ethyl acetate) ~0.42

7.5.2.2 3-(4-nitrophenyl)prop-2-ynal (**5.2**)

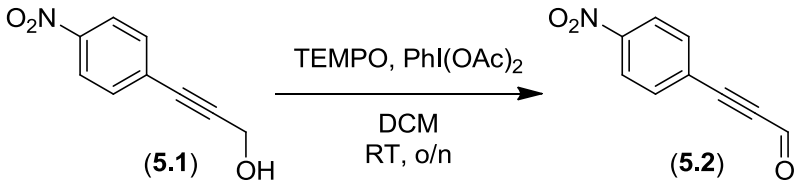

Compound **5.2** was prepared from alcohol **5.1** (3.260 g, 18.40 mmol) according to General Procedure 7.5.1.3 and purified by flash column chromatography (9:1 hexanes:ethyl acetate) to obtain a pale orange powder (1.708 g, 9.752 mmol) in 53% yield.

^{1}H NMR (400 MHz, $CDCl_3$) δ 9.47 (s, 1 H), 8.29 (d, *J*=9.0 Hz, 2 H), 7.78 (d, *J*=9.0 Hz, 2 H)

^{13}C NMR (100 MHz, $CDCl_3$) δ 176.1, 184.8, 133.9, 126.0, 123.9, 90.8, 90.6

HRMS (EI) calc. for [$C_9H_5NO_3$] 175.0269 Da, obt. 175.0243 Da

m.p. 87-89°C (dec.)

R_f (9:1 hexanes:ethyl acetate) ~0.22

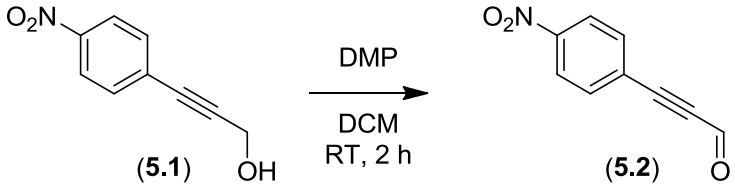

Compound **5.2** was also prepared from alcohol **5.1** (3.203 g, 18.08 mmol) according to General Procedure 7.5.1.4 and purified by flash column chromatography (4:6 DCM:hexanes) to obtain a pale yellow powder (2.987 g, 17.06 mmol) in 94% yield.

^{1}H NMR (400 MHz, $CDCl_3$) δ 9.47 (s, 1 H), 8.29 (d, *J*=9.0 Hz, 2 H), 7.78 (d, *J*=9.0 Hz, 2 H)

7.5.2.3 1-(4-nitrophenyl)penta-1,4-diyn-3-ol (**5.3**)

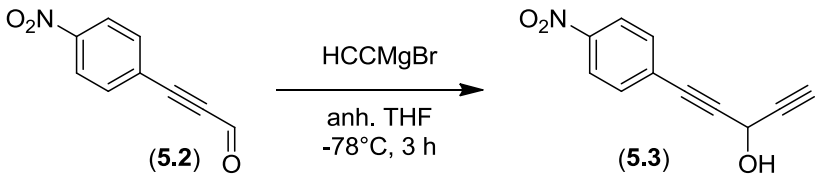

Compound **5.3** was prepared from aldehyde **5.2** (1.708 g, 9.752 mmol) according to General Procedure 7.4.2.4 and purified by flash column chromatography (7:3 hexanes:ethyl acetate) to obtain an orange powder (1.275 g, 6.337 mmol) in 65% yield.

^{1}H NMR (400 MHz, $CDCl_3$) δ 8.22 (d, *J*=8.9 Hz, 2 H), 7.64 (d, *J*=8.9 Hz, 2 H), 5.39 (s, 1 H), 2.68 (s, 1 H), 2.36 (br s, 1 H)

^{13}C NMR (100 MHz, $CDCl_3$) δ 147.6, 132.7, 128.5, 123.6, 90.3, 82.5, 80.0, 73.6, 52.4

HRMS (EI) calc. for [$C_{11}H_7NO_3$] 201.0426 Da, obt. 201.0410 Da

m.p. 109-111°C

R_f (7:3 hexanes:ethyl acetate) ~0.24

7.5.2.4 1-(4-nitrophenyl)penta-1,4-diyn-3-one (**5.4**)

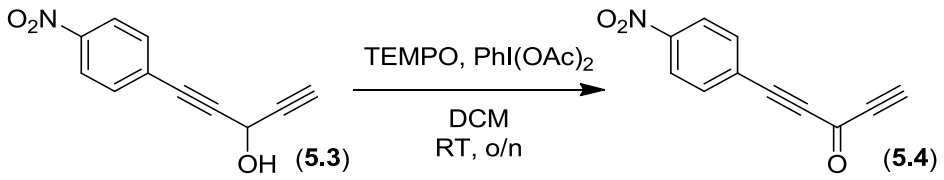

Compound **5.4** was prepared from alcohol **5.3** (1.275 g, 6.337 mmol) according to General Procedure 7.5.1.3 and purified by flash column chromatography (3:7 hexanes:DCM) to obtain a dark orange powder (606 mg, 3.04 mmol) in 48% yield.

^{1}H NMR (400 MHz, $CDCl_3$) δ 8.29 (d, *J*=8.9 Hz, 2 H), 7.80 (d, *J*=8.9 Hz, 2 H), 3.47 (s, 1 H)

^{13}C NMR (100 MHz, $CDCl_3$) δ 159.4, 148.9, 134.0, 125.7, 123.8, 91.1, 88.0, 81.8, 80.3

HRMS (EI) calc. for [$C_{11}H_5NO_3$] 199.0269 Da, obt. 199.0255 Da

m.p. 100-102°C

R_f (3:7 hexanes:DCM) ~0.5

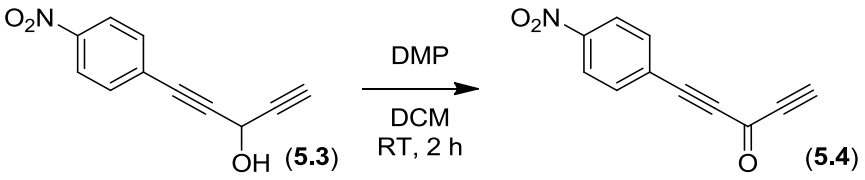

Compound **5.4** was also prepared from alcohol **5.3** (3.131 g, 15.56 mmol) according to General Procedure 7.5.1.4 and purified by flash column chromatography (4:6 hexanes:DCM) to obtain a pale yellow powder (2.741 g, 13.76 mmol) in 88% yield.

^{1}H NMR (400 MHz, $CDCl_3$) δ 8.29 (d, *J*=8.7 Hz, 2 H), 7.80 (d, *J*=8.7 Hz, 2 H), 3.47 (s, 1 H)

7.5.2.5 1-(1-benzyl-1*H*-1,2,3-triazol-4-yl)-3-(4-nitrophenyl)prop-2-yn-1-one (**4.8**)

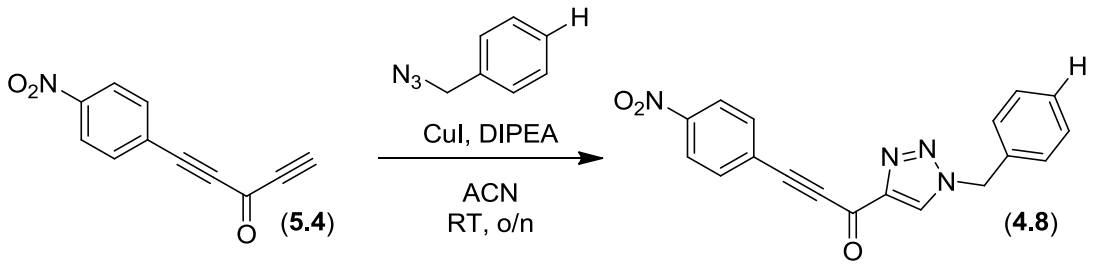

Benzyl azide was prepared from benzyl bromide according to General Procedure 7.4.2.1. Compound **4.8** was prepared from benzyl bromide and ynone **5.4** (100 mg, 0.50 mmol) according to General Procedure 7.5.1.6 and purified by flash column chromatography (1:1 hexanes:ethyl acetate) to obtain an off-white powder (42 mg, 0.13 mmol) in 26% yield.

^{1}H NMR (400 MHz, DMSO-d_6) δ 9.24 (s, 1 H), 8.35 (d, *J*=9.0 Hz, 2 H), 8.04 (d, *J*=9.0 Hz, 2 H), 7.41-7.36 (m, 5 H), 5.73 (s, 2 H)

^{13}C NMR (100 MHz, DMSO-d_6) δ 168.2, 148.4, 146.7, 135.2, 134.2, 130.2, 128.8, 128.3, 127.9, 125.3, 124.0, 89.4, 88.5, 53.2

HRMS (EI) calc. for [$C_{18}H_{12}N_4O_3$] 332.0909 Da, obt. 332.0893 Da

m.p. 154-156°C (dec.)

R_f (1:1 hexanes:ethyl acetate) ~0.33

7.5.2.6 1-(1-(4-nitrobenzyl)-1*H*-1,2,3-triazol-4-yl)-3-(4-nitrophenyl)prop-2-yn-1-one (**4.9**)

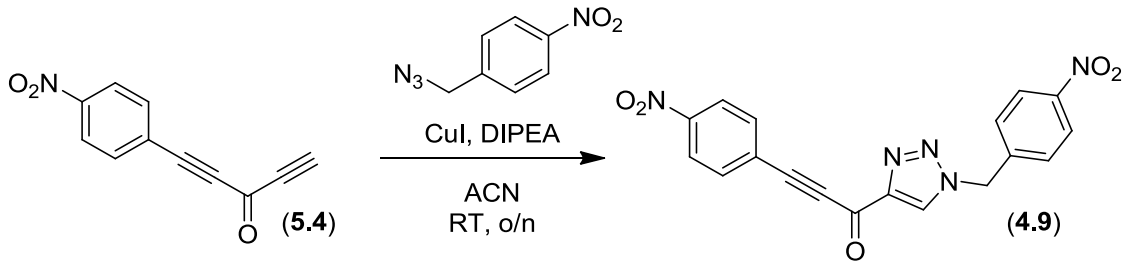

4-Nitrobenzyl azide was prepared from 4-nitrobenzyl bromide according to General Procedure 7.4.2.1. Compound **4.9** was prepared from 4-nitrobenzyl bromide and ynone **5.4** (207 mg, 1.04 mmol) according to General Procedure 7.5.1.6 and purified by flash column chromatography (1-5% ethyl acetate in DCM) to obtain a yellow powder (144 mg, 0.382 mmol) in 39% yield.

^{1}H NMR (400 MHz, DMSO-d_6) δ 9.29 (s, 1 H), 8.35 (d, *J*=8.8 Hz, 2 H), 8.26 (d, *J*=8.8 Hz, 2 H), 8.04 (d, *J*=8.8 Hz, 2 H), 7.60 (d, *J*=8.8 Hz, 2 H), 5.92 (s, 2 H)

^{13}C NMR (100 MHz, DMSO-d_6) δ 168.1, 148.5, 147.3, 146.8, 142.4, 134.2, 130.8, 129.1, 125.3, 124.0, 123.9, 89.4, 88.6, 52.3

HRMS (ESI^{+}) calc. for $[C_{18}H_{11}N_5O_5+Na]^{+}$ 400.0658 Da, obt. 400.0635 Da

m.p. 190-192°C (dec.)

R_f (97:3 DCM:ethyl acetate) ~0.33

7.5.2.7 trimethyl((4-nitrophenyl)ethynyl)silane (**5.6**)

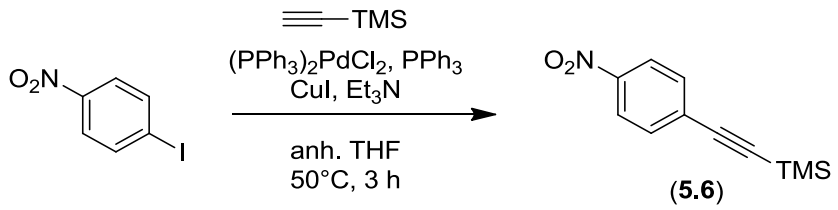

Compound **5.6** was prepared from 4-iodonitrobenzene (1.255 g, 5.000 mmol) and ethynyltrimethylsilane (0.85 mL, 6.0 mmol) according to General Procedure 7.5.1.2 and purified by flash column chromatography (9:1 hexanes:DCM) to obtain an off-white powder (976 mg, 4.45 mmol) in 89% yield.

^{1}H NMR (400 MHz, $CDCl_3$) δ 8.18 (d, *J*=8.9 Hz, 2 H), 7.61 (d, *J*=8.8 Hz, 2 H), 0.29 (s, 9 H)

^{13}C NMR (100 MHz, $CDCl_3$) δ 147.2, 132.7, 130.0, 123.5, 102.7, 100.6, -0.3

R_f (9:1 hexanes:DCM) ~0.20

7.5.2.8 1-ethynyl-4-nitrobenzene (**5.7**)

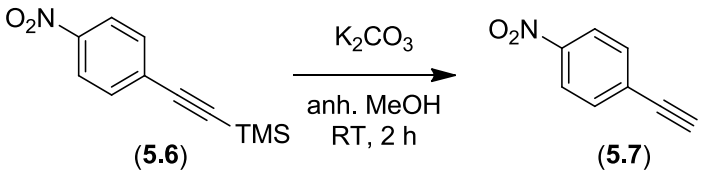

(**5.6**) (**5.7**)

To a suspension of the protected alkyne **5.6** (1.858 g, 8.471 mmol, 1.000 equiv) in anhydrous methanol (30 mL) was added[130] potassium carbonate (2.349 g, 17.00 mmol, 2.007 equiv), resulting in a thick slurry that was stirred at room temperature for 2.5 hours prior to being diluted with diethyl ether (85 mL). This organic phase was washed with water (2 x 40 mL) and brine (40 mL) prior to being dried over anhydrous magnesium sulfate, filtered, and evaporated under reduced pressure. The product **5.7** was purified by flash column chromatography (9:1 hexanes:DCM) to obtain a pastel yellow powder (1.205 g, 8.188 mmol) in 97% yield.

^{1}H NMR (400 MHz, $CDCl_3$) δ 8.21 (d, *J*=8.8 Hz, 2 H), 7.65 (d, *J*=8.9 Hz, 2 H), 3.37 (s, 1 H)

^{13}C NMR (100 MHz, $CDCl_3$) δ 133.0, 128.9, 123.6, 82.3, 81.6. Missing the aromatic C-NO_2

R_f (9:1 hexanes:DCM) ~0.1

7.5.2.9 Attempted coupling between alkyne **5.7** and aldehyde **4.16**

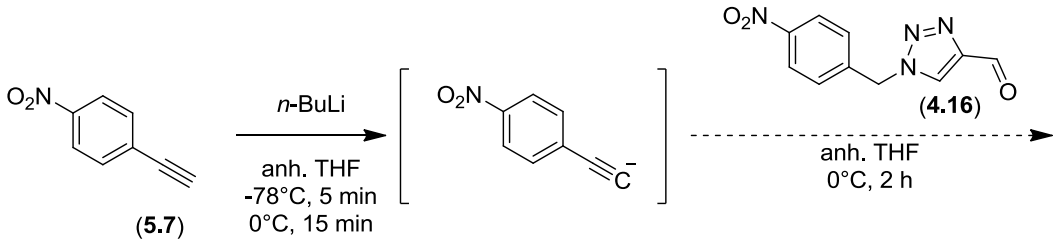

To a solution of alkyne **5.7** (172 mg, 1.17 mmol, 1.00 equiv) in anhydrous THF (3 mL), cooled to -78°C, was added[131] *n*-butyllithium (1.6 M in hexanes, 0.73 mL, 1.17 mmol, 1.00 equiv) prior to stirring at -78°C for 20 minutes. A solution of the aldehyde **4.16** (357 mg, 1.54 mmol, 1.32 equiv) in anhydrous THF (3 mL) was added slowly prior to stirring for 2 hours then quenching the reaction with D_2O (15 mL) and ammonium chloride (0.5 g, 9 mmol). The mixture was then diluted with diethyl ether (15 mL) and ethyl acetate (5 mL, to maximise product solubility). The product was extracted with a 1:1 solution of diethyl ether:ethyl acetate (2 x 15 mL), and the combined organic extracts were washed with water (20 mL) and brine (20 mL) prior to being dried over anhydrous magnesium sulfate, filtered, and evaporated under reduced pressure. The products were separated by flash column chromatography (1:1 hexanes:ethyl acetate) to recover deuterated alkyne **5.7** (119 mg, 0.806 mmol) in 69% yield.

7.5.2.10 1-(4-nitrobenzyl)-1*H*-1,2,3-triazole-4-carboxylic acid (**5.8**)

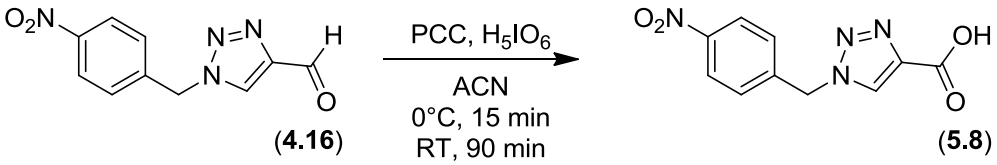

Periodic acid (728 mg, 3.19 mmol, 1.22 equiv) was added[132] to acetonitrile (10 mL) and stirred vigorously for 10 minutes while cooling to 0°C, prior to the addition of aldehyde **4.16** (607 mg, 2.61 mmol, 1.00 equiv) and a solution of pyridinium chlorochromate (12 mg, 58 μmol, 48 mequiv) in acetonitrile (3 mL). The resulting reaction mixture as allowed to gradually warm to room temperature as it was stirred for 90 minutes, resulting in an opaque mixture which was then diluted with ethyl acetate (55 mL), after verifying by TLC that the starting material had been consumed. The product was preliminarily extracted from the organic solution with a solution of 1:1 water:brine (40 mL), saturated aqueous sodium bicarbonate (3 x 40 mL) and brine (40 mL). These aqueous phases were combined and acidified to pH ~1 prior to the extraction of the product with ethyl acetate (3 x 50 mL). The combined organic phases were washed with 1 N HCl (3 x 40 mL) and brine (40 mL), then dried over anhydrous magnesium sulfate, filtered, and evaporated to dryness to obtain product **5.8** as a yellow powder (625 mg, 2.52 mmol) in 98% yield.

^{1}H NMR (400 MHz, $(CD_3)_2CO$) δ 8.68 (s, 1 H), 8.28 (d, *J*=8.7 Hz, 2 H), 7.66 (d, *J*=8.7 Hz, 2 H), 5.94 (s, 2 H)

HRMS (ESI$^+$) calc. for $[C_{10}H_8N_4O_4+Na]^+$ 271.0443 Da, obt. 271.0416 Da

7.5.2.11 Attempted coupling between carboxylic acid **5.8** and alkyne **5.7**

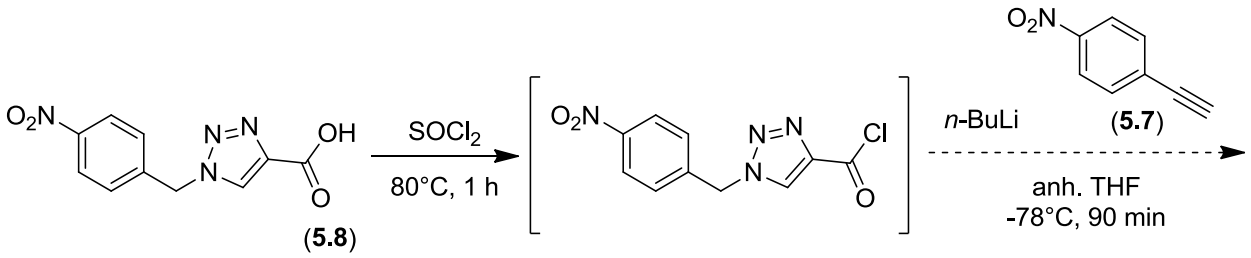

A mixture of carboxylic acid **5.8** (694 mg, 2.80 mmol, 1.10 equiv) in thionyl chloride (7 mL, 0.1 mol, 40 equiv) was stirred at reflux for one hour prior to the removal of the unreacted reagent by distillation. The crude acid chloride product was triturated with hexanes prior to being dried under high vacuum for 3 hours. To a solution of the alkyne **5.7** (374 mg, 2.55 mmol, 1.00 equiv) in anhydrous THF (6 mL), cooled to -78°C, was added[131] a *n*-butyllithium (1.6 M in hexanes, 4.0 mL, 6.4 mmol, 2.5 equiv) prior to stirring at -78°C for 15 minutes. A solution of the acid chloride in anhydrous THF (6 mL) was added dropwise and the mixture was stirred for an additional 90 minutes. The reaction was quenched with D_2O (30 mL) and ammonium chloride (3 g, 56 mmol), and the mixture was diluted with diethyl ether (10 mL) and ethyl acetate (30 mL). The product was additionally extracted with ethyl acetate (2 x 30 mL) and the combined organic extracts were washed with water (35 mL) and brine (35 mL) prior to being dried over anhydrous magnesium sulfate, filtered, and evaporated under reduced pressure. The products were isolated by flash column chromatography (0-10% ethyl acetate in DCM), to obtain decomposition products and alkyne **5.7** that was ~90% deuterated as verified by ^{1}H NMR.

7.5.2.12 3-phenylprop-2-yn-1-ol (**5.9a**)

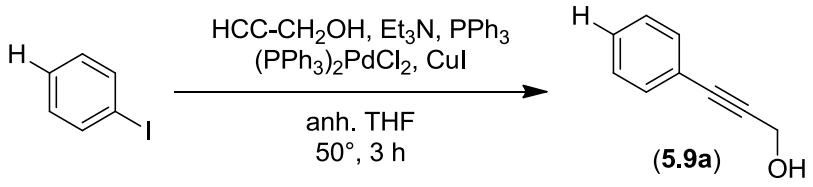

Compound **5.9a** was prepared from iodobenzene (20.00 mmol) according to General Procedure 7.5.1.2 and purified by flash column chromatography (100% DCM) to obtain a yellow oil (2.200 g, 16.65 mmol) in 83% yield.

^{1}H NMR (400 MHz, $CDCl_3$) δ 7.46-7.43 (m, 2 H), 7.35-7.31 (m, 3 H), 4.52 (s, 2H), 1.72 (br d, *J*=2.0 Hz, 1 H)

^{13}C NMR (100 MHz, $CDCl_3$) δ 131.7, 128.5, 128.3, 122.5, 87.7, 85.7, 51.6

HRMS (EI) calc. for [C_9H_8O] 132.0575 Da, obt. 132.0570 Da

R_f (DCM) ~0.34

7.5.2.13 3-phenylprop-2-ynal (**5.10a**)

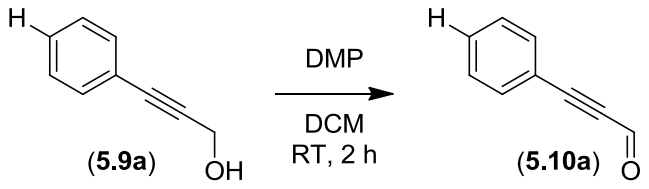

Compound **5.10a** was prepared from alcohol **5.9a** (16.65 mmol) according to General Procedure 7.5.1.4 and purified by flash column chromatography (3:1 hexanes:DCM) to obtain a yellow oil (1.705 g, 13.10 mmol) in 79% yield.

^{1}H NMR (400 MHz, $CDCl_3$) δ 9.44 (s, 1 H), 7.64-7.61 (m, 2 H), 7.53-7.48 (m, 1 H), 7.44-7.40 (m, 2 H)

^{13}C NMR (100 MHz, $CDCl_3$) δ 176.8, 133.3, 131.3, 128.7, 119.4, 95.1, 88.4

R_f (1:1 hexanes:DCM) ~0.46

7.5.2.14 1-phenylpenta-1,4-diyn-3-ol (**5.11a**)

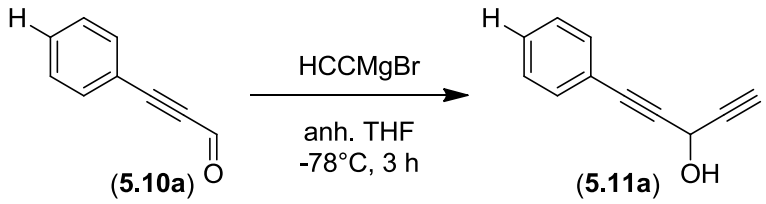

Compound **5.11a** was prepared from aldehyde **5.10a** (13.10 mmol) according to General Procedure 7.5.1.5 and purified by flash column chromatography (7:3 hexanes:DCM) to obtain a yellow oil (1.736 g, 11.12 mmol) in 85% yield.

^{1}H NMR (400 MHz, $CDCl_3$) δ 7.50-7.47 (m, 2 H), 7.38-7.31 (m, 3 H), 5.37 (d, *J*=2.4 Hz, 1 H), 2.63 (d, *J*=2.4 Hz, 1 H), 2.44 (br s, 1 H)

^{13}C NMR (100 MHz, $CDCl_3$) δ 131.8, 128.9, 128.3, 121.7, 85.4, 84.7, 80.8, 72.9, 52.5

HRMS (EI) calc. for [$C_{11}H_8O$] 156.0575 Da, obt. 156.0599 Da

m.p. between -20°C and 20°C

R_f (1:1 hexanes:DCM) ~0.09

7.5.2.15 1-phenylpenta-1,4-diyn-3-one (**5.12a**)

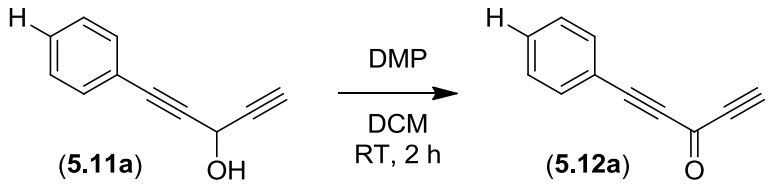

Compound **5.12a** was prepared from alcohol **5.11a** (11.12 mmol) according to General Procedure 7.5.1.4 and purified by flash column chromatography (7:3 hexanes:DCM) to obtain a brown powder (1.456 g, 9.445 mmol) in 85% yield.

^{1}H NMR (400 MHz, $CDCl_3$) δ 7.65-7.63 (m, 2 H), 7.54-7.49 (m, 1 H), 3.80 (s, 1 H)

^{13}C NMR (100 MHz, $CDCl_3$) δ 160.1, 133.5, 131.5, 128.7, 119.1, 92.5, 89.0, 82.2, 79.0

HRMS (EI) calc. for [$C_{11}H_6O$] 154.0419 Da, obt. 154.0411 Da

R_f (1:1 hexanes:DCM) ~0.64

7.5.2.16 1-(1-benzyl-1*H*-1,2,3-triazol-4-yl)-3-phenylprop-2-yn-1-one (**5.13a**)

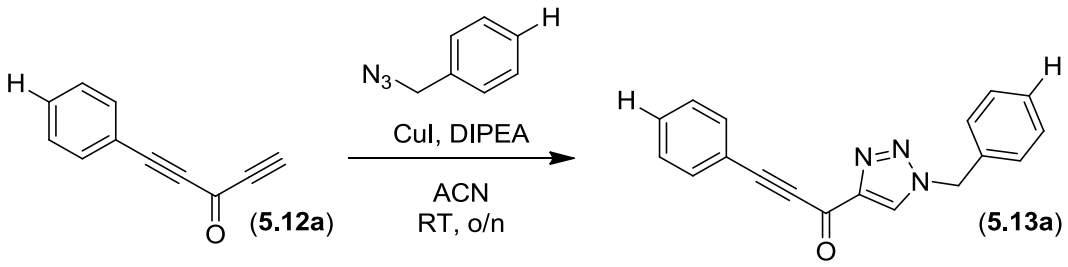

Benzyl azide was prepared from benzyl bromide according to General Procedure 7.4.2.1. Compound **5.13a** was prepared from benzyl azide and ynone **5.12a** (1.00 mmol) according to General Procedure 7.5.1.6 and purified by flash column chromatography (7:3 hexanes:DCM) to obtain a white powder (174 mg, 0.607 mmol) in 61% yield.

^{1}H NMR (400 MHz, $CDCl_3$) δ 8.07 (s, 1 H), 7.73-7.71 (m, 2 H), 7.51-7.47 (m, 1 H), 7.43-7.39 (m, 5 H), 7.34-7.31 (m, 2 H), 5.61 (s, 2 H)

^{13}C NMR (100 MHz, $CDCl_3$) δ 170.1, 148.5, 133.5, 133.44, 131.0, 129.4, 129.3, 128.6, 128.3, 126.7, 119.9, 94.1, 87.1, 54.6

HRMS (EI) calc. for [$C_{18}H_{13}N_3O$] 287.1059 Da, obt. 287.1088 Da

m.p. 144-146°C (dec.)

R_f (DCM) ~0.43

7.5.2.17 1-(1-(4-nitrobenzyl)-1*H*-1,2,3-triazol-4-yl)-3-phenylprop-2-yn-1-one (**5.14a**)

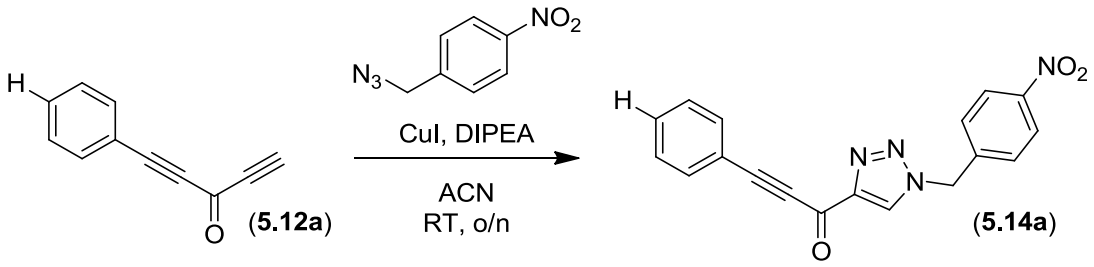

4-Nitrobenzyl azide was prepared from 4-nitrobenzyl bromide according to General Procedure 7.4.2.1. Compound **5.14a** was prepared from 4-nitrobenzyl azide and ynone **5.12a** (1.00 mmol) according to General Procedure 7.5.1.6 and purified by flash column chromatography (100% DCM) to obtain a white powder (140 mg, 0.422 mmol) in 42% yield.

^{1}H NMR (400 MHz, DMSO-d_6) δ 9.23 (s, 1 H), 8.26 (d, *J*=8.8 Hz, 2 H), 7.79-7.76 (m, 2 H), 7.64-7.59 (m, 3 H), 7.56-7.52 (m, 2 H), 5.91 (s, 2 H)

^{13}C NMR (100 MHz, DMSO-d_6) δ 168.5, 147.4, 147.0, 142.6, 133.1, 131.6, 130.6, 129.1, 123.9, 118.8, 91.9, 87.0, 52.3

HRMS (EI) calc. for [$C_{18}H_{12}N_4O_3$] 332.0909 Da, obt.332.0879 Da

m.p. 216-222°C

R_f (DCM) ~0.28

7.5.2.18 *tert*-butyl(4-iodophenoxy)dimethylsilane (**5.15**)

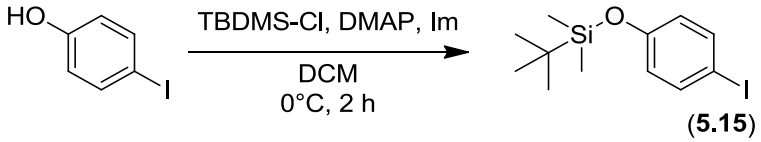

(**5.15**)

To a solution of 4-iodophenol (1.795 g, 8.161 mmol, 1.000 equiv), 4-(dimethylamino)pyridine (60 mg, 0.49 mmol, 60 mequiv) and imidazole (909 mg, 13.3 mmol, 1.63 equiv) in DCM (7.5 mL), cooled to 0°C, was added *t*-butyldimethylsilyl chloride (1.740 g, 11.55 mmol, 1.415 equiv) portionwise prior to stirring for 2 h while allowing the reaction mixture to slowly warm to room temperature. The mixture was filtered and the filtrate was evaporated under reduced pressure prior to the dissolution of the crude residue in DCM (20 mL). The organic solution was washed with 1 N HCl (10 mL), 1 N NaOH (10 mL) and brine prior to being dried over anhydrous magnesium sulfate, filtered, and evaporated to dryness to obtain **5.15** as a yellow oil (2.398 g, 7.174 mmol) in 88% yield.

^{1}H NMR (400 MHz, $CDCl_3$) δ 7.51 (d, *J*=8.8 Hz, 2 H), 6.62 (d, *J*=8.8 Hz, 2 H), 0.98 (s, 9 H), 0.19 (s, 6 H)

^{13}C NMR (100 MHz, $CDCl_3$) δ 153.6, 138.3, 122.5, 83.7, 25.6, 18.2, -4.5

HRMS (EI) calc. for [$C_{12}H_{19}OISi$] 334.0250 Da, obt. 334.0243 Da

7.5.2.19 3-(4-((*tert*-butyldimethylsilyl)oxy)phenyl)prop-2-yn-1-ol (**5.9b**)

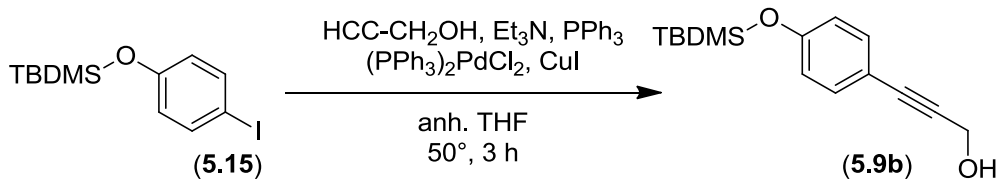

Compound **5.9b** was prepared from iodobenzene **5.15** (7.174 mmol) according to General Procedure 7.5.1.2 and purified by flash column chromatography (100% DCM) to obtain a yellow oil (1.466 g, 5.586 mmol) in 78% yield.

^{1}H NMR (400 MHz, $CDCl_3$) δ 7.33 (d, *J*=8.8 Hz, 2 H), 6.78 (d, *J*=8.8 Hz, 2 H), 4.49 (s, 2 H), 1.66 (br s, 1 H), 0.98 (s, 9 H), 0.21 (s, 6 H)

^{13}C NMR (100 MHz, $CDCl_3$) δ 156.1, 133.2, 120.2, 115.2, 86.0, 85.7, 51.7, 25.6, 18.2, -4.4

HRMS (EI) calc. for [$C_{15}H_{22}O_2Si$] 262.1389 Da, obt. 262.1406 Da

R_f (DCM) ~0.42

7.5.2.20 3-(4-((*tert*-butyldimethylsilyl)oxy)phenyl)prop-2-ynal (**5.10b**)

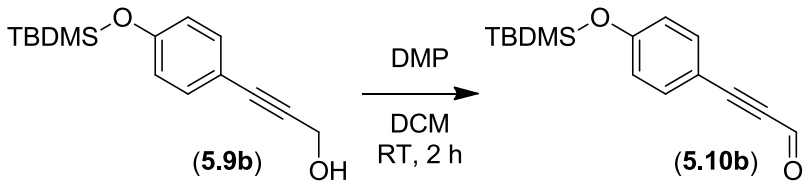

Compound **5.10b** was prepared from alcohol **5.9b** (5.586 mmol) according to General Procedure 7.5.1.4 and purified by gravity column chromatography (100% DCM) to obtain a yellow oil (1.259 g, 4.836 mmol) in 87% yield.

^{1}H NMR (400 MHz, $CDCl_3$) δ 9.40 (s, 1 H), 7.52 (d, *J*=8.8 Hz, 2 H), 6.86 (d, *J*=8.8 Hz, 2 H), 0.99 (s, 9 H), 0.24 (s, 6 H)

^{13}C NMR (100 MHz, $CDCl_3$) δ 176.7, 158.8, 135.4, 120.6, 111.8, 96.5, 88.7, 25.5, 18.2, -4.4

HRMS (EI) calc. for [$C_{15}H_{20}O_2Si$] 260.1233 Da, obt. 260.1235 Da

R_f (DCM) ~0.84

m.p. between -20°C and 20°C

7.5.2.21 1-(4-((*tert*-butyldimethylsilyl)oxy)phenyl)penta-1,4-diyn-3-ol (**5.11b**)

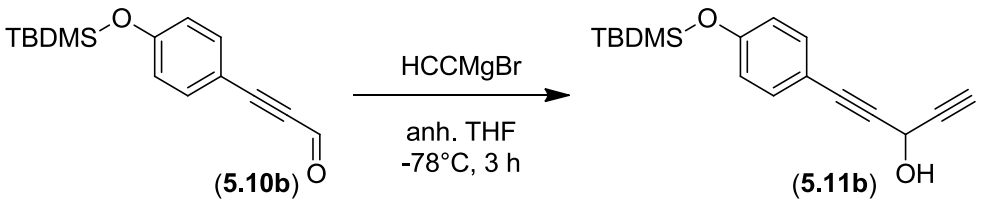

Compound **5.11b** was prepared from aldehyde **5.10b** (4.836 mmol) according to General Procedure 7.5.1.5 and purified by gravity column chromatography (100% DCM) to obtain a yellow oil (711 mg, 2.48 mmol) in 51% yield.

^{1}H NMR (400 MHz, $CDCl_3$) δ 7.36 (d, *J*=8.7 Hz, 2 H), 6.79 (d, *J*=8.7 Hz, 2 H), 5.34 (dd, *J*=7.5 Hz, *J*=2.3 Hz, 1 H), 2.61 (d, *J*=2.2 Hz, 1 H), 2.33 (d, *J*=7.6 Hz, 1 H), 0.98 (s, 9 H), 0.21 (s, 6 H)

^{13}C NMR (100 MHz, $CDCl_3$) δ 156.5, 133.4, 120.2, 114.4, 84.9, 84.3, 81.0, 72.7, 52.6, 25.7, 18.2, -4.4

HRMS (EI) calc. for [$C_{17}H_{22}O_2Si$] 286.1389 Da, obt. 286.1418 Da

R_f (DCM) ~0.38

7.5.2.22 1-(4-((*tert*-butyldimethylsilyl)oxy)phenyl)penta-1,4-diyn-3-one (**5.12b**)

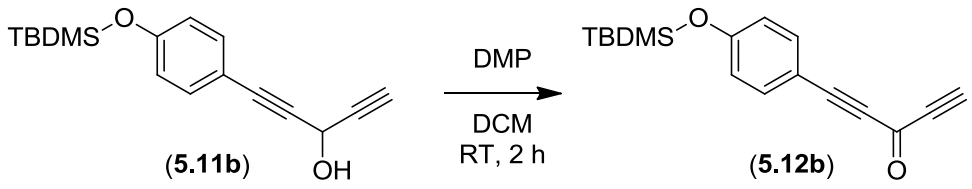

Compound **5.12b** was prepared from alcohol **5.11b** (3.929 mmol) according to General Procedure 7.5.1.4 and purified by gravity column chromatography (100% DCM) to obtain a brown powder (694 mg, 3.38 mmol) in 86% yield.

^{1}H NMR (400 MHz, $CDCl_3$) δ 7.54 (d, *J*=8.7 Hz, 2 H), 6.86 (d, *J*=8.8 Hz, 2 H), 3.34 (s, 1 H), 0.99 (s, 9 H), 0.24 (s, 6 H)

^{13}C NMR (100 MHz, $CDCl_3$) δ 160.1, 159.1, 135.7, 120.6, 111.4, 94.1, 89.5, 82.3, 78.5, 25.5, 18.2, -4.4

HRMS (EI) calc. for [$C_{17}H_{20}O_2Si$] 284.1233 Da, obt. 284.1274 Da

m.p. <50°C

R_f (DCM) ~0.77

7.5.2.23 1-(1-benzyl-1*H*-1,2,3-triazol-4-yl)-3-(4-((tert-butyldimethylsilyl)oxy)phenyl)prop-2-yn-1-one (**5.13b**)

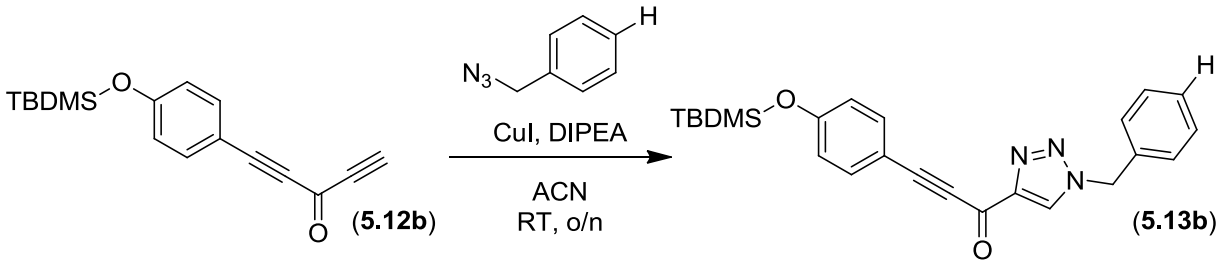

Benzyl azide was prepared from benzyl bromide according to General Procedure 7.4.2.1. Compound **5.13b** was prepared from benzyl azide and ynone **4.12b** (0.986 mmol) according to General Procedure 7.5.1.6 and purified by flash column chromatography (0-2% ethyl acetate in DCM) to obtain a dark orange oil (90 mg, 0.22 mmol) in 22% yield.

^{1}H NMR (400 MHz, $CDCl_3$) δ 8.05 (s, 1 H), 7.62 (d, *J*=8.7 Hz, 2 H), 7.43-7.40 (m 3 H), 7.34-7.31 (m, 2 H), 6.86 (d, *J*=8.7 Hz, 2 H), 5.61 (s, 2 H), 0.99 (s, 9 H), 0.24 (s, 6 H)

^{13}C NMR (100 MHz, $CDCl_3$) δ 170.1, 158.6, 148.6, 135.6, 133.6, 129.4, 129.2, 128.3, 126.5, 120.5, 112.3, 95.4, 87.2, 54.6, 25.6, 18.2, -4.4

HRMS (EI) calc. for [$C_{24}H_{27}N_3O_2Si$] 417.1873 Da, obt. 417.1893 Da

R_f (DCM) ~0.25

7.5.2.24 1-(1-benzyl-1*H*-1,2,3-triazol-4-yl)-3-(4-hydroxyphenyl)prop-2-yn-1-one (**5.16**)

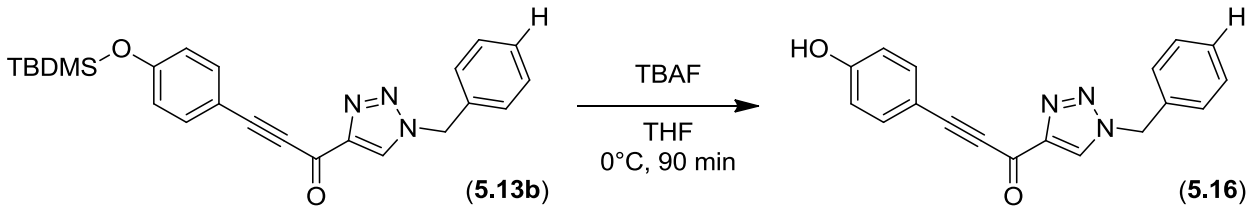

To a solution of silyl ether **5.13b** (83 mg, 0.20 mmol, 1.0 equiv) in THF (1 mL), cooled to 0°C, was added[133] a TBAF solution (1.0 M in THF, 0.70 mL, 0.70 mmol, 3.5 equiv) dropwise prior to stirring at 0°C for 90 minutes, at which point TLC analysis showed complete reactant consumption. The solvent was removed by evaporation under reduced pressure prior to dividing the crude residue between ethyl acetate (1 mL) and water (1 mL). The product was additionally extracted from the aqueous phase with ethyl acetate (2 x 1 mL) and the combined organic extracts were washed with brine (2 mL) prior to being dried over anhydrous magnesium sulfate, filtered, and evaporated under reduced pressure. Compound **5.16** was purified by flash column chromatography (8:2 DCM:ethyl acetate) to obtain a pale pink crystalline powder (40 mg, 0.13 mmol) in 61% yield.

^{1}H NMR (400 MHz, MeOD) δ 8.70 (s, 1 H), 7.63 (d, *J*=8.8 Hz, 2 H), 7.41-7.36 (m, 5 H), 6.86 (d, *J*=8.7 Hz, 2 H), 5.69 (s, 2 H)

^{13}C NMR (100 MHz, MeOD) δ 170.8, 162.5, 149.3, 137.1, 136.4, 130.3, 130.0, 129.7, 129.4, 117.2, 111.1, 96.9, 87.9, 55.4

HRMS (EI) calc. for [$C_{18}H_{13}N_3O_2$] 303.1008 Da, obt. 303.0991 Da

R_f (8:2 DCM:ethyl acetate) ~0.37

7.5.2.25 3-(4-((*tert*-butyldimethylsilyl)oxy)phenyl)-1-(1-(4-nitrobenzyl)-1*H*-1,2,3-triazol-4-yl)prop-2-yn-1-one (**5.14b**)

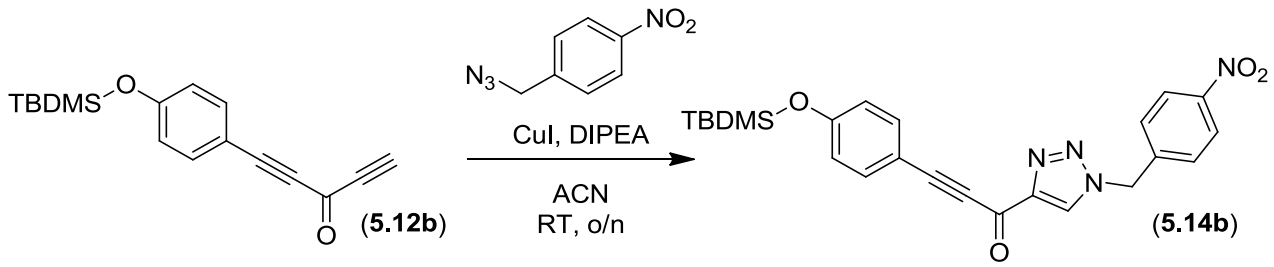

4-Nitrobenzyl azide was prepared from 4-nitrobenzyl bromide according to General Procedure 7.4.2.1. Compound **5.14b** was prepared from 4-nitrobenzyl azide and ynone **5.12b** (0.988 mmol) according to General Procedure 7.5.1.6 and purified by flash column chromatography (0-2% ethyl acetate in DCM) to obtain an off-white powder (170 mg, 0.368 mmol) in 37% yield.

^{1}H NMR (400 MHz, $CDCl_3$) δ 8.28 (d, *J*=8.8 Hz, 2 H), 8.16 (s, 1 H), 7.63 (d, *J*=8.7 Hz, 2 H), 7.47 (d, *J*=8.7 Hz, 2 H), 6.87 (d, *J*=8.7 Hz, 2 H), 5.74 (s, 2 H), 0.99 (s, 9 H), 0.24 (s, 6 H)

^{13}C NMR (100 MHz, $CDCl_3$) δ 169.8, 158.8, 149.0, 148.3, 140.6, 135.6, 128.8, 126.7, 124.5, 120.6, 112.1, 96.0, 87.2, 53.5, 25.6, 18.2, -4.4

HRMS (EI) calc. for [$C_{24}H_{26}N_4O_4Si$] 462.1723 Da, obt. 462.1706 Da

m.p. 155-157°C (dec.)

R_f (DCM) ~0.21

7.5.2.26 3-(4-hydroxyphenyl)-1-(1-(4-nitrobenzyl)-1*H*-1,2,3-triazol-4-yl)prop-2-yn-1-one (**5.17**)

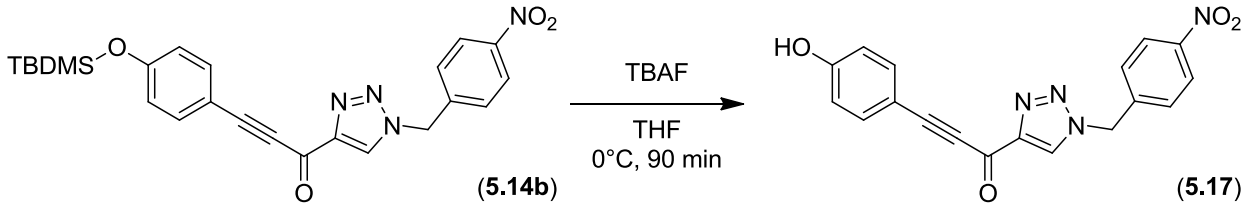

To a solution of the silyl ether **5.14b** (156 mg, 0.338 mmol, 1.00 equiv) in THF (4 mL), cooled to 0°C, was added[133] a TBAF solution (1.0 M in THF, 2.0 mL, 2.0 mmol, 5.9 equiv) dropwise prior to stirring at 0°C for 90 minutes, at which point TLC analysis showed complete reactant consumption. The solvent was removed by evaporation under reduced pressure prior to dividing the crude residue between ethyl acetate (2 mL) and water (2 mL). The product was additionally extracted from the aqueous phase with ethyl acetate (2 x 2 mL) and the combined organic extracts were washed with brine (3 mL) prior to being dried over anhydrous magnesium sulfate, filtered, and evaporated under reduced pressure. Compound **5.17** was purified by flash column chromatography (7:3 DCM:ethyl acetate) to obtain a yellow powder (100 mg, 0.288 mmol) in 81% yield.

^{1}H NMR (400 MHz, DMSO-d_6) δ 10.47 (br s, 1 H), 9.16 (s, 1 H), 8.25 (d, *J*=8.8 Hz, 2 H), 7.62 (d, *J*=8.8 Hz, 2 H), 7.59 (d, *J*=8.8 Hz, 2 H), 6.89 (d, *J*=8.7 Hz, 2 H), 5.89 (s, 2 H)

^{13}C NMR (100 MHz, DMSO-d_6) δ 168.4, 160.8, 147.3, 147.2, 142.7, 135.6, 130.2, 129.1, 123.9, 116.2, 108.5, 94.4, 87.0, 52.3

HRMS (ESI$^+$) calc. for $[C_{18}H_{12}N_4O_4+Na]^+$ 371.0756 Da, obt. 371.0742 Da

m.p.172-174°C (dec.)

R_f (7:3 DCM:ethyl acetate) ~0.40

7.5.2.27 3-(4-methoxyphenyl)prop-2-yn-1-ol (**5.9c**)

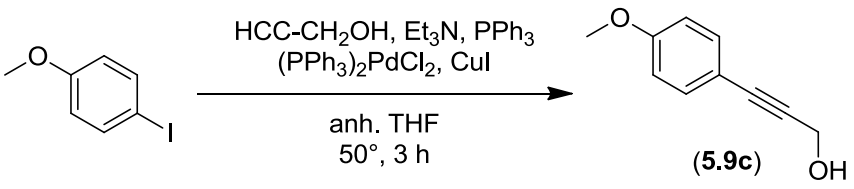

Compound **5.9c** was prepared[123] from 4-iodoanisole (4.68 g, 20.0 mmol) according to General Procedure 7.5.1.2 and purified by flash column chromatography (4:1 hexanes:ethyl acetate) to obtain the product (720 mg, 4.4 mmol) in 22% yield.

^{1}H NMR (400 MHz, $CDCl_3$) δ 7.36 (d, *J*=6.4 Hz, 2 H), 6.82 (d, *J*=6.4 Hz, 2 H), 4.46 (s, 2 H), 3.78 (s, 3 H)

^{13}C NMR (100 MHz, $CDCl_3$) δ 159.8, 133.2, 114.6, 114.0, 85.8, 85.7, 55.3, 51.8

HRMS (EI) calc. for [$C_{10}H_{10}O_2$] 162.0681 Da, obt. 162.0687 Da

7.5.2.28 3-(4-methoxyphenyl)prop-2-ynal (**5.10c**)

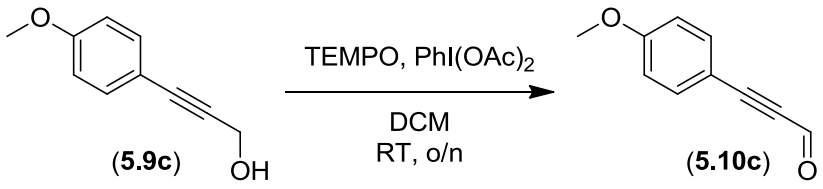

Compound **5.10c** was prepared[123] from alcohol **5.9c** (720 mg, 4.4 mmol) according to General Procedure 7.5.1.3 and purified by flash column chromatography (95:5 hexanes:DCM) to obtain the product (270 mg, 1.7 mmol) in 37% yield.

^{1}H NMR (400 MHz, $CDCl_3$) δ 9.38 (s, 1 H), 7.55 (d, *J*=8.2 Hz, 2 H), 6.91 (d, *J*=8.2 Hz, 2 H), 3.84 (s, 3 H)

^{13}C NMR (100 MHz, $CDCl_3$) δ 176.7, 162.2, 135.4, 114.5, 111.2, 96.6, 88.8, 55.5

HRMS (EI) calc. for [$C_{10}H_8O_2$] 160.0524 Da, obt. 160.0542 Da

7.5.2.29 1-(4-methoxyphenyl)penta-1,4-diyn-3-ol (**5.11c**)

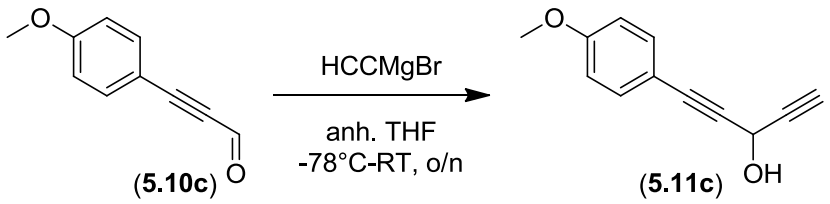

Compound **5.11c** was prepared[123] from aldehyde **5.10c** (270 mg, 1.7 mmol) according to General Procedure 7.4.2.4 and purified by flash column chromatography (4:1 hexanes:ethyl acetate) to obtain the product (217 mg, 1.18 mmol) in 71% yield.

^{1}H NMR (400 MHz, $CDCl_3$) δ 7.29 (d, *J*=11.0 Hz, 2 H), 6.83 (d, *J*=11.1 Hz, 2 H), 5.31 (s, 1 H), 3.79 (s, 3 H), 2.57 (s, 1 H)

^{13}C NMR (100 MHz, $CDCl_3$) δ 160.1, 135.7, 133.4, 114.6, 114.0, 113.8, 84.8, 84.2, 81.0, 55.5, 55.3, 52.6

HRMS (EI) calc. for [$C_{12}H_{10}O_2$] 186.0681 Da, obt. 186.0670 Da

7.5.2.30 1-(4-methoxyphenyl)penta-1,4-diyn-3-one (**5.12c**)

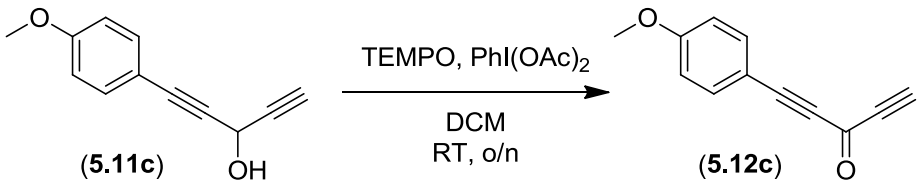

Compound **5.12c** was prepared[123] from alcohol **5.11c** (217 mg, 1.18 mmol) according to General Procedure 7.5.1.3 and purified by flash column chromatography (9:1 hexanes:ethyl acetate) to obtain the product (115 mg, 0.625 mmol) in 53% yield.

^{1}H NMR (400 MHz, $CDCl_3$) δ 7.58 (d, *J*=8.7 Hz, 2 H), 6.90 (d, *J*=8.7 Hz, 2 H), 3.86 (s, 3 H), 3.33 (s, 1 H)

^{13}C NMR (100 MHz, $CDCl_3$) δ 162.4, 135.7, 114.6, 110.8, 94.1, 89.5, 82.2, 78.5, 55.5. Missing one aromatic C

HRMS (EI) calc. for [$C_{12}H_8O_2$] 184.0524 Da, obt. 184.0507 Da

7.5.2.31 1-(1-benzyl-1*H*-1,2,3-triazol-4-yl)-3-(4-methoxyphenyl)prop-2-yn-1-one (**5.13c**)

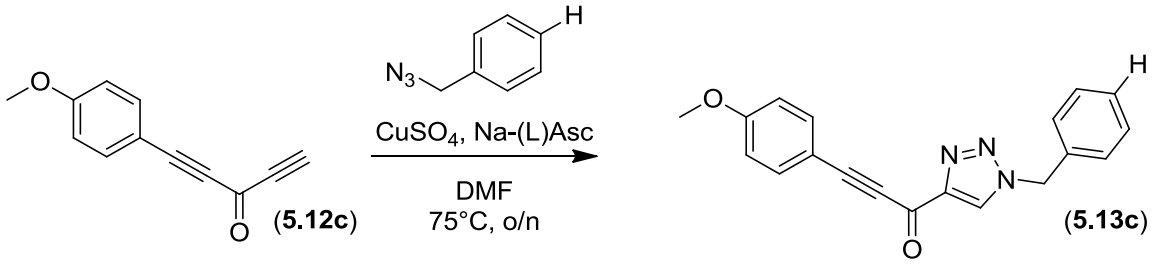

Benzyl azide was prepared from benzyl bromide according to General Procedure 7.4.2.1. Compound **5.13c** was prepared[123] from benzyl azide and ynone **5.12c** (530 mg, 0.987 mmol) according to General Procedure 7.4.2.2 and purified by flash column chromatography to obtain the product (60 mg, 0.23 mmol) in 23% yield.

^{1}H NMR (400 MHz, $CDCl_3$) δ 8.03 (s, 1 H), 7.66 (d, *J*=11.0 Hz, 2 H), 7.38 (m, 3 H), 7.30 (m, 2 H), 6.91 (d, *J*=8.8 Hz, 2 H), 5.58 (s, 2 H), 3.83 (s, 3 H)

^{13}C NMR (100 MHz, $CDCl_3$) δ 170.2, 162.0, 148.7, 135.6, 133.6, 129.4, 128.3, 126.5, 114.4, 111.7, 95.5, 87.3, 55.5, 54.6

HRMS (EI) calc. for [$C_{19}H_{15}N_3O_2$] 317.1164 Da, obt. 317.1190 Da

7.5.2.32 3-(4-methoxyphenyl)-1-(1-(4-nitrobenzyl)-1*H*-1,2,3-triazol-4-yl)prop-2-yn-1-one (**5.14c**)

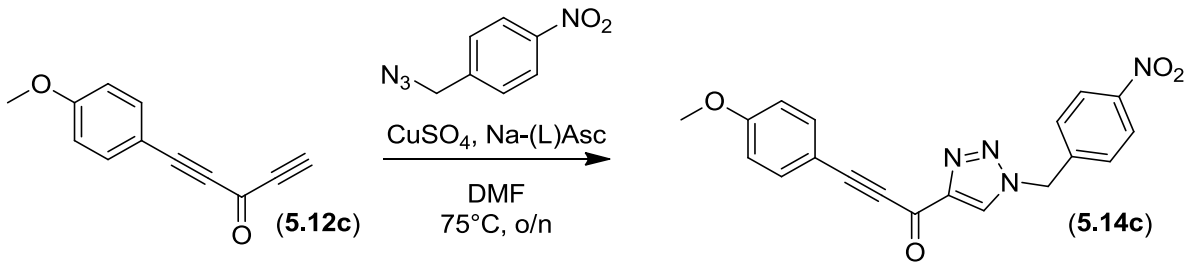

4-Nitrobenzyl azide was prepared from 4-nitrobenzyl bromide according to General Procedure 7.4.2.1. Compound **5.14c** was prepared[123] from 4-nitrobenzyl azide and ynone **5.12c** (125 mg, 0.680 mmol) according to General Procedure 7.4.2.2 and purified by flash column chromatography to obtain the product (86 mg, 0.24 mmol) in 35% yield.

^{1}H NMR (400 MHz, $CDCl_3$) δ 8.26 (d, *J*=7.7 Hz, 2 H), 8.14 (s, 1 H), 7.67 (d, *J*=7.7 Hz, 2 H), 7.46 (d, *J*=7.7 Hz, 2 H), 6.92 (d, *J*=7.7 Hz, 2 H), 5.71 (s, 2 H), 3.85 (s, 3 H)

^{13}C NMR (100 MHz, $CDCl_3$) δ 140.9, 135.5, 128.9, 127.2, 124.3, 114.4, 111.4, 95.5, 55.4, 53.3. Misssing five C's due to low solubility

HRMS (EI) calc. for [$C_{19}H_{14}N_4O_4$] 362.1015 Da, obt. 362.1023 Da

7.5.2.33 3-(4-fluorophenyl)prop-2-yn-1-ol (**5.9d**)

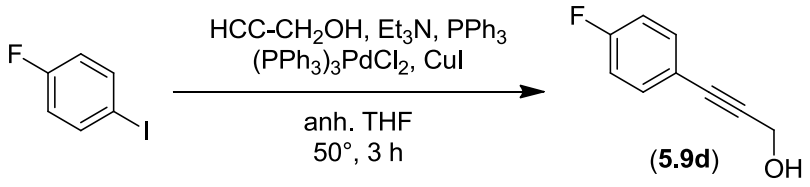

Compound **5.9d** was prepared from 4-fluoroiodobenzene (19 mmol) according to General Procedure 7.5.1.2 and purified by flash column chromatography (100% DCM) to obtain an orange oil (2.474 g, 16.47 mmol) in 86% yield.

^{1}H NMR (400 MHz, $CDCl_3$) δ 7.42 (dd, *J*=8.9 Hz, *J*=5.4 Hz, 2 H), 7.01 (dd, *J*=8.8 Hz, *J*=8.8 Hz, 2 H), 4.49 (s, 2 H), 1.86 (s, 1 H)

^{13}C NMR (100 MHz, $CDCl_3$) δ 162.6 (d, *J*=993 Hz), 133.6 (d, *J*=3.5 Hz), 118.6 (d, *J*=13.1 Hz), 115.6 (d, *J*=87.5 Hz), 86.9 (d, *J*=5.8 Hz), 84.6, 51.6

^{19}F NMR (400 MHz, $CDCl_3$) δ -110.6

HRMS (EI) calc. for [C_9H_7OF] 150.0481 Da, obt. 150.0467 Da

R_f (DCM) ~0.22

7.5.2.34 3-(4-fluorophenyl)prop-2-ynal (**5.10d**)

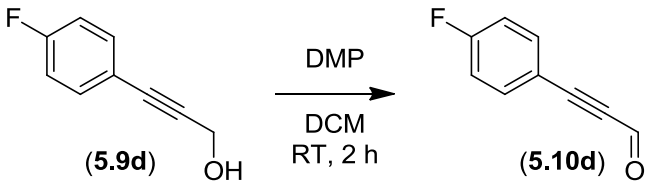

Compound **5.10d** was prepared from alcohol **5.9d** (2.449 g, 16.31 mmol) according to General Procedure 7.5.1.4 and purified by flash column chromatography (100% DCM) to obtain a yellow crystalline powder (2.223 g, 15.01 mmol) in 92% yield.

^{1}H NMR (400 MHz, $CDCl_3$) δ 9.42 (s, 1 H), 7.63 (dd, *J*=9.0 Hz, *J*=5.3 Hz, 2 H), 7.12 (dd, *J*=8.8 Hz, *J*=8.5 Hz, 2 H)

^{13}C NMR (100 MHz, $CDCl_3$) δ 176.6, 164.3 (d, *J*=253 Hz), 135.6 (d, *J*=8.8 Hz), 116.4 (d, *J*=22.6 Hz), 115.6, 94.0, 88.4

^{19}F NMR (400 MHz, $CDCl_3$) δ -105.1

HRMS (EI) calc. for [C_9H_5FO] 148.0324 Da, obt. 148.0341 Da

m.p. <50°C

R_f (DCM) ~0.66

7.5.2.35 1-(4-fluorophenyl)penta-1,4-diyn-3-ol (**5.11d**)

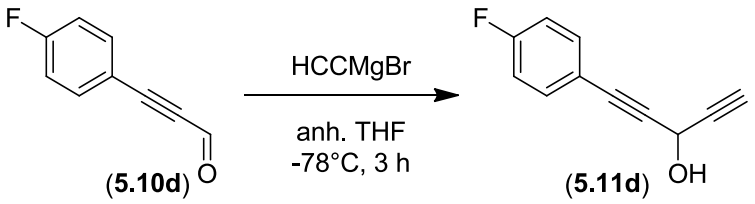

Compound **5.11d** was prepared from aldehyde **5.10d** (2.223 g, 15.01 mmol) according to General Procedure 7.5.1.4 and purified by flash column chromatography (100% DCM) to obtain a pastel yellow powder (2.482 g, 14.26 mmol) in 95% yield.

^{1}H NMR (400 MHz, $CDCl_3$) δ 7.47 (dd, *J*=8.9 Hz, *J*=5.4 Hz, 2 H), 7.03 (dd, *J*=8.7 Hz, *J*=8.7 Hz, 2 H), 5.34 (dd, *J*=7.5 Hz, *J*=2.2 Hz, 1 H), 2.63 (d, *J*=2.4 Hz, 1 H), 2.28 (d, *J*=7.6 Hz, 1 H)

^{13}C NMR (100 MHz, $CDCl_3$) δ 162.9 (d, *J*=249 Hz), 133.9 (d, *J*=8.4 Hz), 117.8, 115.7 (d, *J*=21.9 Hz), 85.2, 83.7, 80.7, 73.0, 52.5

^{19}F NMR (400 MHz, $CDCl_3$) δ -109.7

HRMS (EI) calc. for $[C_{11}H_6FO]^{\cdot}$ 173.0403 Da, obt. 173.0394 Da

m.p. 55-57°C

R_f (DCM) ~0.24

7.5.2.36 1-(4-fluorophenyl)penta-1,4-diyn-3-one (**5.12d**)

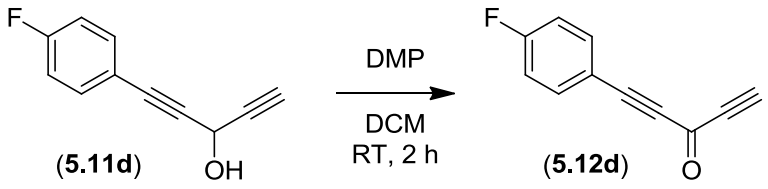

Compound **5.12d** was prepared from alcohol **5.11d** (2.463 g, 14.14 mmol) according to General Procedure 7.5.1.4 and purified by flash column chromatography (100% DCM) to obtain an off-white powder (2.197 g, 12.76 mmol) in 90% yield.

^{1}H NMR (400 MHz, $CDCl_3$) δ 7.65 (dd, *J*=8.9 Hz, *J*=5.3 Hz, 2 H), 7.12 (dd, *J*=8.8 Hz, *J*=8.5 Hz, 2 H), 3.38 (s, 1 H)

^{13}C NMR (100 MHz, $CDCl_3$) δ 164.5 (d, *J*=253 Hz), 160.0, 135.9 (d, *J*=8.7 Hz), 116.4 (d, *J*=22.2 Hz), 115.2, 91.4, 89.0, 82.1, 79.1

^{19}F NMR (400 MHz, $CDCl_3$) δ -104.6

HRMS (EI) calc. for [$C_{11}H_5OF$] 172.0324 Da, obt. 172.0308 Da

m.p. 74-76°C (dec.)

R_f (DCM) ~0.64

7.5.2.37 1-(1-benzyl-1H-1,2,3-triazol-4-yl)-3-(4-fluorophenyl)prop-2-yn-1-one (**5.13d**)

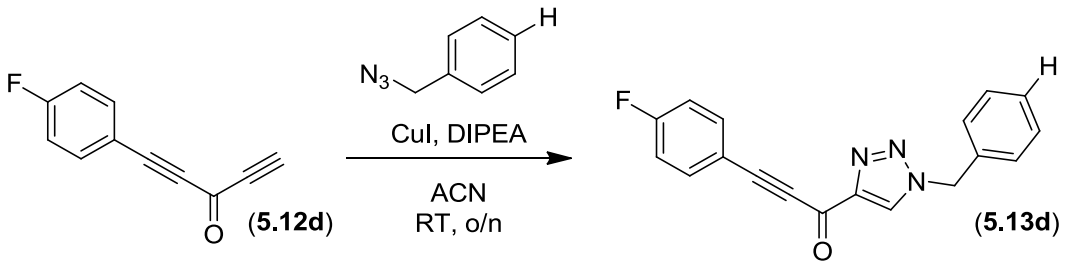

Benzyl azide was prepared from benzyl bromide according to General Procedure 7.4.2.1. Compound **5.13d** was prepared from benzyl azide (60 mg, 0.45 mmol) and ynone **5.12d** according to General Procedure 7.5.1.6 and purified by flash column chromatography (0-10% ethyl acetate in DCM) to obtain an orange-yellow powder (106 mg, 0.347 mmol) in 76% yield.

^{1}H NMR (400 MHz, $CDCl_3$) δ 8.06 (s, 1 H), 7.73 (dd, *J*=9.0 Hz, *J*=5.3 Hz, 2 H), 7.44-7.40 (m, 3 H), 7.33-7.31 (m, 2 H), 7.12 (dd, *J*=8.8 Hz, *J*=8.6 Hz, 2 H), 5.61 (s, 2 H)

^{13}C NMR (100 MHz, $CDCl_3$) δ 170.1, 164.2 (d, *J*=253 Hz), 148.5, 135.8 (d, *J*=9.1 Hz), 133.4, 129.4, 129.3, 128.3, 126.6, 116.2 (d, *J*=22.2 Hz), 116.0 (d, *J*=3.6 Hz), 93.0, 87.0, 54.6

^{19}F NMR (400 MHz, $CDCl_3$) δ -105.7

HRMS (EI) calc. for [$C_{18}H_{12}N_3OF$] 305.0964 Da, obt. 305.0960 Da

m.p. 108-110°C (dec.)

R_f (9:1 DCM:ethyl acetate) ~0.62

7.5.2.38 3-(4-fluorophenyl)-1-(1-(4-nitrobenzyl)-1*H*-1,2,3-triazol-4-yl)prop-2-yn-1-one (**5.14d**)

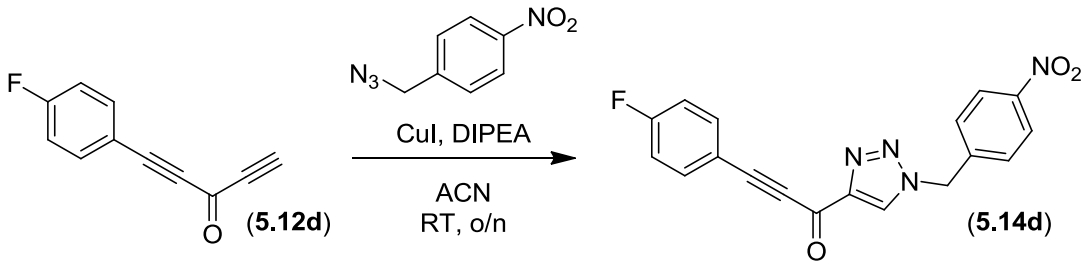

4-Nitrobenzyl azide was prepared from 4-nitrobenzyl bromide according to General Procedure 7.4.2.1. Compound **5.14d** was prepared from 4-nitrobenzyl azide and ynone **5.12d** (176 mg, 1.02 mmol) according to General Procedure 7.5.1.6 and purified by flash column chromatography (0-10% ethyl acetate in DCM) to obtain a white powder (66 mg, 0.19 mmol) in 18% yield.

^{1}H NMR (400 MHz, DMSO-d_6) δ 9.24 (s, 1 H), 8.26 (d, *J*=8.8 Hz, 2 H), 7.87 (dd, *J*=9.0 Hz, *J*=5.4 Hz, 2 H), 7.60 (d, *J*=8.8 Hz, 2 H), 7.40 (dd, *J*=8.9 Hz, *J*=8.9 Hz, 2 H), 5.9 (s, 2 H)

^{13}C NMR (100 MHz, DMSO-d_6) δ 168.3, 162.4, 147.3, 146.9, 142.5, 135.8 (d, *J*=9.1 Hz), 130.5, 129.1, 123.9, 116.5 (d, *J*=22.2 Hz), 115.2 (d, *J*=3.3 Hz), 90.9, 86.8, 52.3

^{19}F NMR (400 MHz, $CDCl_3$) δ -105.3

HRMS (EI) calc. for [$C_{18}H_{11}N_4O_3F$] 350.0815 Da, obt. 350.0843 Da

m.p. 214-216°C (dec.)

R_f (9:1 DCM:ethyl acetate) ~0.47

7.5.2.39 methyl 4-(3-hydroxyprop-1-yn-1-yl)benzoate (**5.9e**)

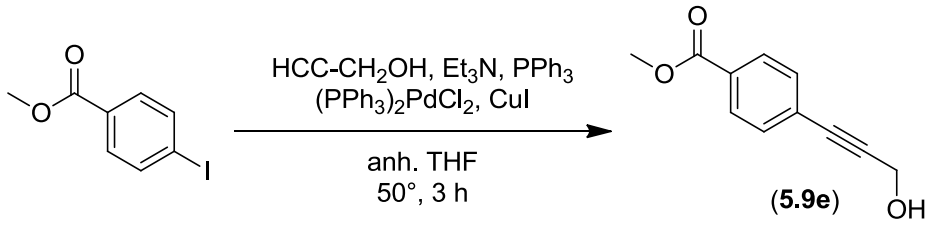

Compound **5.9e** was prepared from methyl 4-iodobenzoate (2.626 g, 10.02 mmol) according to General Procedure 7.5.1.2 and purified by flash column chromatography (0-10% ethyl acetate in DCM) to obtain an off-white powder (1.605 g, 8.436 mmol) in 84% yield.

^{1}H NMR (400 MHz, $CDCl_3$) δ 8.00 (d, *J*=8.6 Hz, 2 H), 7.50 (d, *J*=8.6 Hz, 2 H), 4.53 (s, 2 H), 3.93 (s, 3 H), 1.65 (br s, 1 H)

^{13}C NMR (100 MHz, $CDCl_3$) δ 166.5, 131.6, 129.8, 129.5, 127.2, 90.1, 85.0, 52.2, 51.6

HRMS (EI) calc. for [$C_{11}H_{10}O_3$] 190.0630 Da, obt. 190.0646 Da

R_f (9:1 DCM:ethyl aceate) ~0.39

7.5.2.40 methyl 4-(3-oxoprop-1-yn-1-yl)benzoate (**5.10e**)

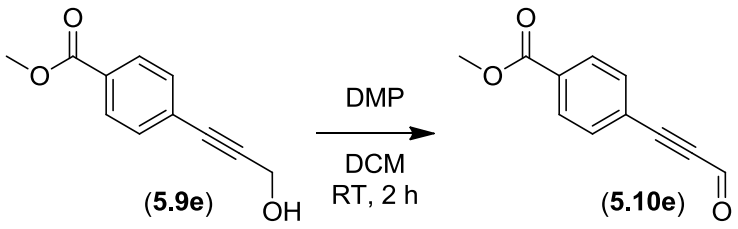

Compound **5.10e** was prepared from alcohol **5.9e** (1.605 g, 8.436 mmol) according to General Procedure 7.5.1.4 and purified by flash column chromatography (100% DCM) to obtain a yellow powder (1.460 g, 7.759 mmol) in 92% yield.

^{1}H NMR (400 MHz, $CDCl_3$) δ 9.45 (s, 1 H), 8.08 (d, *J*=8.6 Hz, 2 H), 7.67 (d, *J*=8.7 Hz, 2 H), 3.95 (s, 3 H)

^{13}C NMR (100 MHz, $CDCl_3$) δ 176.4, 165.9, 133.0, 132.2, 129.7, 123.8, 93.0, 89.6, 52.5

HRMS (EI) calc. for [$C_{11}H_8O_3$] 188.0473 Da, obt. 188.0460 Da

m.p. 88-91°C

R_f (DCM) ~0.70

7.5.2.41 methyl 4-(3-hydroxypenta-1,4-diyn-1-yl)benzoate (**5.11e**)

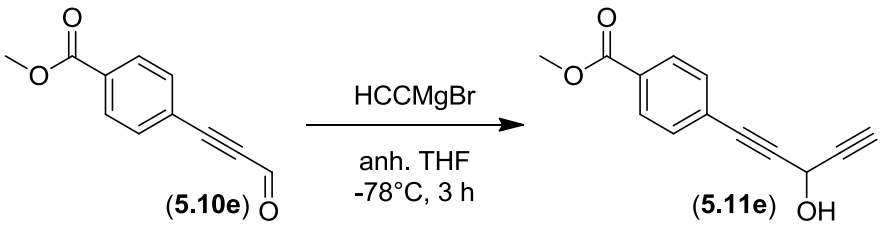

Compound **5.11e** was prepared from aldehyde **5.10e** (1.460 g, 7.759 mmol) according to General Procedure 7.5.1.5 and purified by flash column chromatography (0-10% ethyl acetate in DCM) to obtain a yellow powder (1.159 g, 7.089 mmol) in 91% yield.

^{1}H NMR (400 MHz, $CDCl_3$) δ 8.00 (d, *J*=8.6 Hz, 2 H), 7.53 (d, *J*=8.5 Hz, 2 H), 5.37 (d, *J*=2.2 Hz, 1 H), 3.93 (s, 3 H), 2.65 (d, *J*=2.3 Hz, 1 H)

^{13}C NMR (100 MHz, $CDCl_3$) δ 166.4, 131.8, 130.2, 129.5, 126.4, 88.2, 83.8, 80.4, 73.2, 52.5, 52.3

HRMS (EI) calc. for [$C_{13}H_{10}O_3$] 214.0630 Da, obt. 214.0618 Da

m.p. 90-92°C (dec.)

R_f (DCM) ~0.23

7.5.2.42 methyl 4-(3-oxopenta-1,4-diyn-1-yl)benzoate (**5.12e**)

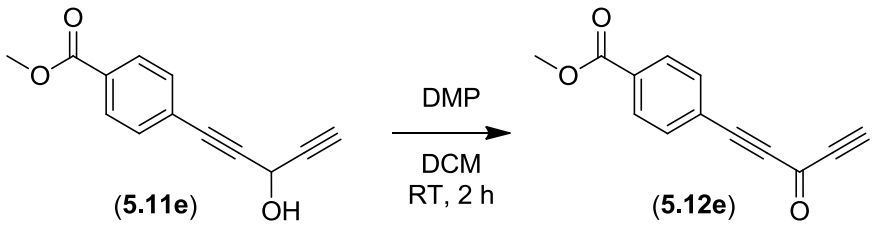

Compound **5.12e** was prepared from alcohol **5.11e** (1.519 g, 7.089 mmol) according to General Procedure 7.5.1.4 and purified by flash column chromatography (100% DCM) to obtain an orange powder (1.362 g, 6.420 mmol) in 91% yield.

^{1}H NMR (400 MHz, $CDCl_3$) δ 8.08 (d, *J*=8.6 Hz, 2 H), 7.70 (d, *J*=8.6 Hz, 2 H), 3.96 (s, 3 H), 3.42 (s, 1 H)

^{13}C NMR (100 MHz, $CDCl_3$) δ 165.9, 159.8, 133.2, 132.4, 129.7, 123.5, 90.4, 90.2, 82.0, 79.6, 52.5

HRMS (EI) calc. for [$C_{13}H_8O_3$] 212.0473 Da, obt. 212.0476 Da

m.p. 101-103°C (dec.)

R_f (DCM) ~0.61

7.5.2.43 methyl 4-(3-(1-benzyl-1*H*-1,2,3-triazol-4-yl)-3-oxoprop-1-yn-1-yl)benzoate (**5.13e**)

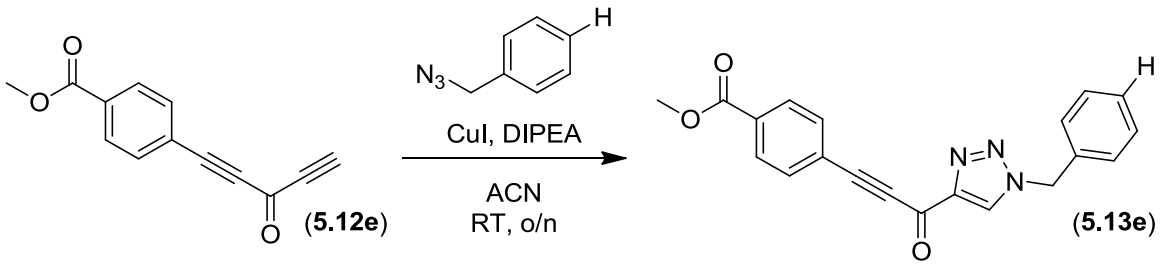

Benzyl azide was prepared from benzyl bromide according to General Procedure 7.4.2.1. Compound **5.13e** was prepared from benzyl azide and ynone **5.12e** (213 mg, 1.00 mmol) according to General Procedure 7.5.1.6 and purified by flash column chromatography (0-8% ethyl acetate in DCM) to obtain an off-white powder (243 mg, 0.702 mmol) in 70% yield.

^{1}H NMR (400 MHz, DMSO-d_6) δ 9.21 (s, 1 H), 8.07 (d, *J*=8.7 Hz, 2 H), 7.91 (d, *J*=8.6 Hz, 2 H), 7.42-7.33 (m, 5 H), 5.72 (s, 2 H), 3.89 (s, 3 H)

^{13}C NMR (100 MHz, DMSO-d_6) δ 168.4, 165.4, 146.9, 135.3, 133.3, 131.6, 130.2, 129.6, 128.8, 128.4, 128.0, 123.4, 89.9, 88.5, 53.2, 52.5

HRMS (EI) calc. for [$C_{20}H_{15}N_3O_3$] 345.1113 Da, obt. 345.1090 Da

m.p. 192-194°C (dec.)

R_f (DCM) ~0.21

7.5.2.44 methyl 4-(3-(1-(4-nitrobenzyl)-1*H*-1,2,3-triazol-4-yl)-3-oxoprop-1-yn-1-yl)benzoate (**5.14e**)

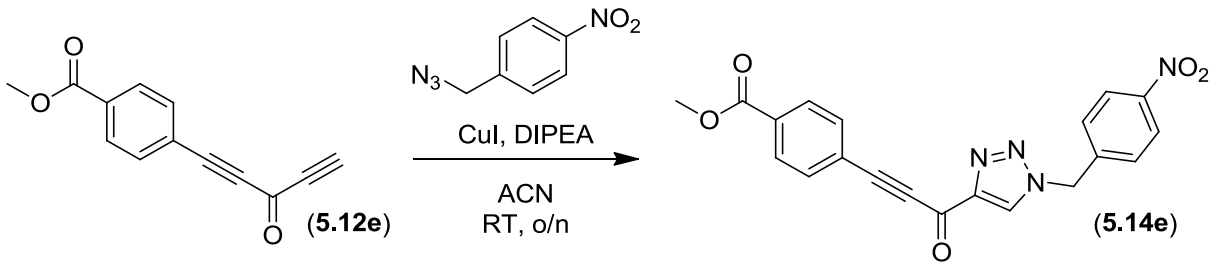

4-Nitrobenzyl azide was prepared from 4-nitrobenzyl bromide according to General Procedure 7.4.2.1. Compound **5.14e** was prepared from 4-nitrobenzyl azide and ynone **5.12e** (0.213 g, 1.00 mmol) according to General Procedure 7.5.1.6 and purified by flash column chromatography (0-7% ethyl acetate in DCM) to obtain a pale yellow crystalline powder (140 mg, 0.358 mmol) in 36% yield.

^{1}H NMR (400 MHz, DMSO-d_6) δ 9.27 (s, 1 H), 8.26 (d, *J*=8.8 Hz, 2 H), 8.07 (d, *J*=8.6 Hz, 2 H), 7.9 (d, *J*=8.6 Hz, 2 H), 7.60 (d, *J*=8.9 Hz, 2 H), 5.91 (s, 2 H), 3.89 (s, 3 H)

^{13}C NMR (100 MHz, DMSO-d_6) δ 168.3, 165.4, 147.4, 146.9, 142.6, 133.3, 131.6, 130.8, 129.6, 129.2, 124.0, 123.4, 90.0, 88.5, 52.5, 52.4

HRMS (EI) calc. for [$C_{20}H_{14}N_4O_5$] 390.0964 Da, obt. 390.0959 Da

m.p. 199-206°C

R_f (DCM) ~0.08

R_f (95:5 DCM:ethyl acetate) ~0.36

7.5.2.45 1-(4-(3-hydroxyprop-1-yn-1-yl)phenyl)ethanone (**5.9f**)

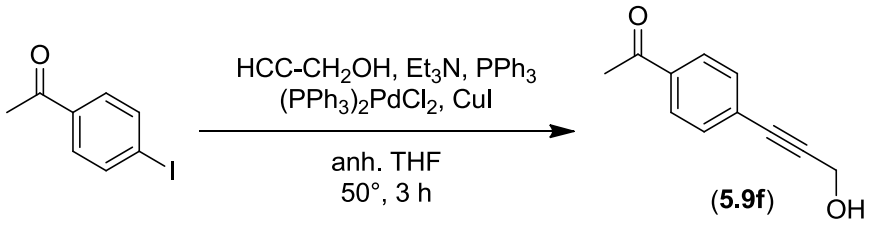

Compound **5.9f** was prepared from 4'-iodoacetophenone (2.462 g, 10.00 mmol) according to General Procedure 7.5.1.2 and purified by flash column chromatography (9:1 to 2:1 DCM:ethyl acetate) to obtain an off-white powder (1.523 g, 8.745 mmol) in 87% yield.

^{1}H NMR (400 MHz, $CDCl_3$) δ 7.92 (d, *J*=8.5 Hz, 2 H), 7.53 (d, *J*=8.5 Hz, 2 H), 4.54 (s, 2 H), 2.61 (s, 3 H)

^{13}C NMR (100 MHz, $CDCl_3$) δ 197.3, 136.5, 131.8, 128.2, 127.4, 90.4, 84.9, 51.6, 26.6

HRMS (EI) calc. for [$C_{11}H_{10}O_2$] 174.0681 Da, obt. 174.0703 Da

m.p. 83-85°C

R_f (9:1 DCM:ethyl acetate) ~0.45

7.5.2.46 3-(4-acetylphenyl)prop-2-ynal (**5.10f**)

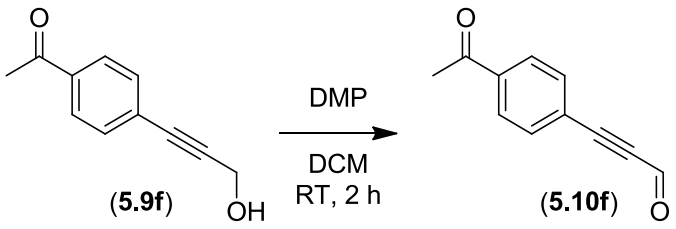

Compound **5.10f** was prepared from alcohol **5.9f** (1.521 g, 8.733 mmol) according to General Procedure 7.5.1.4 and purified by flash column chromatography (95:5 DCM:ethyl acetate) to obtain a yellow crystalline powder (1.355 g, 7.871 mmol) in 90% yield.

^{1}H NMR (400 MHz, $CDCl_3$) δ 9.46 (s, 1 H), 7.99 (d, *J*=8.7 Hz, 2 H), 7.71 (d, *J*=8.7 Hz, 2 H), 2.64 (s, 3 H)

^{13}C NMR (100 MHz, $CDCl_3$) δ 196.9, 176.4, 138.5, 133.3, 128.4, 123.9, 92.9, 89.8, 26.7

HRMS (EI) calc. for [$C_{11}H_8O_2$] 172.0524 Da, obt. 172.0528 Da

m.p. 96-100°C

R_f (9:1 DCM:ethyl acetate) ~0.76

7.5.2.47 1-(4-(3-hydroxypenta-1,4-diyn-1-yl)phenyl)ethanone (**5.11f**)

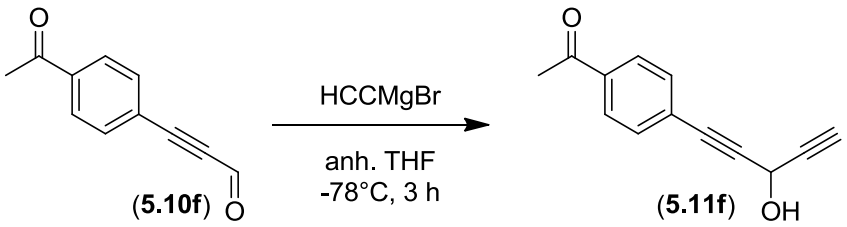

Compound **5.11f** was prepared from aldehyde **5.10f** (1.355 g, 7.871 mmol) according to General Procedure 7.5.1.5 and purified by flash column chromatography (0-10% ethyl acetate in DCM) to obtain an orange oil (1.179 g, 5.950 mmol) in 76% yield.

^{1}H NMR (400 MHz, $CDCl_3$) δ 7.92 (d, *J*=8.5 Hz, 2 H), 7.55 (d, *J*=8.6 Hz, 2 H), 5.38 (br d, *J*=2.1 Hz, 1 H), 2.65 (d, *J*=2.2 Hz, 1 H), 2.61 (s, 3 H)

^{13}C NMR (100 MHz, $CDCl_3$) δ 197.4, 136.8, 132.0, 128.2, 126.6, 88.5, 83.7, 80.4, 73.3, 52.5, 26.6

HRMS (EI) calc. for [$C_{13}H_{10}O_2$] 198.0681 Da, obt. 198.0716 Da

R_f (DCM) ~0.09

R_f (9:1 DCM:ethyl acetate) ~0.47

7.5.2.48 1-(4-acetylphenyl)penta-1,4-diyn-3-one (**5.12f**)

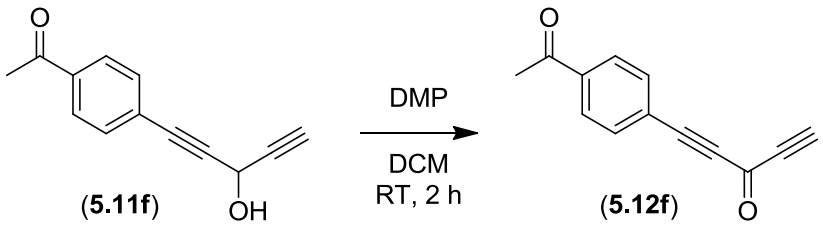

Compound **5.12f** was prepared from alcohol **5.11f** (1.179 g, 5.950 mmol) according to General Procedure 7.5.1.4 and purified by flash column chromatography (100% DCM) to obtain a grey powder (994 mg, 5.07 mmol) in 85% yield.

^{1}H NMR (400 MHz, $CDCl_3$) δ 7.99 (d, *J*=8.7 Hz, 2 H), 7.73 (d, *J*=8.7 Hz, 2 H), 3.43 (s, 1 H), 2.64 (s, 3 H)

^{13}C NMR (100 MHz, $CDCl_3$) δ 196.9, 159.8, 138.6, 133.5, 128.4, 123.6, 90.4, 90.2, 82.0, 79.7, 26.7

HRMS (EI) calc. for [$C_{13}H_8O_2$] 196.0524 Da, obt. 196.0497 Da

m.p. 102-104°C (dec.)

R_f (DCM) ~0.41

7.5.2.49 3-(4-acetylphenyl)-1-(1-benzyl-1*H*-1,2,3-triazol-4-yl)prop-2-yn-1-one (**5.13f**)

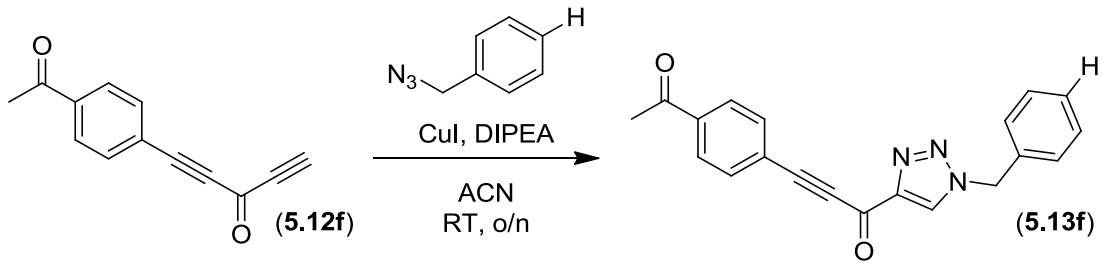

Benzyl azide was prepared from benzyl bromide according to General Procedure 7.4.2.1. Compound **5.13f** was prepared from benzyl azide and ynone **5.12f** (195 mg, 0.995 mmol) according to General Procedure 7.5.1.6 and purified by flash column chromatography (0-15% ethyl acetate in DCM) to obtain a pale yellow powder (202 mg, 0.614 mmol) in 62% yield.

^{1}H NMR (400 MHz, DMSO-d_6) δ 9.21 (s, 1 H), 8.07 (d, *J*=8.6 Hz, 2 H), 7.91 (d, *J*=8.6 Hz, 2 H), 7.42-7.34 (m, 5 H), 5.73 (s, 2 H), 2.63 (s, 3 H)

^{13}C NMR (100 MHz, DMSO-d_6) δ 197.3, 168.3, 146.8, 138.1, 135.2, 133.2, 130.1, 128.8, 128.5, 128.3, 127.9, 123.1, 90.1, 88.5, 53.2, 26.8

HRMS (EI) calc. for [$C_{20}H_{15}N_3O_2$] 329.1164 Da, obt. 329.1178 Da

m.p. 184-186°C (dec.)

R_f (8:2 DCM:ethyl acetate) ~0.69

7.5.2.50 3-(4-acetylphenyl)-1-(1-(4-nitrobenzyl)-1*H*-1,2,3-triazol-4-yl)prop-2-yn-1-one (**5.14f**)

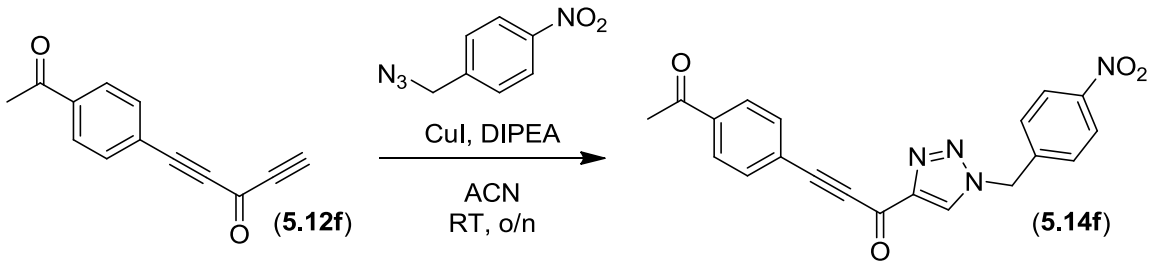

4-Nitrobenzyl azide was prepared from 4-nitrobenzyl bromide according to General Procedure 7.4.2.1. Compound **5.14f** was prepared from 4-nitrobenzyl azide and ynone **5.12f** (197 mg, 1.00 mmol) according to General Procedure 7.5.1.6 and purified by flash column chromatography (0-15% ethyl acetate in DCM) to obtain an off-white powder (200 mg, 0.534 mmol) in 53% yield.

^{1}H NMR (400 MHz, DMSO-d_6) δ 9.26 (s, 1 H), 8.26 (d, *J*=8.9 Hz, 2 H), 8.07 (d, *J*=8.6 Hz, 2 H), 7.91 (d, *J*=8.6 Hz, 2 H), 7.60 (d, *J*=8.8 Hz, 2 H), 5.92 (s, 2 H), 2.64 (s, 3 H)

^{13}C NMR (100 MHz, $CDCl_3$) δ 197.3, 168.3, 147.3, 146.9, 142.5, 138.2, 133.2, 130.6, 129.1, 128.5, 123.9, 123.0, 90.2, 88.5, 52.3, 26.8

HRMS (EI) calc. for [$C_{20}H_{14}N_4O_4$] 374.1015 Da, obt. 374.0996 Da

m.p. 193-196°C

R_f (8:2 DCM:ethyl acetate) ~0.47

References

1. Brown, A. C.; Fraser, T. R., On the Connection between Chemical Constitution and Physiological Action; with special reference to the Physiological Action of the Salts of the Ammonium Bases derived from Strychnia, Brucia, Thebaia, Codeia, Morphia, and Nicotia. *Journal of anatomy and physiology* **1868,** *2* (2), 224-42.

2. Kornek, G.; Selzer, E., Targeted therapies in solid tumours: pinpointing the Tumour's achilles heel. *Current Pharmaceutical Design* **2009,** *15* (2), 207-242.

3. Thomas, H.; Beck, K.; Adamczyk, M.; Aeschlimann, P.; Langley, M.; Oita, R. C.; Thiebach, L.; Hils, M.; Aeschlimann, D., Transglutaminase 6: a protein associated with central nervous system development and motor function. *Amino Acids* **2013,** *44* (1), 161-177.

4. Keillor, J. W.; Clouthier, C. M.; Apperley, K. Y. P.; Akbar, A.; Mulani, A., Acyl transfer mechanisms of tissue transglutaminase. *Bioorg. Chem.* **2014,** *57*, 186-197.

5. Eckert, R. L.; Sturniolo, M. T.; Broome, A.-M.; Ruse, M.; Rorke, E. A., Transglutaminase function in epidermis. *J. Invest. Dermatol.* **2005,** *124* (3), 481-492.

6. Iismaa, S. E.; Holman, S.; Wouters, M. A.; Lorand, L.; Graham, R. M.; Husain, A., Evolutionary specialization of a tryptophan indole group for transition-state stabilization by eukaryotic transglutaminases. *Proc. Natl. Acad. Sci. U. S. A.* **2003,** *100* (22), 12636-12641.

7. Pinkas, D. M.; Strop, P.; Brunger, A. T.; Khosla, C., Transglutaminase 2 undergoes a large conformational change upon activation. *PLoS Biol.* **2007,** *5* (12), 2788-2796.

8. Liu, S.; Cerione, R. A.; Clardy, J., Structural basis for the guanine nucleotide-binding activity of tissue transglutaminase and its regulation of transamidation activity. *Proc. Natl. Acad. Sci. U. S. A.* **2002,** *99* (5), 2743-2747.

9. Mhaouty-Kodja, S., Ghα/tissue transglutaminase 2: an emerging G protein in signal transduction. *Biology of the Cell* **2004,** *96* (5), 363-367.

10. Eckert, R. L.; Kaartinen, M. T.; Nurminskaya, M.; Belkin, A. M.; Colak, G.; Johnson, G. V. W.; Mehta, K., Transglutaminase regulation of cell function. *Physiol. Rev.* **2014,** *94* (2), 383-417.

11. Keillor, J. W.; Apperley, K. Y. P.; Akbar, A., Inhibitors of tissue transglutaminase. *Trends Pharmacol. Sci.* **2015,** *36* (1), 32-40.

12. Ahvazi, B.; Kim, H. C.; Kee, S.-H.; Nemes, Z.; Steinert, P. M., Three-dimensional structure of the human transglutaminase 3 enzyme: binding of calcium ions changes structure for activation. *EMBO Journal* **2002,** *21* (9), 2055-2067.

13. Ahvazi, B.; Boeshans, K. M.; Rastinejad, F., The emerging structural understanding of transglutaminase 3. *Journal of Structural Biology* **2004,** *147* (2), 200-207.

14. Ahvazi, B.; Boeshans, K. M.; Idler, W.; Baxa, U.; Steinert, P. M.; Rastinejad, F., Structural Basis for the Coordinated Regulation of Transglutaminase 3 by Guanine Nucleotides and Calcium/Magnesium. *J. Biol. Chem.* **2004,** *279* (8), 7180-7192.

15. Jiang, W. G.; Ye, L.; Sanders, A. J.; Ruge, F.; Kynaston, H. G.; Ablin, R. J.; Mason, M. D., Prostate transglutaminase (TGase-4, TGaseP) enhances the adhesion of prostate cancer cells to extracellular matrix, the potential role of TGase-core domain. *Journal of Translational Medicine* **2013,** *11*, 269/1-269/12, 12 pp.

16. Aeschlimann, D.; Koeller, M. K.; Allen-Hoffmann, B. L.; Mosher, D. F., Isolation of a cDNA encoding a novel member of the transglutaminase gene family from human keratinocytes. Detection and identification of transglutaminase gene products based on reverse transcription-polymerase chain reaction with degenerate primers. *J. Biol. Chem.* **1998,** *273* (6), 3452-3460.

17. Pietroni, V.; Di Giorgi, S.; Paradisi, A.; Ahvazi, B.; Candi, E.; Melino, G., Inactive and Highly Active, Proteolytically Processed Transglutaminase-5 in Epithelial Cells. *J. Invest. Dermatol.* **2008,** *128* (12), 2760-2766.

18. Candi, E.; Paradisi, A.; Terrinoni, A.; Pietroni, V.; Oddi, S.; Cadot, B.; Jogini, V.; Meiyappan, M.; Clardy, J.; Finazzi-agro, A.; Melino, G., Transglutaminase 5 is regulated by guanine-adenine nucleotides. *Biochem. J.* **2004,** *381* (1), 313-319.

19. Cadot, B.; Rufini, A.; Pietroni, V.; Ramadan, S.; Guerrieri, P.; Melino, G.; Candi, E., Overexpressed transglutaminase 5 triggers cell death. *Amino Acids* **2004,** *26* (4), 405-408.

20. Pigors, M.; Kiritsi, D.; Cobzaru, C.; Schwieger-Briel, A.; Suarez, J.; Faletra, F.; Aho, H.; Maekelae, L.; Kern, J. S.; Bruckner-Tuderman, L.; Has, C., TGM5 Mutations Impact Epidermal Differentiation in Acral Peeling Skin Syndrome. *J. Invest. Dermatol.* **2012,** *132* (10), 2422-2429.

21. Kuramoto, K.; Yamasaki, R.; Shimizu, Y.; Tatsukawa, H.; Hitomi, K., Phage-displayed peptide library screening for preferred human substrate peptide sequences for transglutaminase 7. *Arch. Biochem. Biophys.* **2013,** *537* (1), 138-143.

22. Adany, R.; Bardos, H., Factor XIII subunit A as an intracellular transglutaminase. *Cell. Mol. Life Sci.* **2003,** *60* (6), 1049-1060.

23. Yee, V. C.; Pedersen, L. C.; Trong, I. L.; Bishop, P. D.; Stenkamp, R. E.; Teller, D. C., Three-dimensional structure of a transglutaminase: human blood coagulation factor XIII. *Proc. Natl. Acad. Sci. U. S. A.* **1994,** *91* (15), 7296-300.

24. Korsgren, C.; Lawler, J.; Lambert, S.; Speicher, D.; Cohen, C. M., Complete amino acid sequence and homologies of human erythrocyte membrane protein band 4.2. *Proc. Natl. Acad. Sci. U. S. A.* **1990,** *87* (2), 613-17.

25. Folk, J. E., Mechanism of action of guinea pig liver transglutaminase. VI. Order of substrate addition. *J. Biol. Chem.* **1969,** *244* (13), 3707-13.

26. Leblanc, A.; Gravel, C.; Labelle, J.; Keillor, J. W., Kinetic studies of guinea pig liver transglutaminase reveal a general-base-catalyzed deacylation mechanism. *Biochemistry* **2001,** *40* (28), 8335-8342.

27. Folk, J. E.; Cole, P. W., Structural requirements of specific substrates for guinea pig liver transglutaminase. *J. Biol. Chem.* **1965,** *240* (7), 2951-60.

28. Di Venere, A.; Rossi, A.; De Matteis, F.; Rosato, N.; Agro, A. F.; Mei, G., Opposite effects of Ca^{2+} and GTP binding on tissue transglutaminase tertiary structure. *J. Biol. Chem.* **2000,** *275* (6), 3915-3921.

29. Folk, J. E.; Mullooly, J. P.; Cole, P. W., Mechanism of action of guinea pig liver transglutaminase. II. The role of metal in enzyme activation. *J. Biol. Chem.* **1967,** *242* (8), 1838-44.

30. Lai, T.-S.; Slaughter, T. F.; Peoples, K. A.; Hettasch, J. M.; Greenberg, C. S., Regulation of human tissue transglutaminase function by magnesium-nucleotide complexes. Identification of distinct binding sites for Mg-GTP and Mg-ATP. *J. Biol. Chem.* **1998,** *273* (3), 1776-1781.

31. Griffin, M.; Casadio, R.; Bergamini, C. M., Transglutaminases: Nature's biological glues. *Biochem. J.* **2002,** *368* (2), 377-396.

32. Stamnaes, J.; Pinkas, D. M.; Fleckenstein, B.; Khosla, C.; Sollid, L. M., Redox Regulation of Transglutaminase 2 Activity. *J. Biol. Chem.* **2010,** *285* (33), 25402-25409.

33. Kiraly, R.; Csosz, E.; Kurtan, T.; Antus, S.; Szigeti, K.; Simon-Vecsei, Z.; Korponay-Szabo, I. R.; Keresztessy, Z.; Fesus, L., Functional significance of five noncanonical Ca2+-binding sites of human transglutaminase 2 characterized by site-directed mutagenesis. *FEBS J.* **2009,** *276* (23), 7083-7096.

34. Begg, G. E.; Holman, S. R.; Stokes, P. H.; Matthews, J. M.; Graham, R. M.; Iismaa, S. E., Mutation of a Critical Arginine in the GTP-binding Site of Transglutaminase 2 Disinhibits Intracellular Cross-linking Activity. *J. Biol. Chem.* **2006,** *281* (18), 12603-12609.

35. Mariani, P.; Carsughi, F.; Spinozzi, F.; Romanzetti, S.; Meier, G.; Casadio, R.; Bergamini, C. M., Ligand-induced conformational changes in tissue transglutaminase: Monte Carlo analysis of small-angle scattering data. *Biophysical Journal* **2000,** *78* (6), 3240-3251.

36. (a) Caron, N. S.; Munsie, L. N.; Keillor, J. W.; Truant, R., Using FLIM-FRET to measure conformational changes of transglutaminase type 2 in live cells. *PLoS One* **2012,** *7* (8), e44159; (b) Pavlyukov, M. S.; Antipova, N. V.; Balashova, M. V.; Shakhparonov, M. I., Detection of Transglutaminase 2 conformational changes in living cell. *Biochem. Biophys. Res. Commun.* **2012,** *421* (4), 773-779.

37. Pardin, C.; Roy, I.; Chica, R. A.; Bonneil, E.; Thibault, P.; Lubell, W. D.; Pelletier, J. N.; Keillor, J. W., Photolabeling of Tissue Transglutaminase Reveals the Binding Mode of Potent Cinnamoyl Inhibitors. *Biochemistry* **2009,** *48* (15), 3346-3353.

38. Clouthier, C. M.; Mironov, G. G.; Okhonin, V.; Berezovski, M. V.; Keillor, J. W., Real-Time Monitoring of Protein Conformational Dynamics in Solution Using Kinetic Capillary Electrophoresis. *Angew. Chem., Int. Ed.* **2012,** *51* (50), 12464-12468.

39. Balajthy, Z.; Csomos, K.; Vamosi, G.; Szanto, A.; Lanotte, M.; Fesus, L., Tissue-transglutaminase contributes to neutrophil granulocyte differentiation and functions. *Blood* **2006,** *108* (6), 2045-2054.

40. Melino, G.; Annicchiarico-Petruzzelli, M.; Piredda, L.; Candi, E.; Gentile, V.; Davies, P. J. A.; Piacentini, M., Tissue transglutaminase and apoptosis: sense and antisense transfection studies with human neuroblastoma cells. *Mol. Cell. Biol.* **1994,** *14* (10), 6584-96.

41. Olsen, K. C.; Epa, A. P.; Kulkarni, A. A.; Kottmann, R. M.; McCarthy, C. E.; Johnson, G. V.; Thatcher, T. H.; Phipps, R. P.; Sime, P. J., Inhibition of transglutaminase 2, a novel target for pulmonary fibrosis, by two small electrophilic molecules. *Am. J. Respir. Cell Mol. Biol.* **2014,** *50* (4), 737-747, 11 pp.

42. Boroughs, L. K.; Antonyak, M. A.; Cerione, R. A., A Novel Mechanism by Which Tissue Transglutaminase Activates Signaling Events That Promote Cell Survival. *J. Biol. Chem.* **2014,** *289* (14), 10115-10125.

43. Tucholski, J.; Lesort, M.; Johnson, G. V. W., Tissue transglutaminase is essential for neurite outgrowth in human neuroblastoma SH-SY5Y cells. *Neuroscience (Oxford, United Kingdom)* **2001,** *102* (2), 481-491.

44. Sarang, Z.; Molnar, P.; Nemeth, T.; Gomba, S.; Kardon, T.; Melino, G.; Cotecchia, S.; Fesus, L.; Szondy, Z., Tissue transglutaminase (TG2) acting as G protein protects hepatocytes against Fas-mediated cell death in mice. *Hepatology (Hoboken, NJ, U. S.)* **2005,** *42* (3), 578-587.

45. (a) Rasmussen, L. K.; Sorensen, E. S.; Petersen, T. E.; Gliemann, J.; Jensen, P. H., Identification of glutamine and lysine residues in Alzheimer amyloid βA4 peptide responsible for transglutaminase-catalyzed homopolymerization and crosslinking to α2M receptor. *FEBS Lett.* **1994,** *338* (2), 161-6; (b) Dudek, S. M.; Johnson, G. V. W., Transglutaminase catalyzes the formation of sodium dodecyl sulfate-insoluble, Alz-50-reactive polymers of τ. *J. Neurochem.* **1993,** *61* (3), 1159-62.

46. Johnson, G. V. W.; Cox, T. M.; Lockhart, J. P.; Zinnerman, M. D.; Miller, M. L.; Powers, R. E., Transglutaminase activity is increased in Alzheimer's disease brain. *Brain Res.* **1997,** *751* (2), 323-329.

47. DiFiglia, M.; Sapp, E.; Chase, K. O.; Davies, S. W.; Bates, G.; Vonsattel, J. P.; Aronin, N., Aggregation of huntingtin in neuronal intranuclear inclusions and dystrophic neurites in brain. *Science (Washington, D. C.)* **1997,** *277* (5334), 1990-1993.

48. MacDonald, M. E.; Ambrose, C. M.; Duyao, M. P.; Myers, R. H.; Lin, C.; Srinidhi, L.; Barnes, G.; Taylor, S. A.; James, M.; Groot, N.; MacFarlane, H.; Jenkins, B.; Anderson, M. A.; Wexler, N. S.; Gusella, J. F., A novel gene containing a trinucleotide repeate that is expanded

and unstable on Huntington's disease chromosomes. *Cell (Cambridge, Mass.)* **1993,** *72* (6), 971-83.

49. (a) Kahlem, P.; Terre, C.; Green, H.; Djian, P., Peptides containing glutamine repeats as substrates for transglutaminase-catalyzed crosslinking: relevance to diseases of the nervous system. *Proc. Natl. Acad. Sci. U. S. A.* **1996,** *93* (25), 14580-14585; (b) Lesort, M.; Attanavanich, K.; Zhang, J.; Johnson, G. V. W., Distinct nuclear localization and activity of tissue transglutaminase. *J. Biol. Chem.* **1998,** *273* (20), 11991-11994.

50. Scarpellini, A.; Huang, L.; Burhan, I.; Schroeder, N.; Funck, M.; Johnson, T. S.; Verderio, E. A. M., Syndecan-4 knockout leads to reduced extracellular transglutaminase-2 and protects against tubulointerstitial fibrosis. *J. Am. Soc. Nephrol.* **2014,** *25* (5), 1013-1027.

51. Aeschlimann, D.; Paulsson, M., Transglutaminases: protein crosslinking enzymes in tissues and body fluids. *Thromb. Haemostasis* **1994,** *71* (4), 402-15.

52. Bowness, J. M.; Tarr, A. H.; Wiebe, R. I., Transglutaminase-catalyzed cross-linking: a potential mechanism for the interaction of fibrinogen, low density lipoprotein and arterial type III procollagen. *Thromb. Res.* **1989,** *54* (4), 357-67.

53. Olsen, K. C.; Sapinoro, R. E.; Kottmann, R. M.; Kulkarni, A. A.; Iismaa, S. E.; Johnson, G. V. W.; Thatcher, T. H.; Phipps, R. P.; Sime, P. J., Transglutaminase 2 and its role in pulmonary fibrosis. *Am. J. Respir. Crit. Care Med.* **2011,** *184* (6), 699-707.

54. Griffin, M.; Mongeot, A.; Collighan, R.; Saint, R. E.; Jones, R. A.; Coutts, I. G. C.; Rathbone, D. L., Synthesis of potent water-soluble tissue transglutaminase inhibitors. *Bioorg. Med. Chem. Lett.* **2008,** *18* (20), 5559-5562.

55. Daneshpour, N.; Griffin, M.; Collighan, R.; Perrie, Y., Targeted delivery of a novel group of site-directed transglutaminase inhibitors to the liver using liposomes: a new approach for the potential treatment of liver fibrosis. *J. Drug Targeting* **2011,** *19* (8), 624-631.

56. Kumar, S.; Donti, T. R.; Agnihotri, N.; Mehta, K., Transglutaminase 2 reprogramming of glucose metabolism in mammary epithelial cells via activation of inflammatory signaling pathways. *Int. J. Cancer* **2014,** *134* (12), 2798-2807.

57. Han, A. L.; Kumar, S.; Fok, J. Y.; Tyagi, A. K.; Mehta, K., Tissue transglutaminase expression promotes castration-resistant phenotype and transcriptional repression of androgen receptor. *Eur. J. Cancer* **2014,** *50* (9), 1685-1696.

58. Monteagudo, A.; Ji, C.; Akbar, A.; Keillor, J. W.; Johnson, G. V. W., Inhibition or ablation of transglutaminase 2 impairs astrocyte migration. *Biochem. Biophys. Res. Commun.* **2017,** *482* (4), 942-947.

59. Dieterich, W.; Ehnis, T.; Bauer, M.; Donner, P.; Volta, U.; Riecken, E. O.; Schuppan, D., Identification of tissue transglutaminase as the autoantigen of celiac disease. *Nat. Med. (N. Y.)* **1997,** *3* (7), 797-801.

60. Ciccocioppo, R.; di Sabatino, A.; Corazza, G. R., The immune recognition of gluten in coeliac disease. *Clinical and Experimental Immunology* **2005,** *140* (3), 408-416.

61. Fleckenstein, B.; Molberg, O.; Qiao, S.-W.; Schmid, D. G.; von der Mulbe, F.; Elgstoen, K.; Jung, G.; Sollid, L. M., Gliadin T Cell Epitope Selection by Tissue Transglutaminase in Celiac Disease. Role of enzyme specificity and pH influence on the transamidation versus deamidation reactions. *J. Biol. Chem.* **2002,** *277* (37), 34109-34116.

62. Di Sabatino, A.; Vanoli, A.; Giuffrida, P.; Luinetti, O.; Solcia, E.; Corazza, G. R., The function of tissue transglutaminase in celiac disease. *Autoimmun. Rev.* **2012,** *11* (10), 746-753.

63. Giersiepen, K.; Lelgemann, M.; Stuhldreher, N.; Ronfani, L.; Husby, S.; Koletzko, S.; Korponay-Szabo, I. R., Accuracy of Diagnostic Antibody Tests for Coeliac Disease in Children: Summary of an Evidence Report. *J. Pediatr. Gastroenterol. Nutr.* **2012,** *54* (2), 229-241.

64. Nadalutti, C. A.; Korponay-Szabo, I. R.; Kaukinen, K.; Griffin, M.; Maki, M.; Lindfors, K., Celiac disease patient IgA antibodies induce endothelial adhesion and cell polarization defects via extracellular transglutaminase 2. *Cell. Mol. Life Sci.* **2014,** *71* (7), 1315-1326.

65. Caccamo, D.; Curro, M.; Ientile, R., Potential of transglutaminase 2 as a therapeutic target. *Expert Opin. Ther. Targets* **2010,** *14* (9), 989-1003.

66. Keillor, J. W.; Apperley, K. Y. P., Transglutaminase inhibitors: a patent review. *Expert Opin. Ther. Pat.* **2016,** *26* (1), 49-63.

67. Choi, K.; Siegel, M.; Piper, J. L.; Yuan, L.; Cho, E.; Strnad, P.; Omary, B.; Rich, K. M.; Khosla, C., Chemistry and Biology of Dihydroisoxazole Derivatives: Selective Inhibitors of Human Transglutaminase 2. *Chem. Biol.* **2005,** *12* (4), 469-475.

68. Klöck, C.; Herrera, Z.; Albertelli, M.; Khosla, C., Discovery of Potent and Specific Dihydroisoxazole Inhibitors of Human Transglutaminase 2. *J. Med. Chem.* **2014,** *57* (21), 9042-9064.

69. Dafik, L.; Albertelli, M.; Stamnaes, J.; Sollid, L. M.; Khosla, C., Activation and inhibition of transglutaminase 2 in mice. *PLoS One* **2012,** *7* (2), e30642.

70. Keillor, J. W.; Chica, R. A.; Chabot, N.; Vinci, V.; Pardin, C.; Fortin, E.; Gillet, S. M. F. G.; Nakano, Y.; Kaartinen, M. T.; Pelletier, J. N.; Lubell, W. D., The bioorganic chemistry of transglutaminase - from mechanism to inhibition and engineering. *Can. J. Chem.* **2008,** *86* (4), 271-276.

71. Colak, G.; Keillor Jeffrey, W.; Johnson Gail, V. W., Cytosolic guanine nucledotide binding deficient form of transglutaminase 2 (R580a) potentiates cell death in oxygen glucose deprivation. *PLoS One* **2011,** *6* (1), e16665.

72. Zedira Dr. Falk Pharma and Zedira enter phase I clinical trials for a celiac disease drug. Press release. http://zedira.com/News/Press-Release-Dr-Falk-Pharma-and-Zedira-enter-phase-I-clinical-trials-for-a-celiac-disease-drug_71 (accessed 2 September 2015).

73. Gentile, V.; Cooper, A. J. L., Transglutaminases - possible drug targets in human diseases. *Curr. Drug Targets CNS Neurol. Disord.* **2004,** *3* (2), 99-104.

74. Duval, E.; Case, A.; Stein, R. L.; Cuny, G. D., Structure-activity relationship study of novel tissue transglutaminase inhibitors. *Bioorg. Med. Chem. Lett.* **2005,** *15* (7), 1885-1889.

75. Case, A.; Stein, R. L., Kinetic Analysis of the Interaction of Tissue Transglutaminase with a Nonpeptidic Slow-Binding Inhibitor. *Biochemistry* **2007,** *46* (4), 1106-1115.

76. Schaertl, S.; Prime, M.; Wityak, J.; Dominguez, C.; Munoz-Sanjuan, I.; Pacifici, R. E.; Courtney, S.; Scheel, A.; MacDonald, D., A profiling platform for the characterization of transglutaminase 2 (TG2) inhibitors. *J. Biomol. Screening* **2010,** *15* (5), 478-487.

77. Klöck, C.; Jin, X.; Choi, K.; Khosla, C.; Madrid, P. B.; Spencer, A.; Raimundo, B. C.; Boardman, P.; Lanza, G.; Griffin, J. H., Acylideneoxoindoles: A new class of reversible inhibitors of human transglutaminase 2. *Bioorg. Med. Chem. Lett.* **2011,** *21* (9), 2692-2696.

78. Pardin, C.; Pelletier, J. N.; Lubell, W. D.; Keillor, J. W., Cinnamoyl Inhibitors of Tissue Transglutaminase. *J. Org. Chem.* **2008,** *73* (15), 5766-5775.

79. Chica, R. A.; Gagnon, P.; Keillor, J. W.; Pelletier, J. N., Tissue transglutaminase acylation: proposed role of conserved active site Tyr and Trp residues revealed by molecular modeling of peptide substrate binding. *Protein Sci.* **2004,** *13* (4), 979-991.

80. Pardin, C.; Roy, I.; Lubell, W. D.; Keillor, J. W., Reversible and competitive cinnamoyl triazole inhibitors of tissue transglutaminase. *Chem. Biol. Drug Des.* **2008,** *72* (3), 189-196.

81. Roy, I. Inhibition réversible et photomarquage de la transglutaminase tissulaire. Doctoral thesis, Université de Montréal, 2014.

82. Noguchi, K.; Ishikawa, K.; Yokoyama, K.-I.; Ohtsuka, T.; Nio, N.; Suzuki, E.-I., Crystal structure of red sea bream transglutaminase. *J. Biol. Chem.* **2001,** *276* (15), 12055-12059.

83. Nietlispach, D.; Clowes, R. T.; Broadhurst, R. W.; Ito, Y.; Keeler, J.; Kelly, M.; Ashurst, J.; Oschkinat, H.; Domaille, P. J.; Laue, E. D., An Approach to the Structure Determination of Larger Proteins Using Triple Resonance NMR Experiments in Conjunction with Random Fractional Deuteration. *J. Am. Chem. Soc.* **1996,** *118* (2), 407-15.

84. Ong, S.-E.; Mann, M., A practical recipe for stable isotope labeling by amino acids in cell culture (SILAC). *Nature Protocols* **2006,** *1* (6), 2650-2660.

85. Campbell-Valois, F.-X.; Trost, M.; Chemali, M.; Dill, B. D.; Laplante, A.; Duclos, S.; Sadeghi, S.; Rondeau, C.; Morrow, I. C.; Bell, C.; Gagnon, E.; Hatsuzawa, K.; Thibault, P.; Desjardinsa, M., Quantitative proteomics reveals that only a subset of the endoplasmic reticulum contributes to the phagosome. *Molecular and Cellular Proteomics* **2012,** *11* (7), M111 016378, 13 pp.

86. Stigers, D. J.; Watts, Z. I.; Hennessy, J. E.; Kim, H.-K.; Martini, R.; Taylor, M. C.; Ozawa, K.; Keillor, J. W.; Dixon, N. E.; Easton, C. J., Incorporation of chlorinated analogues of aliphatic amino acids during cell-free protein synthesis. *Chem. Commun. (Cambridge, U. K.)* **2011,** *47* (6), 1839-1841.

87. Zinn, N.; Winter, D.; Lehmann, W. D., Recombinant Isotope Labeled and Selenium Quantified Proteins for Absolute Protein Quantification. *Analytical Chemistry (Washington, DC, United States)* **2010,** *82* (6), 2334-2340.

88. Ping, L.; Zhang, H.; Zhai, L.; Dammer, E. B.; Duong, D. M.; Li, N.; Yan, Z.; Wu, J.; Xu, P., Quantitative proteomics reveals significant changes in cell shape and an energy shift after IPTG induction via an optimized SILAC approach for Escherichia coli. *J Proteome Res* **2013,** *12* (12), 5978-88.

89. Roy, I.; Smith, O.; Clouthier, C. M.; Keillor, J. W., Expression, purification and kinetic characterisation of human tissue transglutaminase. *Protein Expres. Purif.* **2013,** *87* (1), 41-6.

90. Gillet, S. M. F. G.; Chica, R. A.; Keillor, J. W.; Pelletier, J. N., Expression and rapid purification of highly active hexahistidine-tagged guinea pig liver transglutaminase. *Protein Expression Purif.* **2004,** *33* (2), 256-264.

91. Studier, F. W., Protein production by auto-induction in high-density shaking cultures. *Protein Expression Purif.* **2005,** *41* (1), 207-234.

92. Yu, H., Extending the size limit of protein nuclear magnetic resonance. *Proc. Natl. Acad. Sci. U. S. A.* **1999,** *96* (2), 332-334.

93. Luy, B., Approaching the megadalton: NMR spectroscopy of protein complexes. *Angew. Chem., Int. Ed.* **2007,** *46* (23), 4214-4216.

94. Smith, E.; Collins, I., Photoaffinity labeling in target- and binding-site identification. *Future Medicinal Chemistry* **2015,** *7* (2), 159-183.

95. Mesange, F.; Sebbar, M.; Capdevielle, J.; Guillemot, J.-C.; Ferrara, P.; Bayard, F.; Poirot, M.; Faye, J.-C., Identification of Two Tamoxifen Target Proteins by Photolabeling with 4-(2-Morpholinoethoxy)benzophenone. *Bioconjugate Chemistry* **2002,** *13* (4), 766-772.

96. Brunner, J.; Senn, H.; Richards, F. M., 3-Trifluoromethyl-3-phenyldiazirine. A new carbene generating group for photolabeling reagents. *J. Biol. Chem.* **1980,** *255* (8), 3313-18.

97. Jessen, K. A.; English, N. M.; Wang, J. Y.; Maliartchouk, S.; Archer, S. P.; Qiu, L.; Brand, R.; Kuemmerle, J.; Zhang, H.-Z.; Gehlsen, K.; Drewe, J.; Tseng, B.; Cai, S. X.; Kasibhatla, S., The discovery and mechanism of action of novel tumor-selective and apoptosis-

inducing 3,5-diaryl-1,2,4-oxadiazole series using a chemical genetics approach. *Mol. Cancer Ther.* **2005,** *4* (5), 761-771.

98. Hamouda, A. K.; Stewart, D. S.; Chiara, D. C.; Savechenkov, P. Y.; Bruzik, K. S.; Cohen, J. B., Identifying barbiturate binding sites in a nicotinic acetylcholine receptor with [3H]allyl m-trifluoromethyldiazirine mephobarbital, a photoreactive barbiturate. *Molecular Pharmacology* **2014,** *85* (5), 735-746, 12 pp.

99. Kumar, A. B.; Tipton, J. D.; Manetsch, R., 3-Trifluoromethyl-3-aryldiazirine photolabels with enhanced ambient light stability. *Chem. Commun. (Cambridge, U. K.)* **2016,** *52* (13), 2729-2732.

100. Lee, K.; Ban, H. S.; Naik, R.; Hong, Y. S.; Son, S.; Kim, B.-K.; Xia, Y.; Song, K. B.; Lee, H.-S.; Won, M., Identification of Malate Dehydrogenase 2 as a Target Protein of the HIF-1 Inhibitor LW6 using Chemical Probes. *Angew. Chem., Int. Ed.* **2013,** *52* (39), 10286-10289.

101. Savechenkov, P. Y.; Zhang, X.; Chiara, D. C.; Stewart, D. S.; Ge, R. L.; Zhou, X. J.; Raines, D. E.; Cohen, J. B.; Forman, S. A.; Miller, K. W.; Bruzik, K. S., Allyl m-Trifluoromethyldiazirine Mephobarbital: An Unusually Potent Enantioselective and Photoreactive Barbiturate General Anesthetic. *J. Med. Chem.* **2012,** *55* (14), 6554-6565.

102. Kornblum, N.; Jones, W. J.; Anderson, G. J., A new and selective method of oxidation. Conversion of alkyl halides and alkyl tosylates to aldehydes. *J. Am. Chem. Soc.* **1959,** *81*, 4113-14.

103. Zhang, S.; Xu, L.; Trudell, M. L., Selective oxidation of benzylic alcohols and TBDMS ethers to carbonyl compounds with CrO3-H5IO6. *Synthesis* **2005,** (11), 1757-1760.

104. Welle, A.; Billard, F.; Marchand-Brynaert, J., Tri- and tetravalent photoactivable cross-linking agents. *Synthesis* **2012,** *44* (14), 2249-2254.

105. Husain, S. S.; Stewart, D.; Desai, R.; Hamouda, A. K.; Li, S. G.-D.; Kelly, E.; Dostalova, Z.; Zhou, X.; Cotten, J. F.; Raines, D. E.; Olsen, R. W.; Cohen, J. B.; Forman, S. A.; Miller, K. W., p-Trifluoromethyldiazirinyl-etomidate: A Potent Photoreactive General Anesthetic Derivative of Etomidate That Is Selective for Ligand-Gated Cationic Ion Channels. *J. Med. Chem.* **2010,** *53* (17), 6432-6444.

106. Smith, N. W.; Polenz, B. P.; Johnson, S. B.; Dzyuba, S. V., Base and concentration effects on the product distribution in copper-promoted alkyne-azide cycloaddition: additive-free route to 5-iodo-triazoles. *Tetrahedron Lett.* **2010,** *51* (3), 550-553.

107. Cheng, Y.-C.; Prusoff, W. H., Relation between the inhibition constant K1) and the concentration of inhibitor which causes fifty per cent inhibition (I50) of an enzymic reaction. *Biochemical Pharmacology* **1973,** *22* (23), 3099-108.

108. Herner, A.; Marjanovic, J.; Lewandowski, T. M.; Marin, V.; Patterson, M.; Miesbauer, L.; Ready, D.; Williams, J.; Vasudevan, A.; Lin, Q., 2-Aryl-5-carboxytetrazole as a New Photoaffinity Label for Drug Target Identification. *J. Am. Chem. Soc.* **2016,** *138* (44), 14609-14615.

109. Lushchak, V. I., Glutathione homeostasis and functions: potential targets for medical interventions. *Journal of Amino Acids* **2012**, 736837, 26 pp.

110. Chakravarthi, S.; Jessop, C. E.; Bulleid, N. J., The role of glutathione in disulphide bond formation and endoplasmic-reticulum-generated oxidative stress. *EMBO Reports* **2006,** *7* (3), 271-275.

111. Halliwell, B.; Gutteridge, J. M. C., *Free Radicals in Biology and Medicine*. Oxford University Press: 2015.

112. Budke, B.; Kalin, J. H.; Pawlowski, M.; Zelivianskaia, A. S.; Wu, M.; Kozikowski, A. P.; Connell, P. P., An Optimized RAD51 Inhibitor That Disrupts Homologous Recombination without Requiring Michael Acceptor Reactivity. *J. Med. Chem.* **2013,** *56* (1), 254-263.

113. Apperley, K. Y. P.; Roy, I.; Saucier, V.; Brunet-Filion, N.; Piscopo, S.-P.; Pardin, C.; De Francesco, E.; Hao, C.; Keillor, J. W., Development of new scaffolds as reversible tissue transglutaminase inhibitors, with improved potency or resistance to glutathione addition. *MedChemComm* **2017,** *8* (2), 338-345.

114. Wille, F.; Strasser, R., Diethynyl ketone. *Chemische Berichte* **1961,** *94*, 1606-11.

115. Veliev, M. G.; Guseinov, M. M., An improved synthesis of propynal. *Synthesis* **1980,** (6), 461.

116. Gupta, V. P.; Sharma, A., Anharmonic analysis of the vibrational spectra of some cyanides and related molecules of astrophysical importance. *Spectrochimica Acta, Part A: Molecular and Biomolecular Spectroscopy* **2006,** *65A* (3-4), 759-769.

117. (a) McDaniel, D. S.; Brown, H. C., Extended table of Hammett substituent constants based on the ionization of substituted benzoic acids. *J. Org. Chem.* **1958,** *23*, 420-7; (b) Hansch, C.; Leo, A.; Taft, R. W., A survey of Hammett substituent constants and resonance and field parameters. *Chem. Rev.* **1991,** *91* (2), 165-95.

118. Besset, T.; Jubault, P.; Pannecoucke, X.; Poisson, T., New entries toward the synthesis of OCF3-containing molecules. *Organic Chemistry Frontiers* **2016,** *3* (8), 1004-1010.

119. Hao, C. Alkyne bond replacement of alkene bond in para-nitro cinnamoyl triazole compounds for potential reversible and competitive inhibition of tissue transglutaminase. Undergraduate honours thesis, University of Ottawa, 2013.

120. Ai, Y.; Kozytska, M. V.; Zou, Y.; Khartulyari, A. S.; Smith, A. B., Total Synthesis of (-)-Enigmazole A. *J. Am. Chem. Soc.* **2015,** *137* (49), 15426-15429.

121. Hsu, C.-H.; Stedeford, T.; Okochi-Takada, E.; Ushijima, T.; Noguchi, H.; Muro-Cacho, C.; Holder, J. W.; Banasik, M., Framework Analysis for the Carcinogenic Mode of Action of Nitrobenzene. *J. Environ. Sci. Health, Part C Environ. Carcinog. Ecotoxicol. Rev.* **2007,** *25* (2), 155-184.

122. Strauss, M. J., The nitroaromatic group in drug design, pharmacology, and toxicology (for non-pharmacologists). *Industrial & Engineering Chemistry Product Research and Development* **1979,** *18* (3), 158-66.

123. Raymond, M. Synthesis of reversible competitive inhibitors of human tissue transglutaminase: Investigation of substituent effects. Undergraduate honours thesis, University of Ottawa, 2014.

124. Dossetter, A. G., A statistical analysis of in vitro human microsomal metabolic stability of small phenyl group substituents, leading to improved design sets for parallel SAR exploration of a chemical series. *Bioorg. Med. Chem.* **2010,** *18* (12), 4405-4414.

125. Bellamy, F. D.; Ou, K., Selective reduction of aromatic nitro compounds with stannous chloride in nonacidic and nonaqueous medium. *Tetrahedron Lett.* **1984,** *25* (8), 839-42.

126. Presolski, S. I.; Hong, V.; Cho, S.-H.; Finn, M. G., Tailored Ligand Acceleration of the Cu-Catalyzed Azide-Alkyne Cycloaddition Reaction: Practical and Mechanistic Implications. *J. Am. Chem. Soc.* **2010,** *132* (41), 14570-14576.

127. Saucier, V. *Stage d'été 2014*; University of Ottawa: 2014.

128. Rodlert, M.; Harth, E.; Rees, I.; Hawker, C. J., End-group fidelity in nitroxide-mediated living free-radical polymerizations. *Journal of Polymer Science, Part A: Polymer Chemistry* **2000,** *38* (Suppl.), 4749-4763.

129. Vugts, D. J.; Veum, L.; al-Mafraji, K.; Lemmens, R.; Schmitz, R. F.; de Kanter, F. J. J.; Groen, M. B.; Hanefeld, U.; Orru, R. V. A., A mild chemo-enzymatic oxidation-hydrocyanation protocol. *Eur. J. Org. Chem.* **2006,** (7), 1672-1677.

130. Tian, P.-P.; Cai, S.-H.; Liang, Q.-J.; Zhou, X.-Y.; Xu, Y.-H.; Loh, T.-P., Palladium-Catalyzed Difunctionalization of Internal Alkynes via Highly Regioselective 6-Endo Cyclization and Alkenylation of Enynoates: Synthesis of Multisubstituted Pyrones. *Org. Lett.* **2015,** *17* (7), 1636-1639.

131. Spee, M. P. R.; Boersma, J.; Meijer, M. D.; Slagt, M. Q.; van Koten, G.; Geus, J. W., Selective Liquid-Phase Semihydrogenation of Functionalized Acetylenes and Propargylic Alcohols with Silica-Supported Bimetallic Palladium-Copper Catalysts. *J. Org. Chem.* **2001,** *66* (5), 1647-1656.

132. Hunsen, M., Carboxylic acids from primary alcohols and aldehydes by a pyridinium chlorochromate-catalyzed oxidation. *Synthesis* **2005,** (15), 2487-2490.

133. Jeanjot, P.; Bruyneel, F.; Arrault, A.; Gharbi, S.; Cavalier, J.-F.; Abels, A.; Marchand, C.; Touillaux, R.; Rees, J.-F.; Marchand-Brynaert, J., N-(alkyl)-2-amino-1,4-pyrazine derivatives: Synthesis and antioxidative properties of 3- and 3,5-p-hydroxyphenyl-substituted compounds. *Synthesis* **2003,** (4), 513-522.

Appendix

NMR spectra of final compounds

Photolabel (Chapter 3)

3.8

3.1

Bis(triazole)s (Chapter 4)

4.19a to **4.19l**

4.24a and **4.24b**

Alkynes (Chapter 5)

4.8

4.9

5.13a

5.14a

5.16

5.17

5.13b

5.14b

5.13c

5.14c

5.13d

5.14d

5.13e

5.14e

5.13f

5.14f

Comment on inhibitor **4.9**

Compound **3.8**

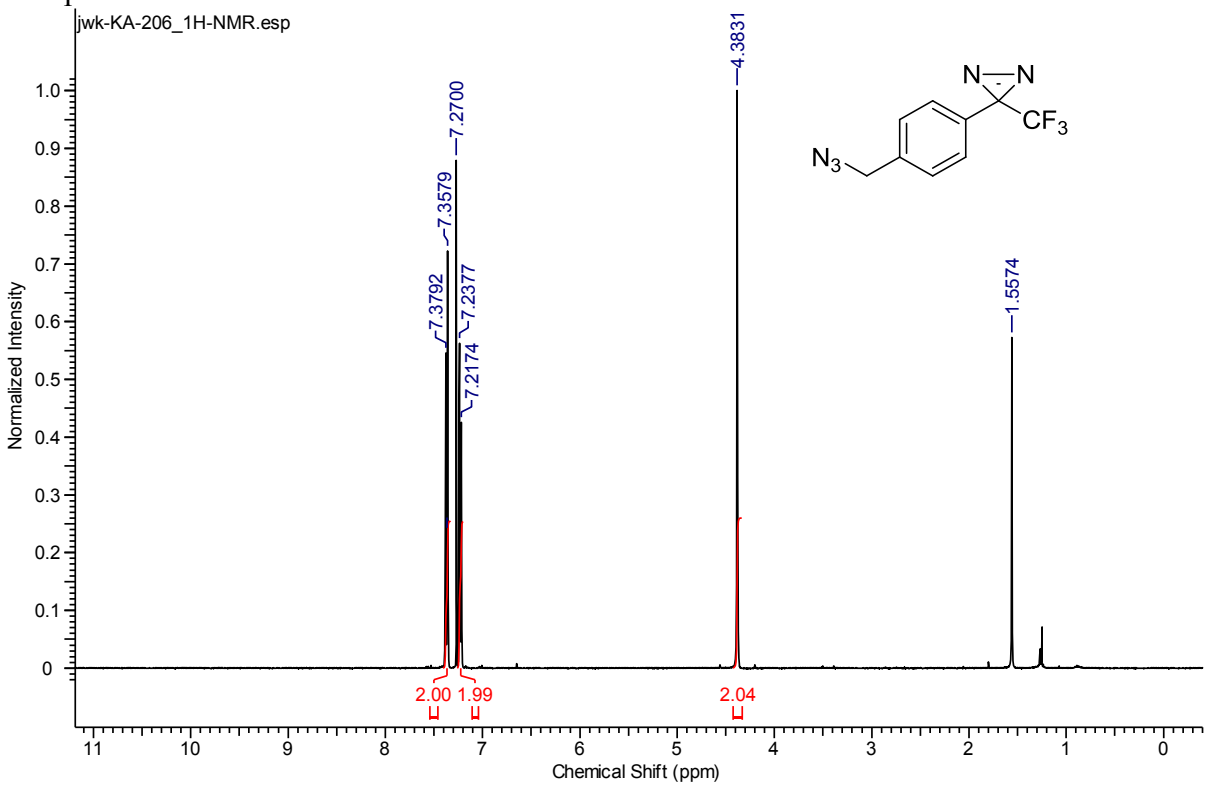
jwk-KA-206_1H-NMR.esp
Normalized Intensity
Chemical Shift (ppm)
4.3831
7.2700
7.3579
7.3792
7.2377
7.2174
1.5574
2.00
1.99
2.04
N
N
CF3
N3

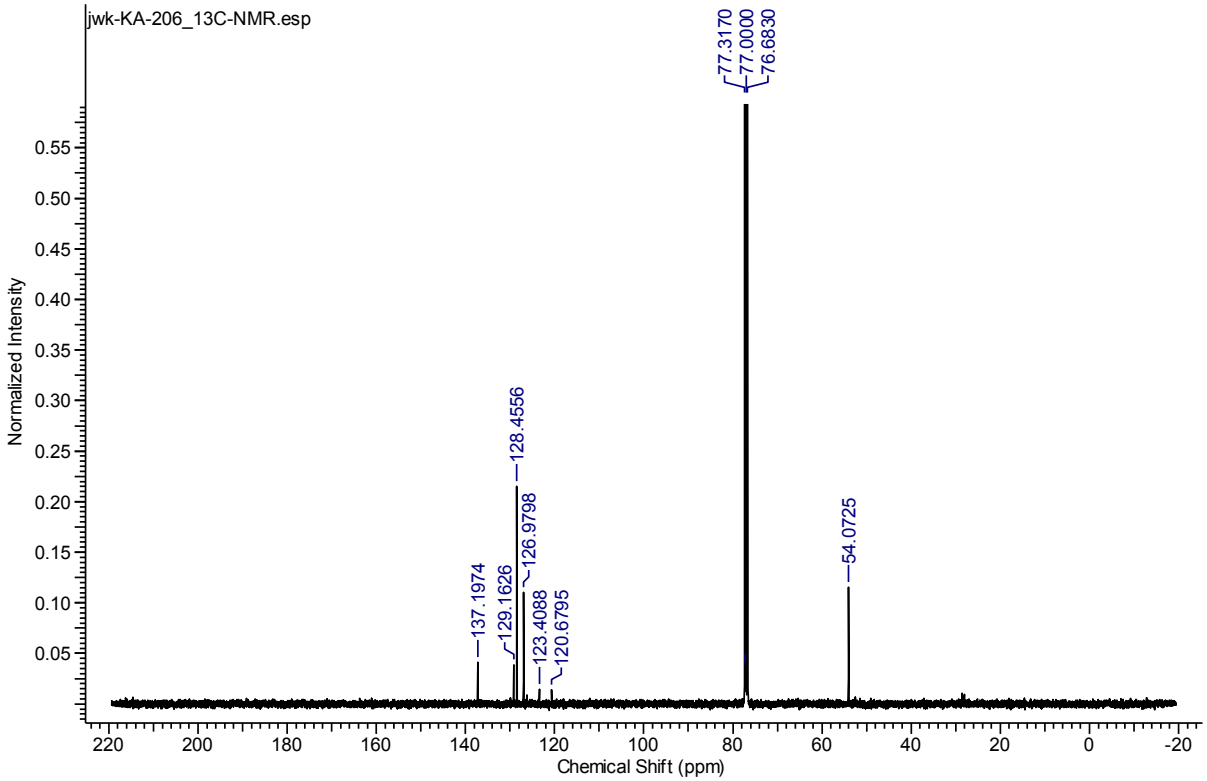
jwk-KA-206_13C-NMR.esp
Normalized Intensity
Chemical Shift (ppm)
77.3170
77.0000
76.6830
128.4556
126.9798
137.1974
129.1626
123.4088
120.6795
54.0725

Compound **3.1**

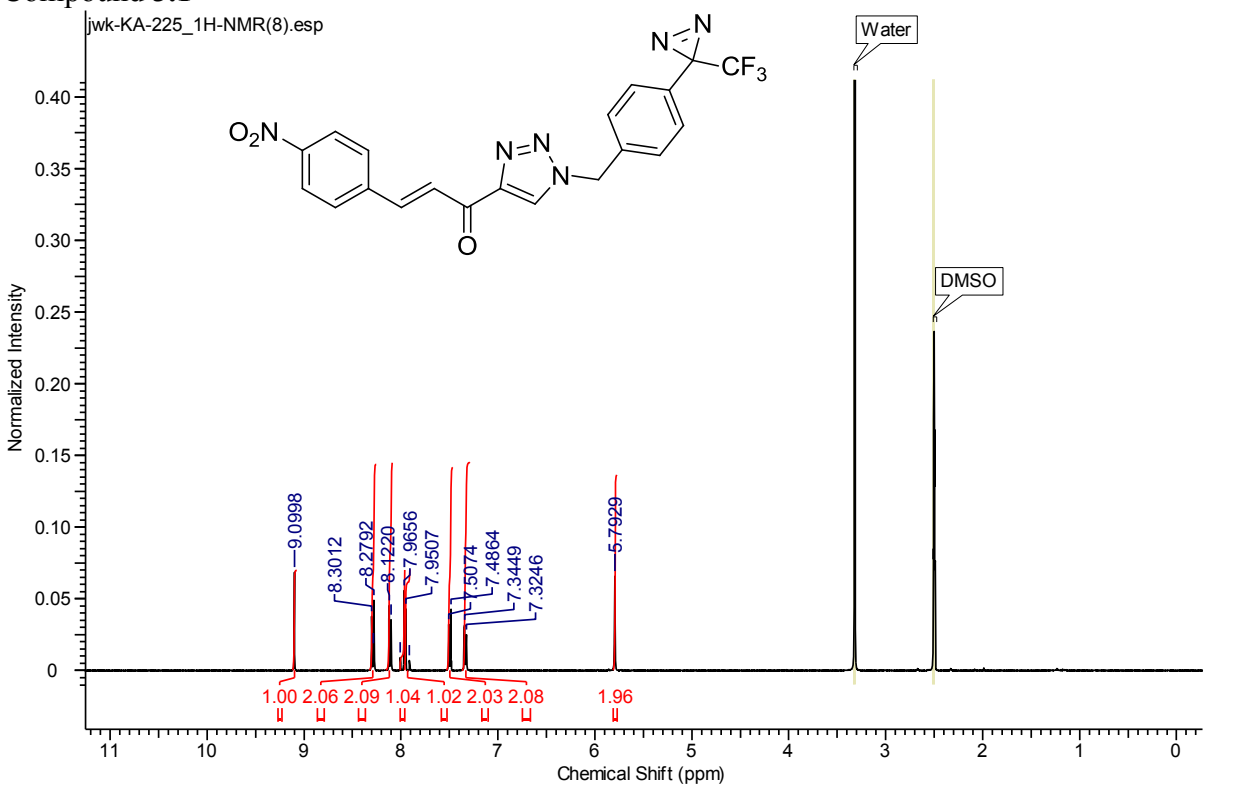
jwk-KA-225_1H-NMR(8).esp
Water
DMSO
9.0998
8.3012
8.2792
8.1220
7.9656
7.9507
7.5074
7.4864
7.3449
7.3246
5.7929
1.00 2.06 2.09 1.04 1.02 2.03 2.08 1.96
Normalized Intensity
Chemical Shift (ppm)

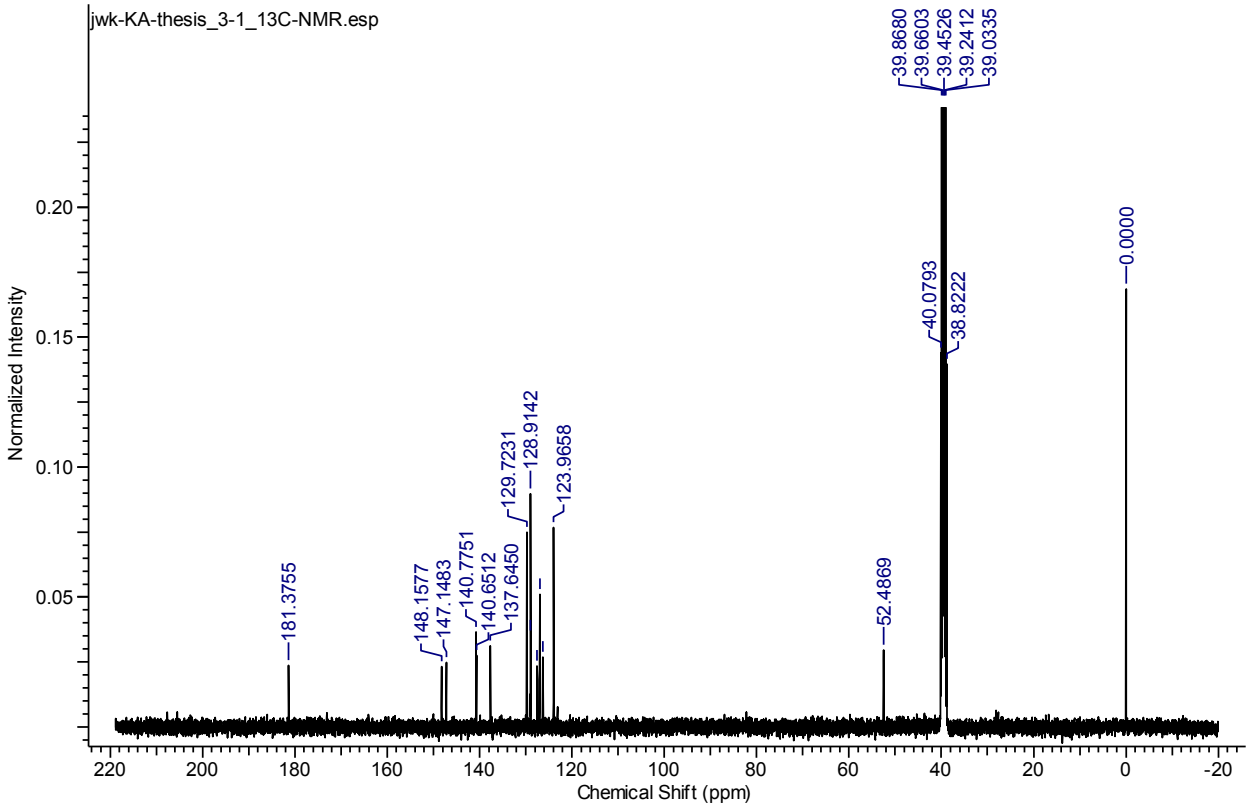
jwk-KA-thesis_3-1_13C-NMR.esp
39.8680
39.6603
39.4526
39.2412
39.0335
40.0793
38.8222
0.0000
181.3755
148.1577
147.1483
140.7751
140.6512
137.6450
129.7231
128.9142
123.9658
52.4869
Normalized Intensity
Chemical Shift (ppm)

Compound **4.19a**

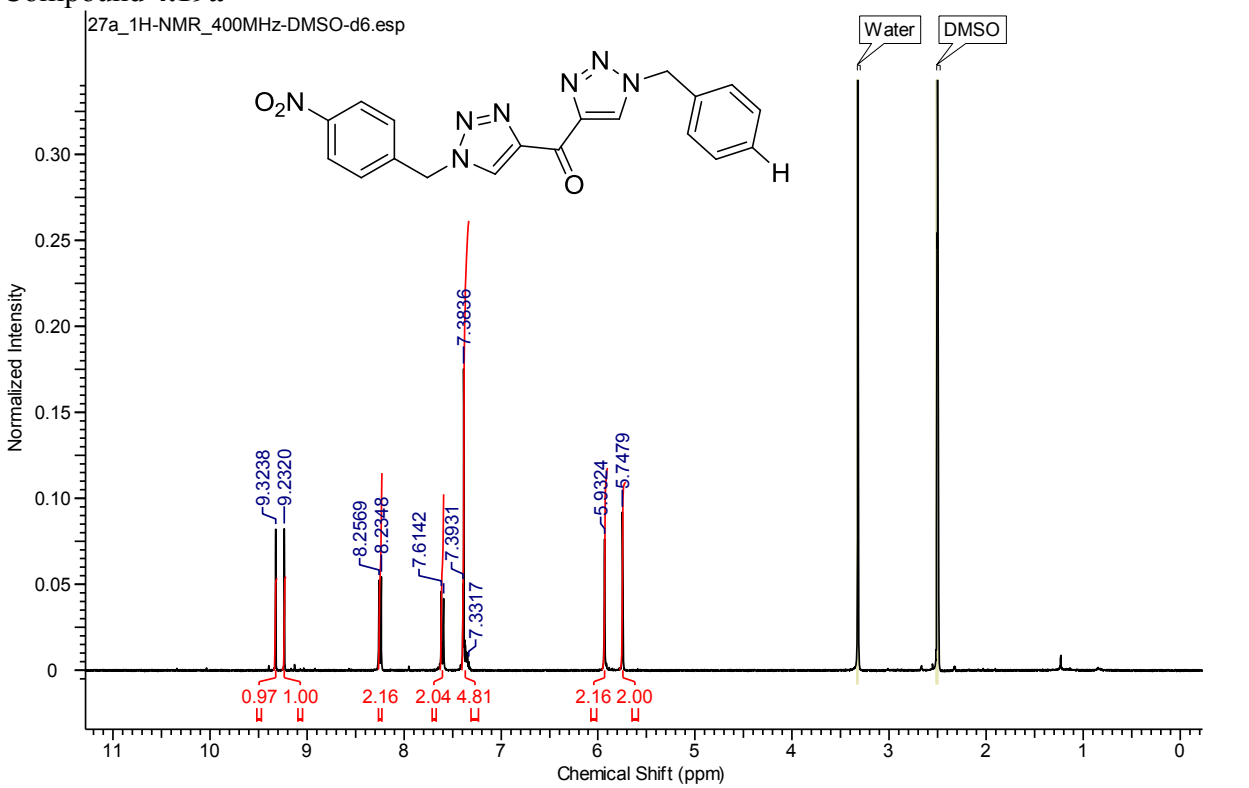

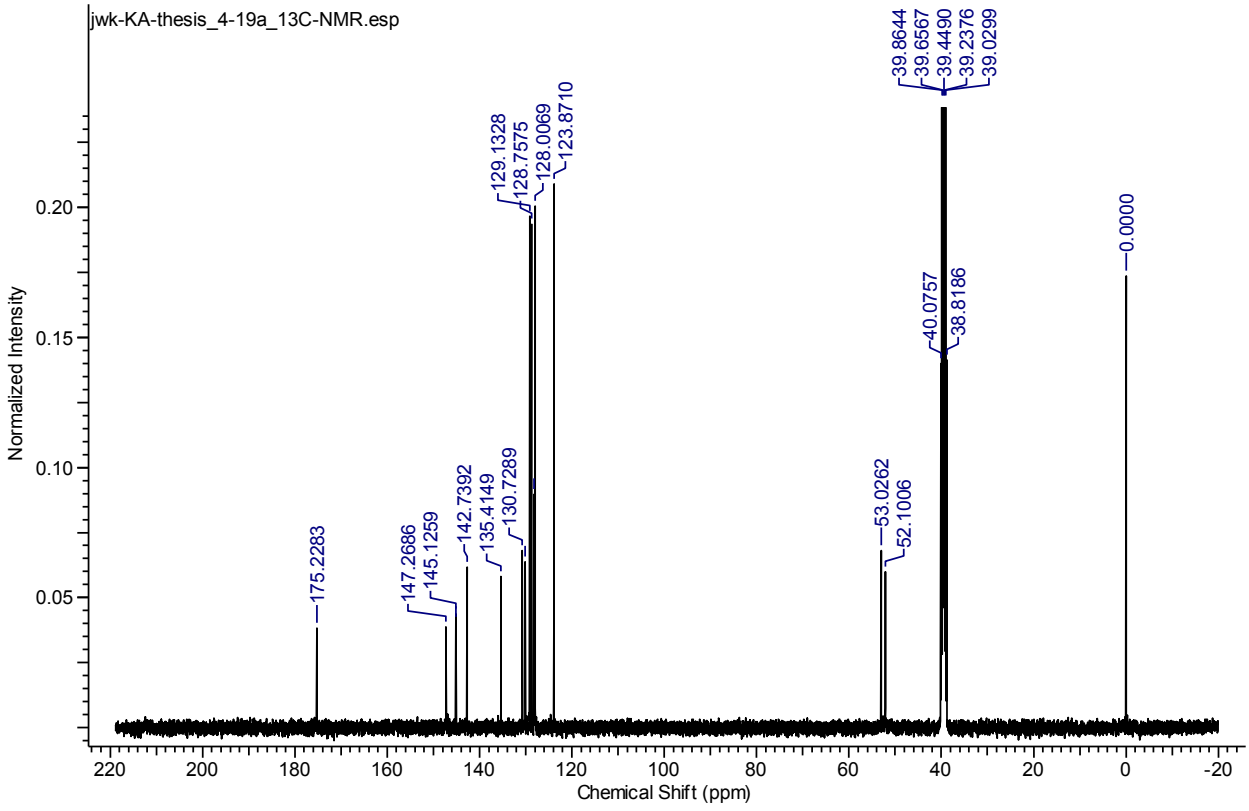

Compound **4.19b**

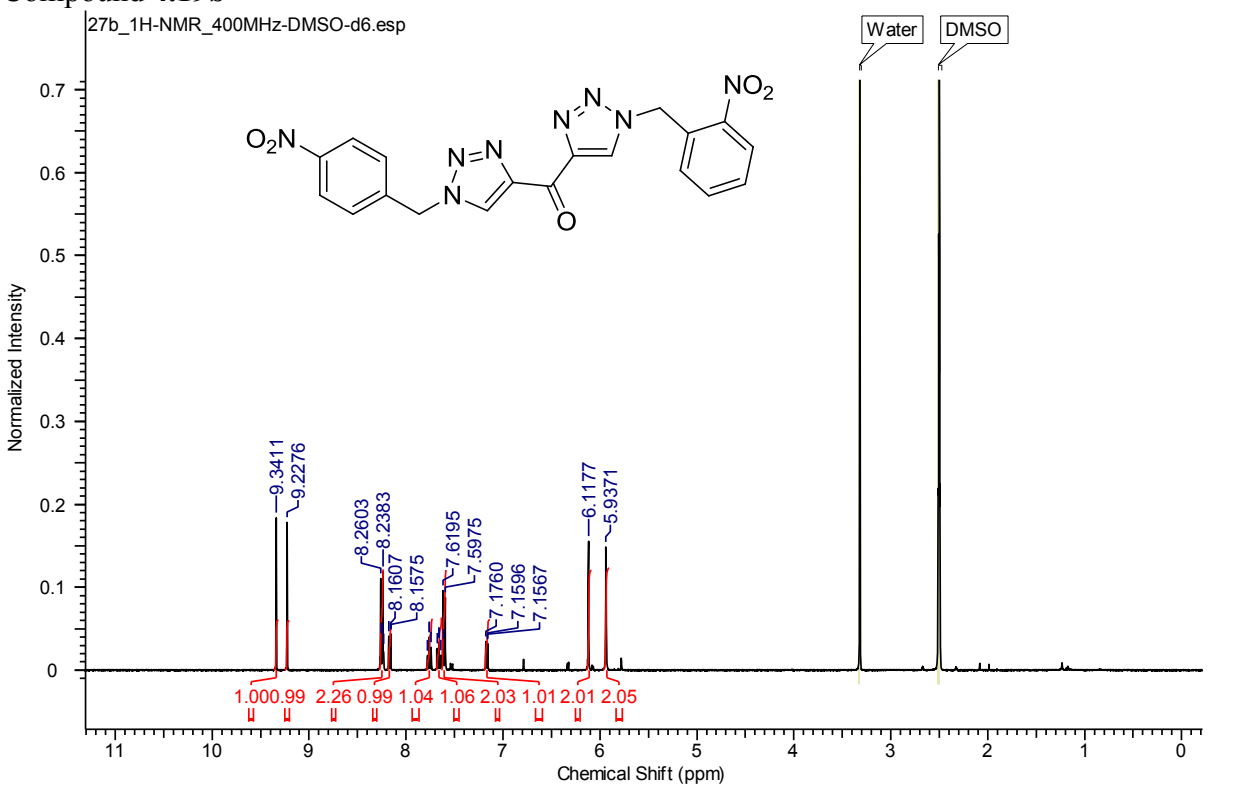

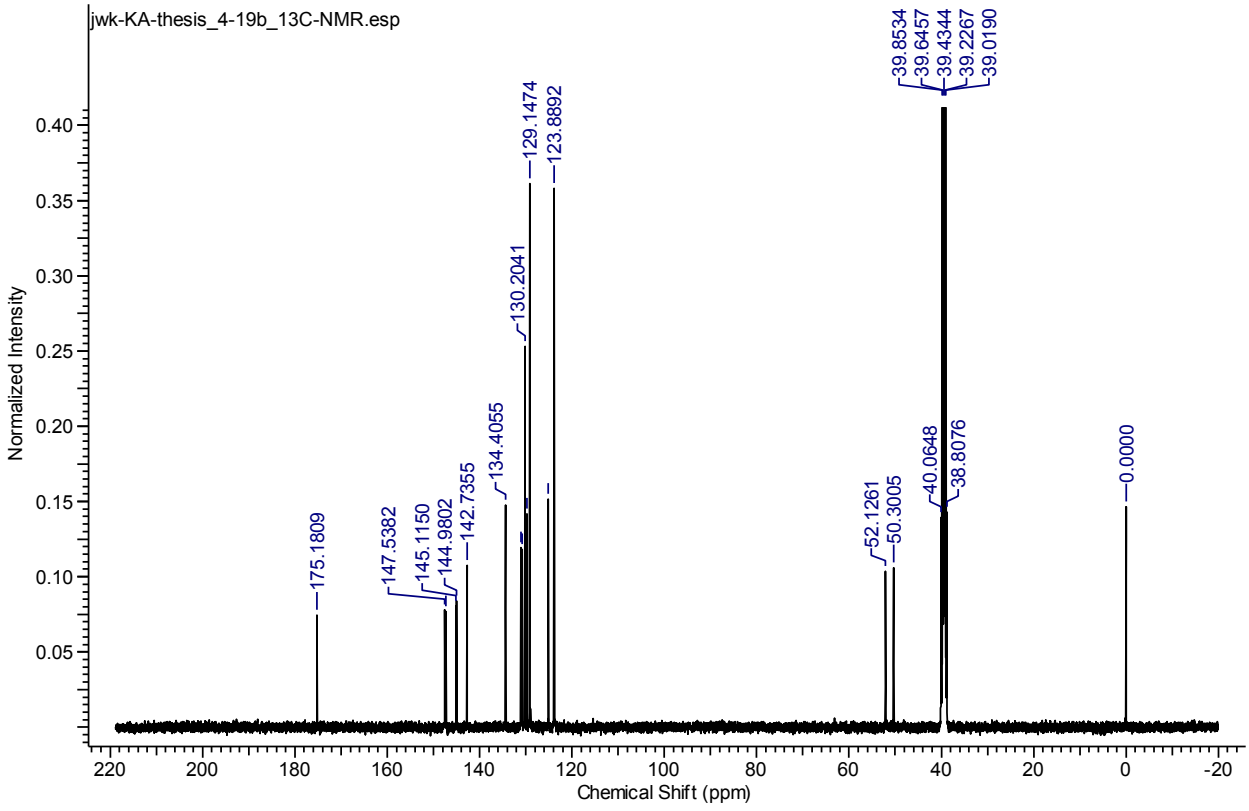

Compound **4.19c**

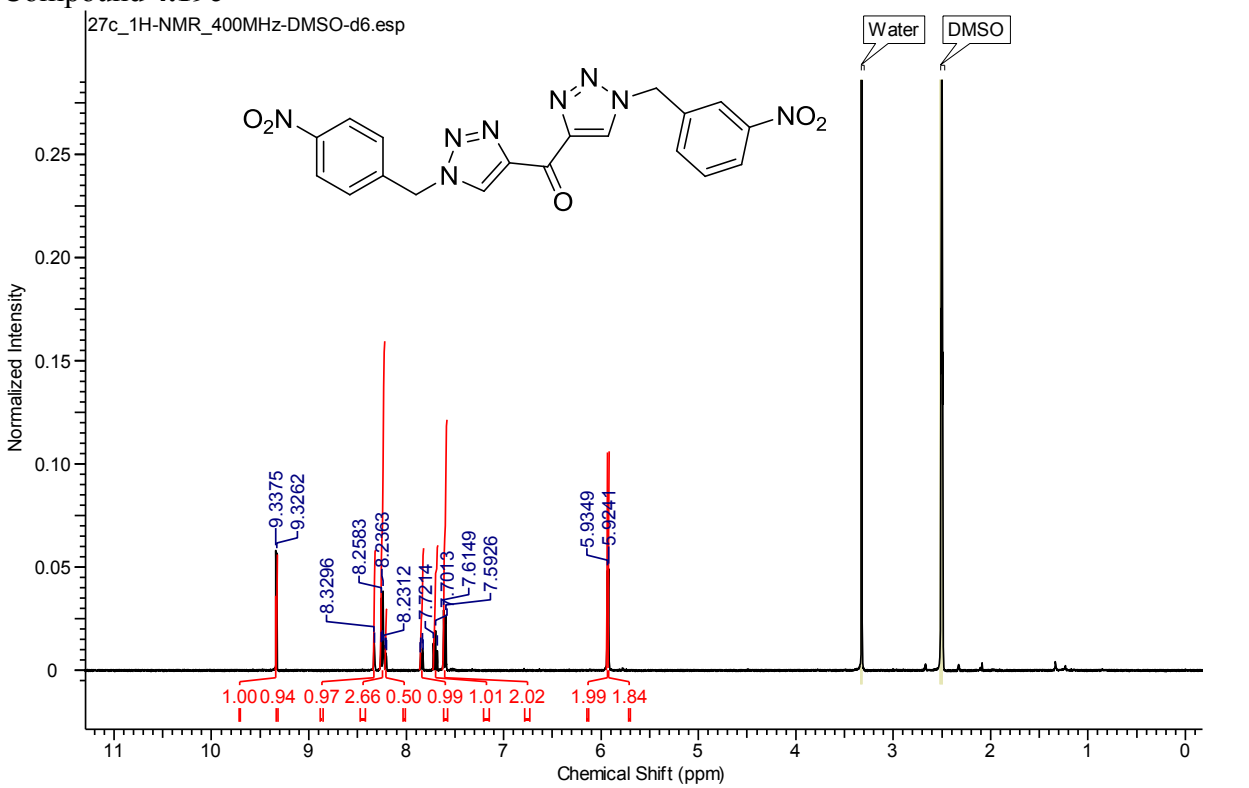

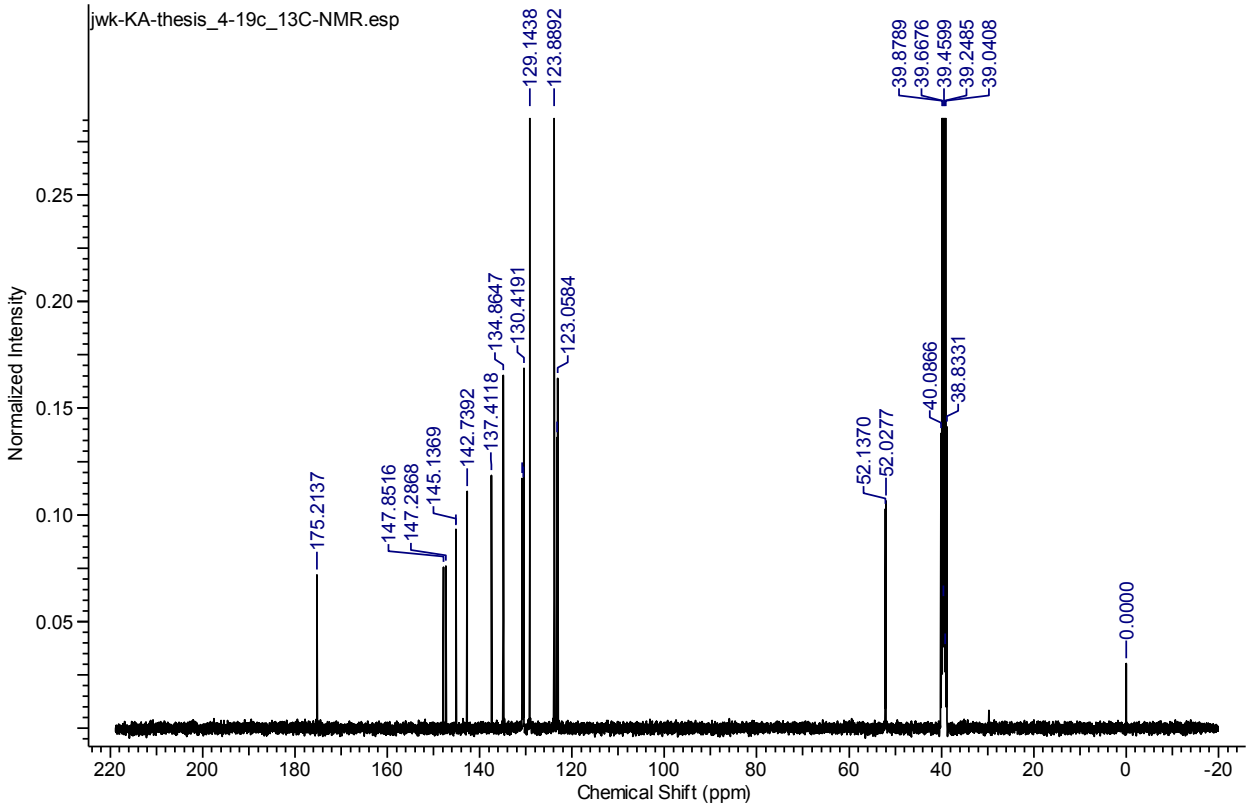

Compound **4.10**

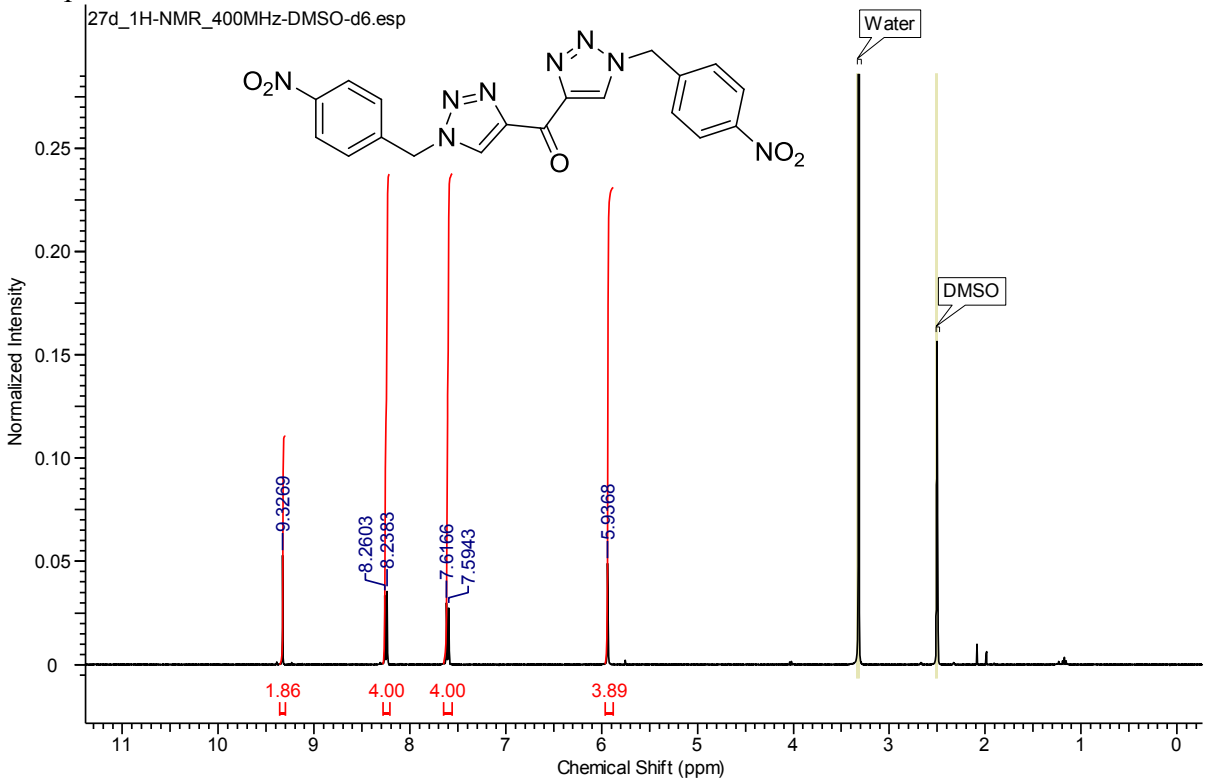

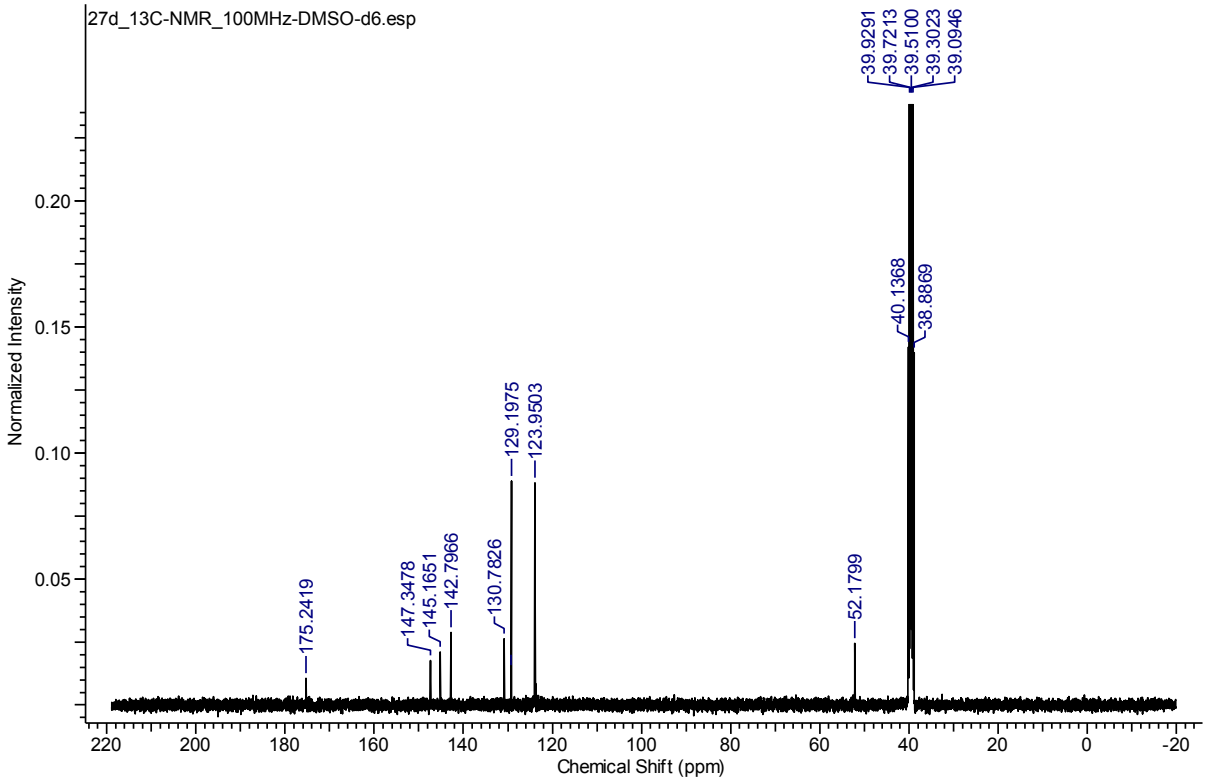

Compound **4.19e**

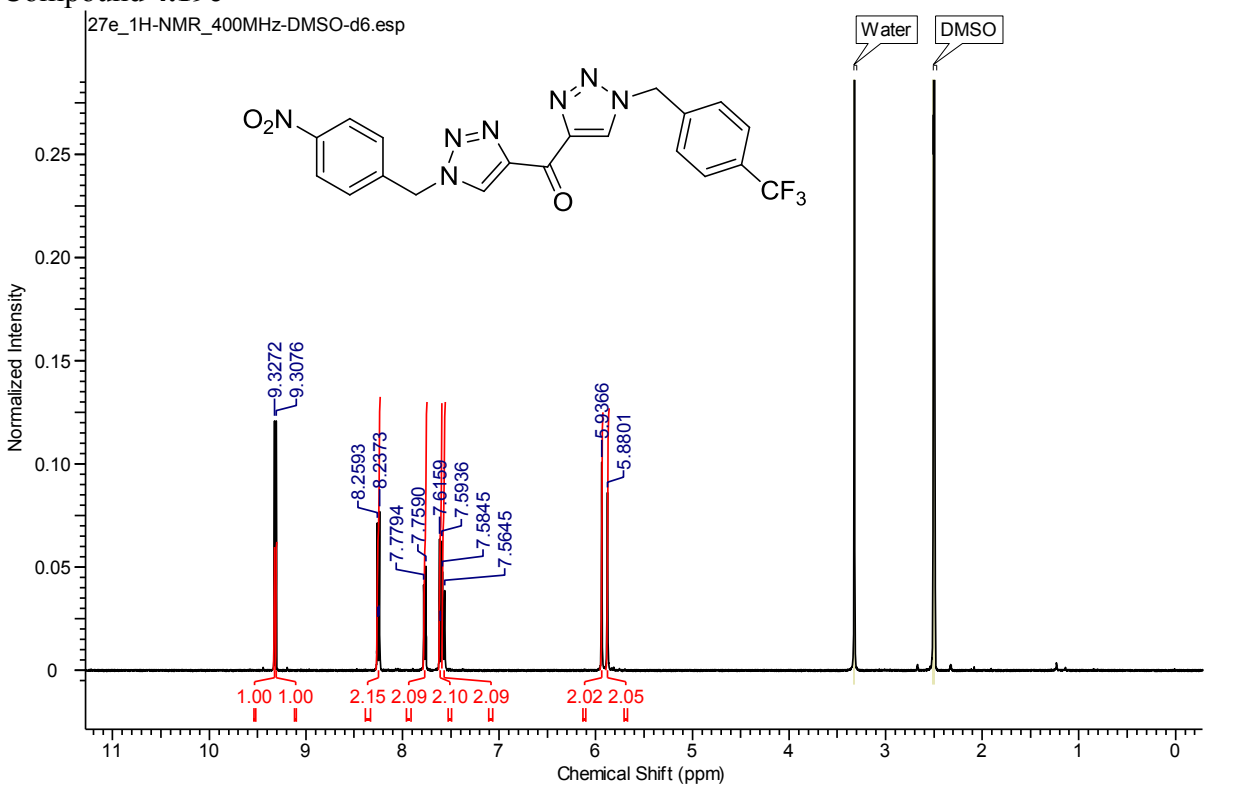

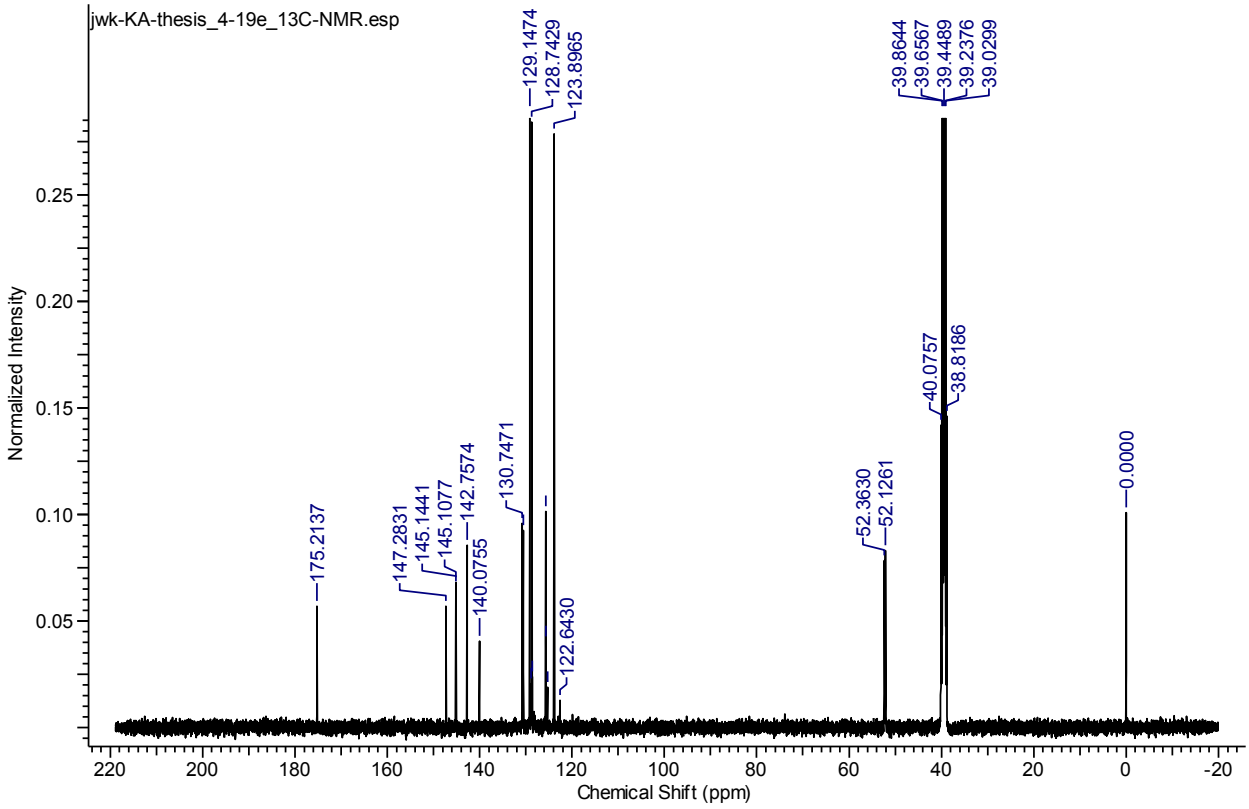

Compound **4.19f**

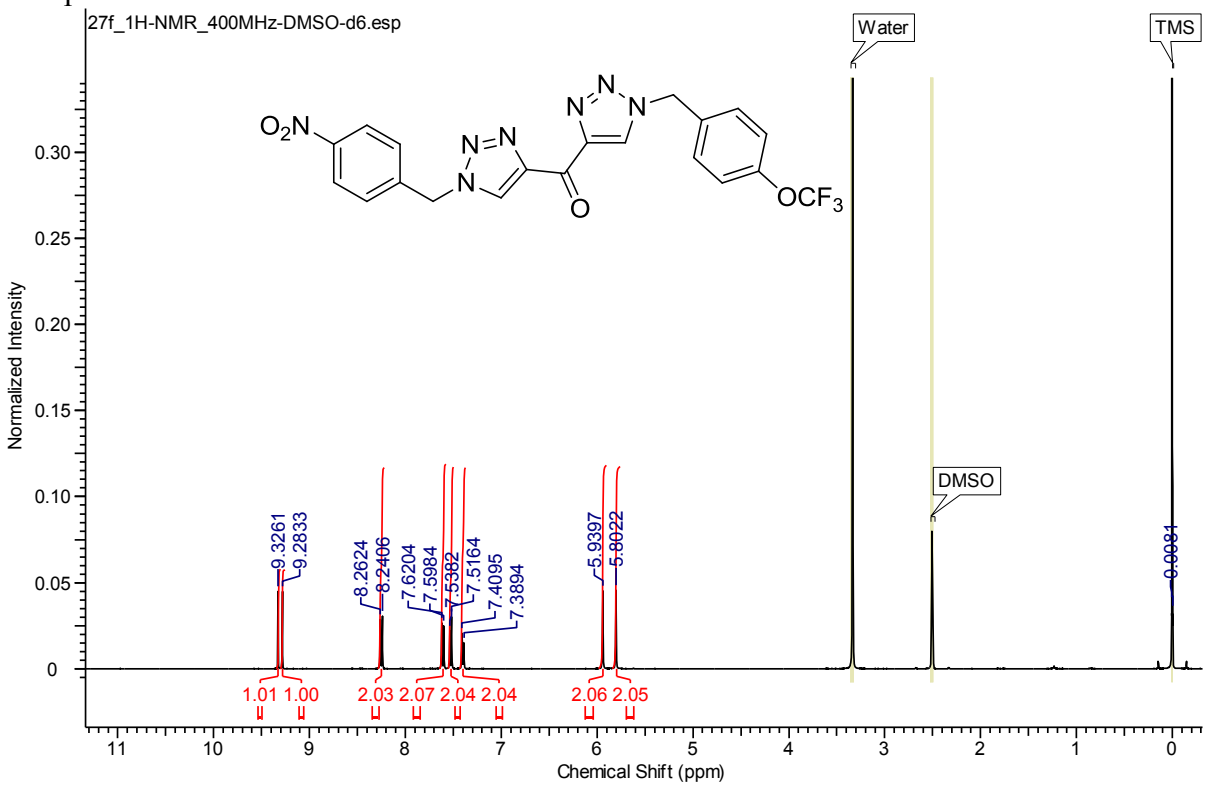

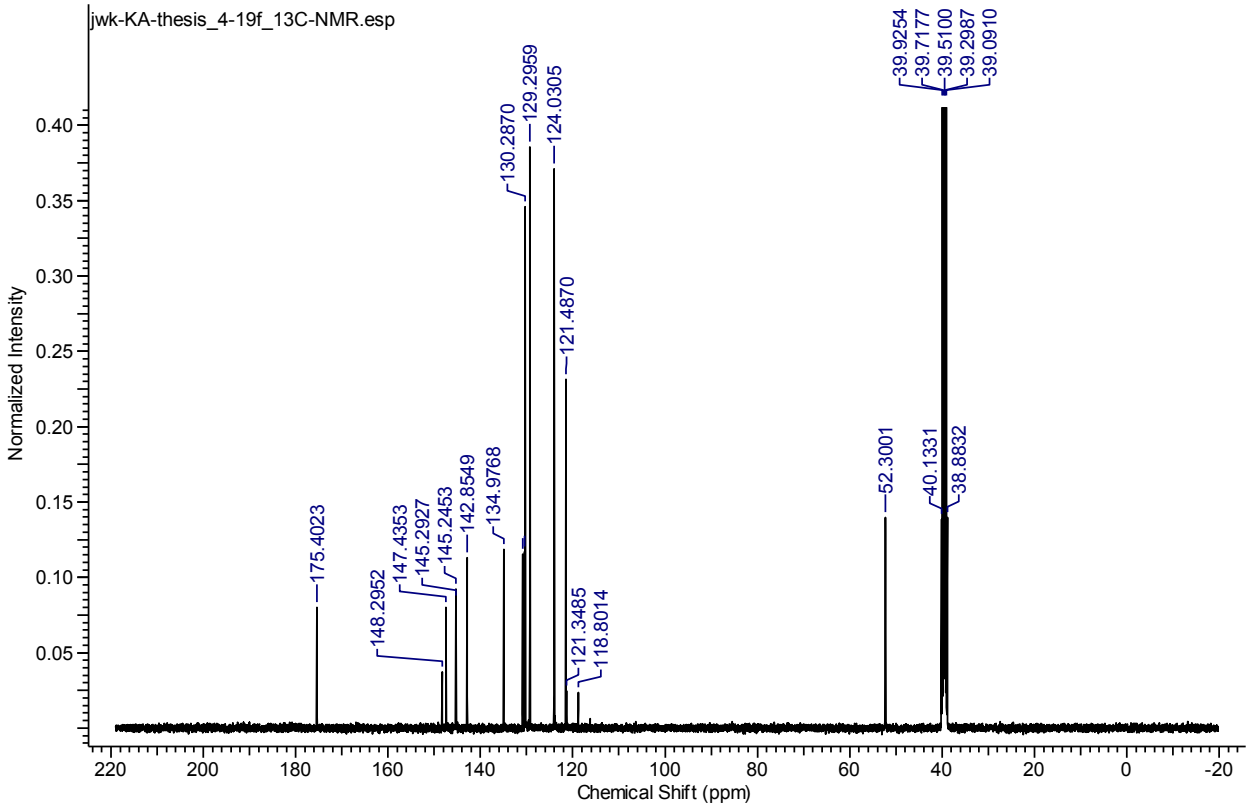

Compound **4.19g**

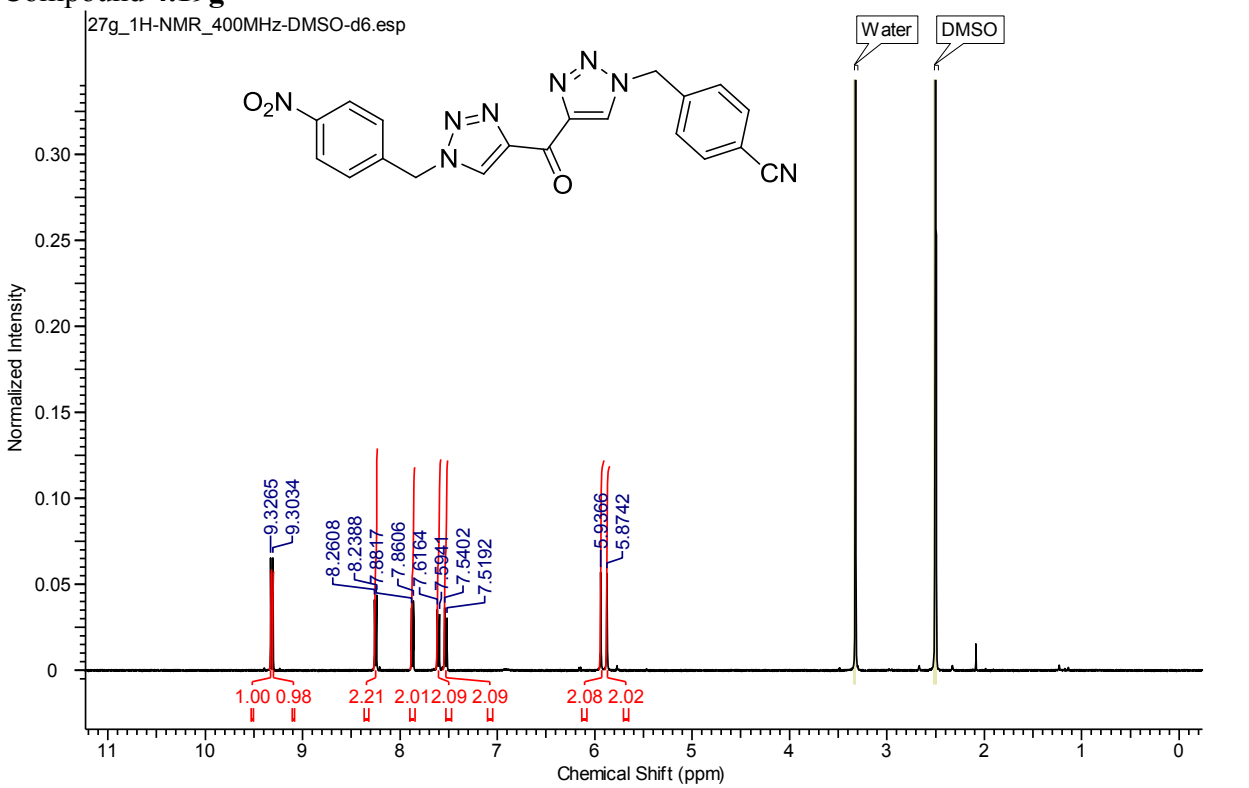

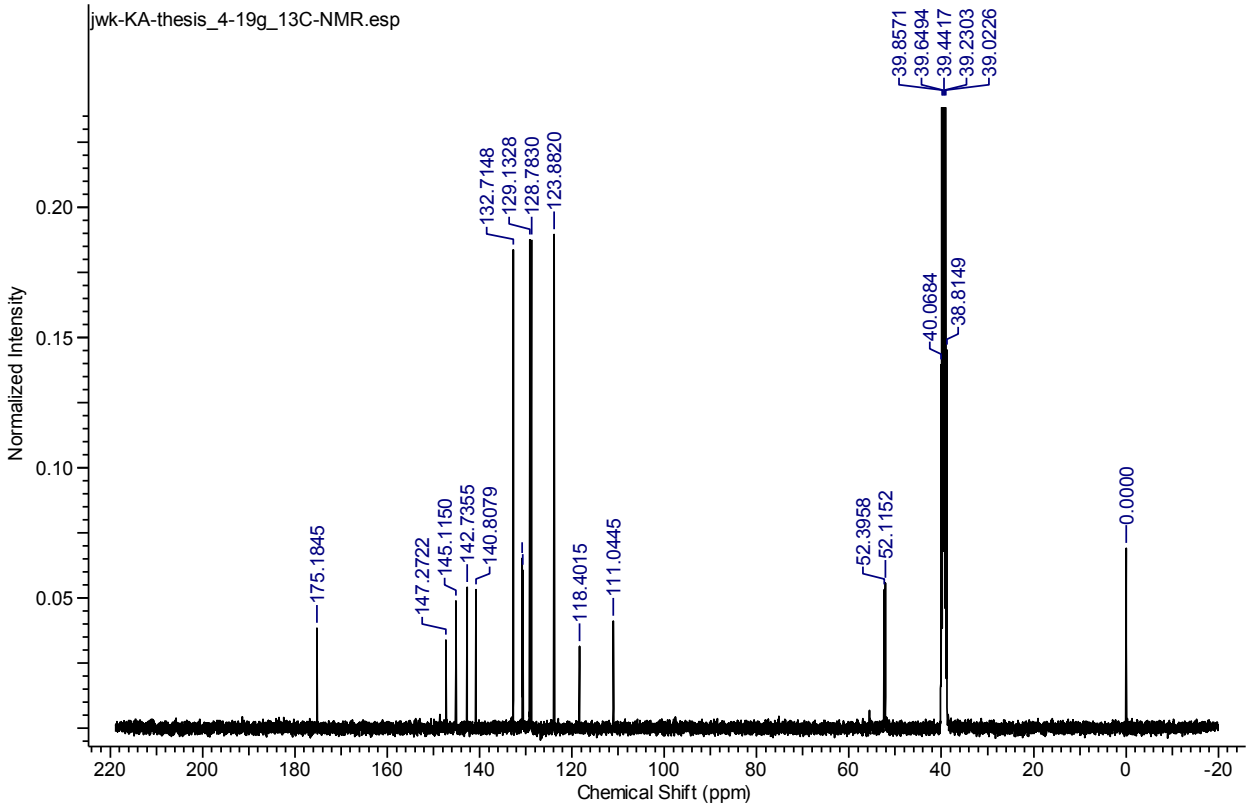

Compound **4.19h**

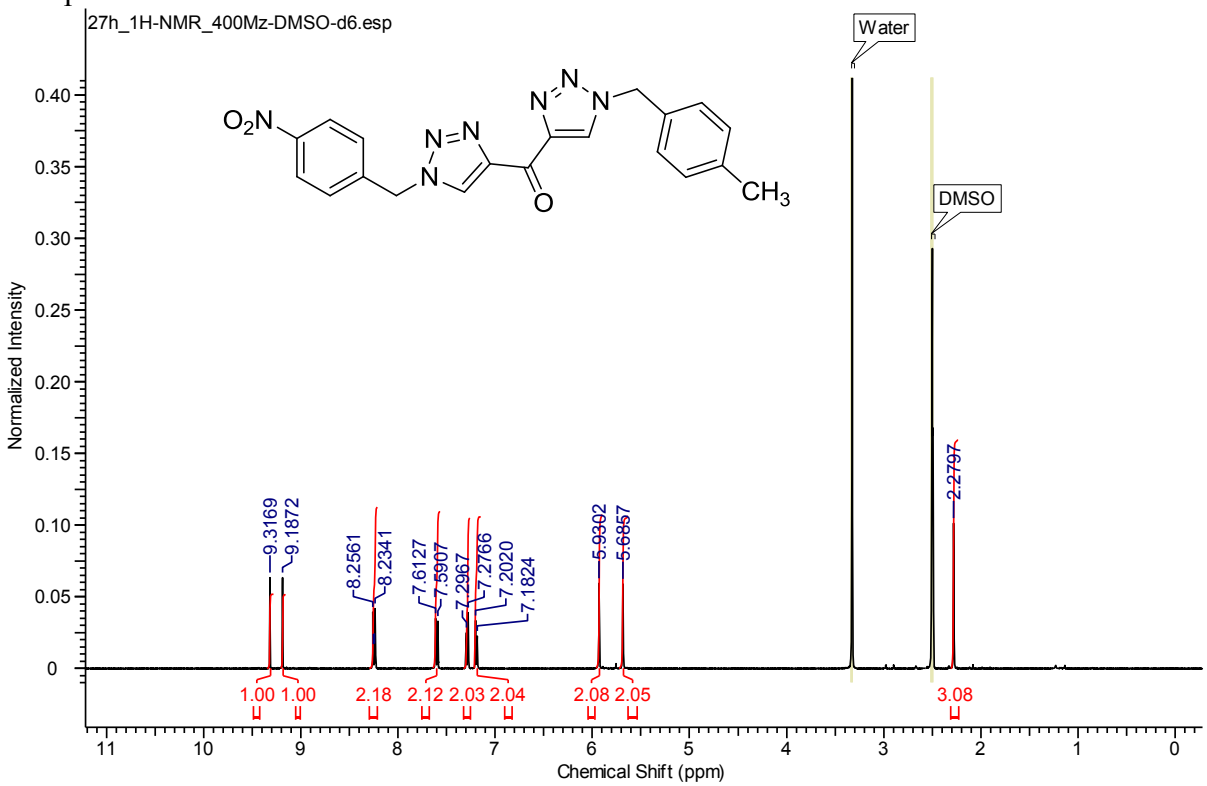

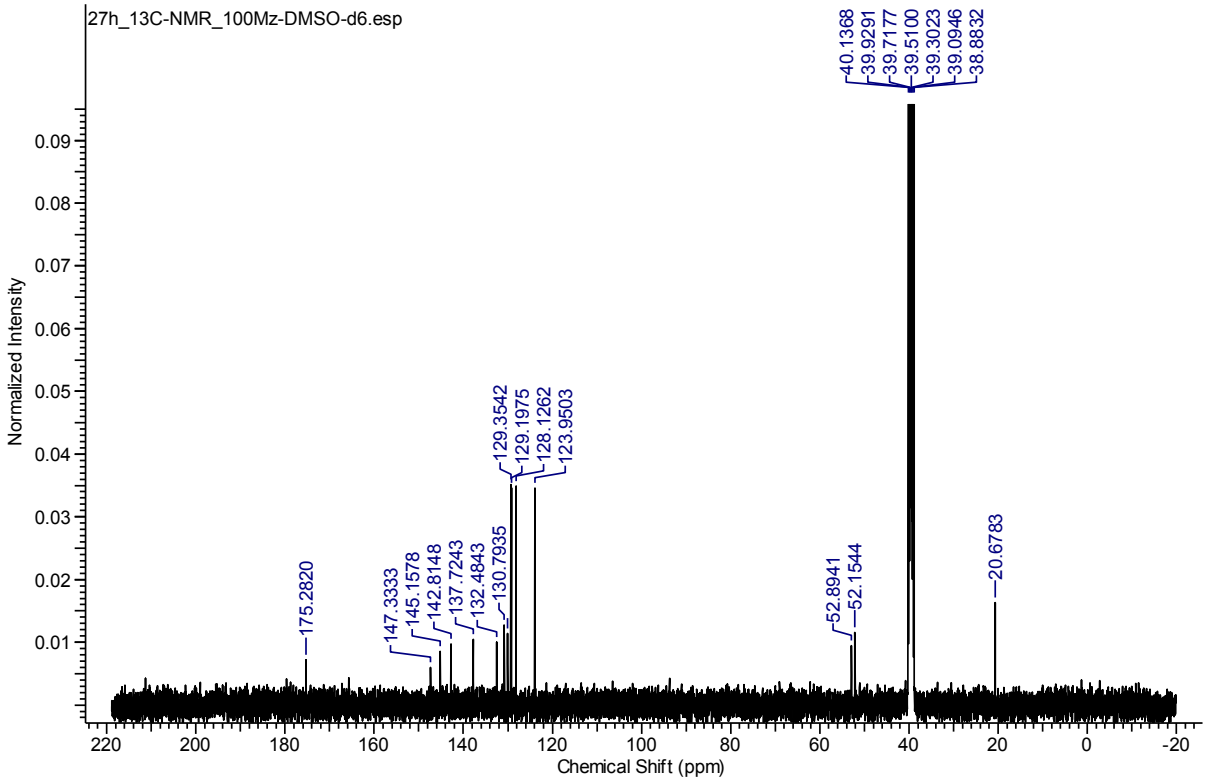

Compound **4.19i**

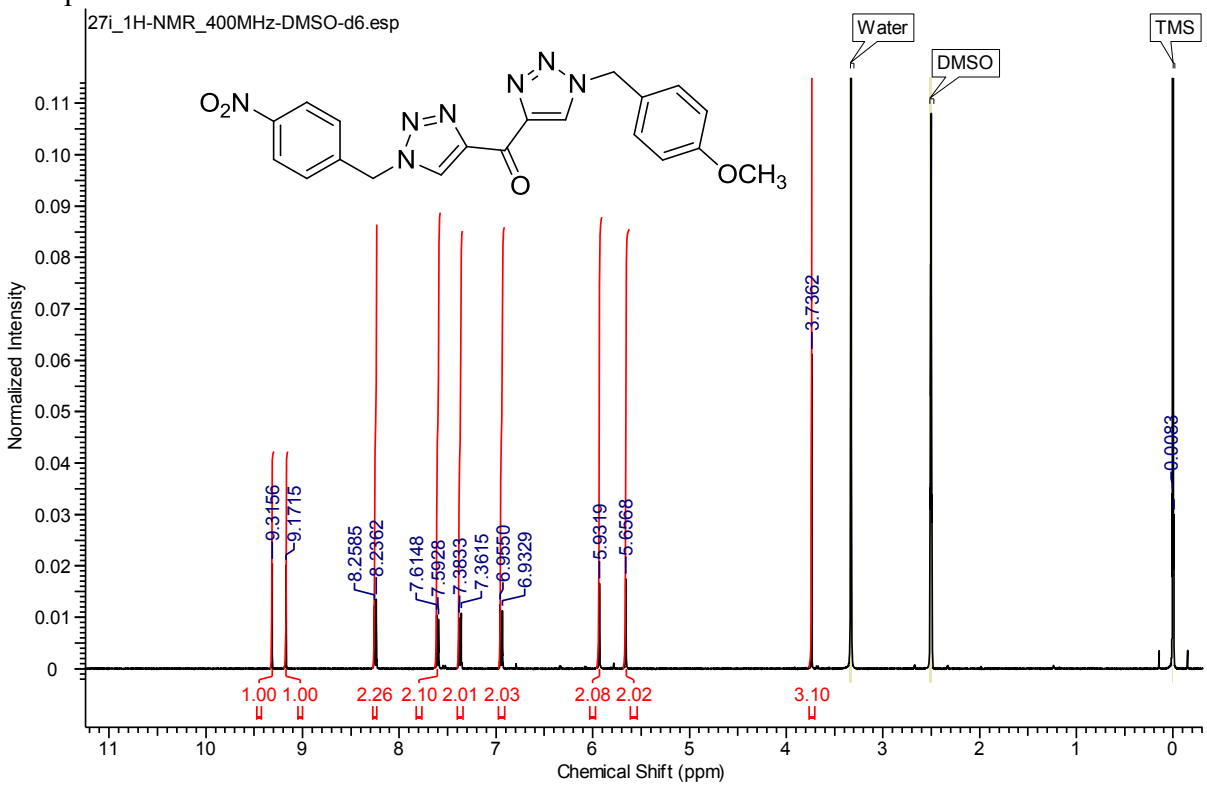

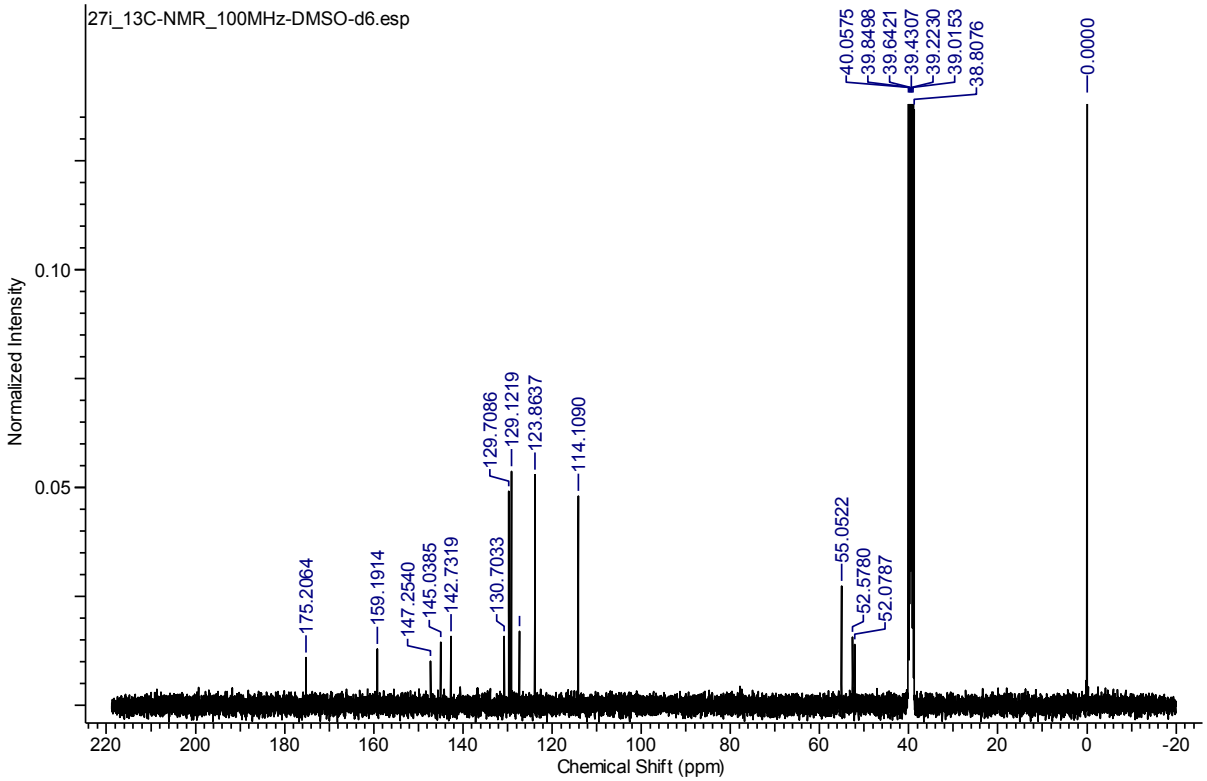

Compound **4.19j**

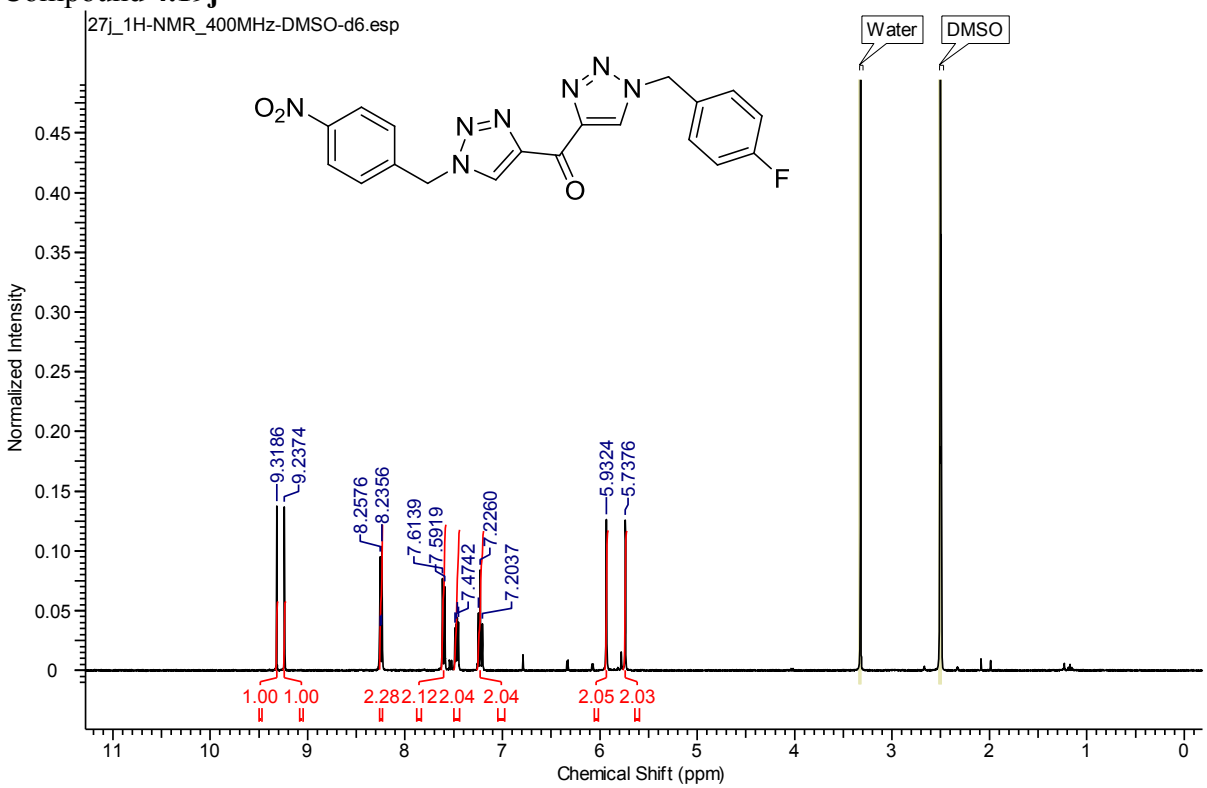

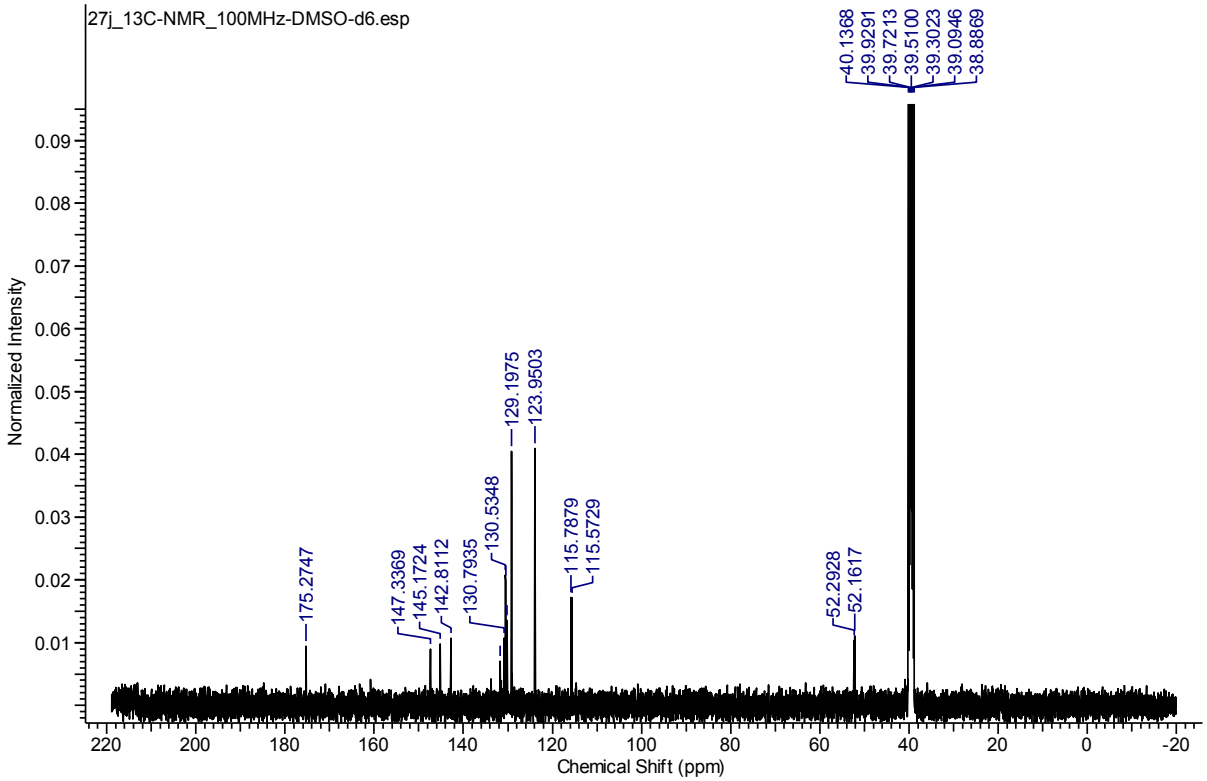

Compound **4.19k**

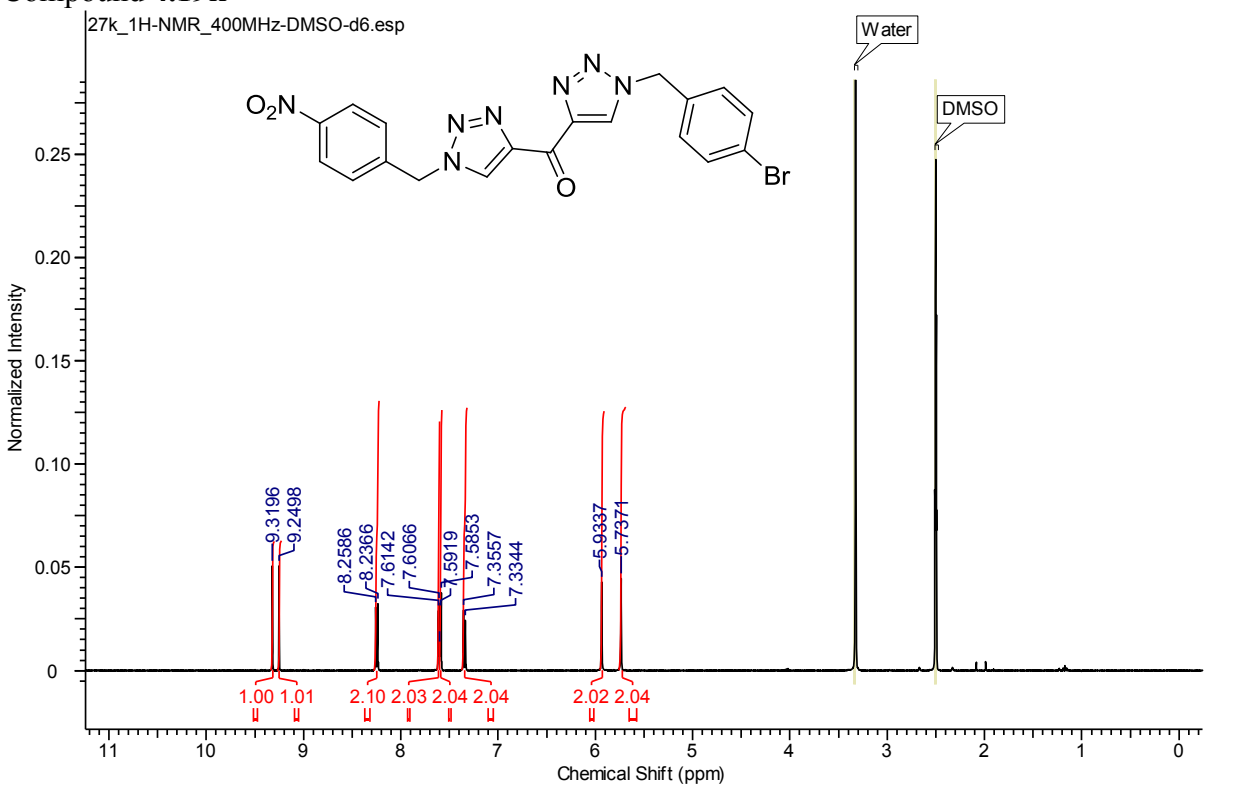

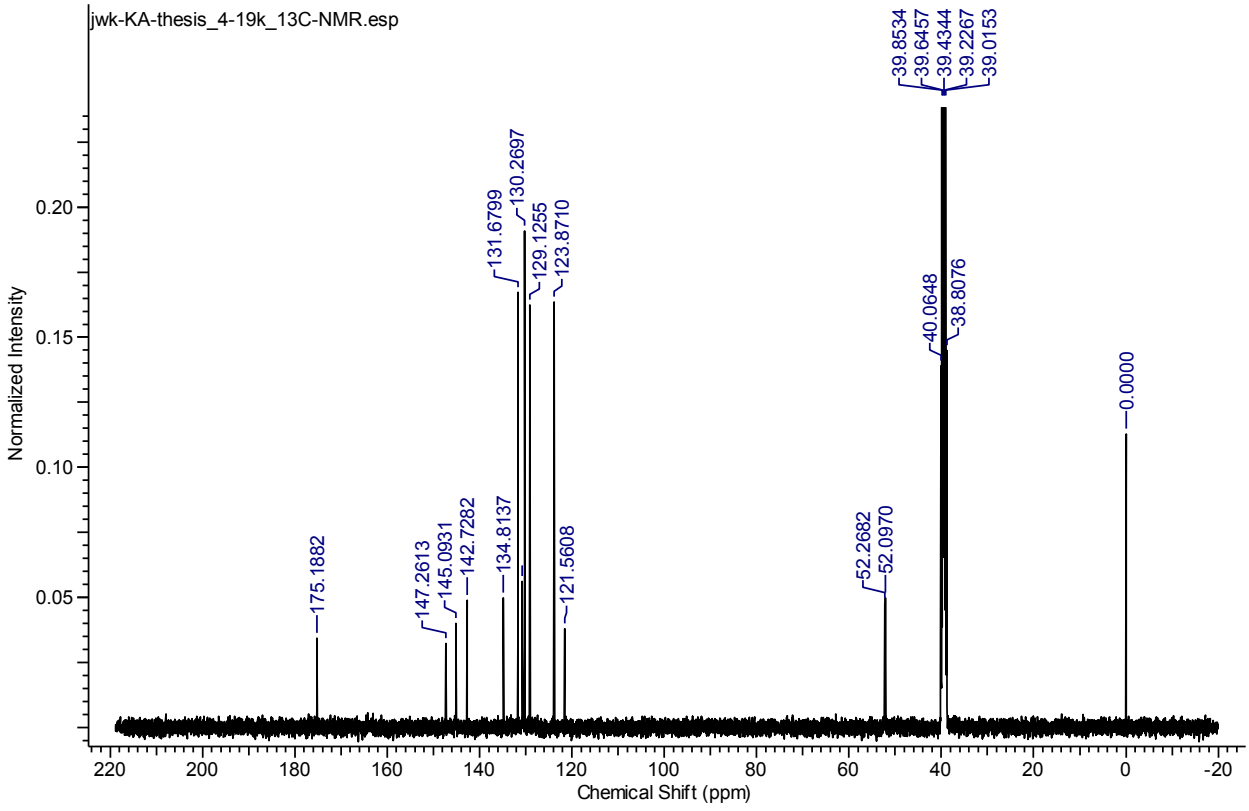

Compound **4.19l**

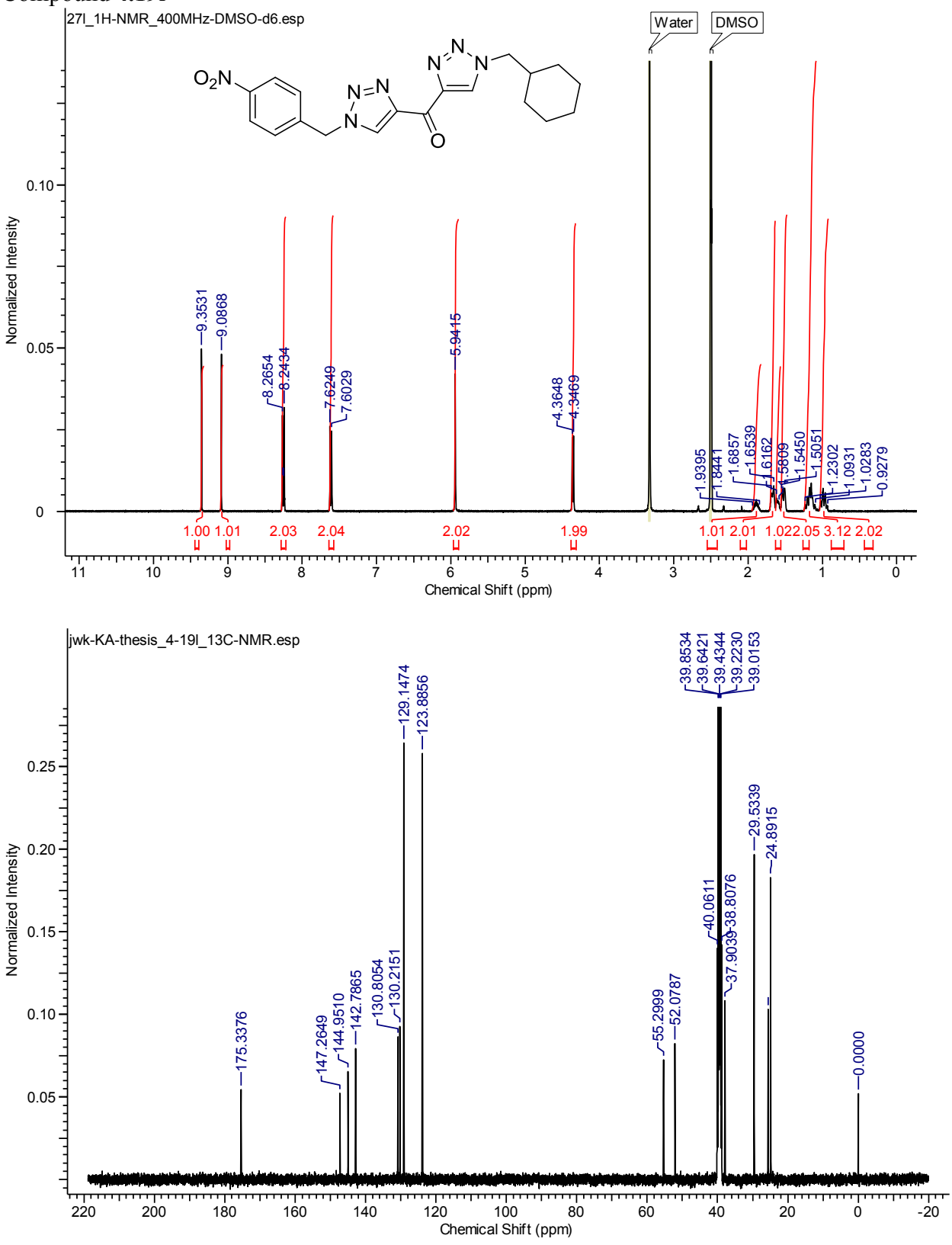

Compound **4.24a**

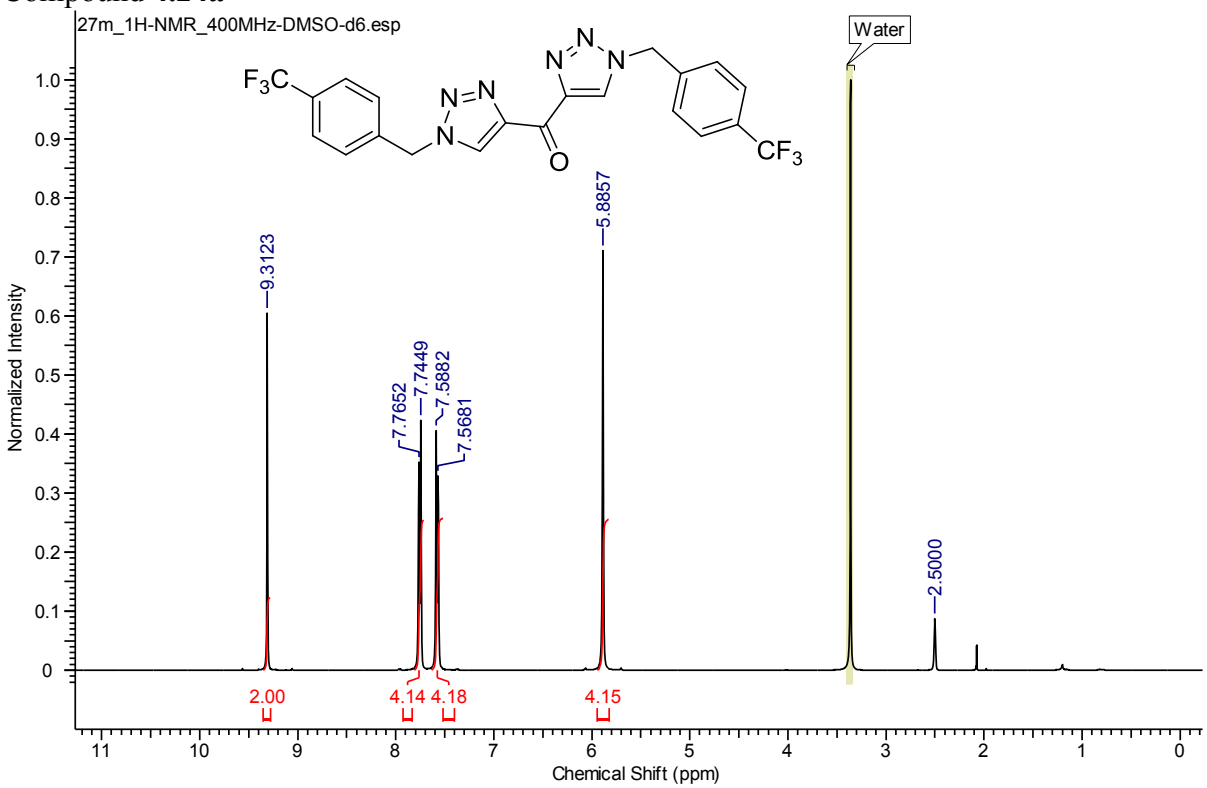

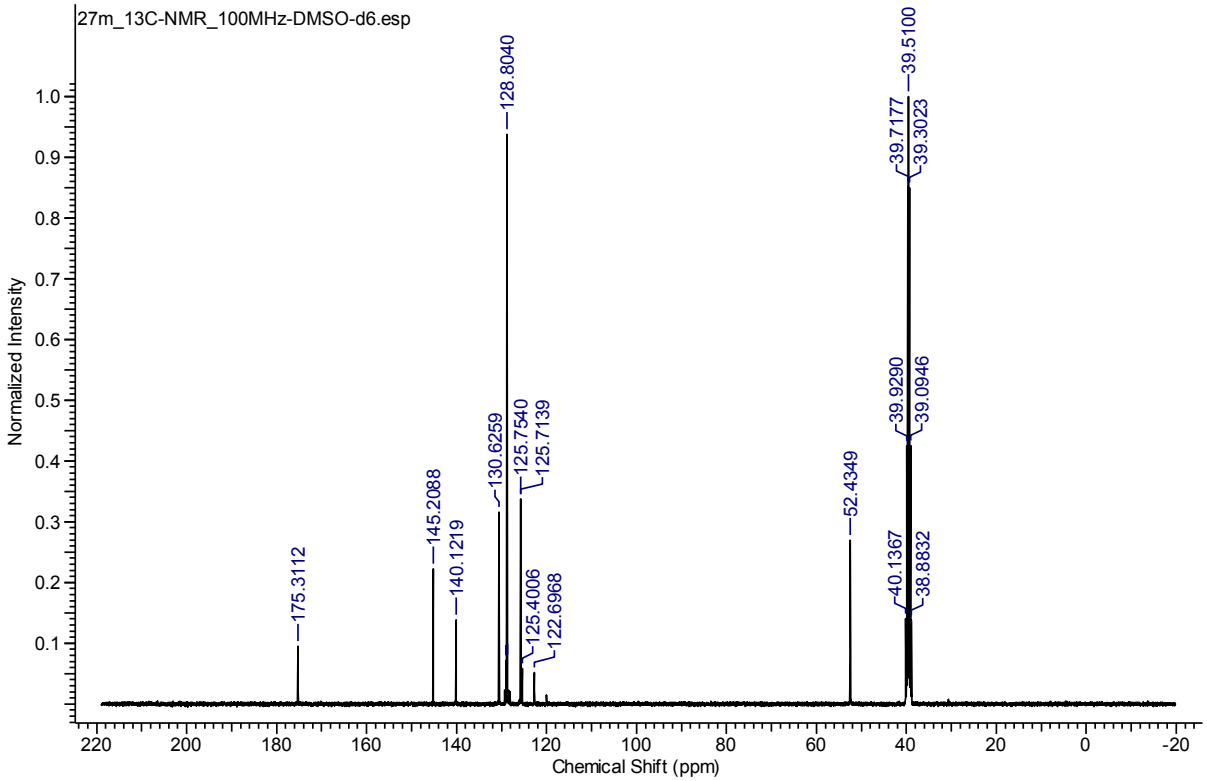

Compound **4.24b**

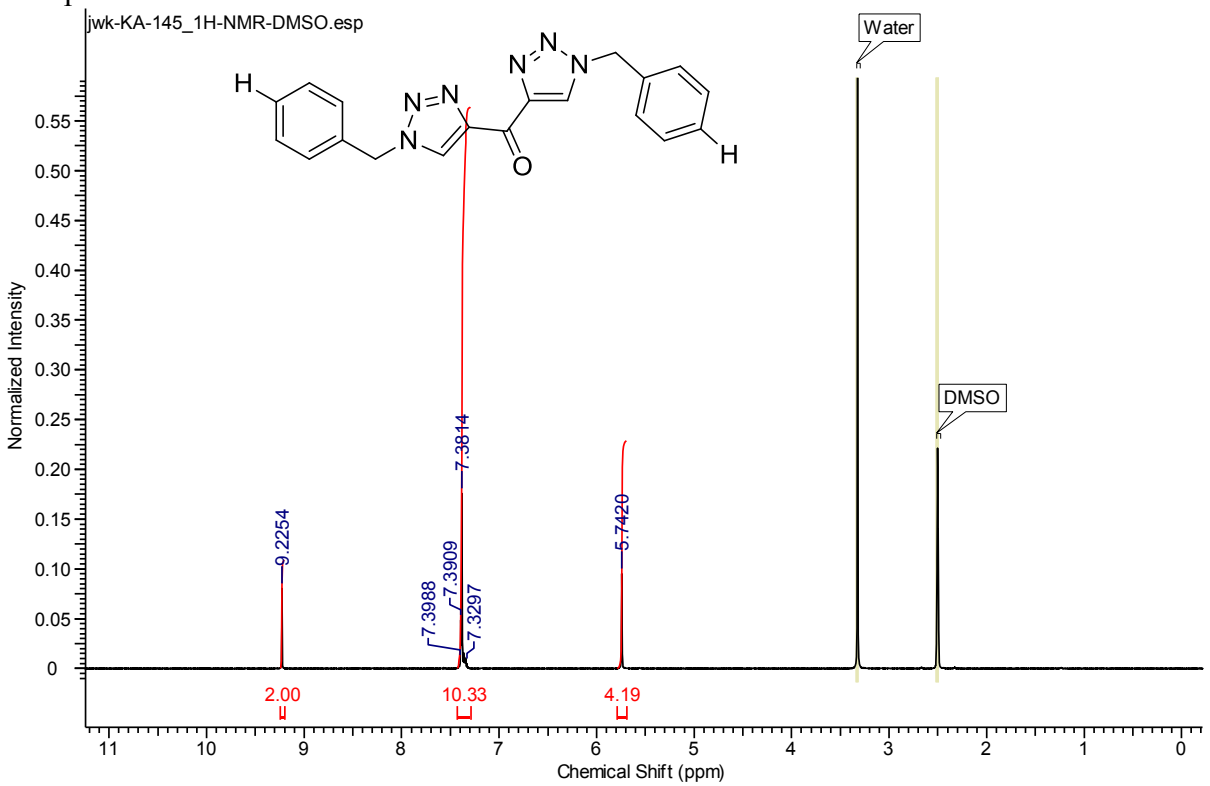

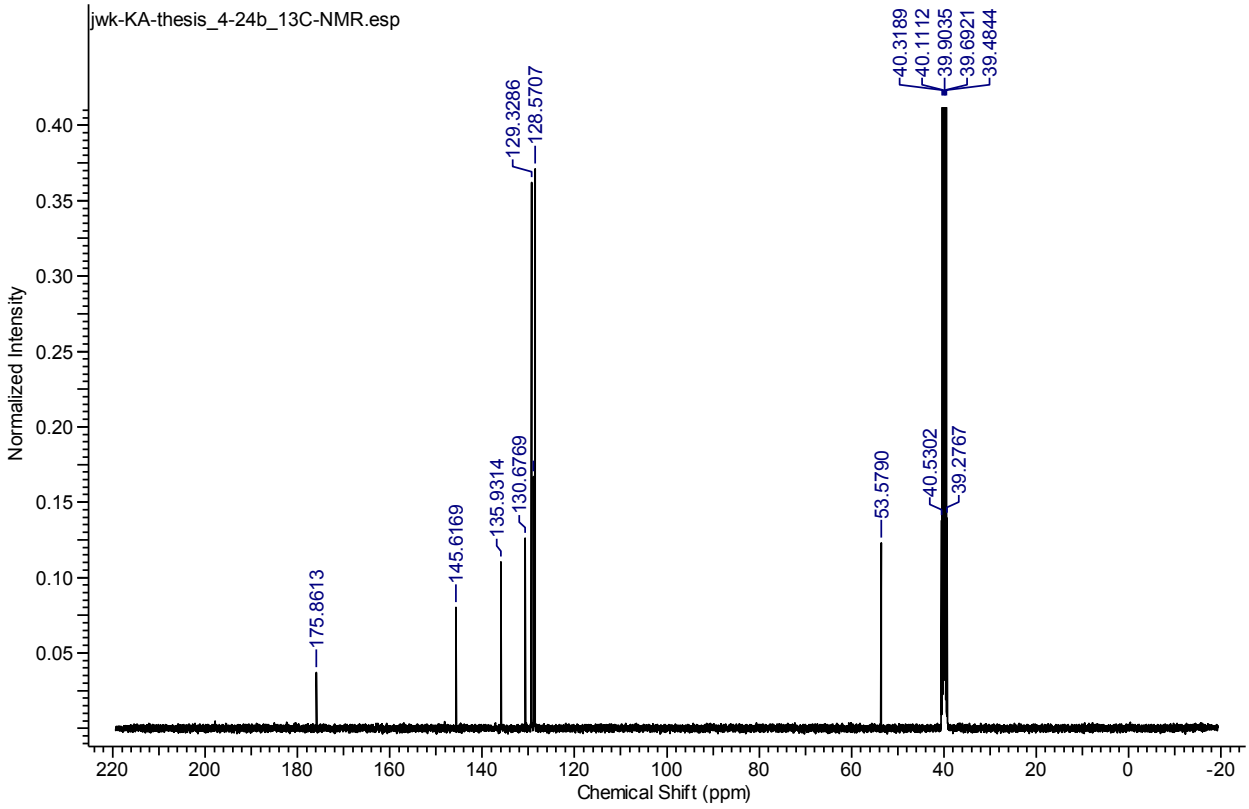

Compound **4.8**

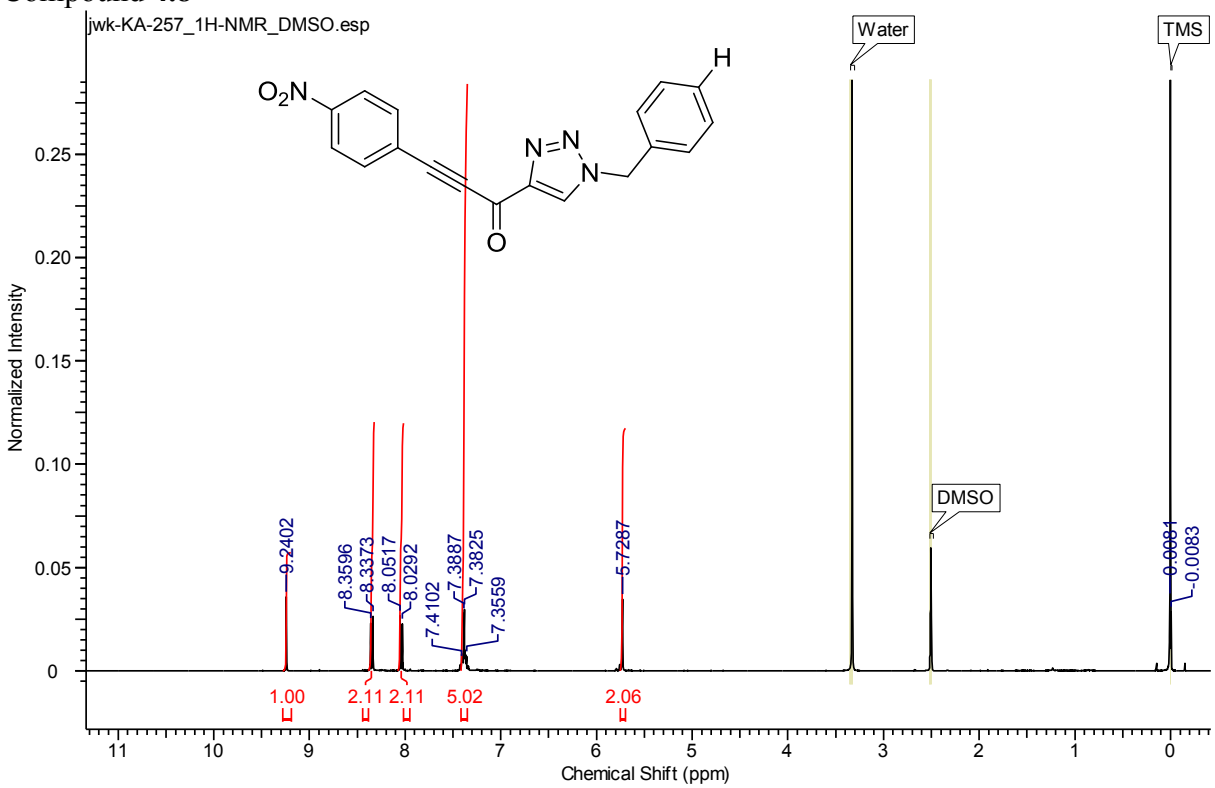
jwk-KA-257_1H-NMR_DMSO.esp
Water
TMS
DMSO
9.2402
8.3596
8.3373
8.0517
8.0292
7.4102
7.3887
7.3825
7.3559
5.7287
0.0084
-0.0083
1.00
2.11
2.11
5.02
2.06
Normalized Intensity
Chemical Shift (ppm)

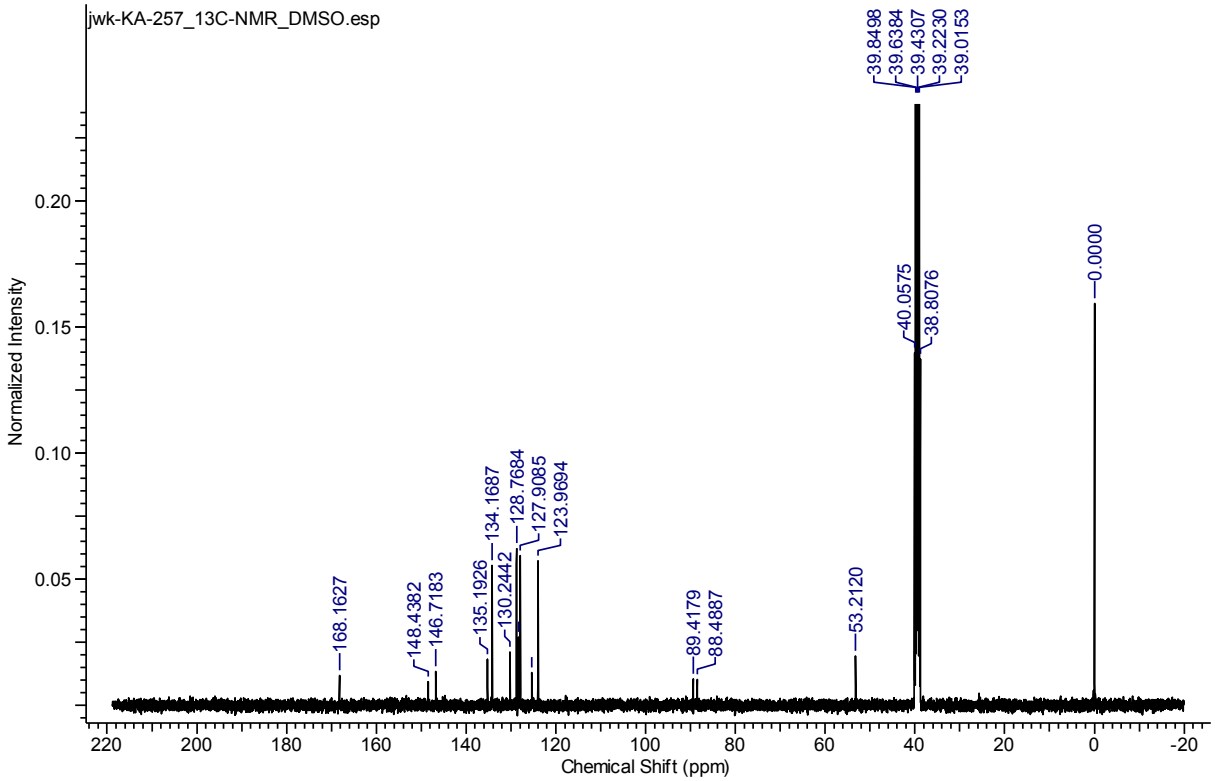
jwk-KA-257_13C-NMR_DMSO.esp
39.8498
39.6384
39.4307
39.2230
39.0153
40.0575
38.8076
0.0000
168.1627
148.4382
146.7183
135.1926
134.1687
130.2442
128.7684
127.9085
123.9694
89.4179
88.4887
53.2120
Normalized Intensity
Chemical Shift (ppm)

Compound **4.9**

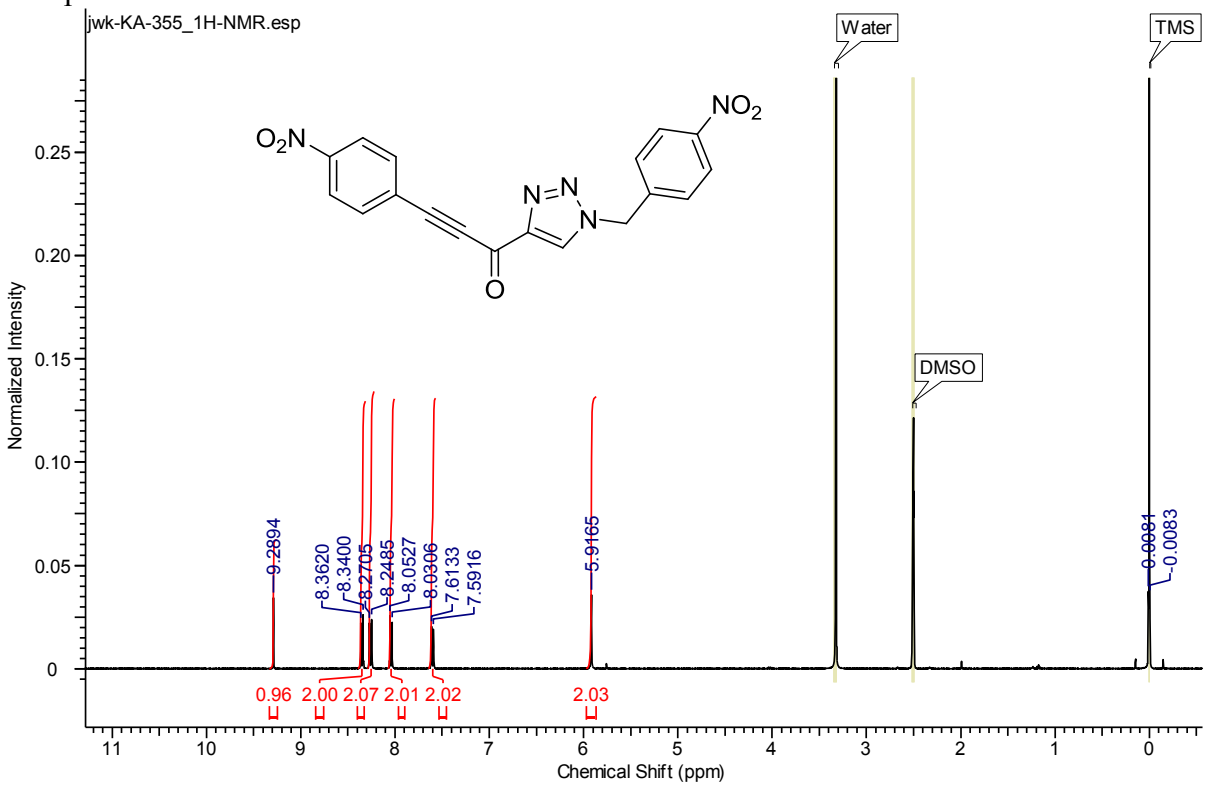
jwk-KA-355_1H-NMR.esp
Water
TMS
DMSO
O_2N
NO_2
N=N
N
O
9.2894
8.3620
8.3400
8.2705
8.2485
8.0527
8.0306
7.6133
7.5916
5.9165
0.0081
-0.0083
0.96
2.00
2.07
2.01
2.02
2.03
Normalized Intensity
Chemical Shift (ppm)

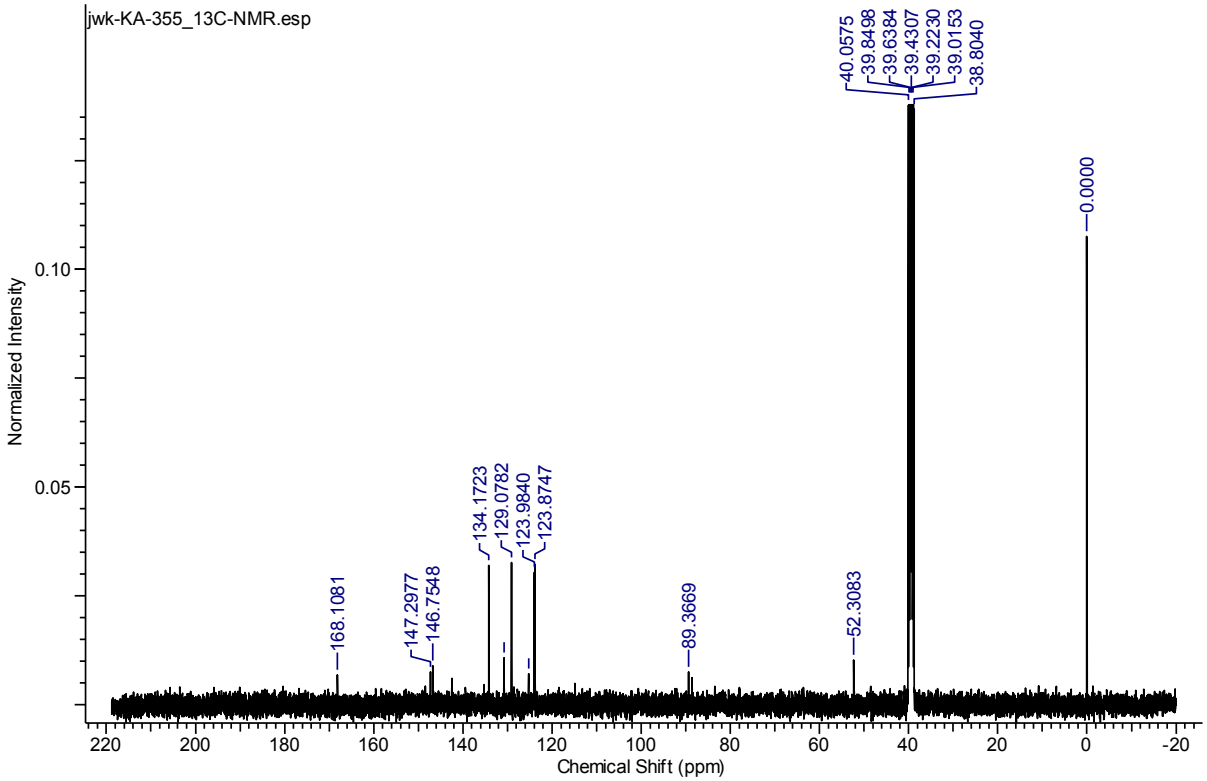
jwk-KA-355_13C-NMR.esp
40.0575
39.8498
39.6384
39.4307
39.2230
39.0153
38.8040
0.0000
168.1081
147.2977
146.7548
134.1723
129.0782
123.9840
123.8747
89.3669
52.3083
Normalized Intensity
Chemical Shift (ppm)

NOESY – Compound **4.9**

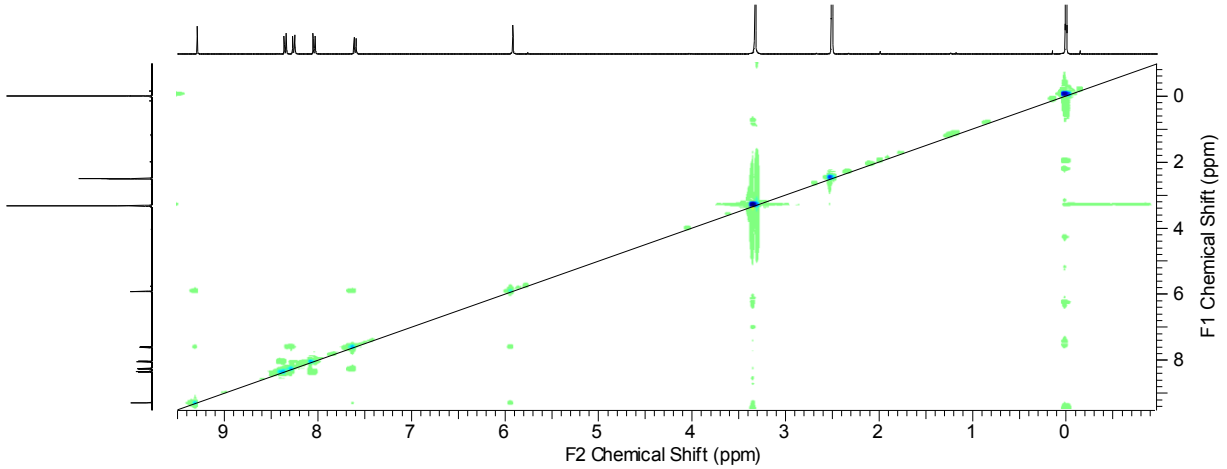

Compound **5.13a**

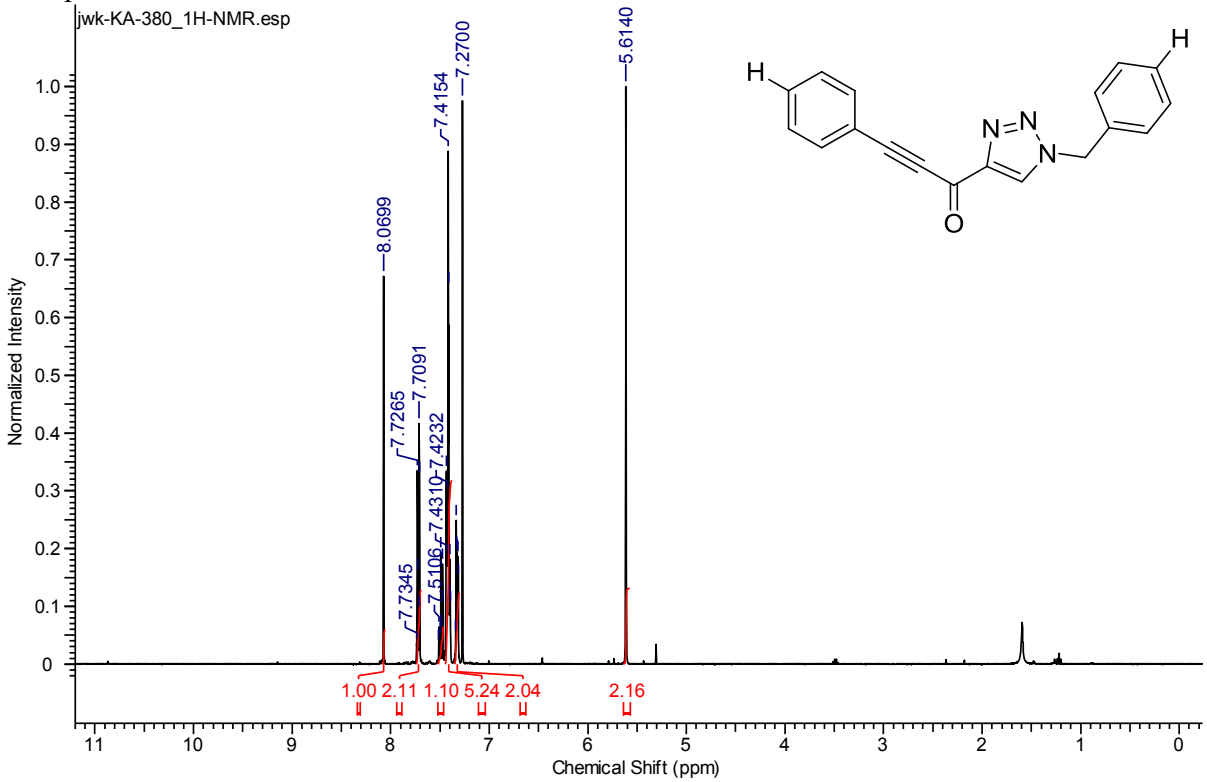

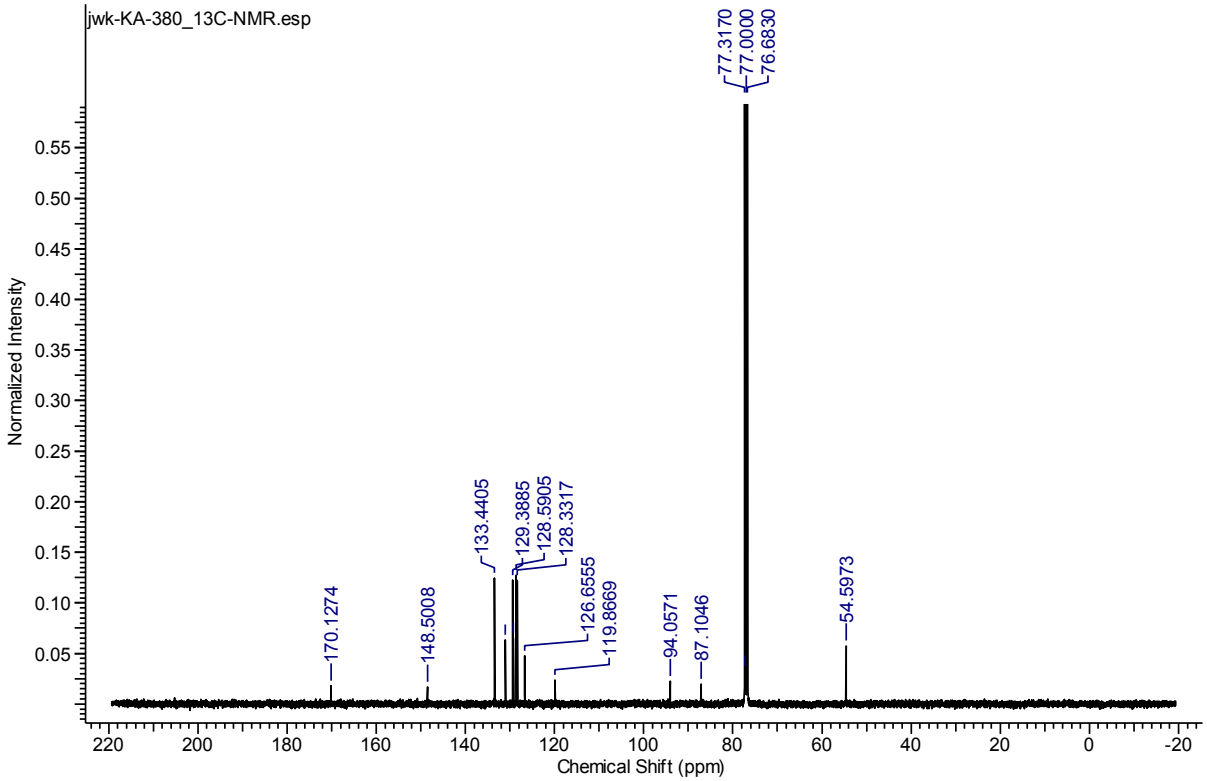

Compound **5.14a**

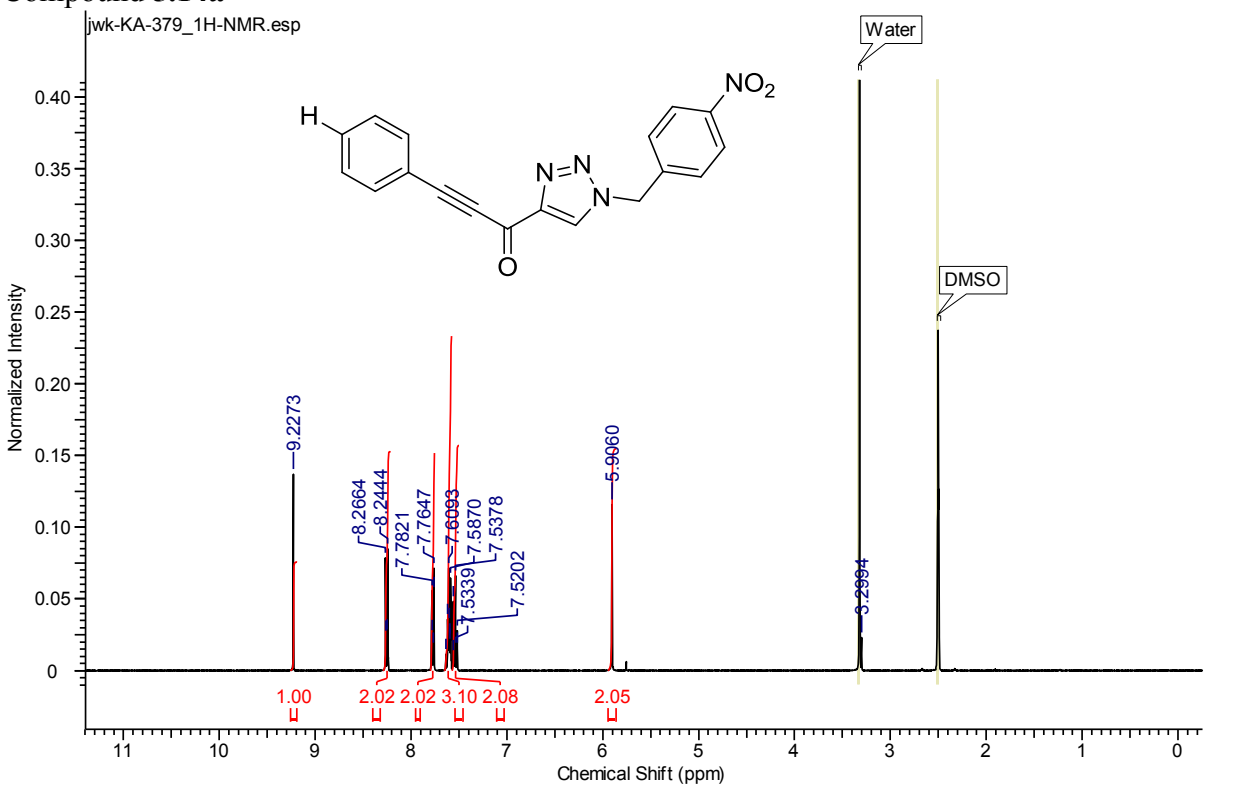

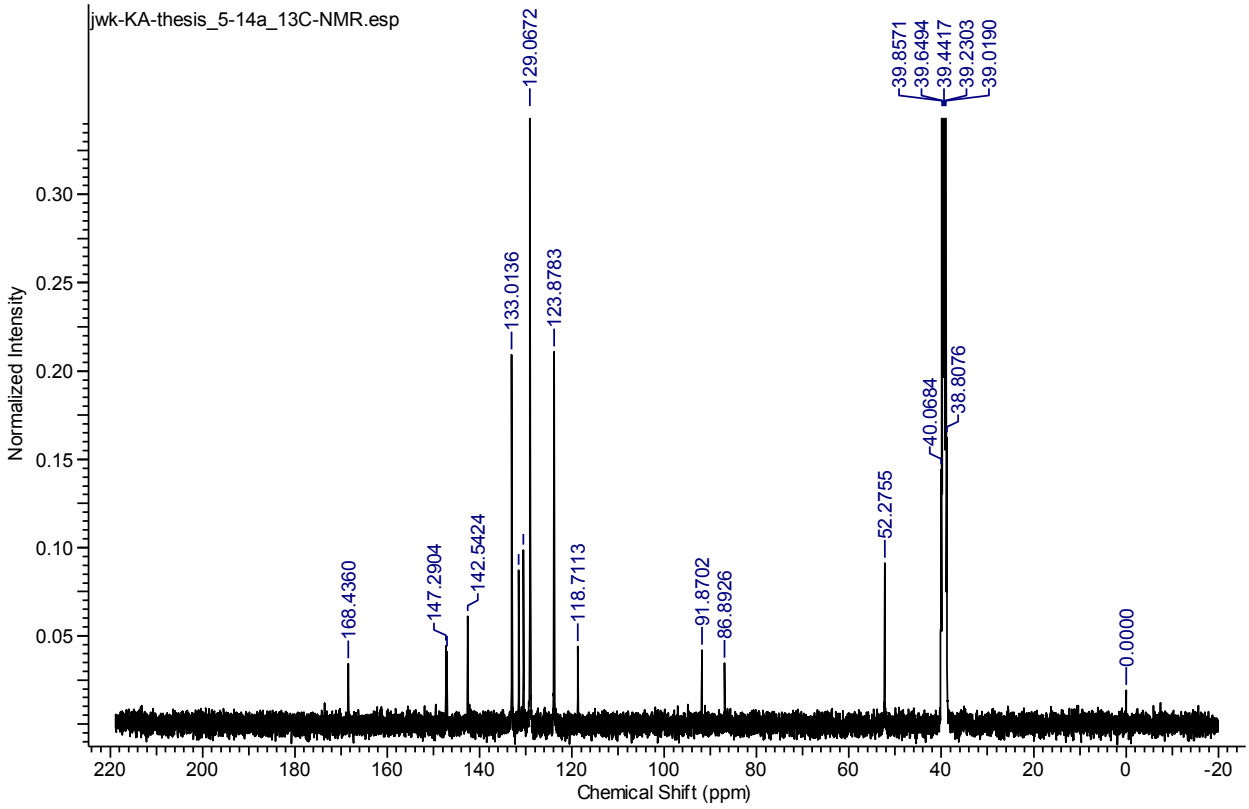

Compound **5.16**

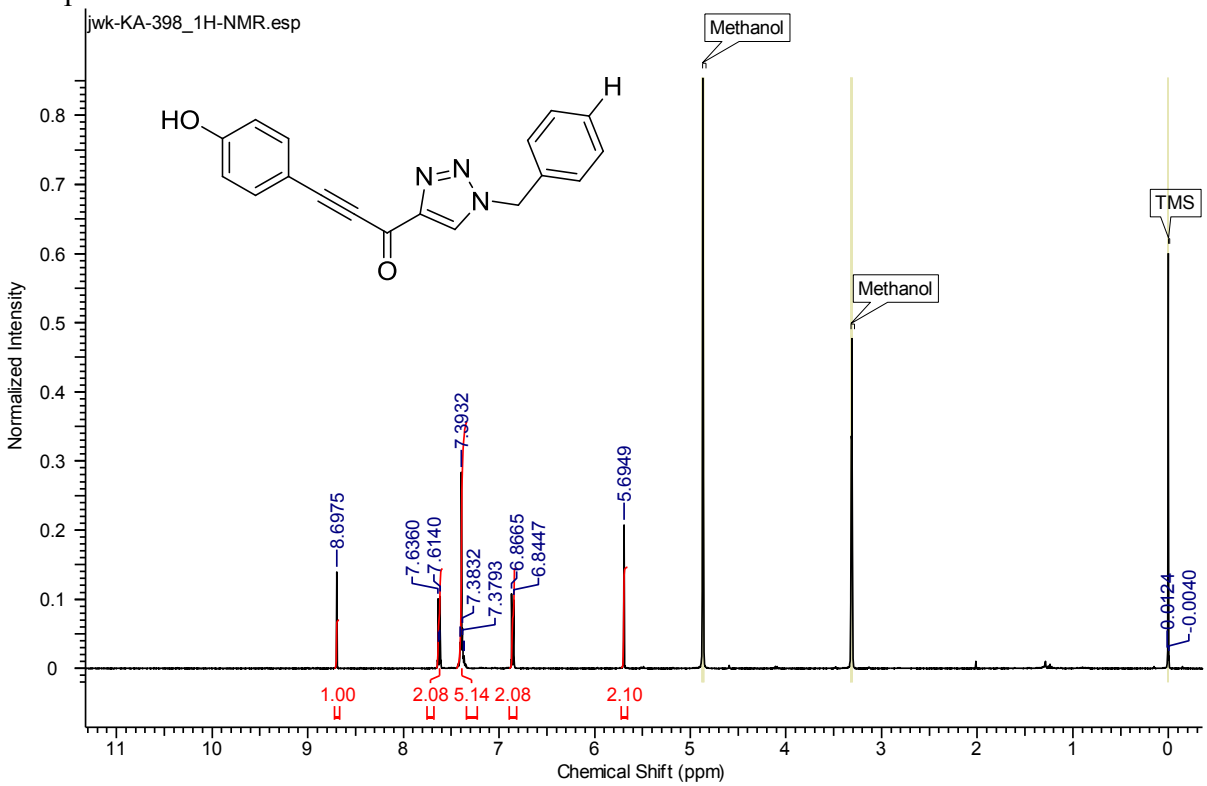

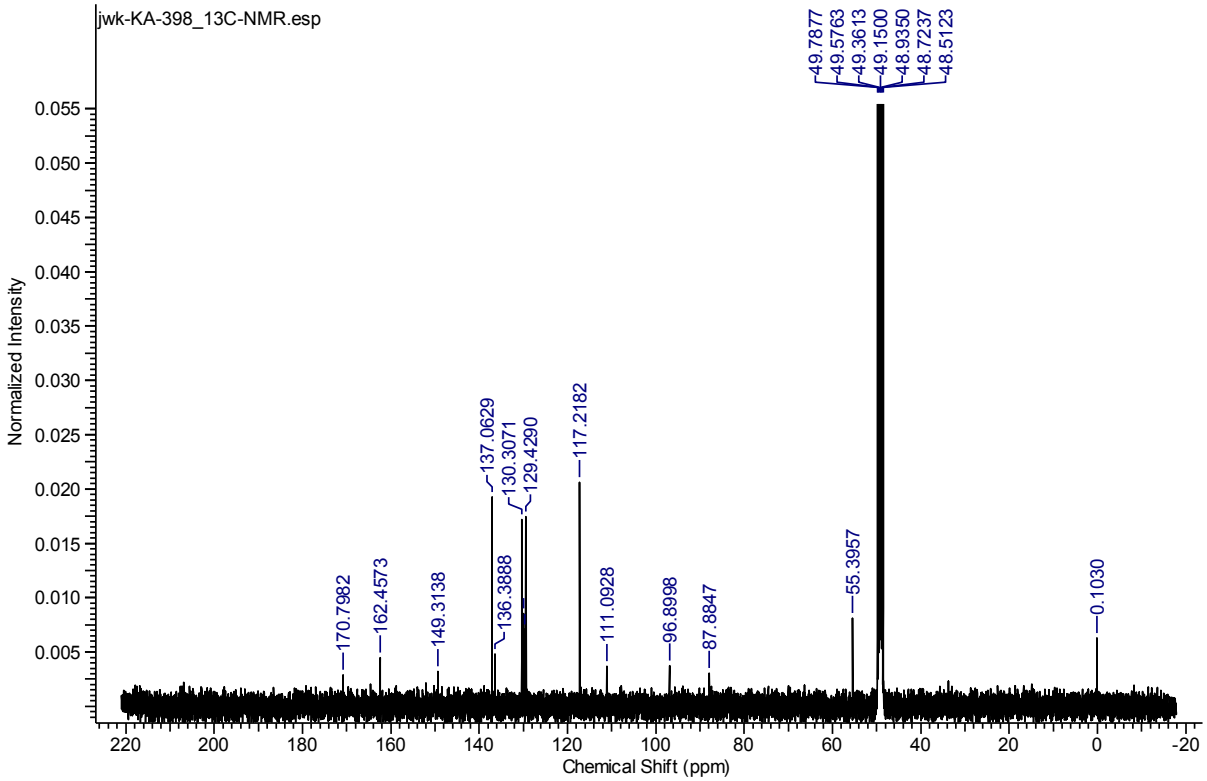

Compound **5.17**

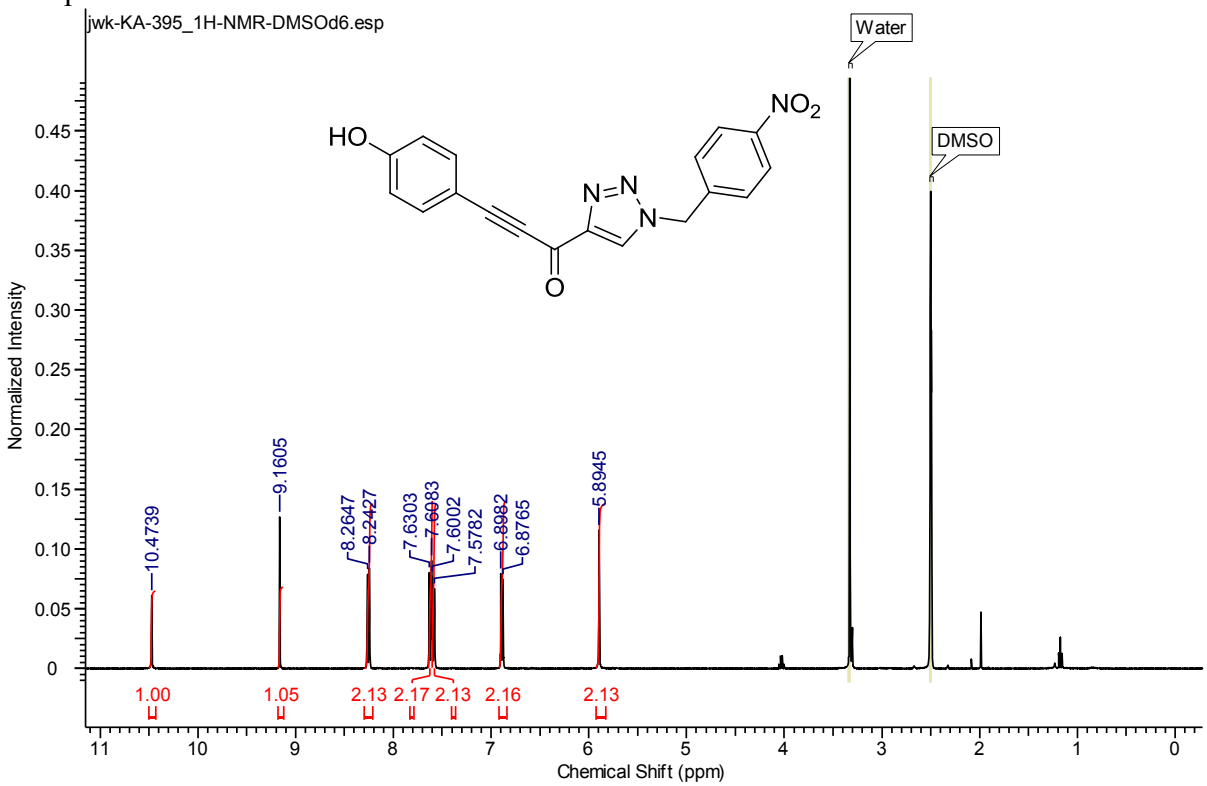

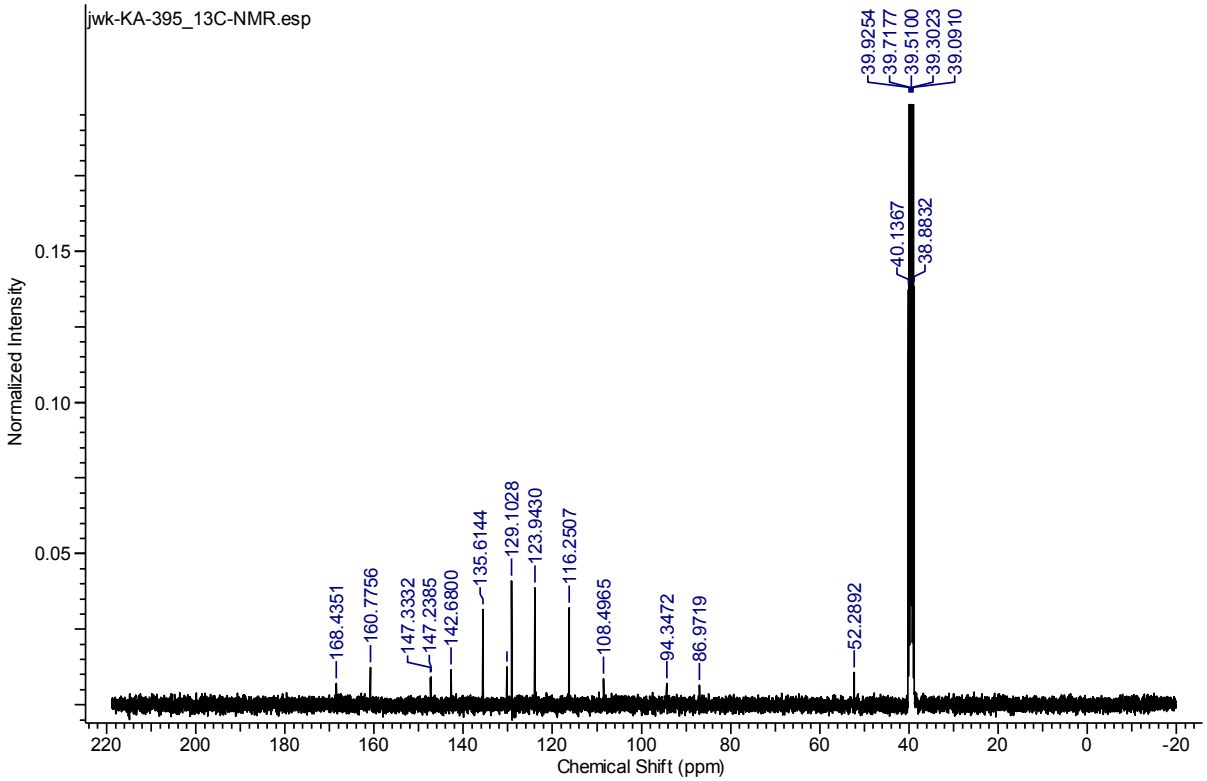

Compound **5.13d**

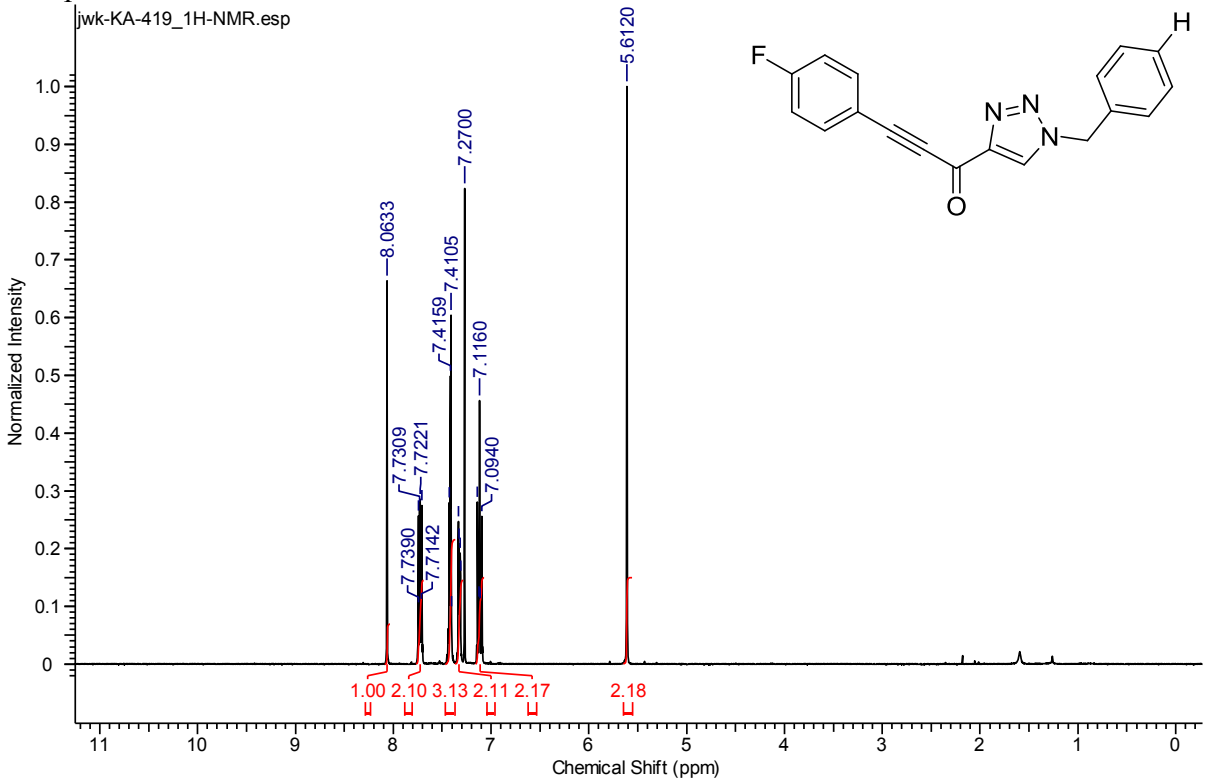

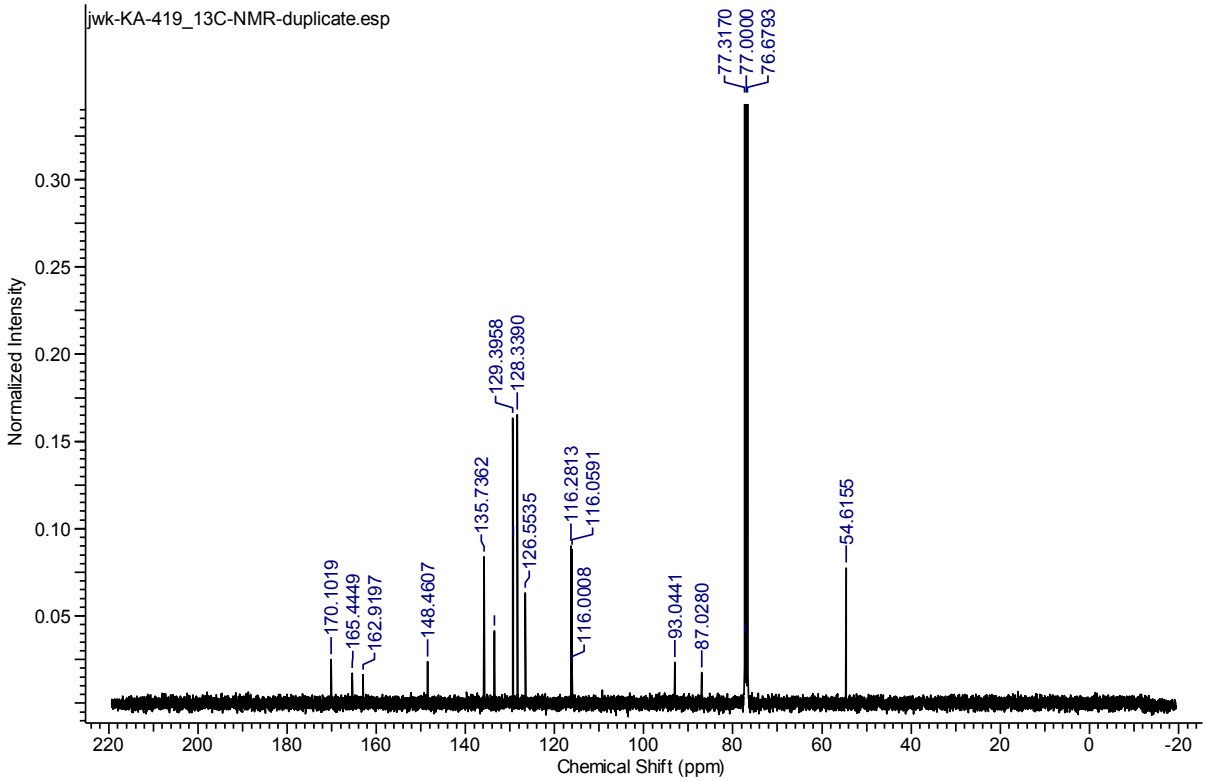

Compound **5.14d**

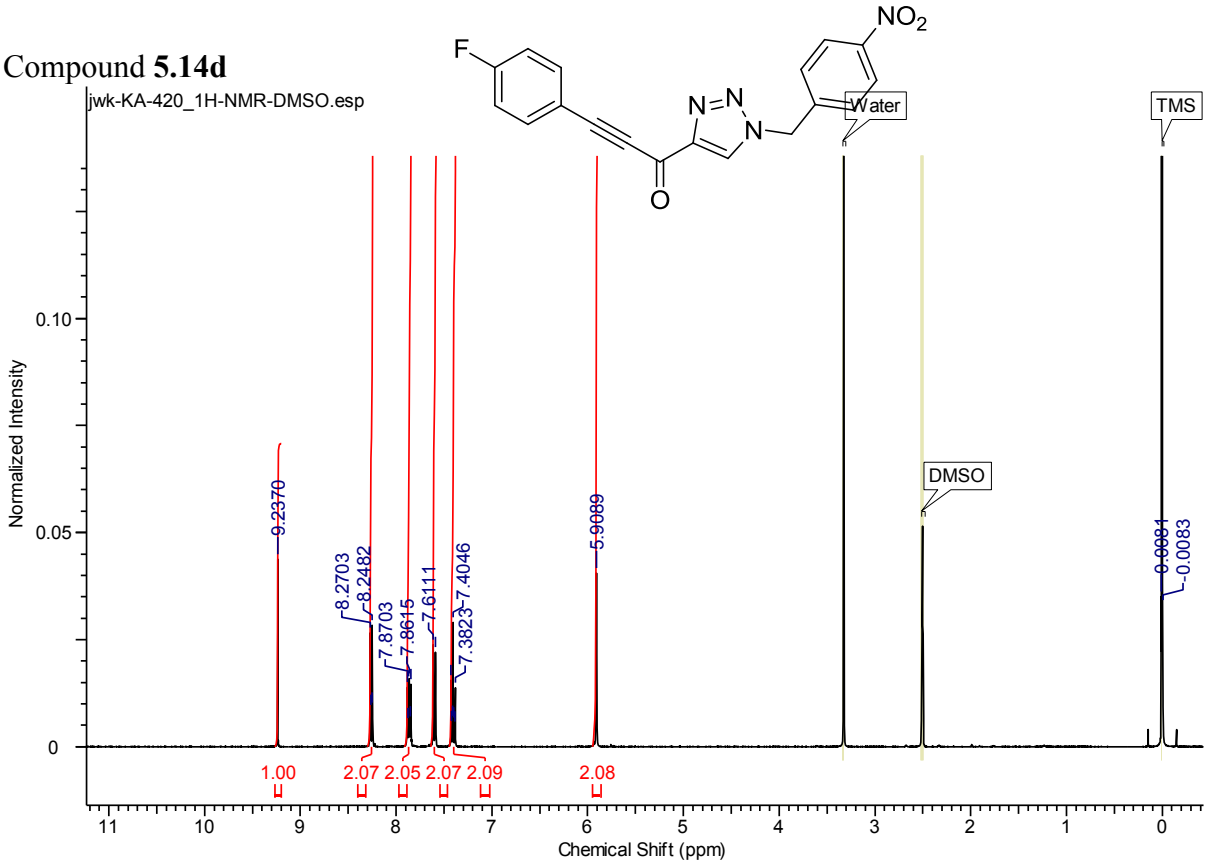

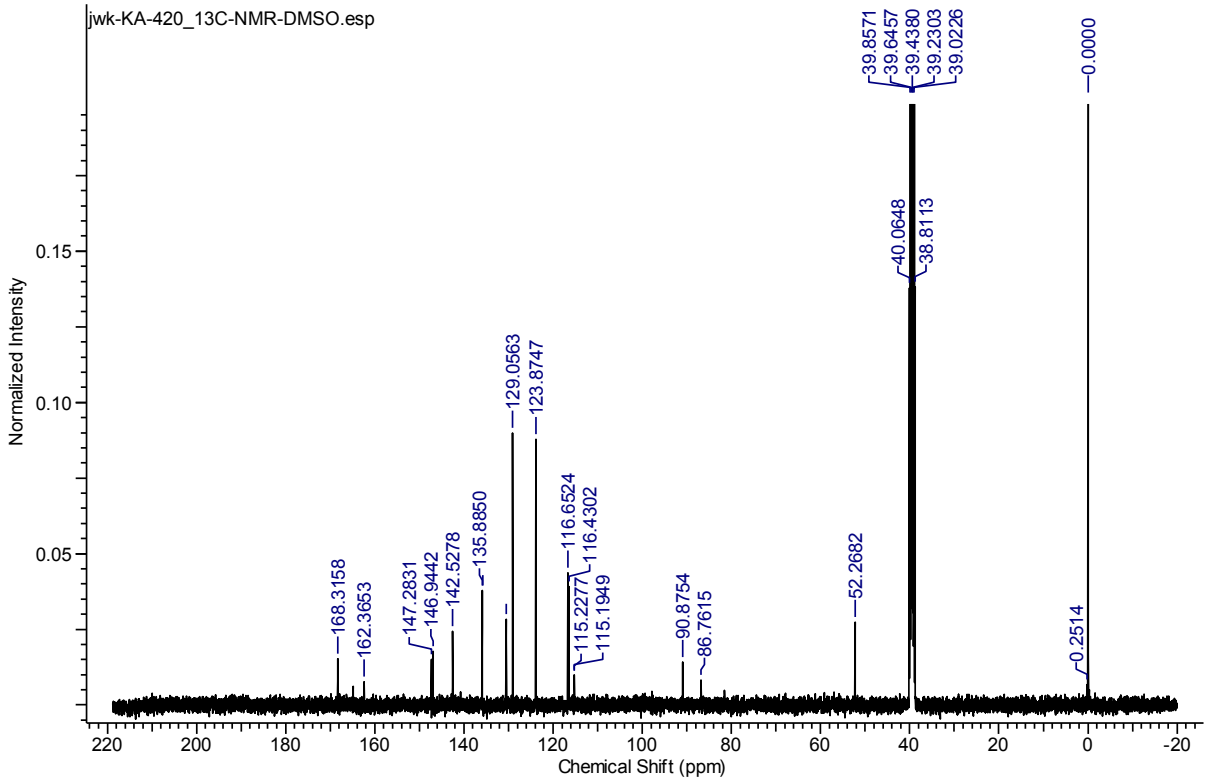

Compound **5.13e**

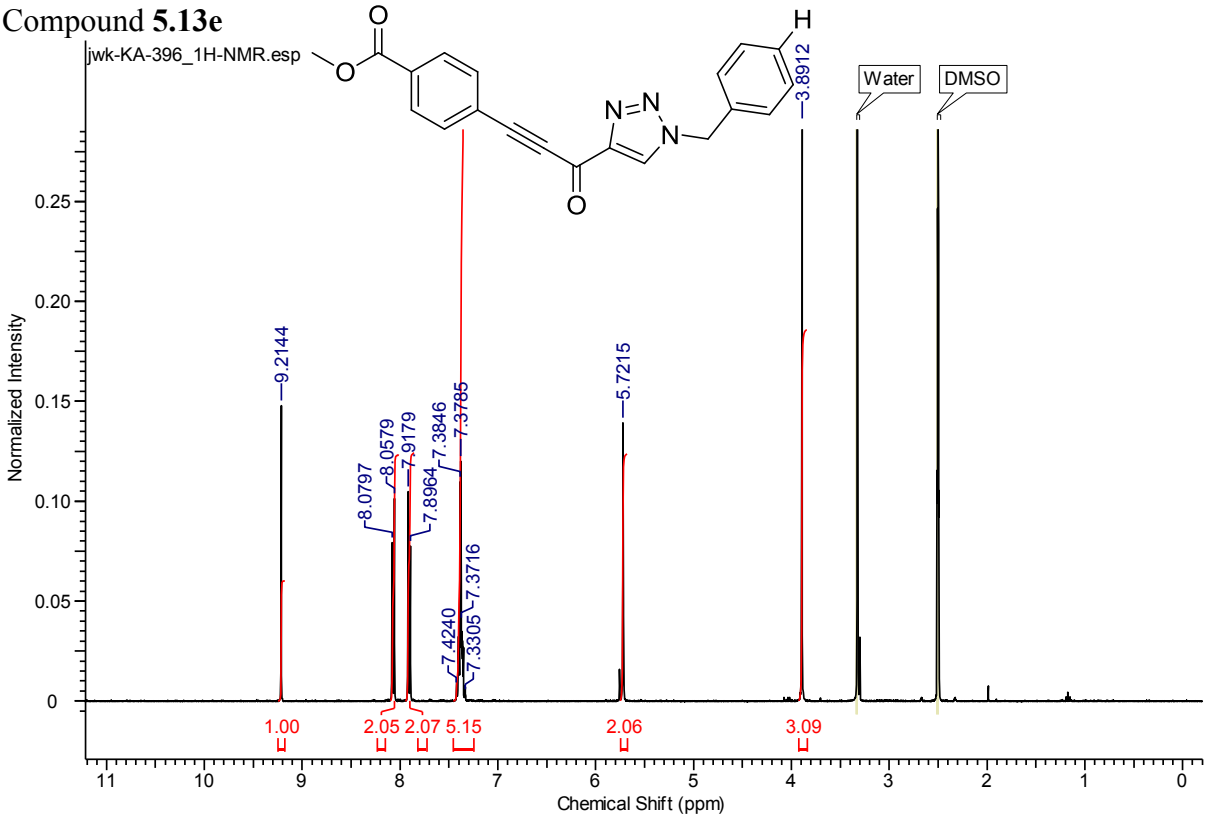

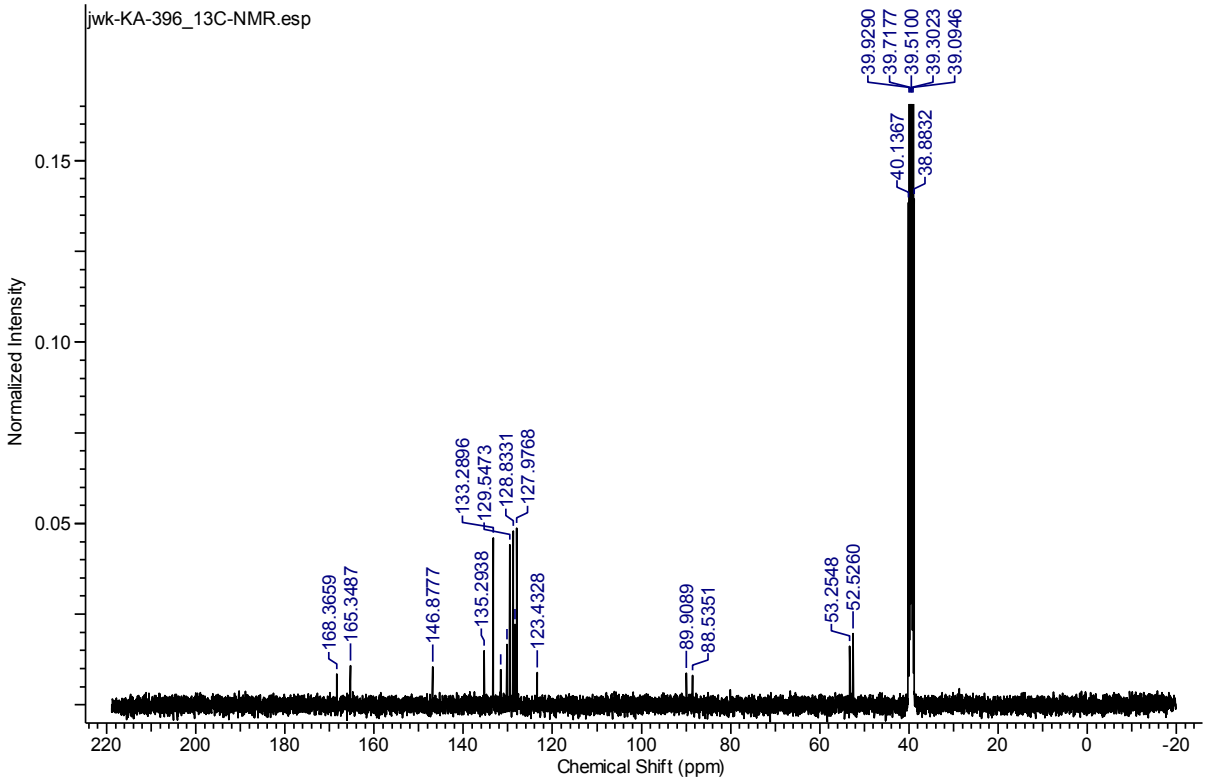

Compound **5.14e**

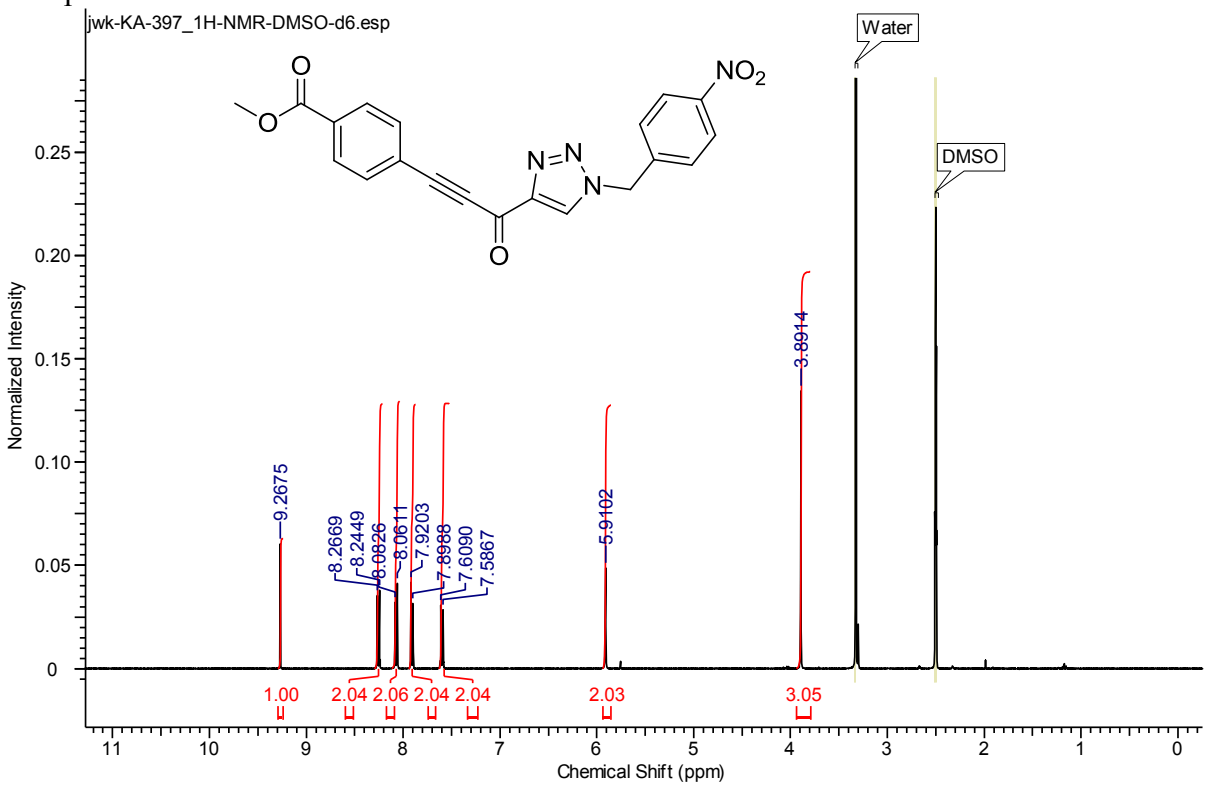

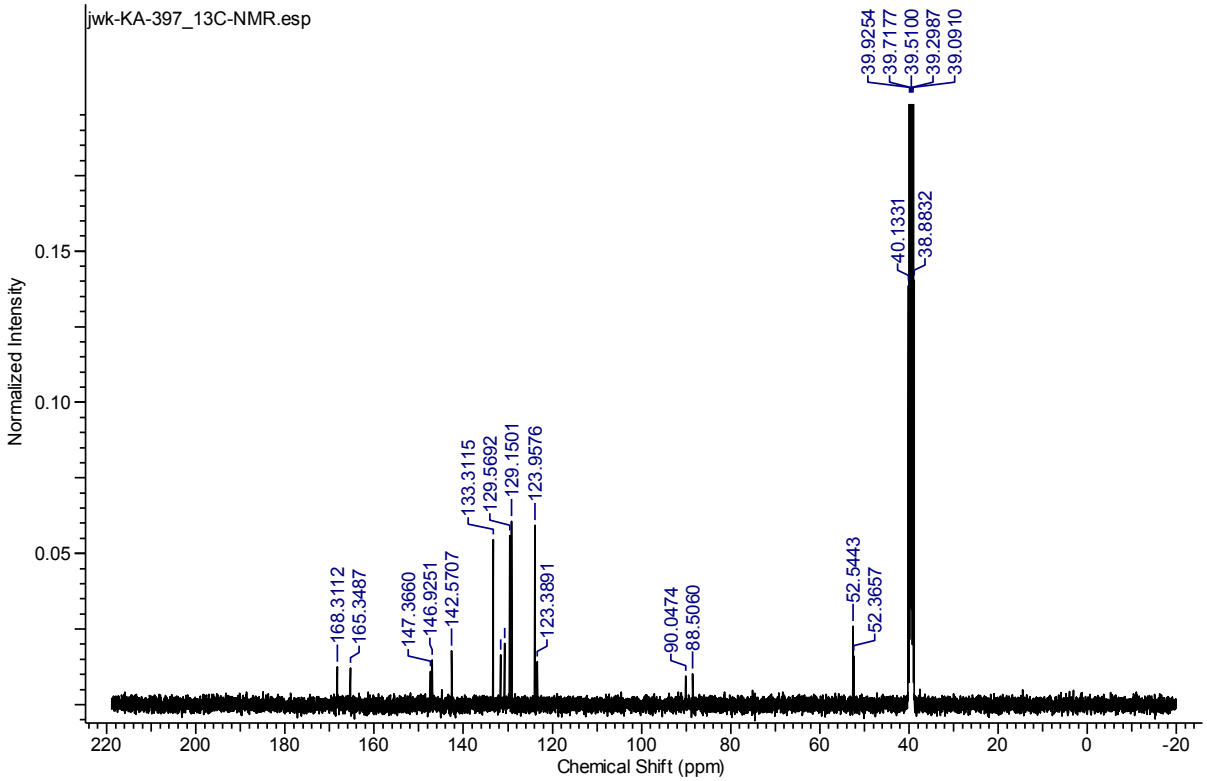

Compound **5.13f**

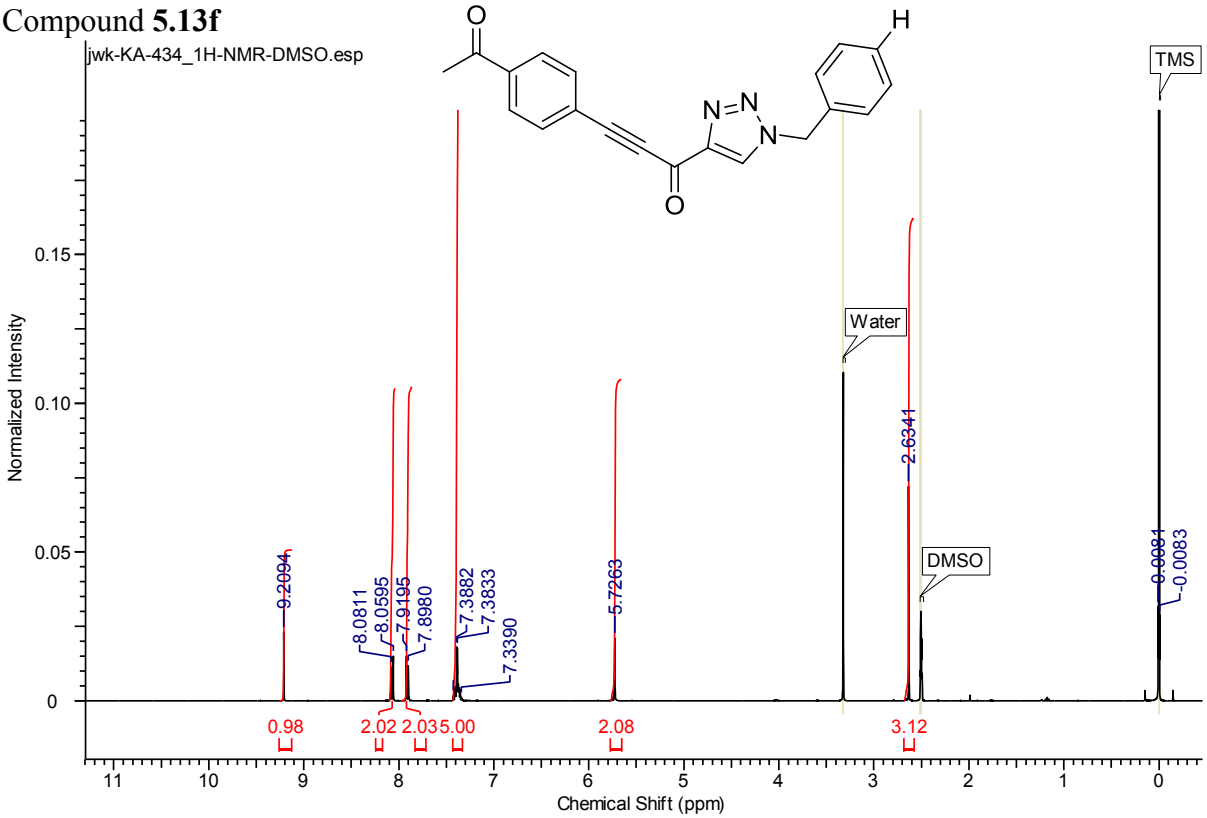

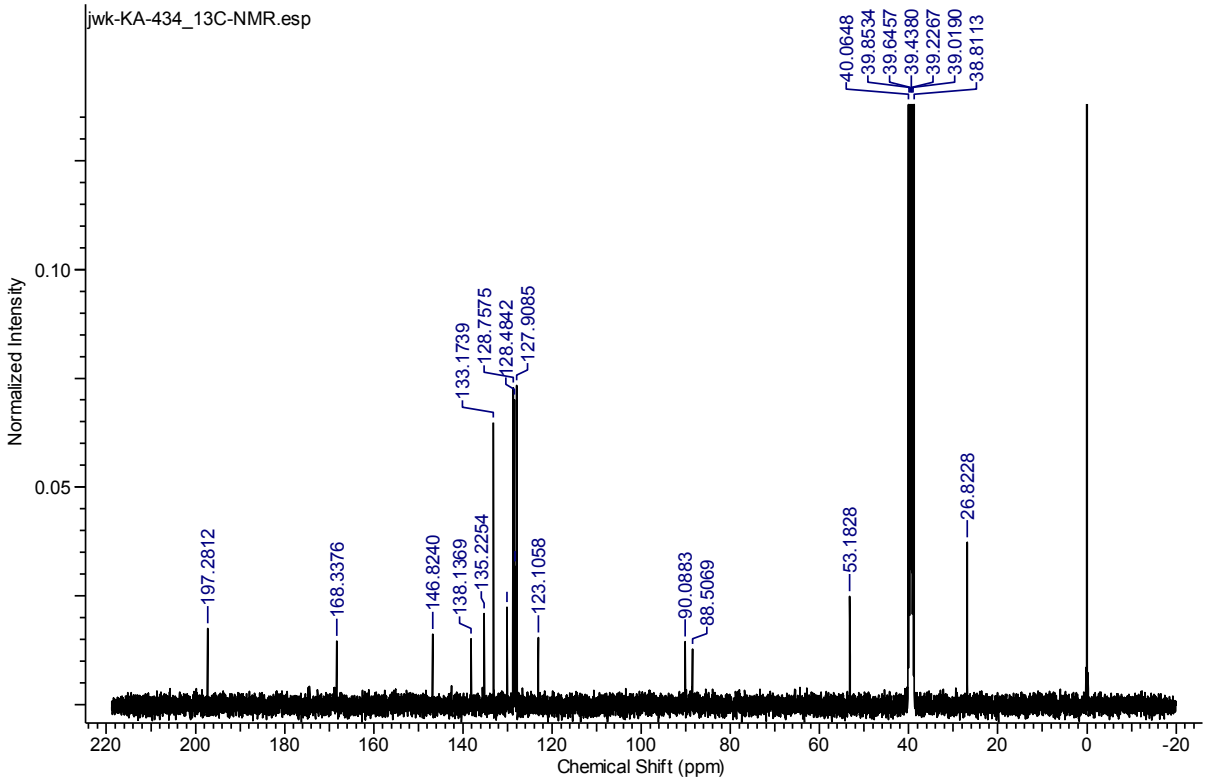

Compound **5.14f**

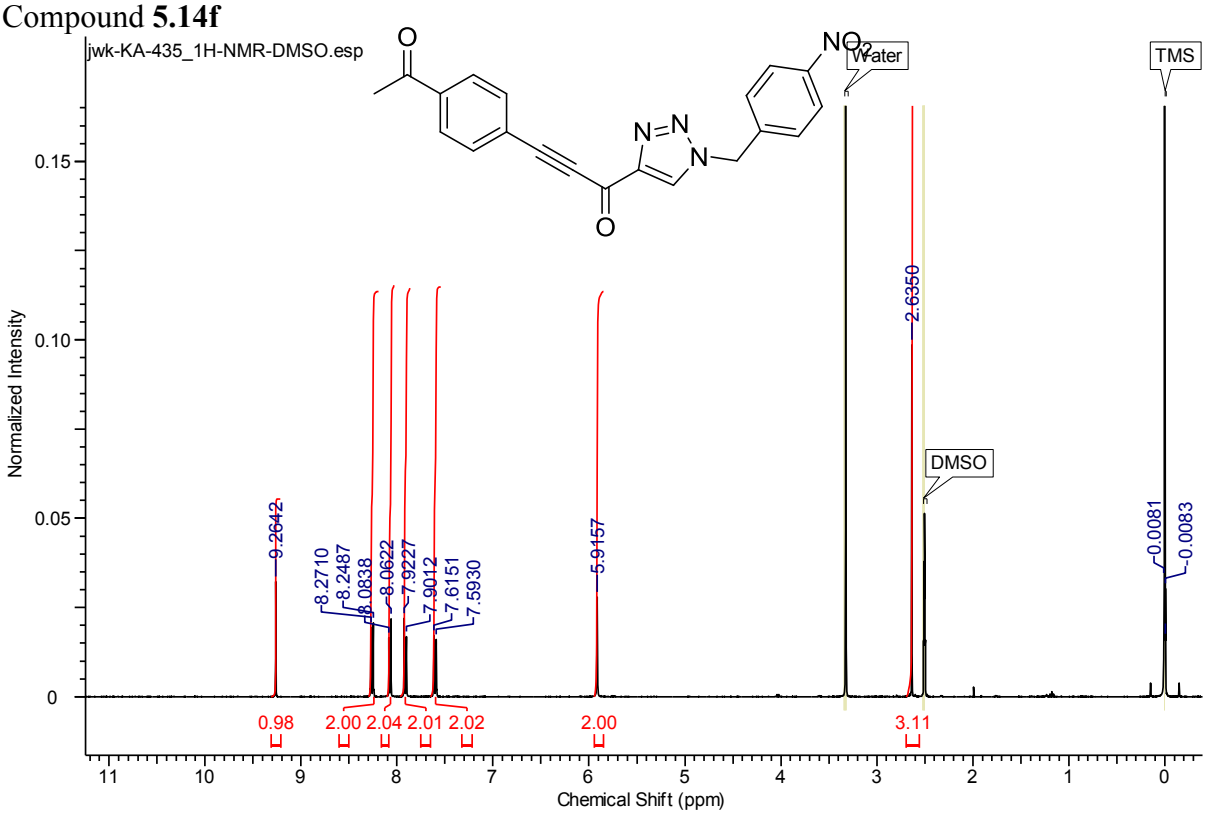

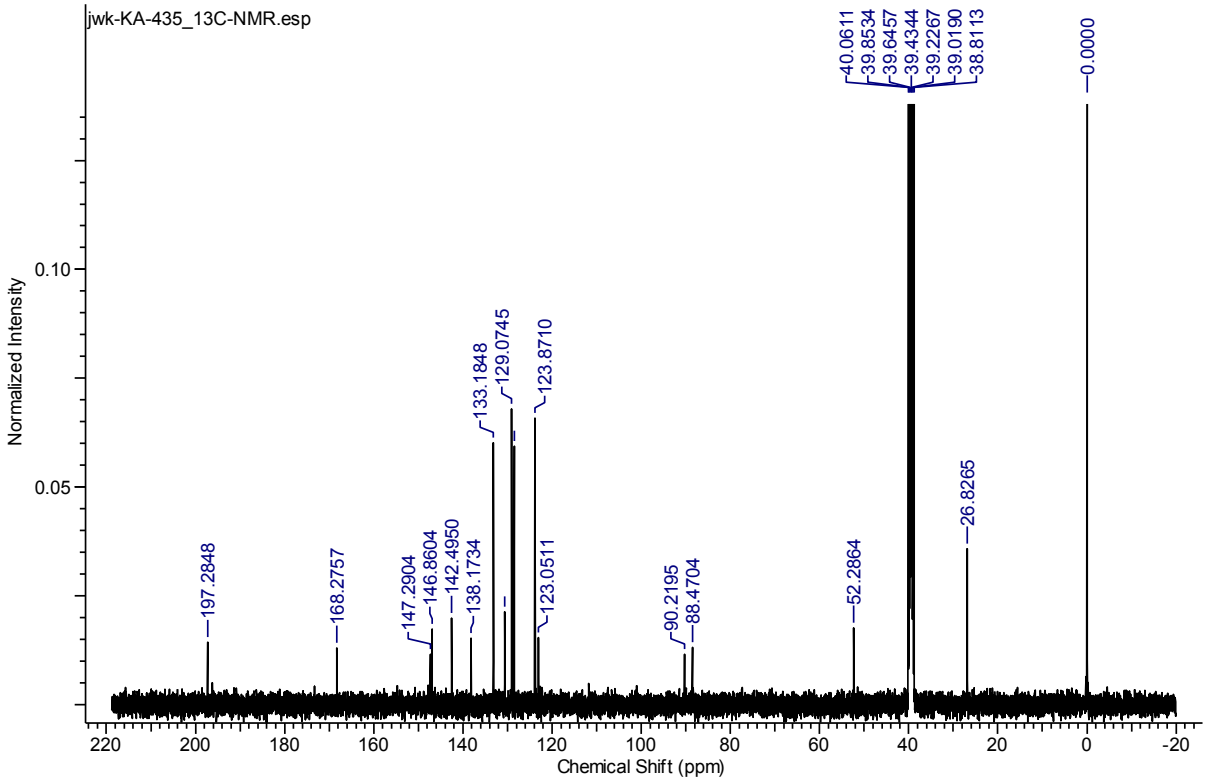

Comment on inhibitor **4.9**

Following the work presented in this thesis, the slow-binding character of compound **4.9** (known as **KA22b**) was investigated further. In a dilution experiment, where the enzyme was incubated in buffer with the inhibitor for fifteen minutes prior to 100-fold dilution into buffer containing **AL5** substrate, we observed less than 10% activity remaining, when compared to a positive control having been incubated with vehicle only. No activity recovery was observed over a 60-minute assay, suggesting that the compound was not dissociating from the enzyme. In a dialysis experiment, where the enzyme and inhibitor solution was dialysed into cleavage buffer overnight after a 15-minute incubation period, we again saw no recovery of activity, suggesting an irreversible reaction between the inhibitor and the enzyme, unlike compound **CP4d**, which was verified to be reversible.

In evaluating compound **4.9** as an irreversible inhibitor under Kitz and Wilson conditions, we determined kinetic parameters of k_{inact} = 4.24 min^{-1} and K_I = 3.93 μM, therefore an overall k_{inact}/K_I = 1.08 x 10^6 M^{-1} min^{-1}. In those experiments, we used a K_M value of 200 μM for **AL5**.